Universitat Autònoma de Barcelona

Study of the resistance to Cucumber mosaic virus controlled by Vacuolar protein sorting 41 in Cucumis melo

Núria Real Tortosa

UNIVERSITAT AUTÒNOMA DE BARCELONA

Facultat de Biociències

Dept. Biologia Animal, Biologia Vegetal i Ecologia

Study of the resistance to *Cucumber mosaic virus* controlled by Vacuolar protein sorting 41 in *Cucumis melo*

Núria Real Tortosa

Barcelona, May 2022

Universitat Autònoma de Barcelona

Facultat de Biociències

Dept. Biologia Animal, Biologia Vegetal i Ecologia

Estudis de Doctorat en Biologia i Biotecnologia Vegetal

PhD thesis

Study of the resistance to *Cucumber mosaic virus* controlled by Vacuolar protein sorting 41 in *Cucumis melo*

Dissertation presented by Núria Real Tortosa for the degree of Doctor of Biology and Plant Biotechnology by Universitat Autònoma de Barcelona (UAB)

This work was performed in

Centre de Recerca en Agrigenòmica (CRAG), Bellaterra.

Thesis director	Tutor	PhD candidate
Dra. Ana Montserrat Martín Hernández	Dra. Ana Montserrat Martín Hernández	Núria Real Tortosa

Barcelona, May 2022

This thesis has been carried out in the department of Plant Genetics of the Centre de Recerca en Agrigenòmica (CRAG) CSIC-IRTA- UAB-UB, Barcelona, and in a 3-months stage in the group of Dr. Hirofumi Nakagami in the department of Plant Microbe Interactions of the Max Planck Institute for Plant Breeding (MPIPZ), Cologne.

I think at times we feel or we are made to feel that we champion different causes. But for me, I see commonality. I think whether we're talking about gender inequality, racism, queer rights, indigenous rights, or animal rights, we're talking about the fight against injustice. We're talking about the fight against the belief that one nation, one people, one race, one gender, or one species has the right to dominate, control, use, and exploit another with impunity.

I think we've become very disconnected from the natural world. And many of us are guilty of an egocentric world view. The believe that we are the center of the Universe. We go into the natural word and we drain it from its resources. We feel entitled to artificially inseminate a cow and when she gives birth we steal her baby, even though her cries of anguish are unmistakable. And then we take her milk that's intended for the calf, and we put it in our coffee and cereal. We fear the idea of personal change because we think we have to sacrifice something; to give something up. But human beings at our best are so creative and inventive, and when we use love and compassion as our guiding principles we can create, develop, and implement systems of change that are beneficial to all sentient beings and to the environment.

– Joaquin Phoenix, Best actor acceptance speech, Oscars 2021

Agraïments

Encara no em crec que ja estigui acabant la tesis. Definitivament ha sigut un període de transformació i aprenentatge, tant a nivell professional com personal i estic molt contenta de totes les persones que he conegut i de les quals m'emporto un trosset de cadascuna.

Primero de todo, quiero dar las gracias a la Dra. Montserrat Martín, mi directora de tesis. Estoy muy agradecida por la oportunidad que me diste al poder realizar la tesis doctoral en el grupo de Plant Virus. Contigo he podido superarme a nivel profesional y he aprendido a trabajar de un modo mucho más autónomo, a ser más crítica y a hacer siempre un poco más. El período de escritura no ha sido fácil y se ha alargado, pero espero que no estés quemada porque tenemos que escribir más papers juntas (jeje). Te deseo que el grupo continue creciendo y que todas las nuevas incorporaciones traigan buenos resultados. Tengo ganas de ver hacia dónde va la investigación.

I would like to thank Dr. Hirofumi Nakagami. You took me as another member of your group, and I was able to learn a lot and work in a very productive and nice environment. I also appreciate all the help you gave me and good advice. I wish you all the success in your group. I want to specially thank Anne; you were super welcoming from the beginning, and I really liked working with you. I think we were quite coordinated, and we did a lot of work while having fun and sharing some laughs as well. Sara, I thank you for all the effort and help with the data analysis. Katharina thank you for welcoming me, showing me the Institute. Also, I sent my regards to all the other lab members that I met briefly but were all very nice to me.

Liu Bin, I was very glad we could work together. You showed me all the yeast two hybrid tricks and I learned a lot. We worked like crazy, but we always shared some laughs. You are one of my referents and I wish you all the success, you deserve it. It was also a pleasure to meet you at a personal level. I think we connected very well and I'm taking all your advice with me. When I travel to China we should meet with Yan and Rong and you can show me around.

Toni! Moltíssimes gràcies per tota l'ajuda durant l'anàlisi del proteoma. T'estic eternament agraïda. Gràcies a tu em miro la bioinformàtica d'una altra manera. També m'alegro d'haver-te pogut conèixer a nivell personal, ets la canya. Et desitjo una molt bona etapa al CRAG.

A la gent del grup de Plant Virus moltes gràcies a tots els que han passat pel grup i als que hi són ara. Fuensi ets la mare del grup i t'agraeixo tot el que has fet per mi. Ets un sol com a persona i m'has ajudat moltíssim. M'alegro molt d'haver pogut aprendre al teu costat i a més a més ens hem divertit també. Lorena, desde que llegaste encajaste muy bien en el lab, e incluso antes de que entrases al grupo ya nos hicimos amigas. Me ha gustado poder enseñarte y ser de algún modo tu mentora, te deseo que te vaya bien en la recta final. Nicole, ja no estàs al grup però vas ser la millor

estudiant. Treballadora, simpàtica i humil. Moltes gràcies. Andrea gracias por todo lo que compartimos juntas, aprendí muchísimo y no me olvidaré de ti. Paula and Yan, you are not there anymore but you were when I started and you helped me a lot, with your help I felt welcomed to the group right away. Irene and Weina I am glad you can continue the work I started; I wish to you both nice results.

Als companys de laboratori, amb vosaltres cada dia és carnaval. Laura i Nathi us estimo molt nenes, sois amor y tenéis un corazón enorme (aunque Laura vaya de dura). Os agradezco mucho toda la empatía y el dejarme ser yo. Ambas brilláis con luz propia, no dejéis que nadie quite importancia a vuestros méritos, os los habéis ganado. Ari moltes gràcies per tota l'ajuda i per tot el bon rotllo que portes sempre. Carlos muchas gracias por preocuparte y pedirme consejos, ha sido un honor. Bea y Felipe siempre os apuntáis a un bombardeo y sois de lo más majo que hay, me ha gustado compartir con vosotros. Martes i Silvia moltes gràcies per tots els consells i l'ajuda. Elena, eres el abrigo de todos los doctorandos, muchas gracias por preocuparte por mí y por ayudarme siempre.

Al departament, moltíssimes gràcies per acollir-me i fer-me sentir com a casa. Des que vaig entrar vaig notar com em vau integrar, acompanyar i m'heu ajudat molt entre tots. Sobretot a la Noemí per la professionalitat i el caliu m'ha ajudat amb tot el que he necessitat.

Gente del despacho 301, sois luz y me habéis acompañado todo este tiempo. Especialmente Miguel, Chris y Lino. Miguel, me lo he pasado genial a tu lado desde cotillear hasta tener conversaciones científicas y técnicas, siempre estamos del mismo rollo. ¡Te deseo la mejor recta final! Chris, eshque te quiero mucho tío jajaaja amigo te echo de menos, celebrar la vida es uno de nuestros puntos fuertes y ya toca. En Madriz o donde estés, aquí se te echa de menos. Lino, siempre que estuviste nos iluminaste el día con tu buen rollo, muchas gracias.

To my ex-flatmates, Naveen and Arnau, I could not have chosen anyone better to share this whole experience with. Naveen we have grown together at a professional and personal level and it has been a pleasure. Arnau, des del principi fins ara hem estat comentant la jugada i hem encaixat molt bé. Espero que puguis anar a Xile i m'encantaria visitar (jeje ahí lo dejo). Et guardaré sempre molt bon record i espero que puguis aconseguir tot el que et proposes.

A la gent d'altres laboratoris, els que he tingut la oportunitat de conèixer sempre m'heu tractat molt bé i us agraeixo el caliu. Especialment el Carles i l'Ornela. Carles moltes gràcies per totes les passejades pel centre, les birres, els cotilleos i els riures compartits. Ho trobaré a faltar. Ornela, gracias por hacer siempre los congresos y charlas mucho más dinámicos. Estás llena de energía. Tengo ganas de ver que te deparará el futuro.

Als que van marxar abans del lab. Jose, què dir-te? El millor company de poiata i amb qui vaig passar la meitat del meu doctorat enganxats i no ho canviaria per res. I una de les persones que va posar cara i ulls al veganisme. Moltes gràcies. La meva tocaia Núria que i tot i que va estar poc temps va ser molt divertit i vas portar molta bona energia. Neus, una ànima lliure i plena d'amor, moltes gràcies pels moments compartits.

Als meus amics de Sabadell, gràcies per ser-hi sempre. Moltes vegades sense entendre res de la meva feina em doneu suport i m'escolteu igualment, només per això ja us ho mereixeu tot. I Encara que no fem res de l'altre món, teniu la capacitat per convertir cada moment en especial. Amb vosaltres em puc llençar a qualsevol aventura que tot anirà bé. Sobretot, vull agrair al Cesc i la Marina el seu suport; en els dies més negres heu passat la tempesta al meu costat.

A les noietes Parakalo, Sara, Mireia, Elena, Marta, Anna i Laura, gràcies per ser-hi i per entendre'm. Realment crec que en pocs grups d'amics es pot arribar a entendre pel que es passa a nivell professional i en què consisteix fer investigació. Sou unes dones fortes i lluitadores.

Moltes gràcies a la meva família, sobretot mare, pare i Maria, que sempre em doneu suport incondicional, faci el que faci i em trobi en la situació en la que em trobi. Crec que tinc molta sort de tenir una família tan oberta i en la que tots els seus membres volen créixer i estan en constant transformació i aprenentatge. M'heu ensenyat a pensar, a dubtar, a respectar als altres i el món que ens envolta, a gaudir dels viatges, a valorar els luxes i a estimar.

Indexes

Index of contents

Index of figures

Index of tables

Index of the digital supplementary material

Supplementary material 1. Chapter I.

Statistical analysis of Chapter I of CmVPS41 structures.

Supplementary material 2. Chapter II.

A- Statistical analysis tables from CMV-MP interacting proteins for *C. melo* and *N. benthamiana.* Including: raw data and possible candidates' information.

B- GO and KEGG analysis of IP proteins.

Supplementary material 3. Chapter III.

A- Statistical analysis tables from all detected proteins in the proteomes of *C. melo* and *N. benthamiana.*

B- Heatmaps. Input and R scripts.

C- Volcano plots. Input and R scripts.

D- Networks.

   a. Inputs networks and R script.
   b. Density graphs of *N. benthamiana*.
   c. Networks.
   d. Cytoscape networks and modules.
   e. Analysis of modules and hubs.

Summaries

Summary

'Songwhan Charmi', is an exotic *Cucumis melo* (*C. melo*) accession (PI 161375) that presents a qualitative and quantitative resistance to *Cucumber mosaic virus* (CMV), depending on the strain. The main quantitative trait locus (QTL) of resistance is a recessive gene *cmv1,* which confers total resistance to CMV strains of subgroup II, such as CMV-LS. CMV-LS is able to replicate and move cell-to-cell in the inoculated leaf of the resistant line, but it is stopped at the bundle sheath and is not able to reach the phloem. *cmv1* encodes a Vacuolar Protein Sorting 41 (VPS41). In this thesis we have extended the knowledge of VPS41-mediated resistance present in melon.

In the first chapter, we have characterized the cellular localization of CmVPS41 in susceptible and resistant varieties identifying differential structures formed by CmVPS41 that co-localize with the late endosomes. These structures re-localize during CMV infection. Moreover, we found that CmVPS41 associates *in vivo* with the movement protein (MP) of CMV-FNY, the viral virulence factor.

In the second chapter, we have identified 136 candidate interactors of CMV-MP in *C. melo* through two protein-protein interaction methods. One of them, Niemann-Pick C1 protein-like (NPC1) is a cholesterol transporter involved in other viral infections. Its interaction domain was validated through a second approach, and its association with the MPs from CMV-FNY and CMV-LS was confirmed both *in vitro* and *in vivo*.

In the third chapter, we performed a high-throughput proteome analysis in *C. melo* upon CMV challenge. Several co-abundance protein networks were generated to study the different biological pathways involved in CMV infection, both at early and late stages of infection, and in susceptible and resistant melon genotypes. Hub proteins involved in CMV resistance and susceptibility were determined through network analysis. The same approach followed in susceptible, CMV-inoculated *Nicotiana benthamiana (N. benthamiana)* plants, allowed a comparison with *C. melo* networks, and identification of common biological pathways of CMV infection, as well as, key proteins of CMV infection common in both *N. benthamiana* and *C. melo*.

Resumen

'Songwhan Charmi' es una accesión exótica de *Cucumis melo* (*C. melo*) (PI 161375) que presenta una mezcla de resistencia cualitativa y cuantitativa frente a la infección por el *Virus del mosaico del pepino* (CMV), dependiendo de la cepa. El principal locus de rasgos cuantitativo (QTL) de la resistencia es el gen recesivo *cmv1*, que confiere resistencia total a las cepas de CMV del subgrupo II, como CMV-LS. CMV-LS es capaz de replicarse y moverse célula a célula en la hoja inoculada de la línea resistente, pero no puede pasar las células de la vaina (BS), donde queda retenido, y no llega al floema. *cmv1* codifica la Vacuolar Protein Sorting 41 (VPS41). En esta tesis se ha ampliado el conocimiento de la resistencia mediada por VPS41 en melón.

En el primer capítulo, se ha caracterizado la localización celular de CmVPS41 en variedades susceptibles y resistentes y esto ha permitido identificar estructuras diferenciales formadas por CmVPS41 que, a su vez, co-localizan con endosomas tardíos. Estas estructuras se re-localizan durante la infección por CMV. Además, se ha visto que CmVPS41 se asocia *in vivo* con la proteína de movimiento (MP) de CMV-FNY, que es el factor de virulencia del virus.

En el segundo capítulo, se identificaron 136 proteínas que potencialmente interaccionan con CMV-MP en *C. melo* a través de dos métodos de interacción proteína-proteína. Una de estas proteínas, la Niemman-Pick C1 protein-like (NPC1) es un transportador de colesterol involucrado en otras infecciones virales. Su dominio de interacción fue validado a través de un segundo método y su asociación con ambas MP, tanto de CMV-FNY como CMV-LS, fue confirmada tanto *in vitro* como *in vivo*.

En el tercer capítulo, se hizo un análisis de alto rendimiento del proteoma de *C. melo* durante el desafío por CMV. Se generaron distintas redes de proteínas co-abundantes para estudiar los diferentes procesos biológicos involucrados en la infección por CMV en estadios tempranos o tardíos de la infección tanto en genotipos de melón resistentes como susceptibles. El análisis de las redes de proteínas permitió encontrar proteínas centrales involucradas en la resistencia o susceptibilidad a CMV. En la planta susceptible *N. benthamiana* inoculada con CMV se aplicó la misma metodología y se compararon los resultados con la red de *C. melo*, pudiendo así identificar procesos biológicos comunes en ambas infecciones por CMV y también proteínas clave en la infección de CMV comunes en ambas plantas.

Resum

'Songwhan Charmi' és una accessió exòtica de *Cucumis melo* (*C. melo*) (PI 161375) que presenta una barreja de resistència qualitativa i quantitativa davant la infecció pel *Virus del mosaic del cogombre* (CMV), depenent de la soca. El principal locus de trets quantitatius (QTL) de la resistència és el gen recessiu *cmv1*, que confereix resistència total a les soques de CMV del subgrup II, com CMV-LS. CMV-LS es capaç de replicar-se i moure's cèl·lula a cèl·lula a la fulla inoculada de la línia resistent, però no pot passar les cèl·lules de la beina (BS), on queda retingut, i no arriba al floema. *cmv1* codifica la Vacuolar Protein Sorting 41 (VPS41). En aquesta tesis s'ha ampliat el coneixement de la resistència a través de VPS41 en meló.

En el primer capítol, s'ha caracteritzat la localització cel·lular de CmVPS41 en varietats susceptibles i resistents, i això ha permès identificar estructures diferencials formades per CmVPS41, que, alhora, co-localitzen amb endosomes tardans. Aquestes estructures es re-localitzen durant la infecció per CMV. A més a més, s'ha vist que VPS41 s'associa *in vivo* amb la proteïna de moviment (MP) de CMV-FNY, que és el factor de virulència del virus.

En el segon capítol, s'han identificat 136 proteïnes que potencialment interaccionen amb la MP de CMV en *C. melo* a través de dos mètodes d'interacció proteïna-proteïna. Una d'aquestes proteïnes, la Niemman-Pick C1 protein-like (NPC1), és un transportador de colesterol involucrat en altres infeccions virals. El seu domini d'interacció va ser validat a través d'un segon mètode i la seva associació amb ambdues MP de CMV-FNY i CMV-LS va ser confirmada tant *in vitro* com *in vivo*.

En el tercer capítol, s'ha fet un anàlisi d'alt rendiment del proteoma de *C. melo* durant el desafiament per el CMV. Es van generar diverses xarxes de proteïnes co-abundants per estudiar els diferents processos biològics involucrats en la infecció per CMV en estadis primerencs o tardans de la infecció tant en genotips de meló resistents com susceptibles. L'anàlisi de les xarxes de proteïnes va permetre trobar proteïnes centrals involucrades tan en la resistència com la susceptibilitat a CMV. En la planta susceptible *N. benthamiana* inoculada amb CMV també es va generar una xarxa fent servir la mateixa metodologia i es va comparar amb els resultats de *C. melo*. Així, es van poder identificar processos biològics comuns en ambdues infeccions de CMV i també proteïnes claus comunes en ambdues plantes durant la infecció de CMV.

Abbreviations

Abbreviations of viruses

AMV	*Alfalfa mosaic virus*
BCMNV	*Bean common mosaic necrosis virus*
CaMV	*Cauliflower mosaic virus*
CMV	*Cucumber mosaic virus*
CymRSV	*Cymbidium ringspot virus*
EboV	*Zaire ebolavirus* or Ebola virus
FLUAV	*Influenza A virus*
GMMV	*Gayfeather mild mottle virus*
HCV	*Hepatitis C virus*
HIV-1	*Human immunodeficiency virus type 1*
LMV	*Lettuce mosaic virus*
MARV	*Marburgvirus*
MNSV	*Melon necrotic spot virus*
M-PMV	*Mason-Pfizer monkey virus*
RCNMV	*Red clover necrotic mosaic virus*
PNRSV	*Prunus necrotic ringspot virus*
PSV	*Peanut stunt virus*
PVY	*Potato virus Y*
PVX	*Potato virus X*
SMV	*Soybean Mosaic Virus*
TAV	*Tomato aspermy virus*
TBSV	*Tomato bushy stunt virus*
TBV	*Tulip breaking virus*
TMV	*Tobacco mosaic virus*
ToMV	*Tomato mosaic virus*
TSWV	*Tomato spotted wilt virus*
TYLCV	*Tomato yellow leaf curl virus*
TYMV	*Turnip yellow mosaic virus*
WMV	*Watermelon mosaic virus*
ZYMV	*Zucchini yellow mosaic virus*

Other abbreviations

aa: Aminoacid

AbA: Aureobasidin A

Ade: Adenine

ANOVA: Analysis of variance

BAC: Bacterial artificial chromosome

BIFC: Bimolecular fluorescence complementation assay

BS: Bundle sheath

CC: Companion cell

cDNA: Complementary DNA

cM: centimorgan

CmAO4 *C. melo* L-ascorbate oxidase 4 homologue

COP: Coat protein complex

CORVET: Class C core vacuole/endosome tethering factor

CP: Coat protein

CRISPR: Clustered regularly interspaced short palindromic repeats

CV: Cabo Verde

DHL: Doubled haploid line

Dpi: Days post-inoculation

dsDNA: Double-stranded DNA

dsRNA: Double-stranded RNA

ER: Endoplasmic reticulum

ERAD: ER-associated degradation

FC: Freeman's cucumber

GA: Golgi apparatus

Gal: Galactosidase

OD_{600} optical density measured at a wavelength of 600 nm

GFP: Green fluorescent protein

GO: Gene ontology

GO:BP: Biological process category of GO terms

GO:CC: Cellular component category of GO terms

GO:MF: Molecular function category of GO terms

His: Histidine

HOPS: Homotypic fusion and protein sorting

IC: Intermediary cell

IP: Immunoprecipitation

KDa: Kilodaltons

KEGG: Kyoto encyclopedia of genes and genomes

Leu: Leucine

LG: Linkage group

mCherry: Monomeric cherry fluorescent protein

MP: Movement protein

NIL: Near isogenic line

NPC1: Niemann-Pick C1 protein-like

nt: Nucleotide

ORF: Open reading frames

p-adj: p-adjusted value

PCR: Polymerase chain reaction

PD: Plasmodesmata

PDIL: protein disulfide isomerase-like

PPI: protein-protein interaction

PM: Plasma membrane

PPU: Pore plasmodesma unit

PS: Piel de Sapo

QTL: Quantitative trait locus

Raf: Raffinose

RFP: Red fluorescent protein

RIL: Recombinant inbred line

RT: Reverse transcription

SC: Songwhan Charmi

SD: Synthetic minimal

SE: Sieve element

SEL: Size exclusion limit

SG: Subgroup

SNARE: Specific vesicle soluble methylmaleimide sensitive factor attachment protein receptor

SNP: Single nucleotide polymorphism

ssDNA: Single-stranded DNA

ssRNA: Single-stranded RNA

TGN: Trans-golgi network

Trp: Tryptophan

TVS: Trans-vacuolar strands

UTR: Untranslated region

VP: Vascular parenchyma

VPS: Vacuolar sorting protein

vRNA: Viral RNA

vRNP: Viral ribonucleoprotein complexes

vsiRNA: Viral small interfering RNA

VSR: Vacuolar sorting receptor

VRC: Viral replication complex

YC: C-terminal part of the yellow fluorescent protein

YFP: Yellow fluorescent protein

YN: N-terminal part of the yellow fluorescent protein

Y2H: Yeast two hybrid

Genetic code

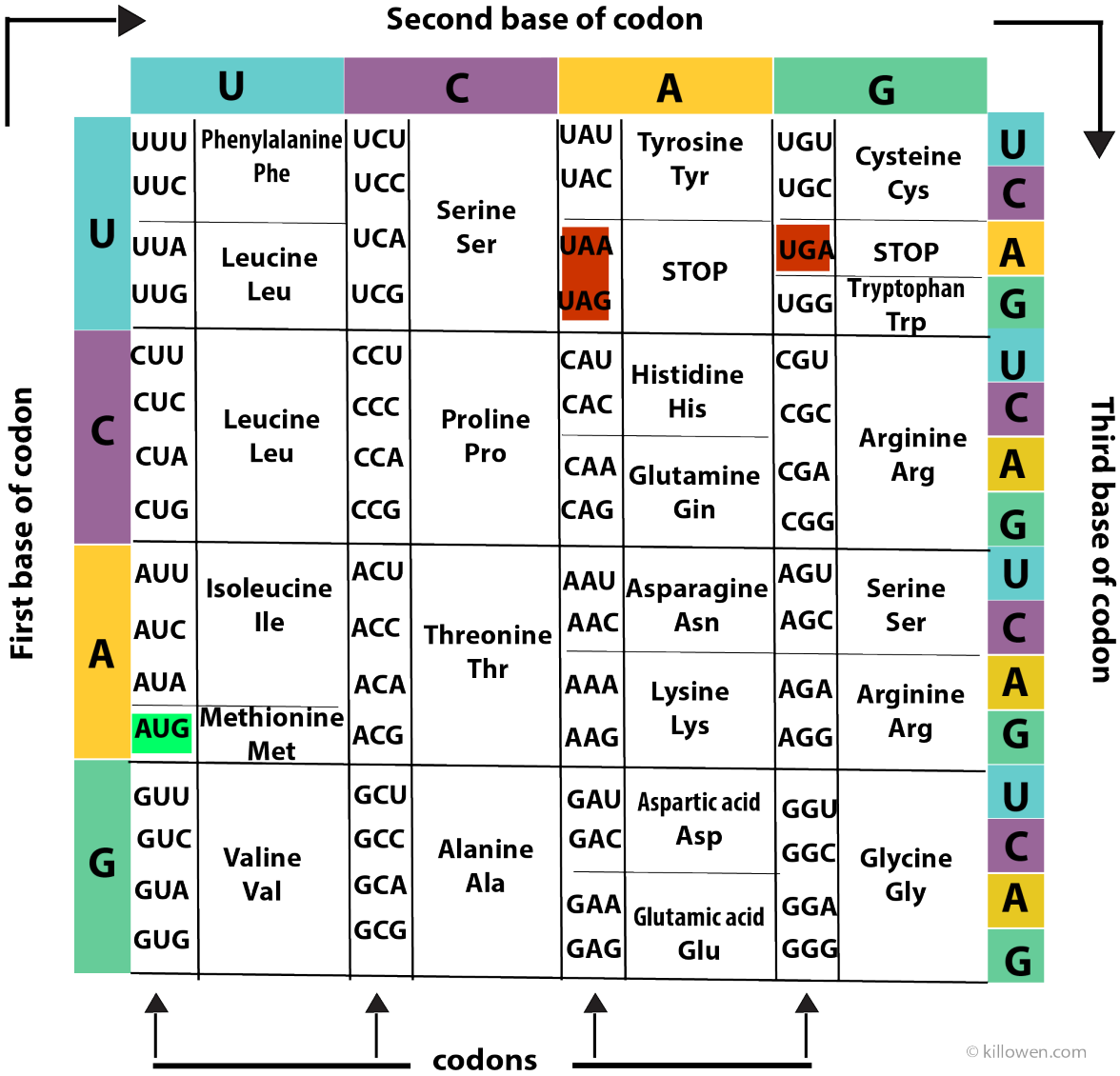

I. General Introduction

GI.1 Cucumis melo L.

GI.1.1. Economic importance and origin

Melon (*Cucumis melo L.*) is the model species of the Cucurbitaceae family; that has been cultivated for over 4,000 years. Melon was first described in the "Species planetarum" by Carolus Linneaus in 1753 and, in the last decades, has become a very important crop because of its great economic value and is cultivated worldwide. In 2020, melon production around the globe was estimated at more than 28 million tones (Mt) (**Figure GI.1**) by the Food and Agriculture Organization of the United Nations (FAO) (https://www.fao.org/faostat/en/#data/QC) (Accessed 30 January 2022) and Spain is at the top ten producers with China in the leading production with almost 14 Mt per year.

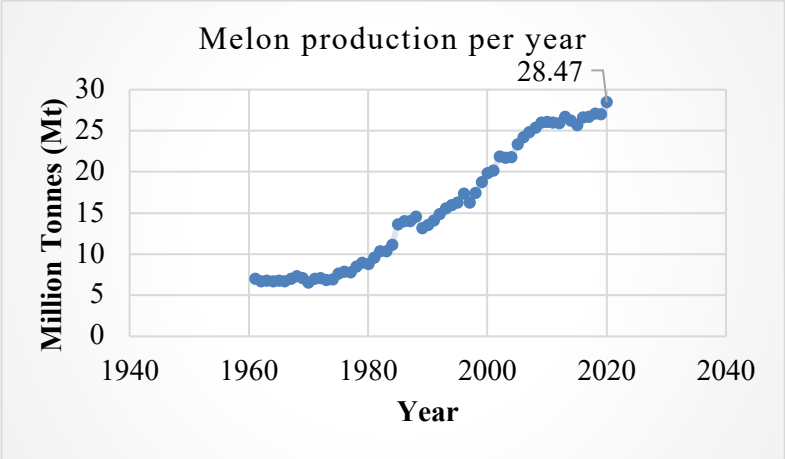

Figure GI.1. Melon production worldwide from 1961 to 2020. Data collected from FAOSTAT (https://www.fao.org/faostat/en/#data/QC).

C. melo is a diploid plant species (2n = 2x = 24). The Cucurbitaceae family comprehends around a thousand species, with 10 worldwide important crops and 23 crops of local commercial importance, being *Cucumis* and *Citrullus* genus the most economically important. Major domesticated cucurbit crops include: cucumber (*Cucumis sativus*), watermelon (*Citrullus lanatus*), pumpkin and squash (*Cucurbita* spp.), wax gourd (*Benicasa hispida*), bottle gourd (*Lagenaria siceraria*), bitter gourd (*Momordica charantia*) and silverseed gourd (*Cucurbita argyrosperma*) (Chomicki et al., 2020).

The species *Cucumis melo L.* is further divided into several botanical varieties (**Figure GI.2**) or types, according mainly to fruit traits such as size, shape, external appearance, but also seed characteristics. The three most important varieties are cantalupensis, inodorus and reticulatus, although a total of 19 groups are included (Pitrat, 2016).

Figure GI.2. Diversity of melon varieties according to Pitrat (2008). **A**. Inodorus (Piel de Sapo). **B**. Conomon (Shiro Uri Okayama). **C**. Momordica (PI124112) **D**. Chate (Carosello Barese). **E**. Dudaim (Queen Anne's pocket melon). **F**. Acidulous (TGR-1551). **G**. Makuwa (Ginsen Makuwa). **H**. Ameri (Kizil Uruk) **I**. Cantalupensis (Vedrantais). **J**. Reticulatus (Dulce). **K**. Flexuosus (Arya). **L**. Tibish (Tibish). **M**. Chinensis (Songwhan Charmi). **N**. Wild melon (trigonus). Adopted from Monforte et al. (2014).

The origin of melon has been widely discussed. Traditional studies place its origin in Africa, where a high number of wild species, the oldest melon seeds and a diversity of chromosomes are found (Davis, 1962; van Zeist and de Roller, 1993; El Hadidi et al., 1996; Robinson and Decker-Walters, 1999). Other studies present the idea of a wild ancestor in Asia, supported by high landraces in India and East Asia (Sebastian et al., 2010). Moreover, discovery of wild melons in Australia added a third component to the discussion (Sebastian et al., 2010). Up to date, the most comprehensive phylogenetic study by Endl et al. (2018) reveals three genetically distinct melon lineages of different geographic origins, one African, another with wild melon accessions from Australia and New Guinea, and a third and large set formed by Asian wild melon accessions. Moreover, only Asian and African cultivars were domesticated and in consequence all modern cultivars come from either the Asian lineage, including

'Inodorus', 'Cantaloupe', 'Galia' and 'Yellow Honeydew' varieties and a few cultivars of African origin ('Moussa', 'Tirama') as well (H1 in **Figure GI.3**), or the African lineage, which includes the 'Fadasi' and 'Tibish' melons (H13, H14 in **Figure GI.3**) (Endl et al., 2018).

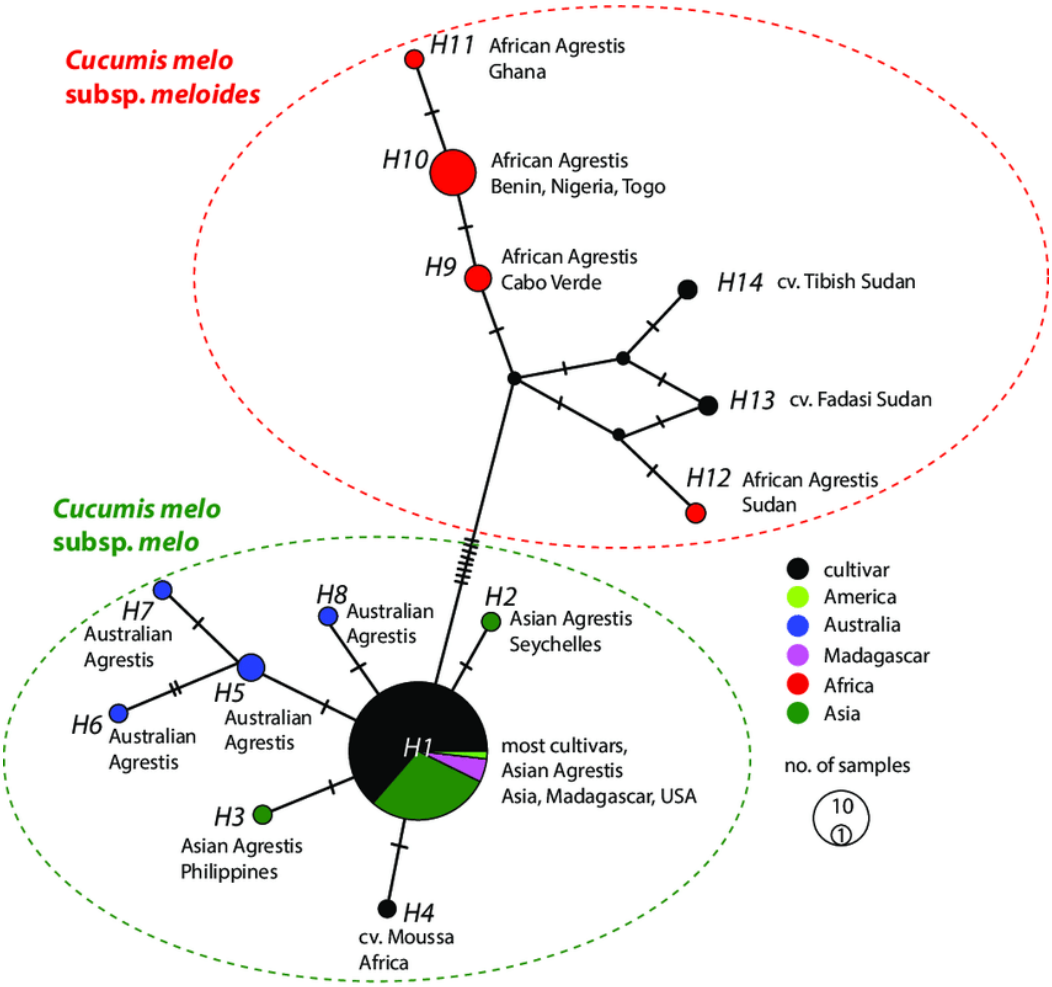

Figure GI.3. *Cucumis melo* geographic origin. Median-joining network of the *Cucumis melo* clade. The nuclear ribosomal internal transcribed spacer (ITS) region haplotypes are represented by circles. Circle diameter indicates number of accessions sampled and colour its geographic origin. Hatch marks on the lines connecting the different haplotypes indicate the haplotypes had not samples. Adopted from Endl et al. (2018).

GI.1.1. Genetic and genomic resources

Its economic value and broad phenotypic differences among cultivars make melon an attractive model to study agronomical traits for breeding programs. This interest has generated a number of molecular tools including a *de novo* sequencing of the melon genome (Garcia-Mas et al., 2012), collections of Near Isogenic lines (NILs) (Eduardo et al., 2005), Double haploid lines (DHLs) (Gonzalo et al., 2011) and recombinant inbred lines (RILs)

(Pereira et al., 2017), genetic maps (Diaz et al., 2011), Expressed Sequence Tags (ESTs) databases (Gonzalez-Ibeas et al., 2007), development of microarrays and microsatellite markers (Ritschel et al., 2004), a BAC-end sequence library, TILLING (Targeting Induced Local Lesions in Genomes) collections (Till et al., 2003; Dahmani-Mardas et al., 2010; González et al., 2011). The most recent is the sequencing of the melon reference genome (Garcia-Mas et al., 2012) and the re-sequencing of several accessions, which allowed to study the evolution of the melon genome and identify transposons and structure variations (Sanseverino et al., 2015) and a large fraction of repetitive elements (Castanera et al., 2020). Functional validation of genes with stable transformation was reported in melon (Giner et al., 2017) and recently gene-editing by CRISPR-Cas9 technique has been efficiently implemented for melon to study genes involved in fruit ripening (Bin et al., 2022; Giordano et al., 2022).

GI.1.1.1. Collection of NILs in melon

The Near Isogenic Line (NIL) population by Eduardo et al. (2005) was developed from a cross between the exotic accession 'Songwhan Charmi' (SC), the donor parent, and the Spanish variety "Piel de Sapo" (PS), the recipient genotype. These two cultivars were chosen for their highest differences in the genome (Garcia-Mas et al., 2000), that correlate as well with differences in climacteric state, flesh characteristics, size of the fruit (Monforte et al., 2004) and resistance to pathogens (Lecoq et al., 1980; Lecoq and Pitrat, 1982).

This allowed to create the NIL population which consisted of a collection of melon plants with homozygous chromosome segments from SC in the genetic background of PS (**Figure GI.4**). The principal use of NIL populations is to characterize complex traits by mendelizing them, this way allowing to perform fine mapping of interesting loci using molecular markers (Rafalski et al., 1996).

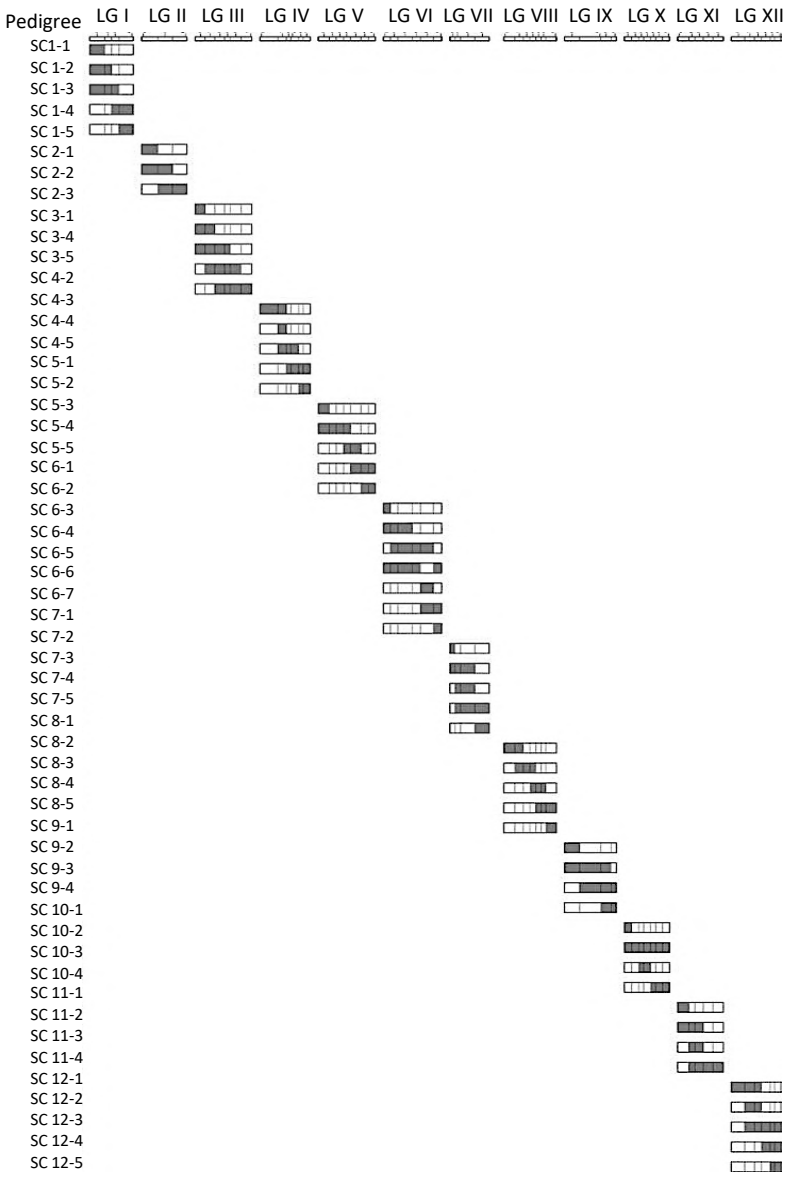

Figure GI.4. Graphic of NILs genotypes. SC: Songwhan Charmi. Grey boxes: introgressions from SC LG: Linkage group. In the pedigree, the first number indicates the LG where the SC introgression maps and the second number, the order of the introgression within the LG. Adopted from Eduardo et al. (2005).

GI.2 The plant cell

GI.1.2. Basic structure

Plants have characteristic eukaryotic cells with differences with their animal counterparts. Their specific organelles and structures are depicted in **Figure GI.5**. Plant cells present plastids, a central vacuole, cell wall, plasmodesmata, while do not have either flagella or centrioles, as animal cells do.

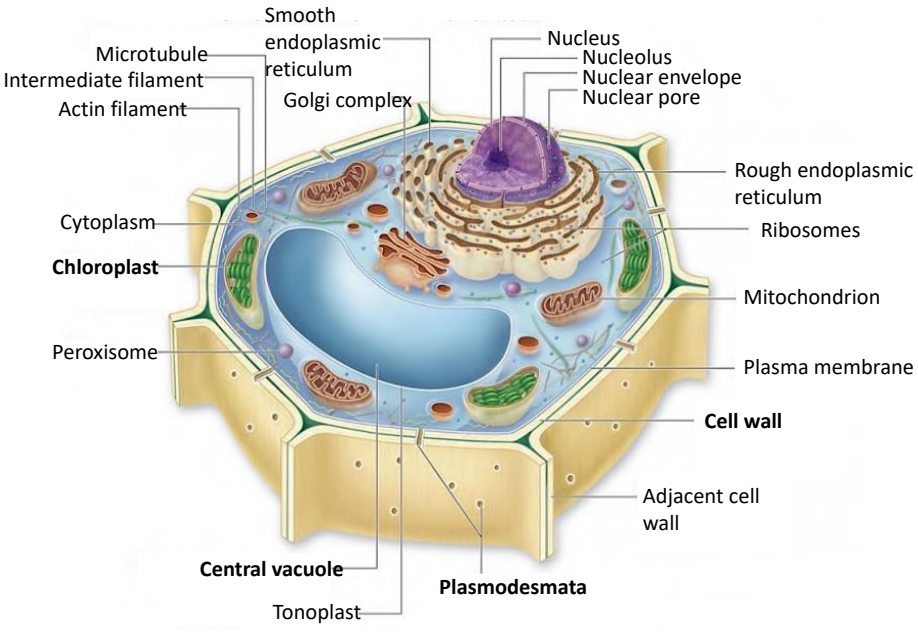

Figure GI.5. Schematic representation of the plant cell organization and its organelles. Specific organelles from plant cells (chloroplast, central vacuole, plasmodesmata and cell wall) are depicted in bold. Modified from Mifflin and Littell (2005).

Cell walls in plants are composed of cellulose, hemicellulose and pectin, while other organisms have other components, such as chitin in fungi or peptoglycan in bacteria. Frequently, an additional layer, composed by lignin or suberin, can be secreted inside the primary cell wall for functional reasons. The new layers of material also contain cellulose but are enriched in lignin and xylans. Cell walls participate in shape, intercellular communication and plant-microbe interactions (Höfte and Voxeur, 2017).

Plasmodesmata (PD) are channels that connect neighbour cells. PDs connect cytoplasm of neighbour cells and have membrane continuity with the Endoplasmic Reticulum (ER) (Maule and Havelda, 2008; Kragler, 2012). In a relaxed state, PDs are composed of desmotubule, an elongation from the ER, specific proteins, cytoskeleton and callose deposits (neck region) and the channel is filled with cytoplasm, which is called the cytoplasmic sleeve (Peters et al., 2021) (**Figure GI.6**A). PDs are involved in transport of molecules, as well as in cellular communication pathways. Specific proteins control movement through the PD (Sager and Lee, 2018).

Plasmodesmata can be classified upon their origin. Primary plasmodesmata are generated during cell division and secondary plasmodesmata are generated afterwards (Burch-Smith et al., 2011). Also, plasmodesmata vary in morphology from simple, twinned or complex

(Kim, 2018) to more specialized in specific tissues (**Figure GI.6**B). Specialized morphologies appear to control movement between certain tissues. The plasmodesmata-pore unit that consists of asymmetric PD located in the walls of sieve elements (SE) and companion cells (CC) that have a large pore in the SE cell wall, while the CC part presents several narrowed channels (Sager and Lee, 2018). Also, in the phloem there is the sieve plate pore which has an enlarged cytoplasmic pore due to previous callose deposition and in the phloem of roots is 'funnel'-shapped PD of SE and pole pericycle cells has a wider opening in the SE side (Ross-Elliott et al., 2017).

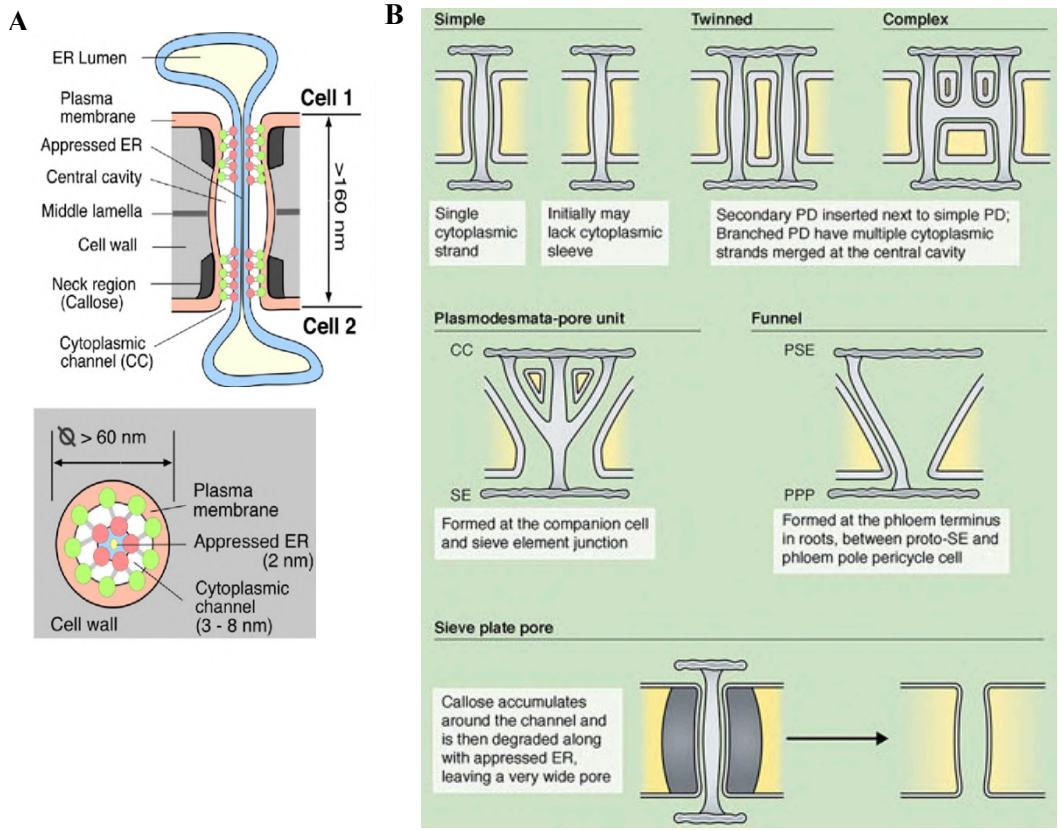

Figure GI.6. Plasmodesmata representation. **A**. Representation of the complex membrane organization of a single plasmodesmata longitudinal section (left), cross section (right). **B**. Types of plasmodesmata morphology. Adopted from Kragler et al. (2013) (A) and Sager and Lee (2018) (B).

Plastids are unique organelles in plants, with a genome encoding approximately 37 genes that have different specialization depending on their type. All plastids have both transcription or translation of the plastid genome with specific roles and essential metabolic functions to the cell. Different types of plastids participate in different processes, several serve as a storage of different compounds, such as pigments and lipids (chromoplast), starch

(amyloplast), fat (elaioplast), proteins (proteinoplast and aleuroplast) or diverse substances (leucoplast), while chloroplasts specific photosynthetic organelles (Rolland et al., 2018).

Vacuoles are the largest compartment in plant cells and are surrounded by a membrane called tonoplast. Plant vacuoles have two functions depending on the tissue. During seed maturation, vacuoles are the storage of different compounds, especially proteins that are synthesized in the ER and transported through the Golgi-independent pathway to the protein storage vacuole. Protein storage vacuoles are converted to lytic vacuoles during germination and this process involves protein storage vacuoles fusion and maturation. Thus, in vegetative tissues there are lytic vacuoles which accumulate other compounds such as proteinases, nucleases and defence proteins (Hunter et al., 2007; Zheng and Staehelin, 2011). Also, other specialized vacuoles containing specific materials can be found in selected tissues. For example, in the seed coat, vacuoles accumulate flavonoids to protect the embryo from UV light. Thus, the role of vacuole and transport of soluble proteins and metabolites has been widely studied (Shimada et al., 2018).

GI.1.3. The plant secretory pathway

The plant secretory pathway consists of the vesicle trafficking pathway with numerous interlinked organelles including ER, the Golgi apparatus (GA), the trans-golgi network (TGN), the endosomes and pre-vacuoles, vacuoles and the plasma membrane (Xiang et al., 2013).

As depicted in **Figure GI.7**, the ER is the first compartment of the secretory pathway (Bassham et al., 2008) and it has a conserved mechanism in yeast, animals and plants (Jürgens, 2004; De Marcos Lousa et al., 2012). From the nuclear envelope, soluble and transmembrane proteins are transported due to their ER signals. Once in the ER, the first quality control of protein folding and assembly occurs (Claessen et al., 2012). In principle, misfolded proteins are recognized by molecular chaperones that retain them in the ER for proper re-folding. However, if proteins are repeatedly misfolded they are transported to the proteasome system for degradation (Ellgaard and Helenius, 2003; Hebert and Molinari, 2007).

From the ER, there are two vesicle traffic systems: Golgi-independent and Golgi-dependent route. In the Golgi-independent pathway (blue arrows **Figure GI.7**), proteins are directly transported from the ER to the plasma membrane or the vacuole (Xiang et al., 2013; Chang

et al., 2017). In the case of vacuolar storage proteins, proteins form aggregates within the ER that produce the precursor-accumulating vesicles (PAC), which transport the proteins into protein storage vacuoles (Hara-Nishimura et al., 1985, 1998). The Golgi-independent pathway from the ER to the vacuole has been demonstrated for proteins in tobacco and humans (Pereira et al., 2013). Direct transport from the ER to the plasma membrane (PM) is not the most usual transport of proteins to the PM. Nevertheless, ER-PM junctions have been described by electron microscopy. In these junctions, enriched proteins have been localized that allow non-vesicular transport of phospholipids and sterols (Chang et al., 2017).

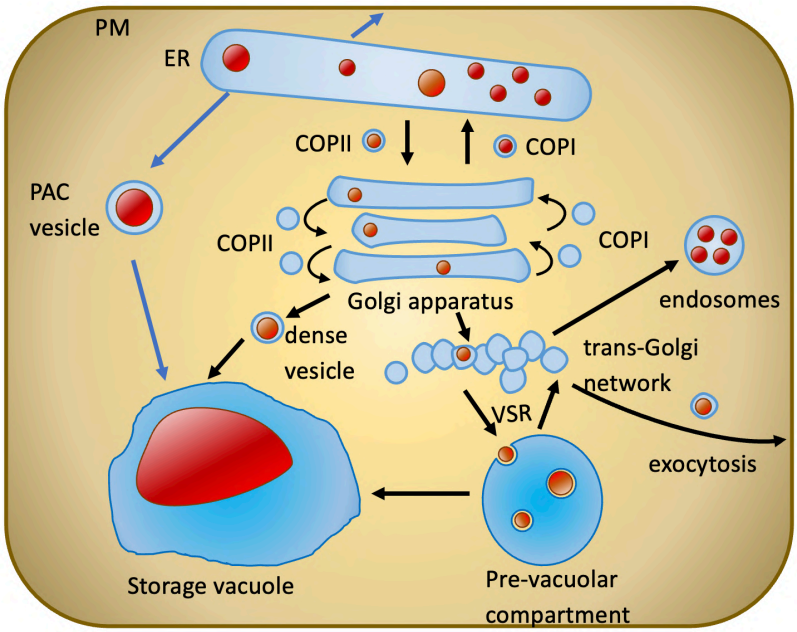

Figure GI.7. Secretory pathway route. From the endoplasmic reticulum (ER) proteins are transported to different organelles through several routes. In the Golgi-independent route (blue arrows) can transport either proteins to the plasma membrane (PM) or storage vacuole proteins with precursor-accumulating (PAC) vesicles. In the Golgi-dependent, the coat protein complex II (COP II) vesicles transport proteins from the ER to the trans-Golgi network (TGN). From the TGN they can be transported to the pre-vacuolar compartment through vacuolar sorting receptors (VSR) either to the endosomes or to the membrane (exocytosis). Return of proteins to the ER involves coat protein complex I (COP I) vesicles.

In the Golgi-dependent pathway (black arrows **Figure GI.7**), proteins are exported at the ER exit sites to coat protein complex II (COPII) vesicles. COPII coat is formed by several Sec proteins and its assembly is initiated by Sar1 a small GTPase (Barlowe and Miller, 2013). One of these Sec proteins, Sec24, participates in recognition of cargo proteins. From the ER, COPII tethering to the GA is mediated by the transport protein particle I (TRAPPI) complex, p115, and the small GTPase Rab1, whereas fusion of the vesicles to the GA is mediated by

specific vesicle soluble methylmaleimide sensitive factor attachment protein receptor (SNARE) proteins, which lead to the fusions of COPII to the GA. Once in the GA, post-translation modifications of proteins, such as glycosylation, sulfation and phosphorylation are performed (Connerly, 2010). However, transport within the GA is still to be unveiled. Different models have been proposed depending in the relationship between the GA , the ER exit sites and the ER subdomain where COPII coat assembly occurs (Shimada et al., 2018). At the TGN, proteins can be either retained, at the Golgi apparatus, or sorted based on their interaction with specific receptors and/or vesicle coats. Delivery can be done to several organelles including the vacuole or pre-vacuolar compartment, plasma membrane, the endolysosomal system or a retrograde return to the ER. Vacuole proteins require vacuolar-sorting signals and vacuolar sorting receptors (VSR) for targeting to the vacuoles (Kang and Hwang, 2014). VSRs are believed to bind their ligands at the TGN and deliver them to the protein storage vacuoles (Künzl et al., 2016). Sorting of proteins to the endolysosomal compartments is mediated by clathrin fusion, which involves adaptor protein complex 1 (AP-1) and other Golgi and clathrin adaptors (Nakatsu et al., 2014). Delivery from TGN to the plasma membrane usually involves the formation of vesicles, but this process is not understood yet (Stalder and Gershlick, 2020). Recycling of cargo receptors or other proteins to the ER is performed through COPI vesicles. COPI is initiated by Arf1, a small GPTase. COPI has an heptameric coat protein complex (α, β, β', γ, δ, ε, ζ) and δ -COP participates in cargo recognition (Arakel and Schwappach, 2018). Dsl1 complex mediates COPI vesicles tethering and facilitates the formation of SNARE complexes (Travis et al., 2020).

GI.3 Plant viruses

GI.1.4. Origin

Plant viral diseases have been observed since the beginning of times. The first record of a viral plant disease was found in a Japanese poem from 752 A.D. (**Figure GI.8**A) which describes the yellow tobacco fields due to the yellowing disease later discovered to be caused by *Tobacco leaf curl Geminivirus* (Suga, 1991). In Europe, paintings of viral diseases appeared in the 17th century when stripped tulips, infected with *Tulip breaking virus* (TBV), were prized varieties (**Figure GI.8**B). However, it was not until the late 19th century when the first virus was documented as a filterable infectious agent (Ivanowski, 1892) and the term virus was used for the first time (Beijerinck, 1898). Later, X-ray technology allowed the establishment of the viral structure (Bernal and Fankuchen, 1937) and the organization and

assembly of the capsid subunits around the viral genome (Holmes, K. C., & Franklin, 1958). The discovery of the DNA structure (Watson and Crick, 1953) allowed to predict the symmetry of the capsid of spherical viruses (Crick and Watson, 1956), which was later verified by electron microscopy methods (Williams and Smith, 1958; Brenner and Horne, 1959) and the atomic study of the first viruses (Abad-Zapatero et al., 1980). In parallel, the establishment of the International Committee on Nomenclature of Viruses (ICNV), later renamed International Committee on Taxonomy of Virus (ICTV) (Joklik and Grossberg, 2006), allowed the classification of hundreds of viruses isolated from different organisms. In the last decades new technological improvements have allowed to focus on studying plant virus replication, diagnosis, and viral genomes.

A **B**

Figure GI.8. First descriptions of phenotypes later discovered to be caused by viruses. **A**. Poem by Empress Koken 752 AD about the appearance of diseased yellow tobacco plants. **B**. Painting by Dutch artist Jacob Marrel (1614-1681) of striped tulips with colour breaking.

GI.1.5. What is a virus?

A virus is an obligate intracellular parasite. Normally viruses are transmissible and cause disease in at least one host. Viral hosts can be found across all kingdoms but nearly half of all known viruses have plants as hosts (Agrios, 2005). Many plant viruses also infect non-plant organisms due to the co-evolution with their plant vectors such as arthropods and fungi (Lefeuvre et al., 2019).

A virion is a virus particle that consists of one or more nucleic acid molecules, called viral genome, which is coated with protein or lipoprotein subunits, called capsid. Additionally, some viruses have an envelope which is an extra layer usually consisting of a lipid bilayer. The nucleic acid molecules consist of either RNA or DNA which in turn may be either single

stranded (ss) or double stranded (ds). Single-stranded nucleic acid molecules may be negative (-) or positive (+) sense indicating if the viral RNA sequence may be directly translated (+) or not (-). From all possible combinations, most plant viruses are single-stranded positive RNA or (+)ssRNA, and can be re-grouped in 20 families and a total of 83 genera (King et al., 2011).

The different types of genomes have different replication strategies. The capsid has a major role in protecting the viral genome, but it can also participate in many other aspects of the viral cycle, such as determining vector transmission, viral movement, symptomatology, and genome activation. The viral genome encodes viral proteins and in the case of RNA viruses it is the regulator of the replication process by participating in various non-template functions such as template recruitment and assembly of the viral replication complexes (VRC) (Callaway et al., 2001; Hull, 2002; Agrios, 2005; Pathak et al., 2011).

GI.1.6. General plant virus cycle

Plant virus entry occurs mostly through wounds in the epidermis caused by a vector, such as, dodder, insects, nematodes, or fungi, or due to abiotic factors like wind or rain. Plant viruses can also be propagated artificially through mechanical inoculation, a mechanism widely used to study plant diseases, or vegetative propagation, mostly used to reproduce ornamental plants (Hull, 2002).

As depicted in **Figure GI.9**, once the virion has entered the plant cell, the viral genome is uncoated and released into the cytoplasm. In positive RNA viruses, viral translation and replication take place in the cytoplasm directly from the genomic RNA. Translation of the viral replicase proteins allows these proteins to recruit, together with several host proteins, the viral RNA to membrane VRCs (Hyodo et al., 2013; Heinlein, 2015a). In the VRCs, the viral RNA (+)ssRNA is the template to produce the complementary RNA strand (-ssRNA) which will be used to synthesize new viral RNA molecules, that are also further translated and replicated. The viral replication involves interactions of the viral encoded polymerase with the host machinery (Hull, 2002; Nagy and Pogany, 2012). Many different host proteins, such as chaperones, RNA-binding proteins, lipids and membrane proteins, participate to remodel the cellular membranes and assembly the viral replicase complex and target the viral factors (Mine and Okuno, 2012). Plant viruses' replication and translation is coupled with movement of the virus to neighbour cells. Plant viruses'. Molecules until 500 kDa can diffuse relatively freely within the cytoplasm, Thus MPs might diffuse to the PD, while vRNP

complexes and virions are transported in an active manner from the site of replication to the neighbour cells (Harries et al., 2010; Niehl and Heinlein, 2011). This intracellular transport can be mediated through Endoplasmic Reticulum (ER) or microtubule filaments depending on the virus. Cell-to-cell movement occurs in epidermal or mesophyll cells through plasmodesmata (PD) with aid of the viral movement protein (MP). The MP enlarges the size exclusion limit (SEL) of plasmodesmata enough to fit the viral ribonucleoproteins or virions and actively transports viruses through them (Wolf et al., 1989; Citovsky et al., 1990, 1992). Plant viruses move cell-to-cell from the epidermis or mesophyll across several different cell types until they arrive to the vascular tissue. In systemic transport from the vascular tissue, viruses first spread to sink tissues (Niehl and Heinlein, 2011) in which again they will move cell-to-cell through plasmodesmata, enter the vascular system until they arrive to distal organs. A successful systemic infection must overcome structural and defence barriers from the host. Some host species might allow the virus spread systemically, while others might restrict the virus movement within specific tissues, inoculated leaves or even cells.

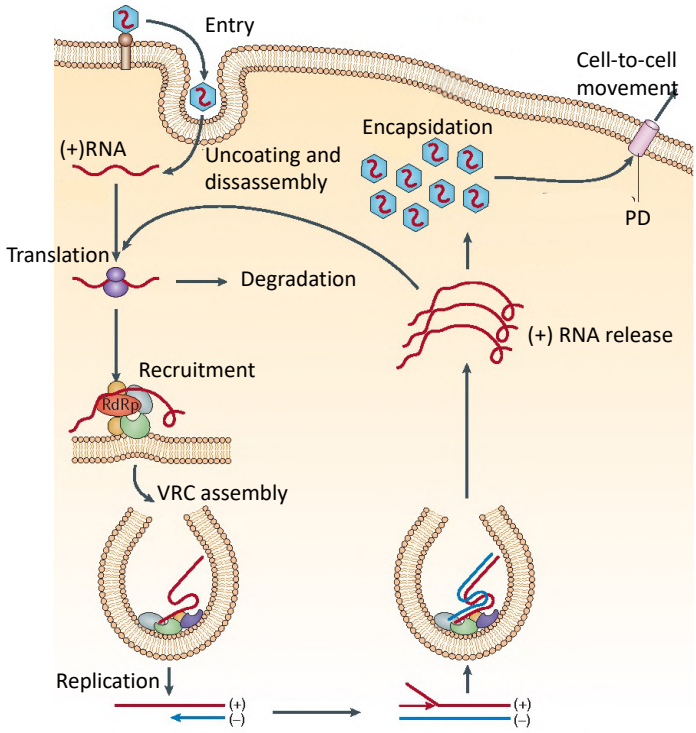

Figure GI.9. Representation of the general cycle of positive-strand RNA plant viruses. VRC: viral replication complexes. RdRp: RNA-dependent RNA polymerase. Modified from Nagy and Pogani (2012).

GI.1.7. Viral transport

GI.1.7.1. Cell-to-cell

Plant viruses need PD to transport themselves from one cell to the neighbour. In a relaxed state (**Figure GI.10**A), PD allows free movement of <1 kDa molecules. However, the size exclusion limit (SEL) of PD can be changed in response to biotic and abiotic stresses (Sun et al., 2019). SEL is changed either with callose accumulation or degradation around the apoplast of the PD, mediated by defence hormones (Wang et al., 2013) or reactive oxygen species (Cui and Lee, 2016), and/or due to specific proteins that can increase SEL directly, such as the movement proteins (MPs) of plant viruses (Niehl and Heinlein, 2011).

The two main mechanisms of plant viruses to move through PD are: (i) non tubule-guided movement of ribonucleoprotein complexes (vRNPs), which diffuse through the desmotubules once the MP allows callose degradation and increases SEL (**Figure GI.10**B) (Peña and Heinlein, 2012; Liu and Nelson, 2013; Zhuang et al., 2018) or through a (ii) tubule-guided movement of virions, in which the MP reorganizes their structure and forms tubules that serve as transport for the viral particles (**Figure GI.10**C) (Ritzenthaler and Hofmann, 2007).

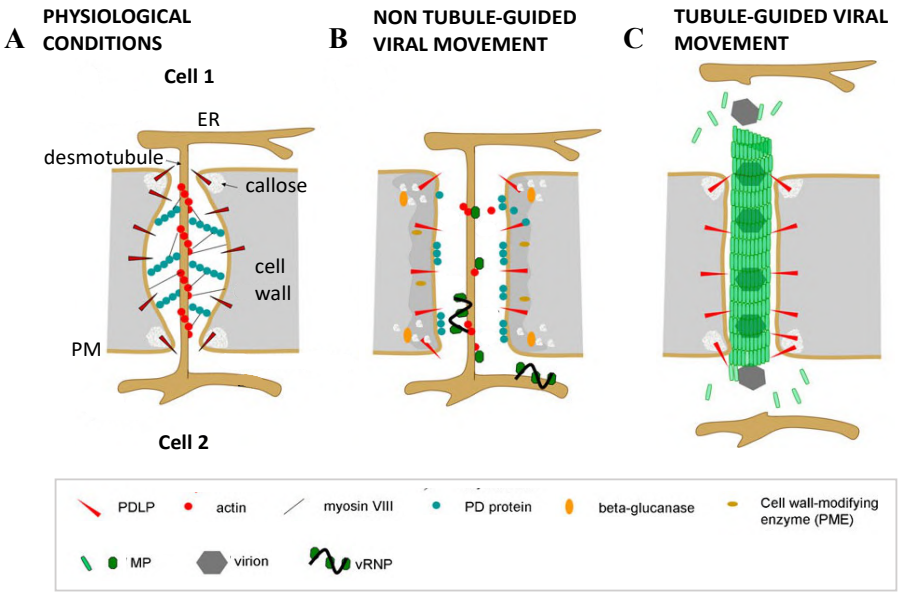

Figure GI.10. Strategies for cell-to-cell movement of plant viruses. **A**. Structure of a PD in physiological conditions, without modifications. **B**. Modified PD through non-tubule guided movement, where MP induces callose degradation that leads to dilation of the PD pore. **C**. Modified PD through tubule-guided movement proteins, where MP-tubule replaces the desmotubule inside plasmodesmata, and virions are transported through tubule assembly. Modified from Niehl and Heinlein (2011).

GI.1.7.2. Intracellular transport of plant viruses

There are many viruses associated with a cell-to-cell movement independent of tubule formation. The most studied example is *Tobacco Mosaic Virus* (TMV). In fact, TMV MP from the 30K superfamily of viral MPs (Melcher, 2000) is the most studied MP regarding intracellular transport (Waigmann et al., 2000; Liu and Nelson, 2013). TMV 126 kDa replicase is also necessary for viral intracellular movement (Asurmendi et al., 2004; Guenoune-Gelbart et al., 2008; Heinlein, 2015a). In this scenario (**Figure GI.11**A), vRNPs are formed with vRNAs and MP in the ER (Christensen et al., 2009) and transported to form, together with more replication proteins, the VRCs (Tilsner et al., 2009) where replication begins. Then, VRCs are transported using the same ER-network to the PDs. TMV MP increases SEL and VRCs can go to the neighbour cell through the desmotubule. It is still not clear how VRCs are transported through the ER network. Nevertheless, microtubules are involved in anchoring VRCs to the ER (Niehl et al., 2013) and their role in TMV movement has been widely evidenced (Kragler et al., 2003; Ashby et al., 2006; Seemanpillai et al., 2006; Boyko et al., 2007; Ouko et al., 2010). Another connection of the cytoskeleton with TMV movement is the interaction of TMV 126 KDa replicase with host elongation factor 1A (EF-1A), which is known to interact with microfilaments and microtubules (Zeenko et al., 2002; Yamaji et al., 2006).

Viruses encoding the double gene block (DGBp1 and DGBp2) and the triple gene block (TGB) movement proteins are also associated with cell-to-cell movement independent of tubule formation. In these viruses the main components and the mechanism of intracellular transport through the PD are not known. For *Melon necrotic spot virus* (MNSV) a DGB virus, Navarro et al. (2019) proposed a plausible model (**Figure GI.11**B) in which DGBp1 would assist transport of vRNPs to the PD while DGBp2s alone would associate with ER and be targeted to the PD. DGBp2 function is still unknown but was demonstrated to be essential for cell-to-cell movement (Navarro et al., 2019). Several genera encode the TGB movement proteins. Most studies indicate that TGBp1 binds to RNA (Verchot-Lubicz et al., 2010) and it is responsible for the formation of vRNP, while TGBp2 and TGBp3 would help deliver TGBp1 to the PD (Solovyev et al., 2012). In *Potato Virus X* (PVX) (**Figure GI.11**C) infection, TGBp2 and TGBp3 would insert in the ER where VRCs are stablished for replication and translation and transported through TGBp2 and TGBp3 to the PD. TGBp1

would participate in VRC anchoring at the PD entry. In this model replication and movement are closely connected at the PD (Tilsner et al., 2013).

The movement of viruses associated with tubule formation includes predominantly viral families *Comoviridae*, *Bunyaviridae*, *Caulimoviridae* and *Bromoviridae*. There is little information about the intracellular transport of the viral particles and most of the work has been focused on the study of *Cauliflower mosaic virus* (CaMV). In CaMV intracellular transport (**Figure GI.11**D), translation occurs in inclusion bodies (IB) composed by CaMV P6 and viral particles which are transported by microfilaments to the PDs (Harries et al., 2009). CaMV MP is targeted to the PD independently, interacts with plasmodesmata-located protein 1 (PDLP1) (den Hollander et al., 2016) and replaces the desmotubule with a MP-tubule. CaMV MP has endocytosis motifs that help its recycling through the trans-Golgi network (Carluccio et al., 2014).

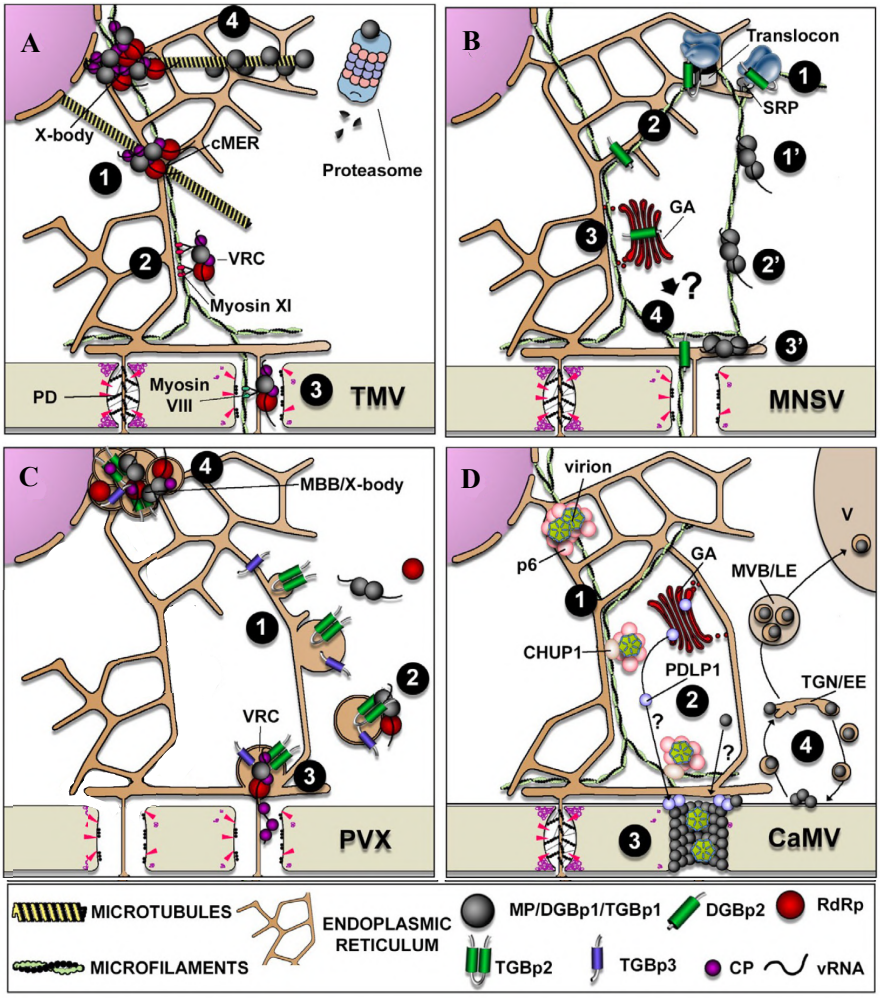

Figure GI.11. Four models for cell-to-cell movement of plant viruses according to Navarro et al. (2019). **A**. *Tobacco Mosaic Virus* (TMV) RNA and MP associate with the endoplasmic reticulum (ER). After recruitment of essential components for replication, viral replication complexes (VRCs)

are thereby established for initial replication (1). Some VRCs may be detached from C-MERs and transported through the actin-ER network (2). Once in the plasmodesmata (PD), the aperture is enlarged by the MP and VRCs move to adjacent cells (3). At middle and late stages of the infection, MPs accumulate at VRCs and microtubules before degradation. Besides, VRCs become large viral factories named X-bodies (4). **B**. *Melon necrotic spot virus* (MNSV) DGBp1 and DGBp2 may use two pathways to arrive to the PDs. Self-interacting DGBp1s bind vRNA to form RNPs (1') that associate with microfilaments (2') and move to the cellular periphery (3'). DGBp2 inserts into ER membranes (1), moves along the Endoplasmic Reticulum (ER) (2) and is exported to the Golgi apparatus (GA) (2) from which is transported to PD (unknown pathway) (4). **C**. *Potato virus X* (PVX) TGBp2 induces the budding of ER vesicles containing TGBp3 and other replication components (1). VRCs would reach the PD through an ER-actin network (2). Once there, the vRNA is transported through the PD in parallel with replication (3). In late stages of the infection, a perinuclear and intricate viral factory or X-body is generated (4). **D**. *Cauliflower mosaic virus* (CaMV) translation of viral proteins occurs at p6 inclusion bodies (IB). At some point, Chloroplast Unusual Positioning 1 (CHUP1) recruits p6 IBs to PD through actin microfilaments(1). CaMV MP moves to PD independently of p6 IB (unknown pathway). Once in the PD, MP and p6 interact with plasmodesmata-located protein 1 (PDLP1), which is transported via GA to the PD (2). CaMV MP replaces the desmotubule from the PD with the MP-tubule. MP then allows CaMV virions through the PD (3). CaMV MP is recycled through trans-Golgi network/early endosome (TGN/EE) route or maybe to the central vacuole (V) (4). Modified from Navarro et al. 2019.

GI.1.7.3. Systemic movement

In long distance movement, most viruses transport themselves through the phloem, with some exceptions that use the xylem (Verchot et al., 2001; Moreno et al., 2004; Wan et al., 2015). The phloem consists of enucleate conducting SE surrounded by non-conducting tissue: CC and phloem parenchyma cells (PP) and all of them surrounded by the bundle sheath (BS) cells, which are differentiated mesophyll cells (**Figure GI.12**). In the different tissues PD frequency and morphology varies and, specialized PD connections can regulate entry and exit to the phloem, which can restrict or reduce long-distance transport of viruses (Lee and Frank, 2018).

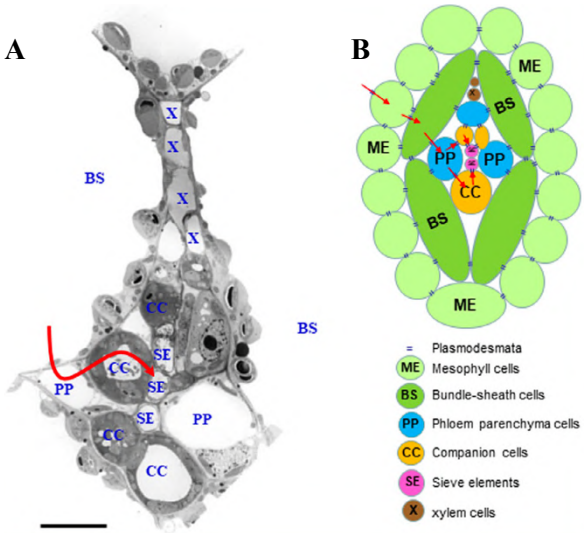

Figure GI.12. Plant viruses' pathway during phloem systemic infection. **A**. Transmission electron microscopy of the phloem cell types. **B**. Schematic representation of the phloem cell types. Red arrows indicate the itinerary of the plant virus to reach the phloem. SE: sieve elements. BS: bundle sheath cells. PP: phloem parenchyma. CC: companion cells. X: xylem. The scale corresponds to 5 µm. Adopted from Navarro et al. (2019).

As shown in **Figure GI.13**, from the infected cell, which is usually in the epidermis, viruses move through different cell types until they reach the vascular tissue. Specifically, from the epidermis, they move to the mesophyll, BS, PP and CC successively, to finally arrive to the conducting SE (Seo and Kim, 2016). Minor veins are the preferred sites for both photosynthate and virus loading. Plant viruses follow the source-to-sink transportation movement within the phloem (Carrington et al., 1996). Virus movement depends on its ability to cross different tissue interphases of the phloem, the participation of cellular organelles and the interaction with host factors (Hong and Ju, 2017). However, it is still a matter of discussion how viral particles are transported through the vasculature, if the viral genomes are transported by themselves or together with other viral proteins or maybe just with the help of phloem proteins with RNA-binding abilities (Folimonova and Tilsner, 2018).

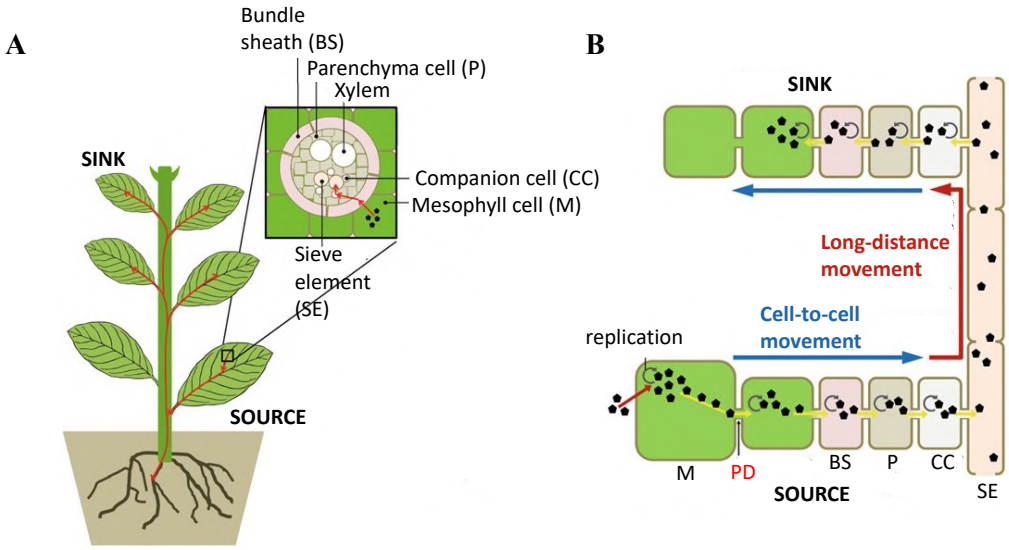

Figure GI.13. Systemic transport of plant viruses. **A**. General view of sink to source viral movement (red arrows). **B**. Detailed cell-to-cell and systemic interphases of viral movement. From the viral entrance into the host (source tissue), plant viruses move from epidermal or mesophyll cells through plasmodesmata (PD) to the vasculature (bundle sheath, parenchyma and companion cells) until loading into sieve elements (SE), which allows its transport to distal sink tissues following the phloem sap. Yellow lines represent cell-to-cell movement through plasmodesmata (PD). Virions are represented as black pentagons. Adapted from Seo and Kim (2016).

GI.1.8. Host factors in the phloem

Key host proteins for long-distance movement are usually host and virus-specific, thus, few have been genetically characterized. Some examples are: pectin methylesterase (PME) in TMV infection in tobacco, that was observed as key for systemic infection at the level of phloem unloading to new tissues (Chen et al., 2000; Chen and Citovsky, 2003), Interacting Protein L (IP-L) in *Tomato mosaic virus* (ToMV) infection in tobacco from which high levels of expression are required for efficient long-distance transport (Li et al., 2005), Tcoi1 in *Cucumber Mosaic Virus* (CMV) infection in *N. tabacum* that interacts with CMV-1a and is required for long-distance movement (Kim et al., 2008a) or P48 in *Cucumis sativus* (*C. sativus*) that is potentially involved in CMV long-distance transport since its interaction with CMV virions facilitates their resistance to RNase A in the phloem (Requena et al., 2006). Also, other cellular determinants can restrict virus long-distance movement, for example, low cadmium environment during TMV and *Turnip vein clearing virus* reduces their systemic movement in tobacco plants (Ueki and Citovsky, 2002, 2005), proteolysis seems to be implicated in PVX degradation in the phloem in *Nicotiana benthamiana (N.benthamiana)* (Mekuria et al., 2008), or constitutive over-expression of salicylic acid in *Arabidopsis thaliana (A. thaliana)* mutants inhibited CaMV long-distance movement (Love et al., 2012) .

GI.1.9. Resistance to viruses

Viruses cause disease by altering the cellular metabolism in the host to create new infecting progeny called virions. Viruses do not use toxins or other mechanisms to damage host cells. However, it is the use of host proteins during the viral cycle what causes disease. In some plants these symptoms can be very clear and severe, however, in other plants the symptoms can be non-existent or easily overlooked due to the resemble of those caused by other pathogens or factors, such as nutrient deficiencies or damage due to insect feeding (Agrios, 2005). As shown in **Figure GI.14**, the most common viral symptoms are mosaics, yellowing, chlorosis, and necrosis of the leaves. Less common symptomatology cause flower growth abnormalities and fruit distortions. Finally, almost all viruses cause dwarfing or stunting of plants and reduction in their total yield in different degrees.

Figure GI.14. Plant virus symptoms. **A**. Mosaic on tobacco leaves. **B**. Yellowing of barley leaves. **C**. Lesions on bean leaf. **D**. Change of tulip flower colour (stripped tulips). **E**. Mosaic on yellow squash. **F**. Ringspots on peach fruit and mosaic on leaves. Adopted from the American Society of Phytopathology (https://www.apsnet.org/Pages/default.aspx).

GI.1.10. Plant Immunity

The first layer of plant immune response is called PAMP-triggered immunity (PTI) and it arises from the detection of the pathogen at the cell surface by using pattern recognition receptors (PRR) that recognize pathogen-associated molecular patterns (PAMPs). PAMPs are essential molecules for microbes but can be recognized by plants; RNA, DNA, proteins, carbohydrates and polysaccharides can be PAMPs (Pisetsky, 2012; Albert, 2013; Niehl et al., 2016). PRRs can be divided in plasma-membrane-localized receptor kinases (RKs), which have several signalling domains, and receptor-like proteins (RLPs), that do not have those domains (Boutrot and Zipfel, 2017). Upon detection of PAMPs, PRRs associate with cofactors and trigger downstream cascades of signalling that progress in stress responses (oxidative burst, calcium burst, defence hormones) that activate Mitogen-Activated Protein Kinases (MAPKs) which in turn start resistance responses, such as callose deposition at the PD or even changes in the cellular wall. PTI leads to the hypersensitive response (HR) which consists of programmed cell death to limit pathogen progression (Bigeard et al., 2015). However, this first barrier can be overcome by pathogens that can produce pathogen-derived proteins, referred as effectors, to overcome PTI defence. At this point, a second layer of defence called the effector-triggered immunity (ETI) may be activated. ETI is characterized by the recognition of pathogen effectors by intracellular receptors called R proteins.

Plant immunity against viruses does not follow a classical immune response and it is still largely unknown. Viruses' resistance (**Figure GI.15**) consists either of modified immunity responses (PTI and ETI) or passive resistance (Nicaise, 2014).

PTI-responses against viruses are largely unknown although more PAMPs are being identified, such as dsRNA that prompts RNA silencing or interference (RNAi) (Niehl et al., 2016; Woo et al., 2016; Perraki et al., 2018). RNAi is sometimes classified apart from innate immunity because it does not follow a typical immune response through PR gene expression and HR and is independent of signalling molecules. However, it does perceive viral dsRNA and conducts signalling cascades well established, by RISC and AGO complex machinery, to establish resistance in non-infected tissues (Alexander and Cilia, 2016). Moreover, several PTI-suppressors are being identified, such as the movement protein (MP) of CMV or the P6 Protein of CaMV both in Arabidopsis (Love et al., 2012; Kong et al., 2018).

ETI-responses against viruses are also mediated by viral effectors that trigger expression of R genes (Gouveia et al., 2016; Garcia-Ruiz, 2019). R genes usually encode for Nucleotide-Binding and Leucine-Rich Repeat domain (NB-LRR) proteins and give resistance to multiple pathogens. In fact, there is nothing special about the NB-LRR proteins that helps them recognize different organisms. Besides, NB-LRR working against viruses resemble or are the same that recognize other organisms (Moffett, 2017). Also, some dominant resistance genes do not encode the classical NB-LRR proteins. In ETI response, the detection of an effector by an R protein triggers signalling leading to resistance responses that usually involve HR. Examples of R genes against viruses are several such as the N gene in tobacco against TMV (Whitham et al., 1994), the Rx gene in potato for PVX (Bendahmane et al., 1999), *Tm-1* gene, although it is not a classic NB-LRR protein, gives resistance to ToMV in tomato by impeding its multiplication without inducing a defence response (Ishibashi and Ishikawa, 2013, 2014). These two layers of defence (PTI and ETI) induce the production of mobile signals that travel to uninoculated distal tissues to start the systemic acquired resistance (SAR) to protect the rest of the plant from secondary infection. These signals include methyl salicylic acid, lipid-transfer protein DIR1, jasmonic acid, azelaic acid, glycerol3-phosphate, among others. SAR consists of a cascade of transcriptional reprogramming initiated by Non-expressor of PR1 (NPR1) and executed by PR proteins (Fu and Dong, 2013).

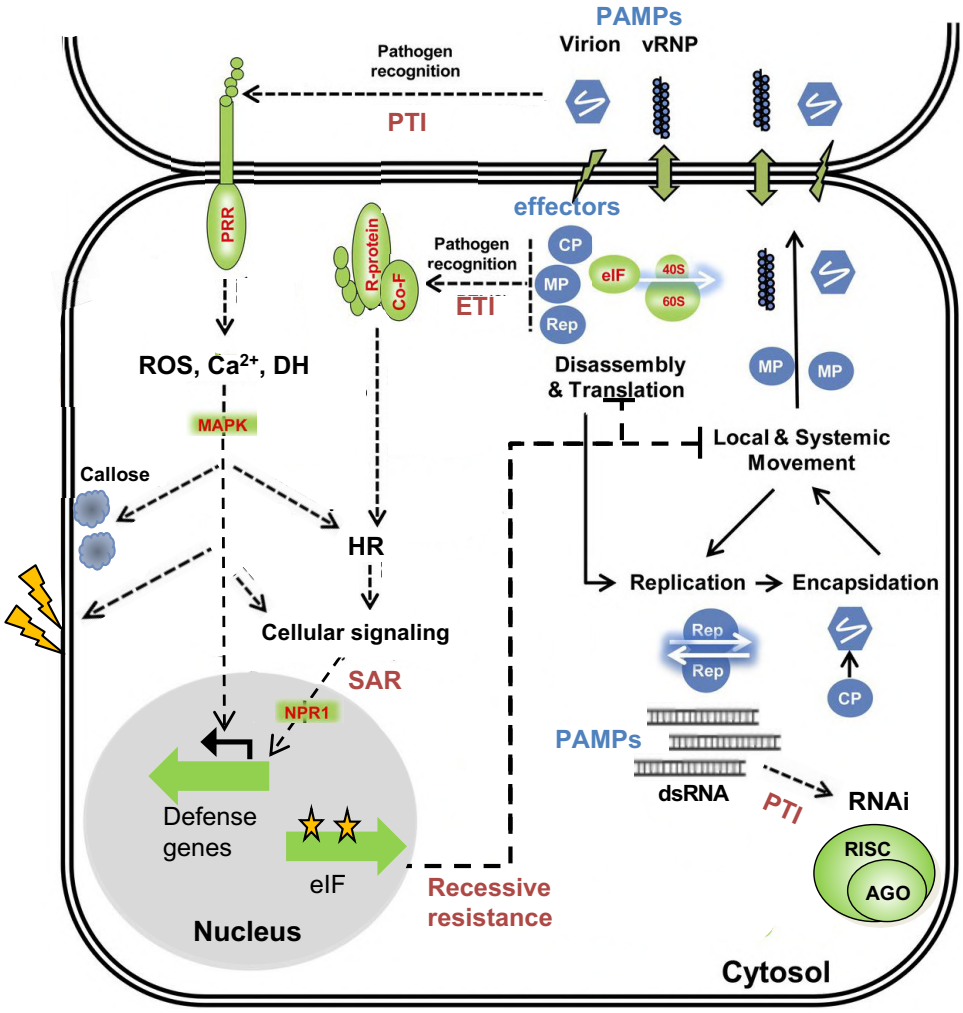

Figure GI.15. Schematic representation of plant antiviral pathways upon virus infection. The name of the different immune responses (PTI, ETI, SAR and recessive resistance) is depicted in dark red. Pathogen-associated molecular patterns (PAMP)-triggered immunity (PTI) can be triggered by viral PAMPs, such as virions and vRNP, that are detected by pattern recognition receptors (PRR) and derive in callose accumulation (represented by the purple cloud), cell wall modifications (represented by the yellow thunderbolt) as an early response and in long term in the hypersensitive response (HR) and local cell death. Another PAMP can be dsRNA but this one follows a different pathway since it is sequestered and degraded by the RNA interference or silencing (RNAi) machinery, represented by the RISC-AGO complex, although other complexes participate. Long term HR can derive in systemic acquired response (SAR) through transcriptional reprogramming of defence genes initiated by Non-expressor of PR1 (NPR1) protein. Plant genes are represented by green arrows. Viruses can release effectors to overcome PTI and a second layer of response may be activated: the effector-triggered immunity (ETI). In ETI effectors are detected through R proteins that might trigger again HR and long term acquired systemic resistance (SAR). Recessive resistance occurs upon deleterious mutations (represented by stars) in host proteins necessary for the virus cycle, such as translation initiation factors (eIF) and others, that impede key steps of the viral cycle (translation, movement). 40S and 60S: ribosomal subunits. CP: coat protein. MP: movement protein. Rep: viral replication machinery. MAPK: Mitogen-Activated Protein Kinases. Co-F: co-factor. RISC (RNA-induced silencing complex). AGO: argonaute. Modified from Mandadi and Scholthof (2013).

In the case of recessive or passive resistance (**Figure GI.15**) there is a loss-of function of host factors needed for plant viruses' infection instead of a direct 'attack', as dominant R proteins induce. This type of resistance corresponds to half of the alleles of resistance to plant viruses (Kang et al., 2005). In most cases the genes affected are translation initiation factors eIF4E and eIF4G and their isoforms, that lose interaction with virus-coded proteins. eIF4Es has been extensively described against potyviruses, either in model species *A. thaliana* (Lellis et al., 2002) or several crops (Ruffel et al., 2002, 2005; Nicaise et al., 2003). Also, eIF4Es-mediated resistance was found in other viral groups, such as bromoviruses, carmoviruses and bymoviruses (Yoshii et al., 1998b, 2004; Kanyuka et al., 2005; Stein et al., 2005; Nieto et al., 2006). More recent studies have found loss-of-function affecting other proteins. Some examples include three vacuolar protein sorting genes; one putative gene in resistance to *Zucchini yellow mosaic virus* (ZYMV) in cucumber (Amano et al., 2013), and two cloned genes, Vacuolar Protein Sorting 41 (CmVPS41) in CMV in melon resistance (Giner et al., 2017) and more recently a Vacuolar Protein Sorting 4 (CmVPS-4) a resistance gene against *Watermelon mosaic virus* (WMV) in melon. Also, another case involves an NB-LRR protein against *Potato virus Y* (PVY) in tobacco (Michel et al., 2018) although in this case it is a tolerance trait more than a resistance mechanism.

GI.4 Bromoviridae family

The *Bromoviridae* family contains important plant viruses distributed worldwide and that includes herbaceous plants, shrubs and trees. *Bromoviridae* has six genera (*Alfamovirus*, *Anulavirus*, *Bromovirus*, *Cucumovirus*, *Ilavirus* and *Oleavirus)* with variable host range, with *Cucumovirus* having the broadest and is being the most important agriculturally (Bujarski, 2021).

Virions of the *Bromoviridae* family members are non-enveloped, with either spherical, icosahedral symmetry (T=3 or T=1) and a diameter of 26-35nm, or bacillus forms with 18 – 26 nm by 30-85 nm. Genomes are positive-stranded tripartite RNAs (RNA1, RNA2, RNA3) of approximately 8 kb of length and packed in separate virions, although *Cucumovirus* genus include as well two subgenomic RNAs and a satellite RNA. Each RNA has a 5' cap-structure while the 3'-terminus can form a tRNA-like or other complex structures. RNA1 and RNA2 encode replicase proteins 1a and 2a, while RNA3 encodes two Open Reading Frames

(ORFs) in which 3a encodes the movement protein and 3b the capsid protein (CP). RNA2 can have a second ORF (**Figure GI.16**C) that encodes the protein 2b, a suppressor of post-transcriptional gene silencing. The number of ORF and their length classify the genome architecture in three groups depicted in (**Figure GI.16**), where *Cucumovirus* and subgroups 1 and 2 from genus *Ilarvirus* present the second ORF in RNA2 (**Figure GI.16**C), while *Ilarvirus* subgroups 3 and 4 do not have protein 2b but have the same ORF length as *Alfamovirus* and *Bromovirus* (**Figure GI.16**A) .

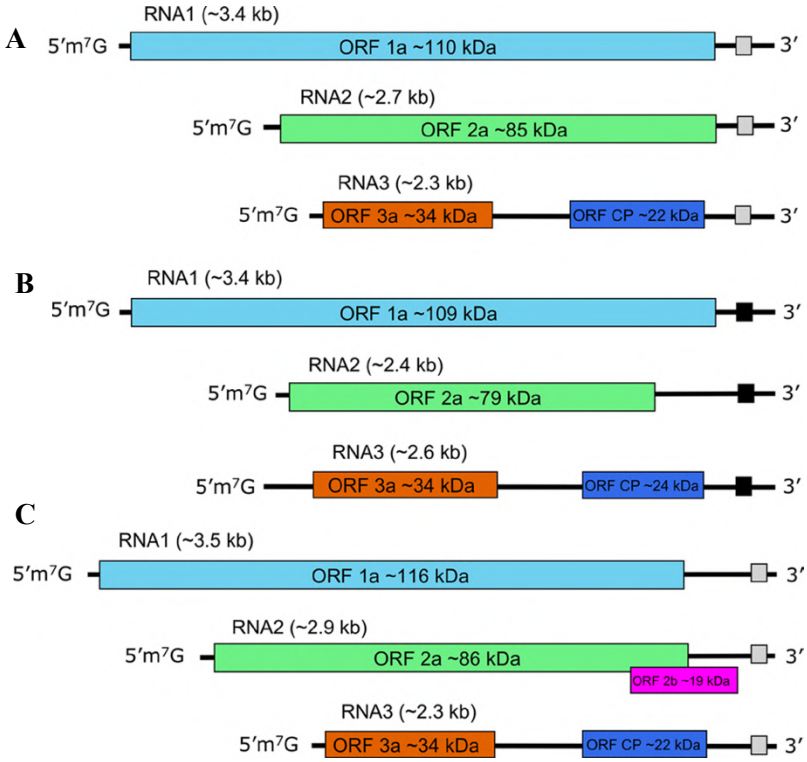

Figure GI.16. Representation of the genome organization in *Bromoviridae*. **A**. Genera *Alfamovirus*, *Bromovirus*, *Ilavirus* subgroups 3 and 4 and *Oleavirus*. **B**. Genus *Anulavirus*. **C**. genera *Cucumovirus* and *Ilarvirus* subgroups 1 and 2. Complex structures are represented by black square boxes in 3' terminus. tRNA-like structures are represented by grey square boxes in 3′ terminus. ORF: open reading frame. CP: coat protein. Adopted from Bujarski (2019).

GI.5 Cucumovirus genus

Cucumoviruses are an important genus that is transmitted by over 80 species of aphids belonging to more than 30 genera. This genus includes four viruses: CMV, *Gayfeather mild mottle virus* (GMMV), *Peanut stunt virus* (PSV) and *Tomato aspermy virus* (TAV).

Cucumoviruses' genomic organization (**Figure GI.17**) differs from the rest of the *Bromoviridae* family in the genomic length of RNAs, presence of 2b gene in RNA2 in

frameshift with ORF of protein 2a and the presence of two subgenomic RNAs (RNA4A and RNA4) which encode the 2b and the capsid protein respectively (Habili and Francki, 1974). In the case of TAV it contains also RNA5 that is a mixture from RNA2 and 3, as well as RNA3B, which corresponds to the 3' end of TAV RNA3 plus 160 nucleotides from its 5' end (Suzuki et al., 2003b). Different strains of Cucumoviruses have a very similar 3'-termini in the three RNAs, as well as 5'-termini of RNA1 and RNA2.

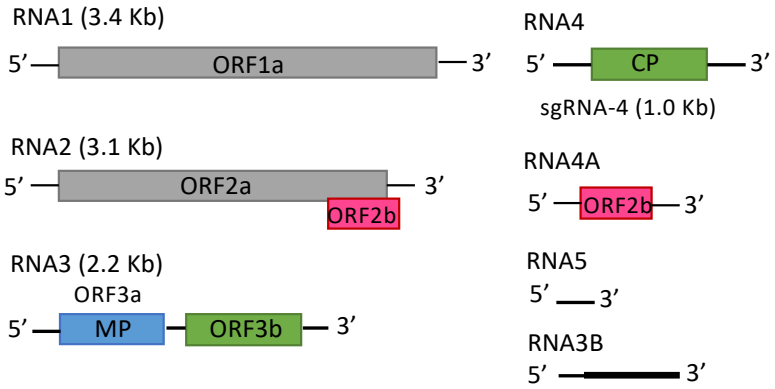

Figure GI.17. Genome architecture of Cucumoviruses. The genomes of CMV, PSV, TAV and GMMV, consist of three genomic RNAs (1-3s) and two major subgenomic RNAs (RNA4 and RNA4A). TAV and some CMV strains contain a minor RNA (RNA5), and TAV contains also a second minor RNA (RNA3B). Adapted from ExPASy database (https://www.expasy.org/).

GI.6 Cucumber mosaic virus

CMV is an important plant virus due to its agronomic impact in crops worldwide, especially in the Mediterranean basin (Martelli et al., 1999; Thackray et al., 2004). CMV is the type member of the genus *Cucumovirus* and in comparison with other genus from this genera, such as TAV and PSV, it infects a larger number of species. CMV can infect about 1,200 host species from more than 100 families (Edwardson and Christie, 2018) that include important crop families, such as Solanaceae, Cucurbitaceae and Cruciferae, as well as wild species that allow it to be persistent all year-round (Jacquemond, 2012). Also, recent discoveries have detected CMV in new kingdoms such as Fungi and Stramenopila (Andika et al., 2017; Mascia et al., 2019).

GI.1.11. Phylogeny

CMV is divided into subgroups I and II (Palukaitis et al., 1992; Anderson et al., 1995) based on serological and chemical properties. Both subgroups share sequence similarity of 70-75 %, a high degree of difference that leads to some researchers to consider them different

species (Jacquemond, 2012). Protein 2b from subgroup I and II strains differs in two regions (N-terminal part and middle), the most notorious being a deletion in aminoacids 62-71 in protein 2b of subgroup II (Du et al., 2008). These differences in the 2b protein correlate with reduced both virulence and ability to suppress RNA silencing in subgroup II strains (Ye et al., 2009).

Subgroup I is further classified into IA and IB strains based on the 5' UTR sequence of RNA3 (Roossinck et al., 1999), whose strains share 92-94 % similarity. Phylogenetic studies proposed CMV had three radiation events that gave rise to subgroup II, subgroup IB and subgroup IA respectively and confirmed this CMV grouping (Roossinck et al., 1999).

GI.1.12. Symptoms

Usually, CMV causes systemic infection, but some plants can remain symptomless, like *Medicago sativa*. Moreover, CMV symptoms can vary depending on the crop infected and the age of the plant upon infection (**Figure GI.18**). Most cucurbits are susceptible to CMV with different severity.

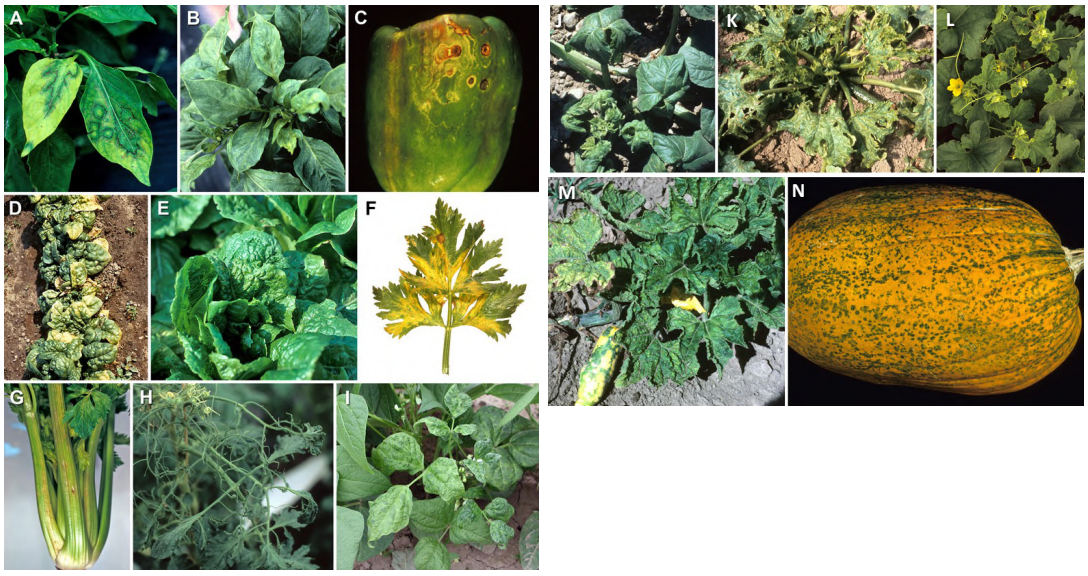

Figure GI.18. CMV infection in several crops. **A-C**. CMV symptoms in pepper including ringspot patterns (A), light green appearance (B), fruit ringspots and rugosity (C). **D**. Leaf chlorosis of CMV infected spinach. **E**. Spots and necrosis within leaf tissues in CMV infected lettuce. **F-G**. CMV symptoms in celery including yellowing and necrosis of veins in the leaves (F) and lesions in the petiole of celery (G). **H**. Filamentous leaf blades in Tomato plants CMV infected. **I**. Leaf curl, green spots and blisters in CMV infected bean leaves. **J-N**. CMV infection in cucurbits. **J**. Severe bending of the petiole and leaf surface in CMV-infected Squash. **K**. Rugosity on in CMV-infected zucchini plant and fruit. **L**. Stunted growing tips in CMV-infected muskmelon. **M**. Change of colour in fruit in CMV-infected yellow squash. **N**. Mosaic pattern in the fruit of in CMV-infected pumpkin. Adopted from American Society of Phytopathology (https://www.apsnet.org/Pages/default.aspx).

GI.1.13. Genome architecture

As depicted in **Figure GI.19**, CMV virions are non-enveloped, spherical, icosahedral, as Cucumoviruses, and have a 29 nm diameter with a T=3 icosahedral symmetry composed by 180 subunits of capsid protein and 18 % RNA (Jacquemond, 2012).

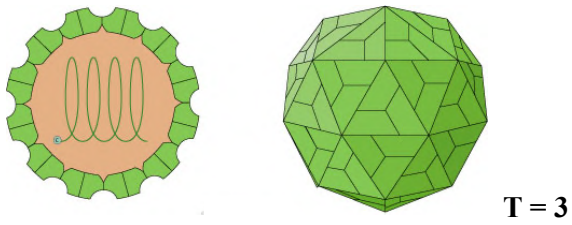

Figure GI.19. CMV virion structure. Non-enveloped, spherical virion about 29 nm in diameter with T=3 icosahedral symmetry, composed of 180 coat proteins: 12 pentamers and 20 hexamers. Adopted from ExPASy (https://www.expasy.org/).

The genome follows a characteristic *Bromoviridae* structure with three (+)ssRNAs, and all have 5'-cap tRNA-like termini and 3'-hydroxylated termini (Jacquemond, 2012). RNA1 has approximately 3,300 nts and it codes for protein 1a, a replicase that has two domains: in the N-terminal part, a putative methyltransferase and in the C-terminal part, a helicase. RNA2 has approximately 3,000 nts and it codes for two proteins: protein 2a is a RNA-dependent RNA polymerase with the typical GDD motif (Ishihama and Barbier, 1994) and protein 2b that is a suppressor of RNA silencing and it has a 1+ frame shift near the 3' terminal of ORF 2a and is expressed from the subgenomic RNA4A. RNA3 has approximately 2200 nts and it encodes the protein 3a, which is the movement protein and has 30 KDa (Boccard and Baulcombe, 1993) approximately, and the protein 3b that is the CP which has approximately 24.5 kDa (Palukaitis et al., 1992) it is encoded by the subgenomic RNA4 (**Figure GI.20**) (Jacquemond, 2012). Moreover, CMV might encapsidate small RNAs: RNA5 and satellite RNAs. RNA5 is encapsidated with CMV subgroup II strains. As previously explained, RNA5 is a mixture of 3' terminal from RNA2 and RNA3 but 5' terminal is not capped, and no translation has been associated with it. Satellite RNAs are noncoding and have no similarity with the viral genome, they use it to complete their cycle. The origin of this satellite RNAs is unknown (Jacquemond and Tepfer, 1998), and it is also not clear whether they benefit the virus, since some studies point out a decrease in viral accumulation and symptoms in some hosts when satellite RNAs are present.

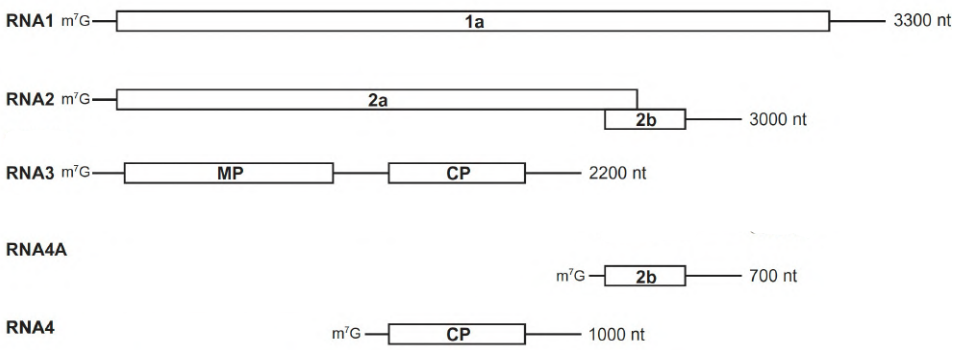

Figure GI.20. CMV genomic architecture. Nt corresponds to approximate nucleotides. Adopted from Jaquemond (2012).

GI.1.14. CMV cycle

GI.1.14.1. Virus replication

Upon viral entry, it follows uncoating of viral particles and translation of CMV (+)ssRNAs to produce viral proteins. In CMV, replication occurs in the tonoplast, the vacuolar membrane where proteins 1a and 2a interact with one another, plus host proteins, to form the replication complex. In tobacco and cucumber, proteins 1a and 2a had differences in tissue distributions. In tobacco, these proteins were observed only in the vascular bundle of minor veins, while in cucumber most were found firstly in the mesophyll and secondly in the epidermis (Cillo et al., 2002). Some of the replication complex interactors are being described in some organisms. In Arabidopsis, TIP proteins (TIP1 and TIP2) interact with protein 1a but not with 2a (Kim et al., 2006), while in tobacco Tsip1 interacts with both proteins in the tonoplast and regulates replication (Huh et al., 2011).

During replication of positive-stranded viruses, such as CMV, there is the synthesis of the minus-stranded RNA. In CMV, this replication is not symmetrical and positive-stranded RNA newly replicated from the minus strand accumulate nearly 100-fold compared to the negative strands (Seo et al., 2009). Also, location of positive-stranded CMV RNAs is found in the cytoplasm while minus-stranded RNAs were barely detectable in hosts tobacco and cucumber (Cillo et al., 2002).

GI.1.14.2. Cell-to-cell movement

CMV MP belongs to the "30K superfamily" of MPs and is encoded by the 3a gene. This MP possesses the main characteristics of MPs such as localization at the plasmodesmata, ability to increase SEL and to bind ssRNAs. CMV MP interacts and severs F-actin filaments (Su et

al., 2010) which is associated with an increase of plasmodesmal SEL. Studies of MP aminoacids have linked several regions with different functions, such as participating in cell-to-cell movement. For example, targeting to the PD and trafficking through it has been associated with cysteine and histidine rich regions, while other aminoacids have been related exclusively to PD targeting or cell-to-cell movement (Sasaki et al., 2006; Sáray et al., 2021).

For cell-to-cell movement, it has been proposed that the coat protein allows a conformational state of the MP (Blackman et al., 1998), although no interaction between these two proteins has been detected *in vitro*. The conformational change would allow the MP to bind the viral RNA to form a ribonucleoprotein complex that travels to the PD. However, it also seems that viral RNA can move through the PD independently of the MP or the coat protein. Thus, it is still uncertain if CMV uses one way or both to migrate to the PD. Other members of the 30K MPs superfamily have different migration methods, either as viral particles or ribonucleic complexes depending on the virus (Kasteel et al., 1993; Kiselyova et al., 2001; Pouwels et al., 2004). Thus, in principle it would not seem easy to extrapolate information by taking the example of other members of the family. However, CMV shares several properties related to viral movement with *Alfalfa mosaic virus* (AMV): MPs form tubules, CP is required for movement and interaction between CP and C-terminal of MPs has been observed, although not essential (Sánchez-Navarro et al., 2006). Moreover, as CMV, AMV can migrate either as viral particles dependent on the CP or as ribonucleic complexes without CP (Sánchez-Navarro et al., 2006).

Also host proteins 2a and 2b have been reported to participate or affect cell-to-cell movement in specific hosts. In the case of protein 2a, it can interact with the MP (Hwang et al., 2005), and in fact specific mutations in both proteins were together show a stronger effect in reducing movement in squash (Hwang et al., 2007). Deletions in protein 2b affect local movement as well as symptomatology of CMV (Lewsey et al., 2009), however it could be an indirect effect of its RNA silencing suppressor activity.

GI.1.14.3. Long distance movement

For long distance transport, CMV uses the phloem following the source-to-sink pathway of assimilates (Moreno et al., 2004). Viral particles arrive to the SE through a cell-to-cell movement from the site of infection (usually the epidermis) from which they follow the mesophyll, BS, PP, CC pathway until the SE, as previously explained.

The first step in long-distance movement starts when the viral particles are loaded in the SE, the conducting tissue of the phloem, that will transport them into distant tissues. In early studies, it was proposed that CMV is trafficked into the minor veins of the SE as a ribonucleoprotein complex that contains viral RNA, CP and 3a MP, and the viral assembly happens in the parietal layer of the SE (Blackman et al., 1998) (**Figure GI.21**). However, no more studies have been focused on this matter, and the exact CMV structure loaded into the SE and where encapsidation occurs remains in question (Jacquemond, 2012). Then, CMV particles are transported within the phloem, in which they interact with host proteins, up to sink tissues. In cucumber, CMV interacts with the phloem protein 1 (PP1) and it is thought to participate either in protection or movement of the ribonucleoprotein complexes (Requena et al., 2006). CMV transcriptome studies show little effect on the phloem transcripts upon CMV infection (Ruiz-Medrano et al., 2007) while proteomic studies in the phloem observed that proteins associated with stress responses were increased upon CMV infection (Malter and Wolf, 2011). The final step of long-distance movement is the unloading from the vascular elements to start an invasion in new tissues. CMV exit from the phloem has not been studied in detail, but most studies show viruses exit from the phloem almost exclusively from major veins (Pallas and García, 2011).

Different studies show that all viral proteins can in some way affect distant movement, however, MP and the CP, that form the ribonucleoprotein complex, as well as the 2b protein are the most important for long distance movement. The CP is essential for efficient long-distance movement of several hosts but not sufficient (Palukaitis & García-Arenal, 2003) and it also participates in the invasion of the shoot apical meristem (SAM) in tobacco (Mochizuki and Ohki, 2005). The MP is associated with the infectivity of CMV-SC strain in soybean (Hong et al., 2007). A mutation in MP aminoacid 60 was shown as temperature sensitive affecting long-distance but not cell-to-cell movement, suggesting different positions of the MP involved in the two types of movement (Li et al., 2001). The 2b protein, the silencing suppressor, is also related to long distance movement in a host dependent manner. In some hosts, such as cucumber, squash and pepper, 2b protein is necessary for long distance movement while in others, such as *Nicotiana* species and *A. thaliana* plants, its deletion only reduces spread or viral accumulation, but does not impede systemic movement (Soards et al., 2002; Lewsey et al., 2009; Masiri et al., 2011). In the case of RNA1, it affects systemic infection rate in squash and controls systemic infection in

lily (Yamaguchi et al., 2005). Protein Tcoi1 in Arabidopsis interacts with protein 1a and modulates viral spread and replication (Kim et al., 2008b).

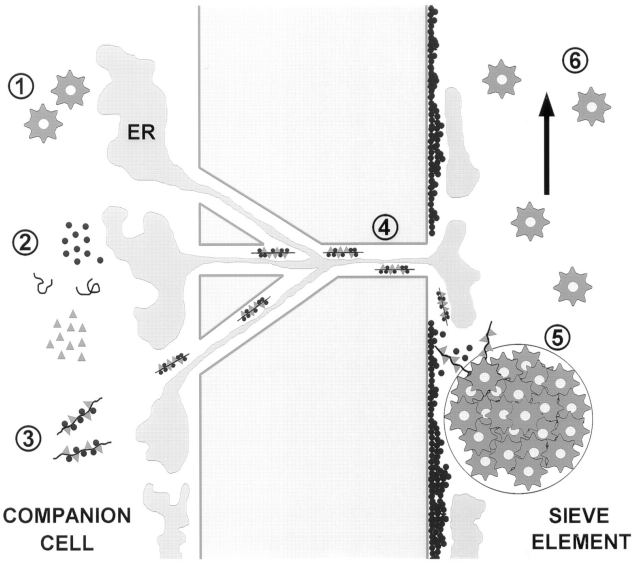

Figure GI.21. Model for CMV movement in minor veins. CMV particles in the CC (1) are disassembled (2) and a linear ribonucleoprotein complex is formed (3) with vRNA, MP (black circles) and CP (grey triangles) to travel through the plasmodesmal pore to the SE (4). In the SE, CP and vRNA form the viral assembly complex (VAC) in the parietal layer (5), while the MP remains dissociated from the complex and in the SE plasma membrane. Once the VAC membrane breaks, assembled virions are released in the stream (6). ER: endoplasmic reticulum. Adopted from Blackman et al. (1998).

GI.1.14.4. Suppression of silencing

In parallel to the virus cycle, CMV protein 2b impedes plant defence through RNA silencing, as the viral suppressor protein. It prevents the initiation of gene silencing at the growing points of plants (Brigneti et al., 1998) by affecting multiple steps in the host RNA silencing pathway. Its ability to bind small interfering RNA (siRNAs), micro RNAs (miRNAs) and Argonautes (AGOs), crucial components of the RNA silencing machinery, allows to block transcriptional and post-transcriptional gene silencing machinery (Wang et al., 2004; Goto et al., 2007; González et al., 2010; Kanazawa et al., 2011; Duan et al., 2012; Hamera et al., 2012). Moreover, in Arabidopsis it was observed that 2b protein works together with protein 1a to control suppression of silencing. Protein 1a regulates 2b interaction with protein AGO1. Limiting the proportion of 2b protein molecules available to bind AGO1, it diminishes 2b-induced symptoms and moderates induction of resistance to CMV, through a second layer of resistance mediated by AGO2 (Watt et al., 2020).

GI.1.15. Virus transmission

In nature CMV is usually transmitted by aphids in a non-persistent manner. The non-persistent manner or non-circulative is characterized by fast acquisition and inoculation. Thus, the virus particles are retained for short times (minutes to few hours) in the mouthparts of the aphid and released rapidly during salivation. At least 80 aphid species in 33 genera transmit CMV (Palukaitis and García-Arenal, 2003). The green peach aphid, *Myzus persicae* and *Aphis gossypii* are the most efficient vectors for CMV (Escriu et al., 2000; Hily et al., 2014). CMV transmission in nature has also been reported through seeds in some crops (Jacquemond, 2012). Artificially, CMV can be transmitted mechanically by humans through cultivating, grafting or manipulation.

Moreover, reservoir host of CMV are found in many wild and weedy plants, where it generally induces a latent infection, as the plants do not develop apparent symptoms. These are the primary source of infection in cultivated crops and serve as seasonal survival hosts and reservoir vectors between crops (Lecoq and Pitrat, 1983; Thackray et al., 2004).

GI.1.16. Resistance to CMV

Natural resistance in CMV has been only observed in few species (**Table GI-1**). Recessive and polygenic resistance is the most common, showing a complex quantitative resistance with QTLs regulating together the resistance. In some cases monogenic and dominant genes are reported as well (Edwardson and Christie, 2018).

Table GI-1. CMV resistance in different plant species.

Type of resistance	Plant species	Resistance gene/QTLs
Dominant	*A. thaliana*	*RCY1*
	Vigna unguiculata	*Cry*
	Capsicum annum L.	*Cmr1*
Recessive	*A. thaliana*	*cum1, cum2*
	C. melo	*cmv1*
	Capsicum annum L.	*cmr2*
Quantitative	*C. sativus*	*cmv6.1*
	C. melo	*cmv1*, *cmvqw3.1* and *cmvqw10.1*
	Capsicum annum L.	*qCmr2.1* and *qCmr11.1*
		cmvP1-5.1 and *cmvP1-10.1*
		qcmv11.1, *qcmv11.2*, *qcmv12.1*

Polygenic resistance is thought to be more durable as the virus must accumulate several mutations to overcome resistance compared to a monogenic one (Jacquemond, 2012). However, it is much more difficult to introduce multiple resistance genes for breeding than introducing a single resistant gene. Over the last decades, most sources of polygenic resistance to CMV have been identified in *Capsicum*. These include several QTLs in different studies (Eun et al., 2016; Guo et al., 2017; Li et al., 2018b) and diverse mechanisms impeding replication, cell-to-cell or long-distance movement (Grube et al., 2000; Caranta et al., 2002; Suzuki et al., 2003a; Kang et al., 2010). In cucumber, a recent study found a QTL in chromosome 6 (Shi et al., 2018). In melon, quantitative oligogenic resistance to CMV was found in the accession PI 161375 (Essafi et al., 2009).

Some examples of single dominant genes against CMV are: (i) *Cry* in cowpea that confers resistance to CMV by inducing a hypersensitive response that restricts local infection (Nasu et al., 1996), (ii) *Cmr1* in Asian pepper cultivar that impedes systemic movement of some CMV strains (Kang et al., 2010), (iii) *RCY1* in *A. thaliana* ecotype C24 that is an NBS-LRR gene that participates in resistance to the CMV strain Y, but not the strain O. The capsid protein of CMV Y is the elicitor of the hypersensitive response that in consequence restricts CMV infection to a local lesion (Takahashi et al., 2001, 2002). In monogenic recessive resistance against CMV we find: (i) SSI2 that acts as a recessive mutant against CMV by restricting it to the inoculated leaves (Sekine et al., 2004), (ii) *cum1* and *cum2* recessive genes, identified as initiation factors eIF4E1 and eIFA4G, that participate independently as single genes in resistance to CMV in *A. thaliana* by affecting efficiency of translation of protein 3a (Yoshii et al., 2004), that in turn, inhibits accumulation and systemic infection of CMV Y (Yoshii et al., 1998b, 1998a), (iii) *cmr2* in Indian pepper cultivar "Lam32" is resistant to CMV-P1 (Choi et al., 2018).

In some cases, the resistant phenotype is well characterized while genetics remain unknown (Palukaitis and García-Arenal, 2003). This is the case for blocking of long-distance movement of CMV in pepper, Japanese radish, and bottle gourd, whereas in maize and pea, resistance affects cell-to-cell movement. In cucumber cv. China (Kyoto) there is inhibition of replication to accomplish CMV resistance, while in *Cucumis figarei*, CMV is stopped before entering the vascular system (Kobori et al., 2000).

GI.7 Resistance to CMV in melon

In melon, there are a few sources of resistance against CMV that were discovered in studies challenging CMV to a high number of exotic and commercial accessions from different geographic origins. Frequent resistance sources include the Japanese "Freeman's Cucumber" melon and the Korean accession PI 161375 cultivar SC (Karchi et al., 1975; Risser, 1977). Other studies involve two Japanese accessions C-189 (Diaz et al., 2003) and Yamatouri (Daryono et al., 2010), 11 Indian accessions (Dhillon et al., 2009; Fergany et al., 2011; Malik et al., 2014) and some Iranian accessions as well (Dhillon et al., 2007; Fergany et al., 2011; Malik et al., 2014; Argyris et al., 2015). Most recently, Pascual et al. (2019) used 52 melon accessions and identified seven additional melon resistant genotypes belonging to horticultural groups Conomon, Makuwa and Dudaim (Pascual et al., 2019).

GI.1.17. Songwhan Charmi resistance to CMV

GI.1.17.1. Genetic basis

The resistance to CMV in SC is recessive, oligogenic (Karchi et al., 1975), quantitative (Dogimont et al., 2000) and strain-specific (Guiu-Aragonés et al., 2014). The major QTL in LGXII was further characterized by Essafi et al. (2009) using a collection of NILs with introgressions of SC in the background genome of the susceptible accession PS. This mapping allowed to limit the region of resistance, named *cmv1*, to a 2.2 cM interval and it was observed that *cmv1* confers total resistance to strains of subgroup II, but not to strains of subgroup I (Essafi et al., 2009; Guiu-Aragonés et al., 2015). Later, a screening of the double haploid lines (DHL) population (Gonzalo et al., 2011) and QTL analysis revealed that the resistance of SC to the strain M6, from CMV subgroup I, was governed by at least three QTLs: *cmvqw12.1*, in LGXII where *cmv1* is located, *cmvqw3.1* in LGIII, and *cmvqw10.1* in LGX (Guiu-Aragonés et al., 2014). Therefore, this suggests that *cmv1*/*cmvqw12.1* is necessary to establish resistance against CMV-M6 but is not sufficient. Also, a possible fourth QTL could cooperate in the resistance to this strain when either *cmvqw3.1* or *cmvqw10.1* is missing.

GI.1.17.2. Resistance at tissue level

Immunogold labelling coupled to electron microscopy allowed to observe that in the resistant melon, CMV-LS was restricted to the BS cells and never reached the vascular parenchyma (VP) or the Intermediary cells (IC). CMV-LS can replicate and move cell-to-

cell but it cannot enter the phloem and perform a systemic infection, while *cmv1* is not able to impede CMV-FNY transport through the BS cells and it can perform a systemic infection (**Figure GI.22**). In grafting experiments with CMV-LS infected PS scions grafted with healthy SC12-1-99 scions did not develop systemic infection. Thus, *cmv1* also affects transport or exit from the phloem. Overall, *cmv1* acts as a gate for systemic infection depending on the CMV strain subgroup (Guiu-Aragonés et al., 2016).

A

	Melon PS	NIL12-1-99
CMV FNY	**S**	**S**
CMV LS	**S**	R

B

	Melon PS	NIL12-1-99
CMV FNY	S	S
CMV LS	S	**R**

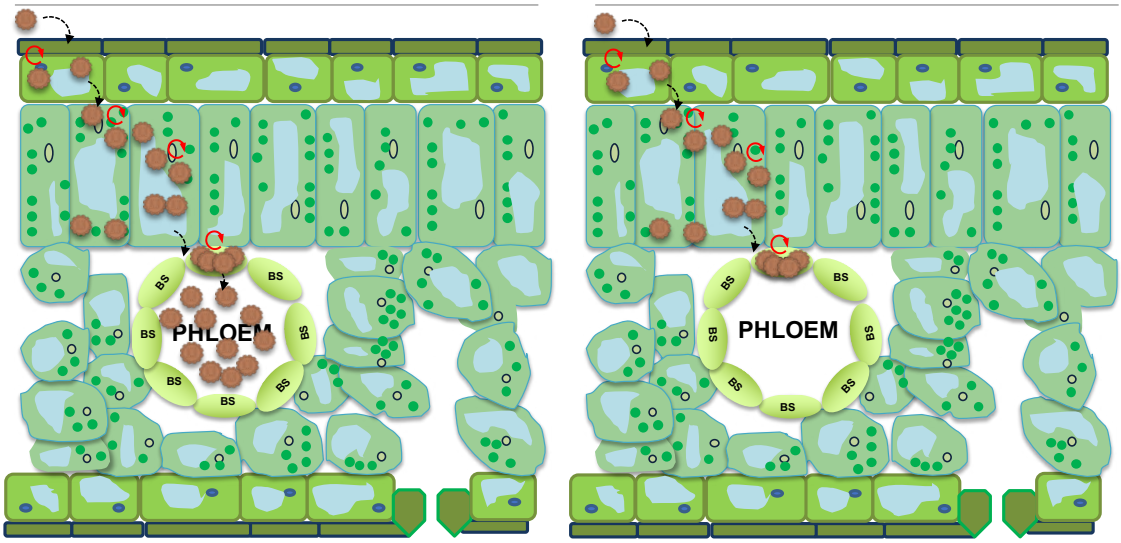

Figure GI.22. Representation of CMV movement in resistant and susceptible melons cells. CMV virions travel from epidermis or mesophyll following cell-to-cell movement through PD and replicating in each cell. **A**. In susceptible melon Piel de Sapo (PS) both CMV strains (FNY and LS) can replicate and move cell-to-cell, reaching the phloem. **B**. In NIL12-1-99 CMV-LS can replicate and move ell-to-cell but it is stopped in the bundle sheath cells (BS). S: susceptible melon to the corresponding CMV strain. R: resistant melon to the corresponding CMV strain. Brown circle: CMV.

GI.1.17.3. The movement protein is the virulence factor from CMV

The use of viral chimaeras between CMV strain LS (SG II) and CMV strain FNY (SG I) allowed to find that the movement protein is the virulence factor of CMV against *cmv1* (Guiu-Aragonés et al., 2015). Comparison of the sequences of this region allowed to find five differential positions between SG II strains and those of SG I. Mutagenesis of the CMV-LS clone by introducing residues from CMV-FNY revealed that a combination four positions (changes 64–68 SNNLL to HGRIA, R81C, G171T and A195I) in the MP determines virulence against *cmv1* resistance in melon (Guiu-Aragonés et al., 2015).

GI.1.17.4. cmv1 encodes Vacuolar Protein Sorting 41

A fine mapping was performed to reduce *cmv1* interval to 132 Kb using a F2 population cross from PS and the NIL SC12-1, which carries the resistant *cmv1* allele. *cmv1* interval contained eight genes (Giner et al., 2017). Polymorphism analysis of the candidate genes from both variants PS and SC did not find transposon insertions or structural variations, but 10 SNPs inside the exons of three genes: one in MELO3C004835, encoding a possible Lysosomal Pro-X carboxypeptidase (PCP), another in MELO3C004833, encoding a Crooked neck-like protein 1 (CNL) and three in MELO3C004827, that encodes a Vacuolar protein sorting-associated protein 41 (VPS41). CmVPS41 was later validated as the *cmv1* gene using: transgenic susceptible melon plants expressing the dominant PS allele in SC background and challenged with both CMV strains in which both CMV-LS and CMV-FNY were able to infect the susceptible transgenic lines, (ii) screening of a Targeting Induced Local Lesions In Genomes (TILLING) population from the background of the susceptible accession CharMono (Dahmani-Mardas et al., 2010) that found CmVPS41 mutants with enhanced resistance to CMV-LS. Moreover, comparison from CmVPS41 from PS and SC, found substitution L348R at exon 5 as the most plausible causal polymorphism of resistance due to its high deleterious effect. Gene expression between both variants PS and SC did not change, thus corroborating the effect of the coding sequence rather than other regulatory regions (Giner et al., 2017). In another study, Pascual et al. (2019) confirmed L348R as the most deleterious substitution in exon 5 and discovered a new source of resistance: G85E. G85E was present in Freeman's Cucumber, as well as in four additional melon genotypes. In all the new resistant accessions CMV-LS was able to replicate and move cell-to-cell but could not reach the phloem. Thus, it seems phloem blockage in resistant melons is a general strategy used by CmVPS41 (Pascual et al., 2019).

GI.8 CmVPS41

Vacuolar Protein Sorting 41 (VPS41) is a very conserved protein which has been most studied in yeast. VPS41 is part of the Homotypic Fusion and Vacuole Protein Sorting (HOPS) complex that participates in the transport of cargo proteins from the late trans-Golgi network to the vacuole.

GI.1.18. The HOPS complex

From the trans-Golgi network, cargo proteins are budded into the early endosome compartment (**Figure GI.23**). Early endosomes contain by Rab5, a GTPase, and class C core vacuole/endosome tethering factor (CORVET) complex. From early endosomes, endosome maturation occurs in different states before becoming late endosomes. To do so, the process requires a series of events: intra-lumenal vesicle (ILV) formation, Rab conversion, tethering complex conversion, phosphatidylinositol production (phosphatidylinositol 3-phosphate and phosphatidylinositol 3,5-bisphosphate), endosome motility and other processes. Also, progressive acidification occurs during endosome maturation. Thus, at the late endosome Rab5 has been replaced by Rab7, endosomal sorting complex required for transport (ESCRT) machinery has formed several intra-lumenal vesicles (ILV) and CORVET complex has been replaced by the HOPS complex (Wang et al., 2011).

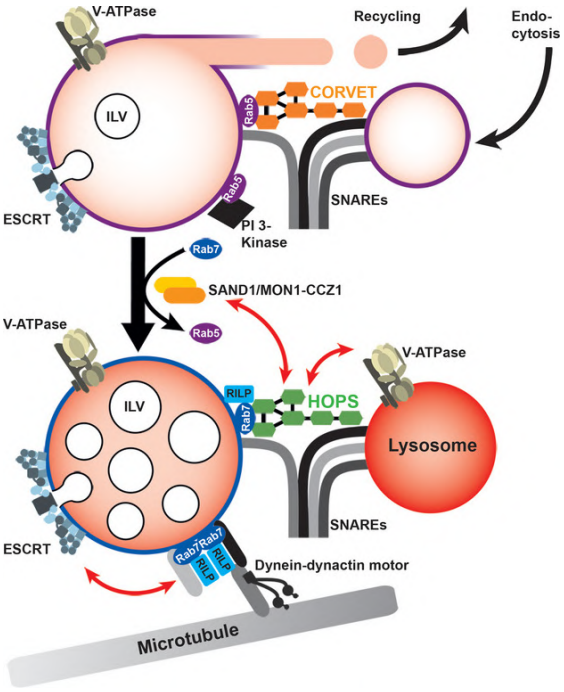

Figure GI.23. Endosome maturation. Major events in the pass from early to late endosomes include: endosomal tethering complexes conversion (from CORVET to HOPS), ILV formation (by ESCRT machinery), acidification (by V-ATPase), Rab conversion (from Rab5 to Rab7), phosphatidylinositol conversion (by phosphatidylinositol (PI) 3-kinases), endosome motility (by microtubules). RILP: Rab-interacting lysosomal protein. ILV: intra-lumenal vesicle. ESCRT: Endosomal sorting complex required for transport machinery. HOPS: Homotypic fusion and vacuole protein sorting complex. CORVET: Class C core vacuole/endosome tethering factor. V-ATPase Vacuolar type ATPase. SNARE: Soluble methylmaleimide sensitive factor attachment protein receptor proteins. Darker shades of red indicate increasing acidification. Red arrows indicate interactions between endosome modules. Adapted from Solinger and Spang (2013).

HOPS and CORVET proteins have been most studied in yeast. The CORVET complex consists of C core proteins (Vps11p, Vps16p, Vps18p and Vps33p) plus Vps8p and Vps3p while the HOPS complex shares four C core proteins together with Vps39p and Vps41p (Takemoto et al., 2018), a total of 6 subunits as well (**Figure GI.24**). Vps33p is the SNARE-interacting subunit that allows to direct their fusogenic activity (Zhang and Hughson, 2021). Vps41p is the tethering subunit that delivers the cargo proteins. Moreover, recruitment to the yeast vacuole membranes needs phosphatidylinositol3-phosphate and 5-phosphate (PtdIns(3)P and PtdIns(4,5)P2) (Stroupe et al., 2006) and vacuolar fusion requires the Mon1-Ccz1 complex which is the guanine nucleotide exchange factor (GEF) for Ypt7 (the yeast homolog of Rab7).

Figure GI.24. CORVET and HOPS subunits and functional distinctions as well as interactions with Rabs and SNARE proteins according to Plemel et al. (2011). Functional interactions between Rabs and other proteins are indicated by dashed red lines. Image adapted from Solinger and Spang (2013).

The differences between CORVET and HOPS change membrane fusion specificity in early and late endosomes. Thus, while the CORVET complex regulates endosome fusion, the HOPS complex is necessary for all fusion events of the vacuole and lysosomes, and it also participates in protein sorting in the vacuole (Balderhaar and Ungermann, 2013). Interestingly, although they both are tethering complexes, have evolved independently and rely on different assemblies and combinations of proteins to perform their function (Solinger and Spang, 2013).

In mammals, several homologs of all HOPS components have been found although their function is little known. In humans, hVps41 and hVps39 localize to the late endosomes and lysosomes and are required for the delivery of cargo proteins to active lysosomes (Pols et al., 2013). Moreover, hVps41 knockdown leads to delay in the transport of low-density lipoprotein (LDL) to the lysosome (Garg et al., 2011). Also, hVps41 has been associated with human pathologies (Ruan et al., 2010; Roy et al., 2011; An et al., 2012) or even as key components in *Zaire ebolavirus* (EboV) infection (Carette et al., 2011b).

In plants, the complete HOPS complex was detected in *Arabidopsis* and it was recently shown to mediate vacuole fusion (Takemoto et al., 2018). However, HOPS function and regulation is not well characterized yet. In *Arabidopsis*, both VPS33 and VPS41 accumulate in late endosomes. VPS41 is also located in the tonoplast, and its location is dependent on phosphoinositides. Moreover, VPS41 regulates vacuole fusion together with VTI11 SNARE. Also, VPS41 and VPS33 are important for pollen fertility and protein storage vacuole maturation in embryos (Brillada et al., 2018). In plants, the HOPS complex can also bind phosphoinositides and these control localization of VPS41 subunit (Stroupe et al., 2006; Brillada et al., 2018).

GI.1.19. The AP-3 complex

Protein transport to the yeast vacuole can also happen through the alkaline phosphatase (ALP) pathway (Piper et al., 1997). The ALP pathway transports several proteins, including Vam3, a vacuolar SNARE protein, that is transported with AP-3 adaptor, whose vesicles revealed the presence of Vps41 on these membranes. Schoppe et al. (2020) confirmed that Vps41 is an interactor of AP-3 vesicles, and it does not influence AP-3 vesicle generation. The model proposed (**Figure GI.25**) consists of AP-3 vesicles forming independently of Vps41 and being transported to the vacuolar membrane. Then, AP-3 vesicles require an assembled coat to interact with the HOPS complex in the vacuolar membrane and bind to Vps41. The interaction with SNARE proteins would capture AP-3 vesicles and allow partially uncoating to finally allow vacuolar fusion through both SNARE proteins and HOPS complex (Schoppe et al., 2020).

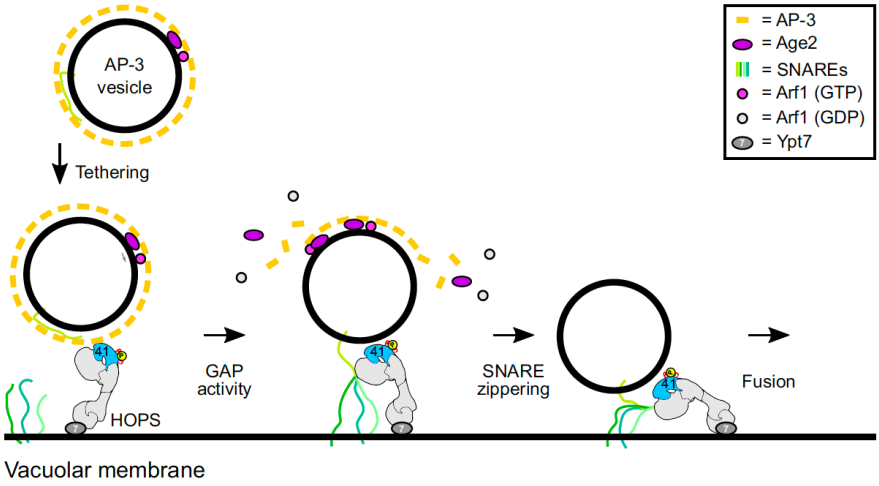

Figure GI.25. Model of AP-3 vesicle tethering and fusion at the vacuole. AP-3 vesicles require an assembled coat to interact with vacuole-localized HOPS and bind to Vps41. Interaction with vesicle SNAREs capture AP-3 vesicles stably and allow partial uncoating via the Arf GAP Age2. SNARE and HOPS interactions then drive fusion with the vacuole. Adopted from Schoppe et al. (2020).

Overall, CmVPS41 is the gatekeeper protein in *C. melo* resistance to CMV-LS in the bundle sheath cells, but its cellular mechanism to confer resistance it is still unknown. This thesis would like to study CmVPS41 at a cellular level and its relationship with the virulence factor CMV-MP.

Objectives

The main objective of this thesis is to study how the *C. melo* Vacuolar Protein Sorting 41 (CmVPS41) and the viral movement protein (MP) of CMV participate in the resistance or infection mechanism depending on the *C. melo* cultivar.

The specific objectives are:

(i) Investigate the localization pattern of CmVPS41 from both, susceptible and resistant melon genotypes, the localization of CmVPS41 carrying only the mutations causing the resistance and the response of CmVPS41 to the presence of the viral MP or the whole virus. This objective will allow to understand CmVPS41 function in the plant cell, and observe CmVPS41 relationship with CMV and MP.

(ii) Identification of melon proteins that interact with the Movement Protein during CMV infection. Studying the interactome of the MP during CMV infection will give more information about the partners playing a role in CMV infection in *C. melo*.

(iii) Characterize the biological response of *C. melo* to CMV inoculation in susceptible and resistant melon cultivars and in the susceptible species *N. benthamiana*. This objective will allow to study the molecular pathways activated or repressed during CMV infection or resistance in melon plants and to find key proteins working in both species during CMV infection.

Chapter I. Mutations in CmVPS41 controlling resistance to *Cucumber mosaic virus* display specific subcellular localizations.

Mutations in CmVPS41 controlling resistance to *Cucumber mosaic virus* display specific subcellular localizations

Núria Real[1], Irene Serrano[2+], Cèlia Guiu-Aragonés[1] and Ana Montserrat Martín-Hernández[1,3]*

[1] Centre for Research in Agricultural Genomics (CRAG) CSIC-IRTA-UAB-UB, C/Vall Moronta, Edifici CRAG, Bellaterra (Cerdanyola del Vallés), Barcelona, Spain, [2] Laboratoire des Interactions des Plantes et Microorganismes, CNRS, Toulouse, France, [3] Institut de Recerca i Tecnologia Agroalimentàries (IRTA), Campus UAB, Bellaterra, Barcelona, Spain,

[+]Current address: Albrecht-von-Haller-Institute for Plant Sciences, Georg-August-University Göttingen, 37077 Göttingen, Germany.

*Corresponding author. Mailing address: Centre for Research in Agricultural Genomics (CRAG) CSIC-IRTA-UAB-UB, C/Vall Moronta, Edifici CRAG, Bellaterra (Cerdanyola del Vallés), Barcelona, Spain. Email address: montse.martin@irta.es

Short running head: Subcellular localization of CmVPS41

Article submitted to Plant Physiology journal on May 2022.

I.1. Abstract

Resistance to *Cucumber mosaic virus* (CMV) in melon has been described in several exotic accessions. It is controlled by a recessive resistance gene, *cmv1*, which encodes a Vacuolar Protein Sorting 41 (CmVPS41). *Cvm1* prevents systemic infection by restricting the virus to the bundle sheath cells, preventing viral phloem entry. CmVPS41 from different resistant accessions carried two causal mutations, either a G85E change, found in the accessions Pat-81 and Freeman's Cucumber, or L348R found in PI 161375, cultivar 'Songwhan Charmi' (SC). The analysis of the subcellular localization of CmVPS41 in *Nicotiana benthamiana (N. benthamiana)* has revealed differential structures in resistant and susceptible accessions. Susceptible accessions showed nuclear and membrane spots and many transvacuolar strands, whereas the resistant accessions showed many intravacuolar invaginations. All these structures colocalize with the late endosomes. Artificial CmVPS41 carrying individual causal mutations in the genetic background of CmVPS41 from susceptible variety Piel de Sapo (PS), revealed that the structure most correlated with resistance was the absence of transvacuolar strands. Co-expression of CmVPS41 with the viral MPs, the determinant of virulence, did not change these localizations; however, infiltration of CmVPS41 from either SC or PS accessions in CMV-infected *N. benthamiana* leaves showed a localization pattern closer to each other, with an increase in membrane spots in the CmVPS41 from SC and lower number of transvacuolar strands in CmVPS41 from PS. Our results suggest that the distribution of CmVPS41PS in the late endosomes produces transvacuolar strands that facilitate CMV infection and that CmVPS41 is re-localized during viral infection.

I.2. Introduction

When viruses enter the plant, they must replicate, move cell-to-cell through plasmodesmata, up to the veins, surrounded by the bundle sheath (BS) cells, and invade the phloem cells, namely vascular parenchyma (VP) cells and companion cells (CC) to finally invade the whole plant, producing a systemic infection (Hipper et al., 2013). Since viruses have a small and compact genome, encoding only a few genes, they must request the participation of many host factors to complete their cycle. Mutations in those host factors develop a loss of susceptibility that can either limit or prevent viral infection, thus, becoming resistance genes that are recessively inherited (Hashimoto et al., 2016a). Therefore, understanding how viral proteins and virions interact with host factors is key to prevent viral diseases.

Cucumber Mosaic Virus (CMV) is a single positive-stranded RNA virus able to infect over 1200 plant species, including members of three important crop families, Solanaceae, Cruciferae and Cucurbitaceae (Edwardson and Christie, 1991). CMV genome has three genomic and two subgenomic RNAs that encode five viral proteins. CMV strains are divided in two subgroups, I (SG I) and II (SG II) which share 70% of their sequence and present differences in their serological and chemical properties (Roossinck, 2001). In melon few sources of resistance to CMV have been identified (Karchi et al., 1975; Pascual et al., 2019; Martín-Hernández and Picó, 2021), among them the Korean cultivar 'Songwhan Charmi', PI 161375 (from now on SC). SC shows an oligogenic and recessive resistance (Karchi et al., 1975), with a major gene, *cmv1*, conferring resistance to strains of SG II (Essafi et al., 2009; Guiu-Aragonés et al., 2015), and at least two other Quantitative Trait Loci (QTLs) which, together with *cmv1* confer resistance to SG I strains (Guiu-Aragonés et al., 2014). The resistance conferred by *cmv1* is manifested as a restriction to phloem entry, since in the plants carrying this gene, strains of SG II (such as CMV-LS) can replicate and move cell-to-cell in the mesophyll up to the BS cells but are restricted in these cells and cannot move to the phloem cells. However, strains of SG I (such as CMV-FNY) can overcome this restriction and invade the phloem (Guiu-Aragonés et al., 2016). The viral factor determining this ability is the movement protein (MP), since a viral clone from CMV-LS carrying the MP from FNY can invade the phloem of the plant carrying the gene *cmv1* (Guiu-Aragonés et al., 2015).

Map-based cloning in melon demonstrated that *cmv1* encodes a Vacuolar Protein Sorting 41 (CmVPS41) (Giner et al., 2017), a protein involved in the intracellular vesicle transport of

cargo proteins from the late Golgi to the vacuole as part of the "homotypic fusion and vacuole protein sorting" (HOPS) complex, both via endosomes and through vesicles, via the AP-3 pathway (Balderhaar and Ungermann, 2013; Schoppe et al., 2020). HOPS is a complex of six subunits, four of them shared (VPS11, VPS33, VPS16 and VPS18) with the complex CORVET, another complex involved in endosome life cycle. The remaining two, VPS39 and VPS41 are required for the tethering function, being VPS41 the effector subunit of HOPS to promote vacuole fusion (Price et al., 2000). VPS41 is localized in late endosomes in Arabidopsis (Brillada et al., 2018). In yeast, VPS41p participates in the membrane fusion of cargo proteins between late endosomes and lysosomes (Rehling et al., 1999). In mammals self-assembly of VPS41 is required for the biogenesis of the secretory pathway (Asensio et al., 2013b) and mutations in this protein are related to neurological disorders and abnormal membrane trafficking (Sanderson et al., 2021) associated with lysosomal abnormalities (Steel et al., 2020). In fungi, VPS41 also localizes to endosomes and vacuolar membrane, and it is essential for plant infection and fungal development (Li et al., 2018a). Likewise, deletions in VPS41 in pancreatic B cells cause defects in insulin secretion (Burns et al., 2021). In *Arabidopsis thaliana (A. thaliana)*, AtVPS41 controls pollen tube-stigma interaction and is found in pre-vacuolar compartments and in the tonoplast, where it is required for the late stage of the endocytic pathway (Hao et al., 2016). VPS41 has also been related to Ebola virus infection (Carette et al., 2011a), whereas in plants, it has only been related to CMV infection in melon (Giner et al., 2017).

Although CmVPS41 is a general gatekeeper in many melon genotypes for viral phloem entry and determines the resistance against CMV-LS, its way of action is yet to be characterized. Here we have investigated the localization pattern of CmVPS41 from both, susceptible and resistant melon genotypes, and the localization of CmVPS41 carrying only the mutations causing the resistance from some resistant accessions. We have also investigated their response to the presence of the viral MP and to the whole virus during the infection.

I.3. Material and Methods

Plant material, viral strains, and yeast strains

Cucumis melo L. genotypes, Piel de Sapo (PS), Songwhan Charmi (SC), Freeman's Cucumber (FC), Pat 81 and Cabo Verde (CV), with different susceptibilities to CMV were used to clone their corresponding CmVPS41 genes (Supplementary **Table SI-1**). The list of

CmVPS41 included two chimerical constructs with CmVPS41 genotype from PS carrying the identified causal mutations: (i) causal mutation present in cultivar SC (L348R) (Giner et al., 2017) and (ii) causal mutation found in cultivars FC and Pat 81 (G85E) (Pascual et al., 2019). *Cucumis melo L*. seeds were pre-germinated by soaking them in water overnight, and then maintained for 2-6 days in neutral day at 28 °C. Seedlings were grown in growth chambers SANYO MLR-350H in long-day conditions consisting of 22°C for 16 h with 5000 lux of light and 18°C for 8 h in the dark. For agroinfiltration, *N. benthamiana* plants were grown in the greenhouse in long-day conditions consisting of 24-28°C with 5000 lux of light for 16 h and 22-24°C 8 h in the dark.

CMV strains CMV-LS and CMV-FNY were used for CMV infection assay. *Saccharomyces cereviseae* (*S. cereviseae*) strains Y2HGold and Y187 were used for Yeast Two Hybrid assay (Takara Bio, Mountain View, USA).

Plasmid construction

For co-localization experiments with CmVPS41s, total RNA extractions from the different melon accessions were performed using TriReagent (SIGMA-ALDRICH, St Louis, MO, USA) following the manufacturer's protocol. 200 ng of total RNA were used to synthesize cDNA using oligo (dT)12-18 primer (Invitrogen by Thermo Fisher Scientific, Vilnius, Lithuania) and PrimeScript (Takara Bio, Dalian, China), according to manufacturer's instructions. For cloning the complete CmVPS41 genes, cDNA was PCR-amplified using the PrimeSTAR® GXL DNA Polymerase (Takara Bio, Dalian, China) and the primers annealing at the ends of the gene and carrying the attB sequences (Supplementary **Table SI-1**) and cloned into the pBSDONR P1-P4 (Gu and Innes, 2011) by Gateway BP reaction (MultiSite Gateway® Pro from Invitrogen by Thermo Fisher Scientific, Vilnius, Lithuania). For CmVPS41 clones carrying the causal mutations, CmVPS41 G85E and L348R constructs were generated from CmVPS41 pBSDONR P1-P4 VPS41PS and VPS41SC (for L348R) or VPS41PS and VPS41FC (for G85E) constructs using a combination of specific primers (Supplementary **Table SI-1**) to transfer the fragments containing the causal mutations to the VPS41PS background using Gibson Assembly technology (GeneArt® Seamless PLUS Cloning and Assembly Kit, Invitrogen Corporations, Carlsbad, CA, USA). eGFP (Cormack et al., 1996) and RFP (Campbell et al., 2002) were cloned into pBSDONR P4r-P2 for C-terminal fusion using specific primers (Supplementary **Table SI-1**). The P1-P4 clones were mixed with the corresponding P4r-P2 and the dexamethasone-inducible destination vector

pBAV154 (Vinatzer et al., 2006) in a three-way Gateway LR reaction (MultiSite Gateway® Pro from Invitrogen by Thermo Fisher Scientific, Vilnius, Lithuania).

For MP-localization experiments, the complete MP gene of both strains was PCR amplified using primers that generate BamHI and XhoI at 5' and 3' end of gene respectively. PCR products were cloned into GATEWAY® pENTRTM 3C (InVitrogen Corporations, Carlsbad, CA, USA) at BamHI-XhoI sites. To express C-terminally tagged fluorescent protein fusion of MP:GFP, both pENTR-MP-LS and pENTR-MP-FNY were recombined with destination vector pH7WGF2 (Karimi et al., 2002), using LR clonase mix (Invitrogen Corporations, Carlsbad, CA, USA) according to the manufacturer's instructions. pDLP1:GFP clone was kindly provided by Prof. Andy Maule (John Innes Centre) For Bimolecular Fluorescence Complementation assay (BIFC), MPs and CmVPS41s coding sequences were PCR-amplified using specific primers (Supplementary **Table SI-1**) and cloned into pDONR P1-P4 as described above, and introduced into the expression vector pBAV154 as a C-terminal fusion with either partial N-terminal YFP (YN) (for CmVPS41s) or partial C-terminal YFP (YC) (for CMV-MPs) (Supplementary **Table SI-2**) using Gateway technology, as previously described.

For Yeast Two Hybrid experiments, coding sequences of CMV MPs and CmVPS41s were PCR amplified using specific primers (Supplementary **Table SI-1**) and cloned into plasmid pENTR/D-TOPO (Thermo Scientific by Thermo Fisher Scientific, Vilnius, Lithuania). Both MP genes were cloned into the pGBKT7 vector at the BamHI and EcoRI sites using T4 DNA ligase (Thermo Scientific by Thermo Fisher Scientific, Vilnius, Lithuania) following manufacturer's instructions. CmVPS41s were cloned into pGADT7 vector at the SalI and EcoRI sites using T4 DNA ligase (Thermo Scientific by Thermo Fisher Scientific, Vilnius, Lithuania).

For co-localization of CmVPS41 with organelle markers, *A. thaliana* genes were used (Supplementary **Table SI-2**). Endoplasmic reticulum (35S:HDEL-mCherry), Golgi Apparatus (35S:MAN49-mCherry), Tonoplast (35S:γ-TIP-mCherry) and late endosome (ARA6-mCherry) were from (Serrano et al., 2016). Plasma membrane (35S:Remorin-mCherry) marker was nicely provided by Dr. Núria Sanchez Coll (CSIC, CRAG, Barcelona, Spain) (Marín et al., 2012).

All constructs were verified by sequencing with Sanger method using an ABI 3730 DNA Analyzer (Applied Biosystems) for capillary electrophoresis and fluorescent dye terminator detection. Correct insertion and orientation of all constructs were verified with Sequencher® version 5.0 sequence analysis software (Gene Codes Corporation, Ann Arbor, MI, USA (http://www.genecodes.com). Correct plasmids were transformed in *A. tumefaciens* GV3101.

Transient expression in *Nicotiana benthamiana*

A. tumefaciens cultures carrying the corresponding plasmid were incubated at 28ºC with their corresponding antibiotics for 24-48h and bacterial pellet was collected by centrifugation and resuspended in Induction Buffer (1M $MgCl_2$ and 0.15 M acetosyringone) to 0.4 final OD_{600}, except for the 35S:Remorin 1.3-mCherry experiments, where 0.2 final OD_{600} was used. Bacterial culture was induced for 2h in the dark. For agroinfiltration of more than one plasmid, suspensions were mixed in equal ratio and were infiltrated using a needleless syringe into the abaxial side of expanding leaves of 2–3-week-old *N. benthamiana* plants. For dexamethasone-inducible pBAV154-derived constructs, 24h post infiltration, expression was induced applying 50μM dexamethasone solution with a brush in the adaxial part of the infiltrated leaf (Sigma, St. Louis, USA). Expression of fluorescence was observed at 20 h after dexamethasone induction in pBAV154-derived vectors and 48 h after agroinfiltration in vectors with 35S promoter.

Yeast Two Hybrid assays

Constructs for Yeast Two Hybrid (Y2H) were freshly transformed into *S. cerevisiae* strains before every one-to-one Y2H assay. pGBKT7-MPs, positive control (pGBKT7-53) and negative control bait plasmids (pGBKT7-Lam) were transformed into yeast strain Y2HGold (Takara Bio, Mountain View, USA) while pGADT7-CmVPS41s and pGADT7-T control prey plasmids were transformed into yeast strain Y187 following the Yeastmaker Yeast Transformation System 2 instructions (Clontech by Takara Bio, Mountain View, USA). The transformed cells were grown either in SD/-Trp agar plates for Y2HGold or in SD/-Leu agar plates for Y187 at 30ºC for 3-5 days. Matings between the Y2HGold and Y187 strains carrying the appropriate constructs were performed in 0.5 mL of 2XYPDA in the presence of the corresponding antibiotics following manufacturer's instructions (Clontech's Matchmaker Gold Yeast Two-Hybrid System, Clontech by Takara Bio, Mountain View,

USA). Yeast cells were cultured at 30ºC for 24h and plated in SD/-Trp/-Leu/X-alpha-Gal agar plates. After 3-5 days blue or white colonies appeared and were transferred in a more restrictive media (SD/-Trp/-Leu/X-alpha-Gal/Aureobasidin A agar plates). After 5-7 days blue colonies (or in its defect white colonies) were selected and plated in the most restrictive media (SD/-Ade/-His/-Trp/-Leu/X-α-Gal/AbA). True interaction was assumed when strong blue colonies were able to grow in the more restrictive media.

CMV inoculations

Viral inocula were freshly prepared from infected zucchini squash Chapin F1 (*Cucurbita pepo L.*) (Semillas Fitó SA, Barcelona, Spain). Sap was rub-inoculated in first and second true leaves of 2-week-old *N. benthamiana* plants.

Confocal Laser Scanning Microscopy

For Bimolecular fluorescence complementation (BiFC) and co-localization experiments of plasma membrane or endoplasmic reticulum with CmVPS41 proteins, images were collected on a Leica TCS-SP5 II confocal microscope (Leica Microsystems, Exton, PA USA) using a 63x water immersion objective NA 1.2, zoom 1.6. In BiFC images YFP was excited with the blue argon ion laser (514 nm), and emitted light was collected between 530 nm and 630 nm using a HyD detector. For co-localization, eGFP was excited with the blue argon ion laser (488 nm), and emitted light was collected between 495–535 nm. mCherry and RFP were excited with an orange HeNe laser (594 nm), and emitted light was collected between 570–660 nm. Chloroplasts were excited with the blue argon laser (488 nm), and emitted light was collected at 650-750 nm. eGFP and chloroplasts signals were collected separately from the mCherry or RFP signals and later superimposed. All Images were processed using Fiji imaging software (version 1.52i). Fiji colocalization tool "Colocalization Threshold" was used to calculate the Pearson coefficient of co-localization and to create a colocalized Pixel Map for each combination of CmVPS41 plus organelle marker. To observe CmVPS41 intravacuolar structures IMARIS software (Bitplane AG, Zurich, Switzerland) was used to perform 3D reconstructions of the Z -stacks of confocal images and capture snapshots.

In all other agroinfiltration experiments, images were collected on Olympus FV1000 confocal laser scanning microscope (Olympus, Tokyo, Japan). During scanning, we used a quadruple-dichroic mirror (DM 488/559). For visualization of eGFP, RFP, mCherry and chloroplasts the same emission and collection windows than for the Leica Microscope were

used. The images with co-localization were studied by sequential excitation with each laser separately to avoid crossed fluorescence in the red channel. Images were processed using Olympus FV1000 software (version 04.02). Fiji (1.52i) was used to set the scale bar and calculate the Pearson coefficient for co-localization experiments with CmVPS41 and organelle markers.

I.4. Results

CmVPS41 from both PS and SC associate in vivo with CMV-FNY Movement Protein.

Given that CMV-MP is the determinant of virulence that communicates with CmVPS41, we investigated if there was interaction between these two proteins. For Y2H experiments, yeast clones carrying either MP-FNY or MP-LS were tested against those carrying either CmVPS41PS or CmVPS41SC. After mating and selection in restrictive medium supplemented with X-alpha- Gal, the resulting colonies were as white as the negative control, while the positive control turned blue. This indicated that none of the MPs interacted with none of the CmVPS41s (**Figure I.1**A). This experiment was repeated twice, getting the same result. To confirm this result in vivo, we performed BiFC experiments using the constructs VPS41s-YN and MPs-YC, where the CmVPS41 from either PS or SC carried the N-terminal part of YFP, and the MP from either CMV-FNY or CMV-LS carried the C-terminal part of YFP. Then, co-agroinfiltration of the VPS41s-YN and MPs-YC BiFC constructs showed that MP-FNY was able to interact both with CmVPS41PS and CmVPS41SC in a pattern compatible with their localization at the plasmodesmata, whereas MP-LS was unable to interact with any CmVPS41 (**Figure I.1**C). *C. melo* L-ascorbate-oxidase homologue was used as positive control for interaction with CMV MP. To confirm that CMV-MPs localize at the PDs, we investigated the cellular localization of the CMV-MPs alone. Co-agroinfiltration of a 35S:MP-FNY-GFP or 35S:MP-LS -GFP constructs with the PD marker PDLP1 (Plasmodesmata-located protein 1) (Amari et al., 2010) tagged with RFP, showed that, as expected, both MPs co-localize with PDLP1 at the PDs (**Figure I.1**B). Therefore, the interaction between VPS41s and MP-FNY was taking place at or near the PDs. Altogether, these experiments indicated that, the only possible interaction was between the CmVPS41PS or CmVPS41SC with MP-FNY.

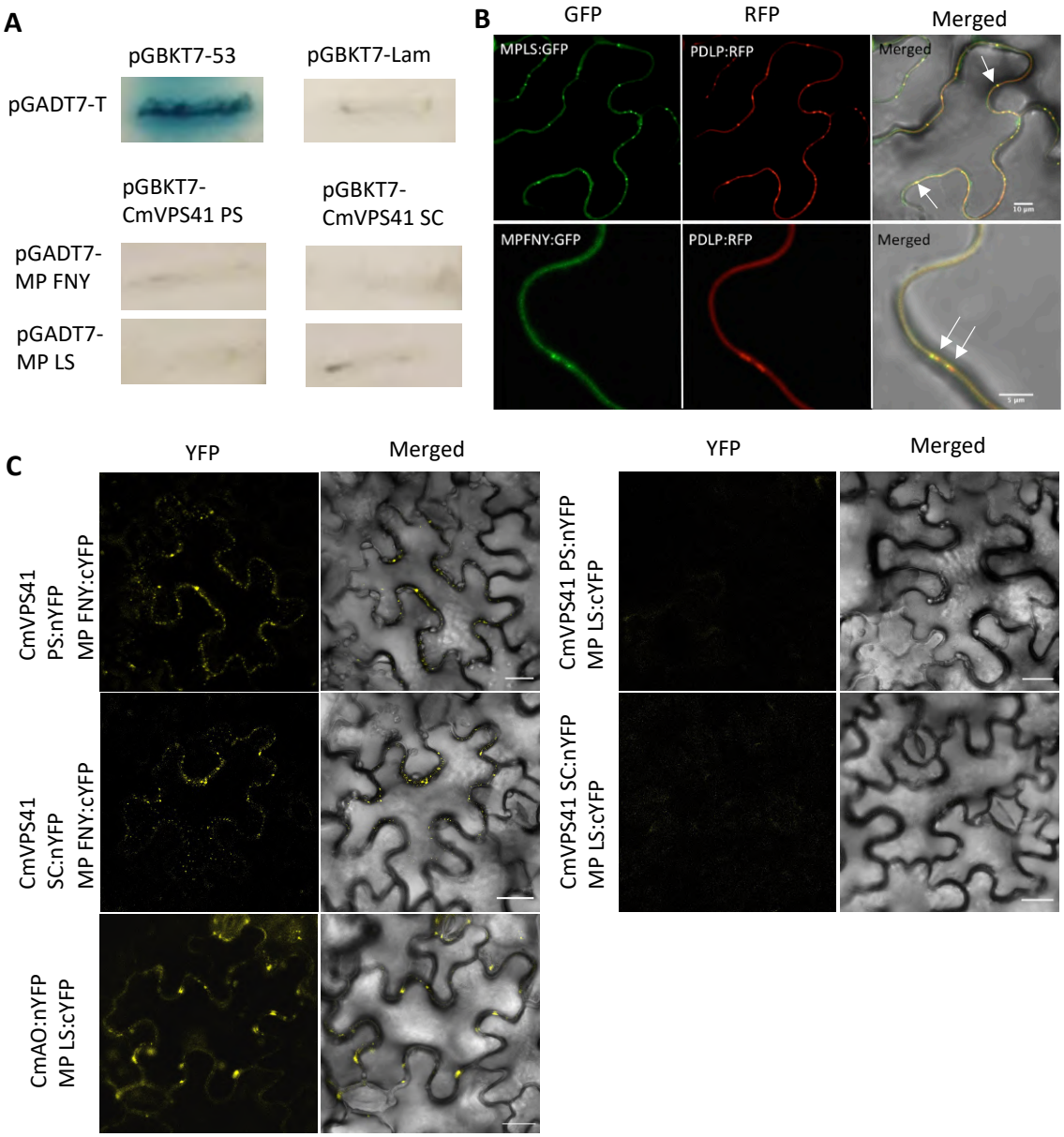

Figure I.1. Interaction between CmVPS41s and CMV-MPs. **A.** Yeast-Two-Hybrid (Y2H) between CmVPS41 and CMV-MPs in SD/-Trp/-Leu/X-alpha-Gal/AbA/-His/-Ade agar plates. Each cell shows the results of Y2H interaction combination of prey in vector pGADT7 per bait in vector pGBKT7. Growth of a strong or light blue colony indicates interaction between prey and bait, whilst absence of growth or white colonies indicates no interaction. Controls are pGADT7-T (prey) in combination with either bait pGBKT7-53 (positive interaction) or bait pGBKT7-Lam (no interaction). **B.** Co-localization of CMV-MPs (MP FNY:GFP or MP LS:GFP) with plasmodesmata marker (PDLP1:RFP). Co-localization of MPs and PDLP can be observed as yellow colour (arrows). **C.** In planta BIFC assay between CmVPS41s and CMV-MPs. L-ascorbate oxidase 4 homologue (CmAO:nYFP) is the positive CMV-MP interacting control. 'Merged': YFP and bright field channel together. BIFC scale bars correspond to 20 µM length.

CmVPS41 from resistant and susceptible melon genotypes have different localization patterns.

To analyse the subcellular localization of CmVPS41s, the genes from both, the susceptible melon genotype PS and the resistant SC, tagged with eGFP, were expressed under a Dexamethasone-inducible promoter in *N. benthamiana* epidermal cells. We observed that 20 hours after Dexamethasone application, both variants seem to localize to the cytoplasm and the nucleus. However, there were some differences in the localization pattern of both CmVPS41 variants. CmVPS41PS localization was very strong as spots in the plasma membrane or in the tonoplast and speckles in both, the nuclear membrane, and the nucleus. Also, there were several trans-vacuolar strands in most cells (**Figure I.2**A, 1 and 2). However, in the cells expressing the resistant allele, CmVPS41SC, there were no membrane spots, the expression inside the nucleus and cytoplasm was smooth, there were no trans-vacuolar strands and there were many tonoplast invaginations towards the vacuole (**Figure I.2**A, 3 and 4). These localization patterns were clearly different from those shown when expressing eGFP alone (Supplementary **Figure SI.1**). A quantification of the cells carrying these distinctive structures showed significant differences among the susceptible PS and the resistant SC variants (**Figure I.2**B). More than 90 % of cells expressing CmVPS41PS showed nuclear speckles, whereas only around 30 % of cells expressing CmVPS41SC showed them. The difference in membrane or tonoplast spots was even more evident, since almost none of the CmVPS41SC-expressing cells showed them, whereas almost all CmVPS41PS presented them. The differences in transvacuolar strands were also significant, with most CmVPS41SC presenting one or none and most CmVPS41PS presenting a mean of four strands. Last, a mean of 75 % of VPS41SC expressing cells showed tonoplast invaginations, whereas those structures were almost absent from CmVPS41PS-expressing cells. Thus, although both proteins localized in the cytoplasm, there were localization patterns clearly different in both CmVPS41 in some structures when expressed in *N. benthamiana* epithelial cells. From those structures some of them (transvacuolar strands and nuclear and membrane/tonoplast spots) would be related with the susceptible variant, whereas the intravacuolar invaginations would be related with the resistant CmVPS41SC variant.

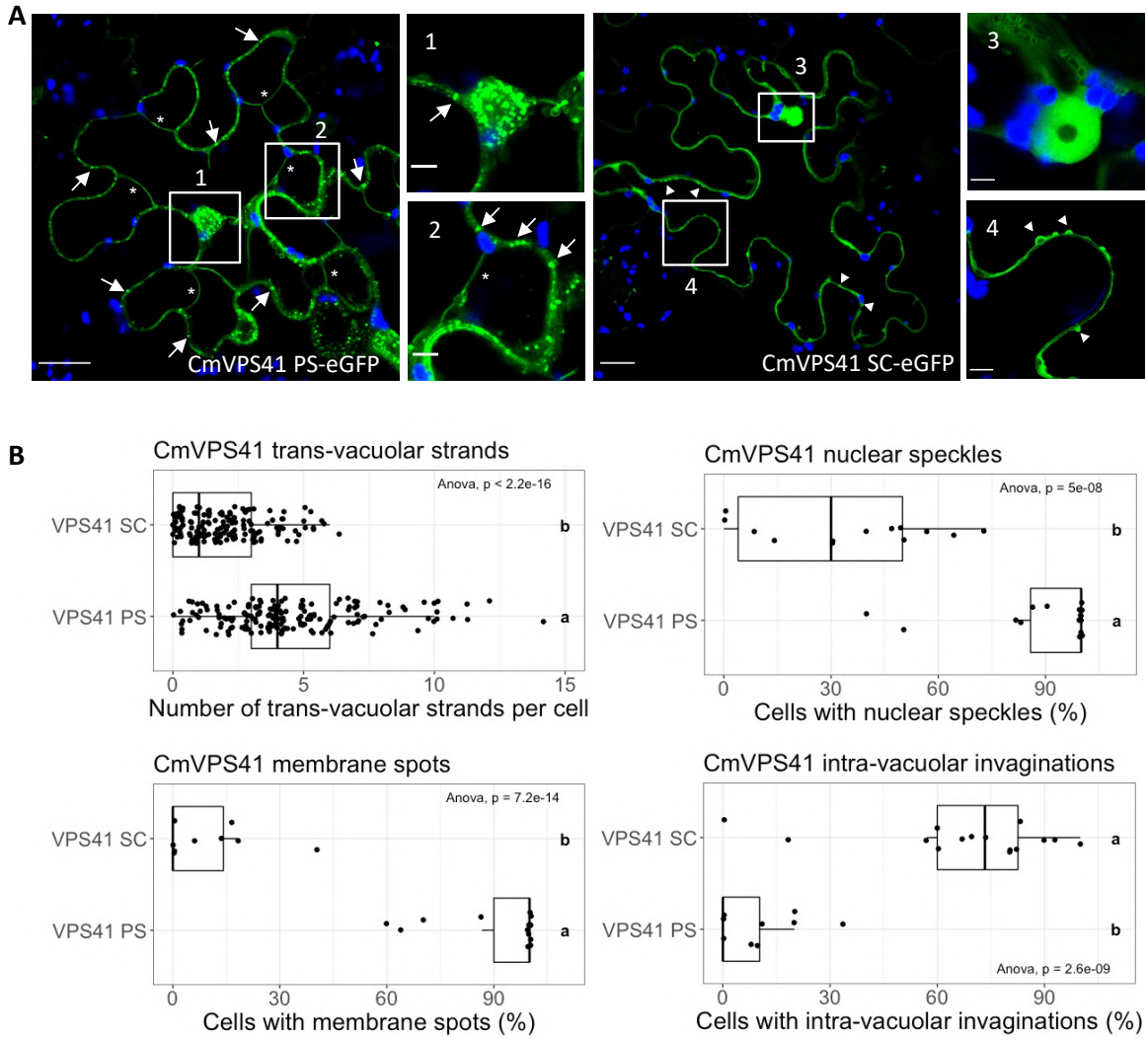

Figure I.2. Localization patterns of CmVPS41. **A.** Localization of CmVPS41 PS (CmVPS41 PS-eGFP) and CmVPS41 SC (CmVPS41 SC-eGFP). In blue, chloroplast autofluorescence. Image scales from whole images correspond to 20µm and amplified images scale is 5 µm. Arrows: membrane speckles. Arrowheads: intravacuolar invaginations. *: Transvacuolar strands. **B.** Boxplots of distinctive structures in CmVPS41 PS and SC-expressing cells. Each boxplot was generated with R package 'ggpubr'. Significant one-way analysis of variance (ANOVA) (p-value<0.05) between each CmVPS41 and specific structures is shown in each boxplot. Post-hoc Tukey results within treatments are indicated with letters. The same letter corresponds to nonsignificant differences between CmVPS41 PS and CmVPS41 SC.

The differential structures co-localize with late endosomes.

VPS41 is a protein involved in the transport of cargo proteins from late Golgi to the vacuole via vesicles or endosomes. To identify the sub-cellular nature of the distinctive structures, a set of cell markers were used. As seen in **Figure I.3**, CmVPS41 from both variants are identified in several organelles, including endoplasmic reticulum, plasma membrane, tonoplast, or late endosomes. However, the transvacuolar strands, the speckles seen in

CmVPS41PS expression and the invaginations from CmVPS41SC colocalize only with late endosome (**Figure I.3**). Thus, the differential structures are derived of the late endosomes, and this suggests that the expression of both variants induce a different distribution of the endosomes throughout the cytoplasm, including crossing the vacuole from side to side and invaginations towards the vacuole.

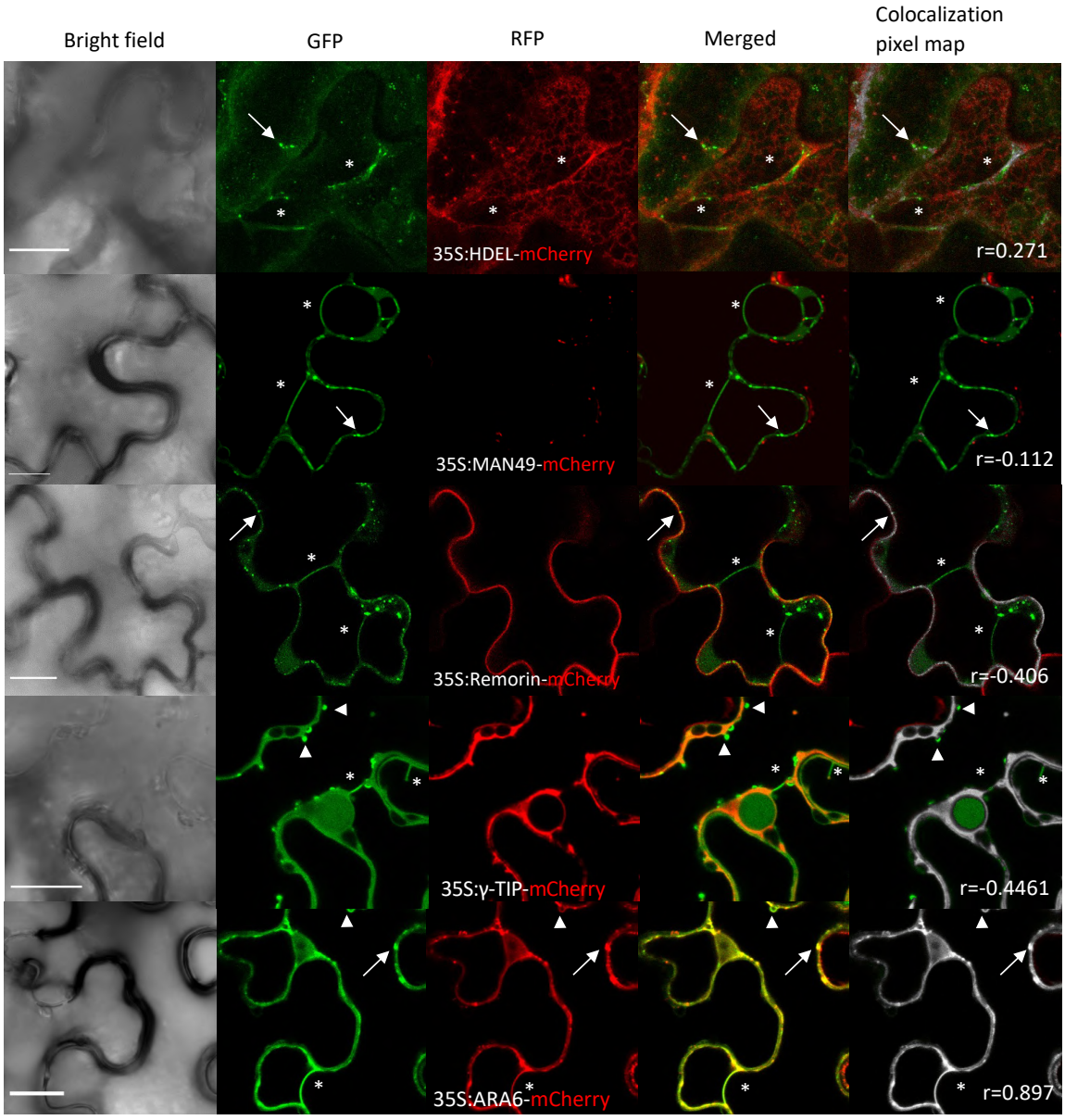

Figure I.3. Colocalization of CmVPS41 with organelle markers**.** GFP channel: CmVPS41s specific structures. RFP channel: different organelle markers, endoplasmic reticulum (35S:HDEL-mCherry), Golgi apparatus (35S:MAN49-mCherry), plasma membrane (35S:Remorin-mCherry), tonoplast (35S:γ-TIP-mCherry) and early endosome (35S:ARA6-mCherry). Merged: co-localization shown as a yellow colour. Colocalization pixel map, shown in grey, while non-colocalized pixels keep the original colour. Pearson correlation coefficient (r) of pixel matching colocalization was calculated with Fiji software analysis tool "Colocalization threshold". Arrows: membrane speckles. Arrowheads: intravacuolar invaginations. *: Transvacuolar strands scale bars are 20 µm.

The different distribution of late endosomes does not change with the co-expression with CMV-MP

The determinant of virulence that relates to the *cmv1* gene (CmVPS41SC) is the MP (Guiu-Aragonés et al., 2015). As the MP from CMV-FNY enables the virus to overcome the resistance posed by *cmv1*, whereas the MP from CMV-LS does not, it might be possible that the localization pattern of CmVPS41SC could change in the presence of FNY-MP. As shown in **Figure I.4**, co-agroinfiltration experiments expressing both CmVPS41s and both CMV MPs showed that the localization pattern of CmVPS41PS does not change significantly in the presence of either MP, showing no significant differences in nuclear speckles, membrane spots and absence of intravacuolar invaginations. Only the presence of either MP seemed to decrease slightly the number of transvacuolar strands per cell (**Figure I.4**B). Likewise, the localization of CmVPS41SC did not change in the presence of either MP-LS or MP-FNY, showing no speckles, very few transvacuolar strands and most cells had tonoplast invaginations, like the pattern of the CmVPS41SC expressed alone (**Figure I.4**B). These experiments were repeated three times with similar results. Therefore, the co-expression of CmVPS41SC with the MP FNY, does not induce any significant change in the localization of the CmVPS41SC that could resemble a susceptible pattern, more similar to that of CmVPS41PS.

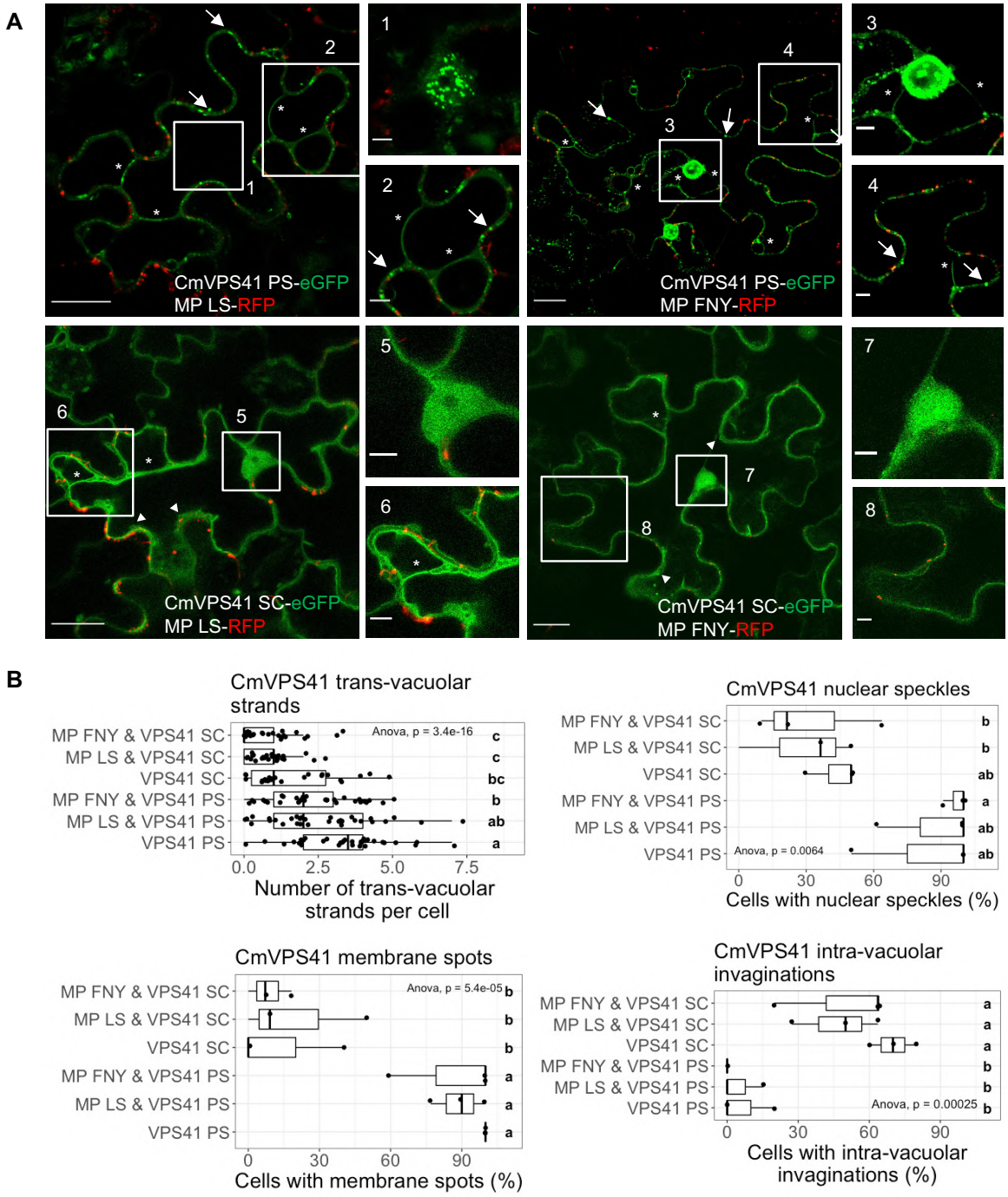

Figure I.4. CMV-MPs effect on CmVPS41-induced structures. **A.** Co-localization of CmVPS41 PS-eGFP or CmVPS41SC-eGFP with CMV MP-FNY-RFP or CMV MP-LS-RFP. Numbers indicate areas amplified on the right. Scale bars are 20 µm (whole image) or 5 µm (amplified image). **B.** Boxplots of CmVPS41-induced structures. Each boxplot was generated with R package 'ggpubr'. Significant one-way analysis of variance (ANOVA) (p-value<0.05) between each treatment and specific CmVPS41 structure is shown in each boxplot. Post-hoc Tukey results of treatments are indicated with letters. The same letter corresponds to nonsignificant differences between CmVPS41PS and CmVPS41SC (co-infiltrated or not with CMV-MPs).

CmVPS41 localization pattern in resistant and susceptible melon genotypes is different.

The analysis of the CmVPS41 gene in 54 melon accessions identified several new resistant genotypes, among them, Freeman's Cucumber (FC) and Pat-81 (Pascual et al., 2019). CmVPS41 from SC, differ from CmVPS41PS in three amino acid positions (P262A, L348R and S620P). However, only the change L348R correlates with resistance to CMV (Giner et al., 2017; Pascual et al., 2019). Pat-81 and FC differ from PS in the same P262A, S620P and also in G85E instead of L348R (Pascual et al., 2019) (**Figure I.5**A). On the contrary, the accession Cabo Verde is a susceptible genotype that shared P262A and S620P amino acid polymorphisms with SC, FC and Pat-81, but lacks any putative causal mutation (**Figure I.5**A), Over-expression of CmVPS41 from both FC and Pat-81 genotypes, as well as from Cabo Verde, confirmed most of the above characteristics. CmVPS41 from Cabo Verde presented membrane spots and nuclear speckles, trans-vacuolar strands and very few intra-vacuolar invaginations, like PS does (**Figure I.5**B,C), whereas CmVPS41 from the accessions FC and Pat-81 showed smooth nuclei and cytoplasm and very few trans-vacuolar bridges, like CmVPS41SC. However, unlike CmVPS41SC, they show very few intra-vacuolar invaginations (**Figure I.5**B, C). Thus, this suggests that the resistance to CMV would not be related to the presence of invaginations of the tonoplast.

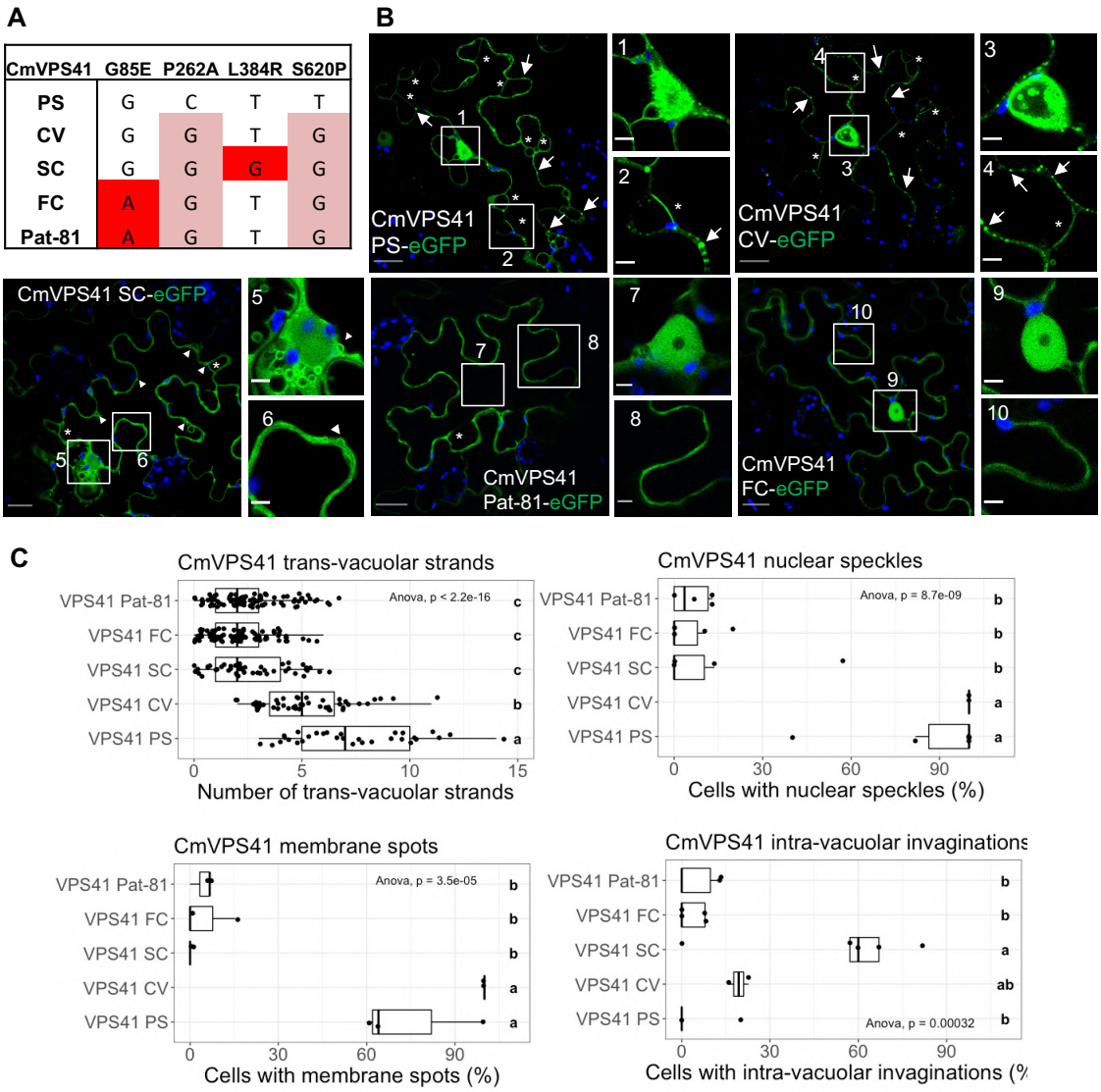

Figure I.5. CmVPS41-induced structures in exotic melon genotypes. **A.** Genotypes of the CmVPS41 melon variants **B.** CmVPS41 distinctive structures in the melon genotypes CV (CmVPS41 CV-eGFP), Pat-81 (CmVPS41Pat-81-eGFP), FC (CmVPS41FC-eGFP), PS (CmVPS41PS-eGFP) and SC (CmVPS41SC-eGFP). CmVPS41Pat-81 amplified nucleus (7) belongs to the same cell from another Z-plane. In blue, chloroplast autofluorescence. Scale bars are 20 µm (whole images) or 5 µM and (amplified images). **C.** Boxplots of CmVPS41 structures in CV, Pat-81 and FC compared to PS and SC. Each boxplot was generated with R package 'ggpubr'. Significant one-way analysis of variance (ANOVA) (p-value<0.05) between each CmVPS41 variant and each specific structure is shown in each boxplot. Post-hoc Tukey results within CmVPS41 genotypes are indicated with letters. The same letter corresponds to nonsignificant differences between CmVPS41 genotypes.

The causal mutations induce a decrease in the number of transvacuolar strands

To determine which of the structures were related to the causal mutations, and hence, to resistance, two new constructs were built. Both kept the sequence of CmVPS41PS, but

carried only the nucleotide change either at nucleotide 254, which produced the amino acid substitution G85E, or at nucleotide 1043 which express a VPS41 protein carrying the L348R change (Pascual et al., 2019). After infiltration into *N. benthamiana* plants, the construct carrying L348R loses the localization pattern of CmVPS41PS and shows many intra-vacuolar invaginations, few spots in the cytoplasm and nucleus, and few trans-vacuolar strands. This is a typical CmVPS41SC localization (**Figure I.6**A, B). Moreover, the number of intra-vacuolar imaginations is higher than when expressing CmVPS41SC and they appear to be generated frequently nearby the nuclear membrane. Therefore, the same mutation responsible for the resistance correlates with changes in the distribution of the late endosome to produce numerous intravacuolar invaginations and few transvacuolar strands. The overexpression of the CmVPS41 construct carrying the G85E causal mutation showed no tonoplast invaginations and very few transvacuolar strands (**Figure I.6**A, B), which confirms the observations made in Pat-81 and FC. The only difference with those was the presence of some cells with a few membrane spots. Altogether, these results indicate that the lack of transvacuolar strands, rather than the presence of tonoplast invaginations, correlate with the mutations that cause resistance to CMV.

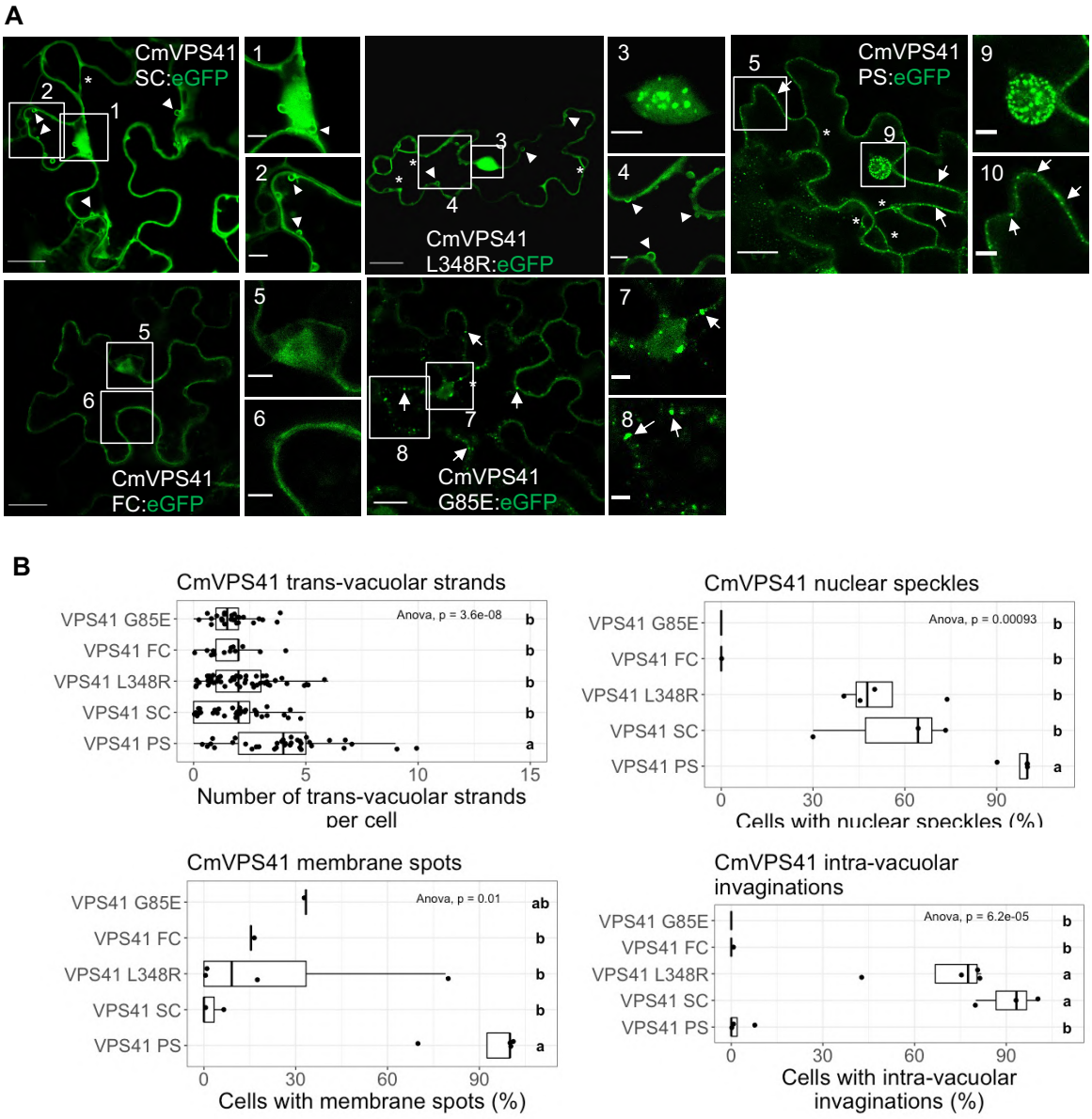

Figure I.6. Effect of causal mutations on CmVPS41 structures. **A.** Localization of CmVPS41 carrying different causal mutations. CmVPS41 G85E-eGFP and CmVPS41 L348R-eGFP carry the causal mutations G85E and L348R, respectively. CmVPS41 PS-eGFP, CmVPS41 SC-eGFP and CmVPS41 FC-eGFP correspond to PS, SC and FC genotypes. Bar scales 20 µm (whole images) or 5 µm (amplified images). **B.** Boxplots of CmVPS41 structures. Each boxplot was generated with R package 'ggpubr'. Significant one-way analysis of variance (ANOVA) (p-value<0.05) is shown in each boxplot. Post-hoc Tukey results within treatments are indicated with letters. The same letter corresponds to nonsignificant differences between different treatments.

Some structures from both, resistant and susceptible CmVPS41s variants, re-localize during the viral infection.

Although the MP is the virulence determinant of CMV against the gene *cmv1*, its co-expression under a strong promoter with CmVPS41 does not show an influence in the VPS41 localization pattern. However, during a real infection the MP can be expressed on due amount and time, and this could lead to a change in the CmVPS41 localization. To analyse this, *N. benthamiana* plants were inoculated either with CMV-FNY or CMV-LS and, after the onset of symptom appearance, new, symptomatic leaves were agroinfiltrated either with CmVPS41PS:GFP or CmVPS41SC:GFP. In these *N. benthamiana* infected cells, both CmVPS41PS and CmVPS41SC-infiltrated plants showed some differences in the localization pattern independently of the virus strain used. Nuclear speckles were present in many VPS41PS expressing cells and much fewer in CmVPS41SC-expressing cells, like in non-infected infiltrated cells shown above (**Figure I.7**). Conversely, the number of cells with membrane spots increased, and the number of tonoplast invaginations decreased in CmVPS41SC-expressing cells with respect to non-infected plants (**Figure I.7**A, B). Interestingly, transvacuolar strands remained very scarce for SC-expressing cells but in PS-infiltrated cells its number decreased significantly during the viral infection, suggesting that these strands could be transiently formed during a real infection and, once the infection is set, they could be no longer needed. Thus, two distinctive structures were differently present in CMV-infected cells with respect to their non-infected counterparts: the number of cells with membrane spots increased in CMV-infected CmVPS41SC-expressing cells and there were fewer transvacuolar strands in CmVPS41PS-expressing cells than in non-infected cells.

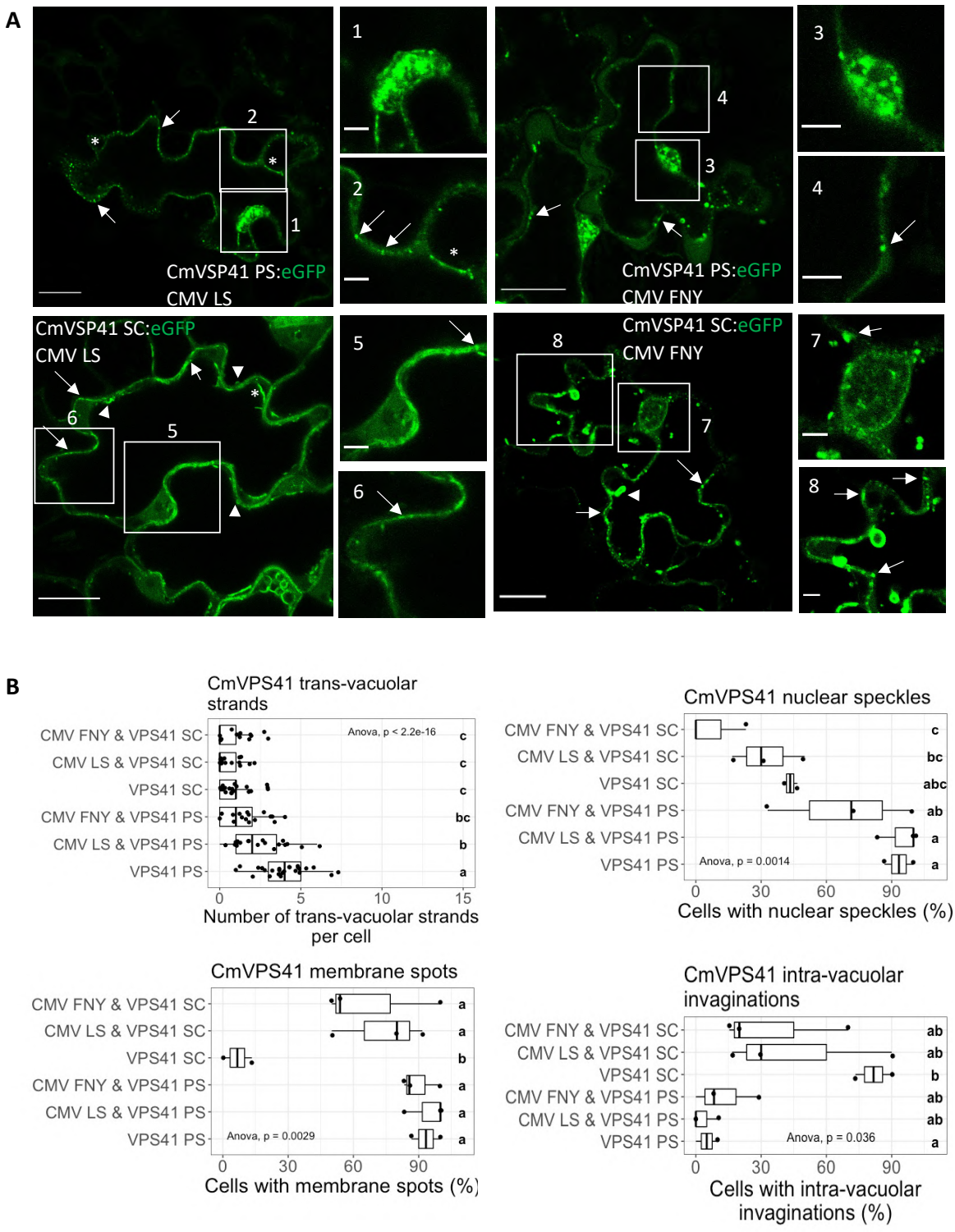

Figure I.7. Effect of CMV infection on CmVPS41 structures. **A.** Localization of CmVPS41 in the presence of CMV-strains LS or FNY. CmVPS41 PS-eGFP or CmVPS41 SC-eGFP in the presence of either CMV-LS or CMV-FNY. Bar scales 20 µm (whole images) or 5 µm (amplified images). **B.** Boxplots of CmVPS41 structures. Each boxplot was generated with R package 'ggpubr'. Significant one-way analysis of variance (ANOVA) (p-value<0.05) is shown in each boxplot. Post-hoc Tukey results within treatments are indicated with letters. The same letter corresponds to nonsignificant differences between different treatments.

I.5. Discussion

VPS41, as a component of the HOPS complex, is a key regulator of cell trafficking. Here we have described the cellular localization of CmVPS41 both from the susceptible cultivar PS and from the resistant exotic cultivar SC, showing that they have differences, mainly in membrane and nuclear speckles, transvacuolar strands and intravacuolar invaginations. Sometimes, these structures moved during the observation. Transvacuolar strands and intra vacuolar invaginations have already been described in soybean (Nebenfuhr et al., 1999) and in several cell types in *A. thaliana*, where these structures are moving and changing their morphology in a manner dependent on actin microfilaments. Furthermore, the movement of the transvacuolar strands were dependent on actin microfilaments (Uemura et al., 2002). Interestingly, CMV MP has been involved in severing acting filaments to increase the size exclusion limit of plasmodesmata (Su et al., 2010). These trans vacuolar structures have been related to the distribution of different solutes, mRNAs and organelles, like Golgi vesicles in the cytoplasm up to the PDs. Moreover, the non-mobile RFP mRNA was targeted to PDs through the transvacuolar strands when co-expressed with *Tobacco mosaic virus* (TMV) MP, suggesting that these strands can be used by a viral MP to direct the virus towards the PDs (Luo et al., 2018). Thus, these structures could well be used also by CMV during the infection through its MP and, together with CmVPS41, for its intracellular movement towards the PDs. The localization of CmVPS41s carrying only the causal mutations for resistance L348R (Giner et al., 2017) and G85E (Pascual et al., 2019), indicated that the resistance was mostly related to the absence of transvacuolar strands, rather than with the presence of intravacuolar invaginations, which supports the idea that those strands could be involved in CMV intracellular trafficking. A more exhaustive analysis with three-dimensional visualization of confocal stack-images shows the structure of these transvacuolar strands, appearing as ropes arranged in a fence-like manner (**Figure I.8**). The special structures colocalize with late endosomes, which is one of the ways the CmVPS41, as part of the HOPS complex, carries cargo proteins to the vacuole. The other way, the AP-3 pathway, skips the endosome pathway and needs VPS41 to drive vesicles directly to the vacuole (Rehling et al., 1999). Thus, the late endosomal localization of the differential structures observed in our experiments suggests that CMV uses CmVPS41 in the endosomal pathway and is independent on the vesicle transport of the AP-3 pathway. Furthermore, as the co-expression with the viral MP does not have an effect in the differential structures

present with CmVPS41SC, probably MP alone is not redirecting endosomal trafficking of CmVPS41 and the way in which these two proteins cooperate remains to be seen.

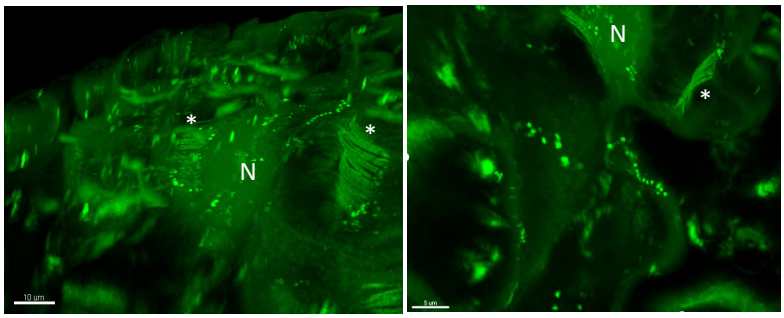

Figure I.8. Three-dimensional reconstruction from Z-stack of CmVPS41PS-GFP derived transvacuolar strands (green). Asterisks (*) indicate trans-vacuolar strands. N indicates nucleus. Scale bars are either 5 or 10 μm.

Despite the MP being the determinant of virulence that communicates with CmVPS41 during infection, overexpression of CmVPS41s with CMV MPs does not change significantly the CmVPS41SC localization. This would suggest that either the differential structures are not really related to resistance to CMV or that the MP does not participate at this step of the infection. Alternatively, in the context of a viral infection, it may need the participation of other viral proteins to fully re-localize those differential structures. In fact, overexpression of CmVPS41s in systemically infected *N. benthamiana* leaves showed a similar localization pattern with both proteins, presenting many cells with membrane spots, very few transvacuolar strands and very few intravacuolar invaginations. Only nuclear speckles were behaving as in the absence of infection, abundant in PS and very few in SC. Membrane spots do not co-localize with PDs, since they do not co-localize with MPs. Besides, membrane spots are not related to cell-to-cell viral movement, since in the resistant accessions, CMV can move cell-to-cell in the inoculated leaf until reaching the bundle sheath cells (Guiu-Aragonés et al., 2016). In the context of viral infection, not only the MP is present, but all viral proteins, whose expression should be tightly regulated. For example, some MPs, accumulate transiently in the first stages of the cell infection (Maule and Palukaitis, 1991). The fact that the transvacuolar strands are dynamic (Uemura et al., 2002), suggests that, when the infection is fully established, these structures may disappear, since they may not be further needed for moving the virus towards the PDs. One possible mechanism for the dynamism of these structures during viral infection may be the timely degradation by the Ubiquitination Proteasome System (UPS). Many viral proteins are

degraded in vivo by the UPS, among them, TMV MP as well as those MPs from *Turnip yellow mosaic virus* (TYMV), *Potato leafroll virus* (PLRV) and TGBp3 from *Potato virus X* (PVX) are known proteasome degraded viral MPs (Reichel and Beachy, 2000; Drugeon and Jupin, 2002; Vogel et al., 2007; Ju et al., 2008). Thus, UPS degradation of viral proteins, and particularly MPs, seems to be a quite extended regulation system in viral infections (for a review, see in (Alcaide-Loridan and Jupin, 2012). Thus, the interplay of all viral proteins and their timely regulation during infection could rend a CmVPS41 localization pattern quite different in different times of the infection and different than when overexpressed with MP. Further work is needed to unveil the role of CmVPS41-produced transvacuolar strands during CMV infection and the link with factors that regulate VPS41 function, such as the levels of phosphatidyl inositol or the role of Rab GTPases (Brillada et al., 2018).

Acknowledgements

We thank Fuensanta Garcia for her technical support. This work was supported by the grants AGL2015-64625-C2-1-R and RTI2018-097665-B-C2, from the Spanish Ministry of Economy and Competitivity (co-funded by FEDER funds) and by the CERCA Programme/Generalitat de Catalunya. We acknowledge financial support from the Spanish Ministry of Science and Innovation-State Research Agency (AEI), through the "Severo Ochoa Programme for Centres of Excellence in R&D" 2016-2019 (SEV-2015-0533) and CEX2019-000902-S.

Author contributions

N.R. performed research and analysed data. I.S. performed research. C.G-A performed research and A.M.M.-H. designed research and wrote the paper.

References

Alcaide-Loridan C, Jupin I (2012) Ubiquitin and plant viruses, let's play together! Plant Physiol 160: 72-82

Amari K, Boutant E, Hofmann C, Schmitt-Keichinger C, Fernandez-Calvino L, Didier P, Lerich A, Mutterer J, Thomas CL, Heinlein M, Mély Y, Maule AJ, Ritzenthaler C (2010) A family of plasmodesmal proteins with receptor-like properties for plant viral movement proteins. PLoS Pathog 6: e1001119

Asensio CS, Sirkis DW, Maas JW, Egami K, To T-L, Brodsky FM, Shu X, Cheng Y, Edwards RH (2013) Self-assembly of VPS41 promotes sorting required for biogenesis of the regulated secretory pathway. Developmental cell 27: 425-437

Balderhaar HJk, Ungermann C (2013) CORVET and HOPS tethering complexes – coordinators of endosome and lysosome fusion. Journal of Cell Science 126: 1307-1316

Brillada C, Zheng J, Krüger F, Rovira-Diaz E, Askani JC, Schumacher K, Rojas-Pierce M (2018) Phosphoinositides control the localization of HOPS subunit VPS41, which together with VPS33 mediates vacuole fusion in plants. Proc Natl Acad Sci U S A 115: E8305-e8314

Campbell RE, Tour O, Palmer AE, Steinbach PA, Baird GS, Zacharias DA, Tsien RY (2002) A monomeric red fluorescent protein. Proc Natl Acad Sci U S A 99: 7877-7882

Carette JE, Raaben M, Wong AC, Herbert AS, Obernosterer G, Mulherkar N, Kuehne AI, Kranzusch PJ, Griffin AM, Ruthel G, Cin PD, Dye JM, Whelan SP, Chandran K, Brummelkamp TR (2011) Ebola virus entry requires the cholesterol transporter Niemann-Pick C1. Nature 477: 340-343

Cormack BP, Valdivia RH, Falkow S (1996) FACS-optimized mutants of the green fluorescent protein (GFP). Gene 173: 33-38

Drugeon G, Jupin I (2002) Stability in vitro of the 69K movement protein of Turnip yellow mosaic virus is regulated by the ubiquitin-mediated proteasome pathway. J Gen Virol 83: 3187-3197

Edwardson JR, Christie RG (1991) Cucumoviruses. In JR Edwardson, RG Christie, eds, CRC Handbook of Viruses Infecting Legumes. CRC Press, Boca Raton, FL., pp 293-319

Essafi A, Diaz-Pendon JA, Moriones E, Monforte AJ, Garcia-Mas J, Martin-Hernandez AM (2009) Dissection of the oligogenic resistance to *Cucumber mosaic virus* in the melon accession PI 161375. Theoretical and Applied Genetics 118: 275-284

Giner A, Pascual L, Bourgeois M, Gyetvai G, Rios P, Picó B, Troadec C, Bendahmane A, Garcia-Mas J, Martín-Hernández AM (2017) A mutation in the melon Vacuolar Protein Sorting 41 prevents systemic infection of Cucumber mosaic virus. Scientific Reports 7: 10471

Gu Y, Innes RW (2011) The KEEP ON GOING protein of Arabidopsis recruits the ENHANCED DISEASE RESISTANCE1 protein to trans-Golgi network/early endosome vesicles. Plant Physiol 155: 1827-1838

Guiu-Aragonés C, Díaz-Pendón JA, Martín-Hernández AM (2015) Four sequence positions of the movement protein of Cucumber mosaic virus determine the virulence against *cmv1*-mediated resistance in melon. Molecular Plant Pathology 16: 675-684

Guiu-Aragonés C, Monforte AJ, Saladié M, Corrêa RX, Garcia-Mas J, Martín-Hernández AM (2014) The complex resistance to Cucumber mosaic cucumovirus (CMV) in the melon accession PI 161375 is governed by one gene and at least two quantitative trait loci. Molecular Breeding 34: 351-362

Guiu-Aragonés C, Sánchez-Pina MA, Díaz-Pendón J, Peña EJ, Heinlein M, Martín-Hernández AM (2016) *cmv1* is a gate for Cucumber mosaic virus transport from bundle sheath cells to phloem in melon. Mol. Plant Pathology 17: 973-984

Hao L, Liu J, Zhong S, Gu H, Qu LJ (2016) AtVPS41-mediated endocytic pathway is essential for pollen tube-stigma interaction in Arabidopsis. Proc Natl Acad Sci U S A 113: 6307-6312

Hashimoto M, Neriya Y, Yamaji Y, Namba S (2016) Recessive Resistance to Plant Viruses: Potential Resistance Genes Beyond Translation Initiation Factors. Frontiers in microbiology 7: 1695-1695

Hipper C, Brault V, Ziegler-Graff V, Revers F (2013) Viral and cellular factors involved in phloem transport of plant viruses. Frontiers in plant science 4: 1-18

Ju HJ, Ye CM, Verchot-Lubicz J (2008) Mutational analysis of PVX TGBp3 links subcellular accumulation and protein turnover. Virology 375: 103-117

Karchi Z, Cohen S, Govers A (1975) Inheritance of resistance to Cucumber Mosaic virus in melons. Phytopathology 65: 479-481

Karimi M, Inzé D, Depicker A (2002) GATEWAY vectors for Agrobacterium-mediated plant transformation. Trends Plant Sci 7: 193-195

Li B, Dong X, Li X, Chen H, Zhang H, Zheng X, Zhang Z (2018) A subunit of the HOPS endocytic tethering complex, FgVps41, is important for fungal development and plant infection in Fusarium graminearum. Environ Microbiol 20: 1436-1451

Luo KR, Huang NC, Yu TS (2018) Selective Targeting of Mobile mRNAs to Plasmodesmata for Cell-to-Cell Movement. Plant Physiol 177: 604-614

Martín-Hernández AM, Picó B (2021) Natural Resistances to Viruses in Cucurbits. Agronomy 11: 23

Maule AJ, Palukaitis P (1991) Virus movement in infected plants. Critical Reviews in Plant Sciences 9: 457-473

Nebenführ A, Gallagher LA, Dunahay TG, Frohlick JA, Mazurkiewicz AM, Meehl JB, Staehelin LA (1999) Stop-and-go movements of plant Golgi stacks are mediated by the acto-myosin system. Plant Physiol 121: 1127-1142

Pascual L, Yan J, Pujol M, Monforte AJ, Picó B, Martín-Hernández AM (2019) CmVPS41 Is a General Gatekeeper for Resistance to Cucumber Mosaic Virus Phloem Entry in Melon. Frontiers in Plant Science 10

Price A, Seals D, Wickner W, Ungermann C (2000) The Docking Stage of Yeast Vacuole Fusion Requires the Transfer of Proteins from a Cis-Snare Complex to a Rab/Ypt Protein. Journal of Cell Biology 148: 1231-1238

Rehling P, Darsow T, Katzmann DJ, Emr SD (1999) Formation of AP-3 transport intermediates requires Vps41 function. Nat Cell Biol 1: 346-353

Reichel C, Beachy RN (2000) Degradation of tobacco mosaic virus movement protein by the 26S proteasome. J Virol 74: 3330-3337

Roossinck MJ (2001) Cucumber mosaic virus, a model for RNA virus evolution. Molecular Plant Pathology 2: 59-63

Sanderson LE, Lanko K, Alsagob M, Almass R, Al-Ahmadi N, Najafi M, Al-Muhaizea MA, Alzaidan H, AlDhalaan H, Perenthaler E, van der Linde HC, Nikoncuk A, Kühn NA, Antony D, Owaidah TM, Raskin S, Vieira L, Mombach R, Ahangari N, Silveira TRD, Ameziane N, Rolfs A, Alharbi A, Sabbagh RM, AlAhmadi K, Alawam B, Ghebeh H, AlHargan A,

Albader AA, Binhumaid FS, Goljan E, Monies D, Mustafa OM, Aldosary M, AlBakheet A, Alyounes B, Almutairi F, Al-Odaib A, Aksoy DB, Basak AN, Palvadeau R, Trabzuni D, Rosenfeld JA, Karimiani EG, Meyer BF, Karakas B, Al-Mohanna F, Arold ST, Colak D, Maroofian R, Houlden H, Bertoli-Avella AM, Schmidts M, Barakat TS, van Ham TJ, Kaya N (2021) Bi-allelic variants in HOPS complex subunit VPS41 cause cerebellar ataxia and abnormal membrane trafficking. Brain 144: 769-780

Schoppe J, Mari M, Yavavli E, Auffarth K, Cabrera M, Walter S, Fröhlich F, Ungermann C (2020) AP-3 vesicle uncoating occurs after HOPS-dependent vacuole tethering. Embo j 39: e105117

Su S, Liu Z, Chen C, Zhang Y, Wang X, Zhu L, Miao L, Wang XC, Yuan M (2010) Cucumber mosaic virus movement protein severs actin filaments to increase the plasmodesmal size exclusion limit in tobacco. Plant Cell 22: 1373-1387

Uemura T, Yoshimura SH, Takeyasu K, Sato MH (2002) Vacuolar membrane dynamics revealed by GFP-AtVam3 fusion protein. Genes Cells 7: 743-753

Vinatzer BA, Teitzel GM, Lee MW, Jelenska J, Hotton S, Fairfax K, Jenrette J, Greenberg JT (2006) The type III effector repertoire of Pseudomonas syringae pv. syringae B728a and its role in survival and disease on host and non-host plants. Mol Microbiol 62: 26-44

Vogel F, Hofius D, Sonnewald U (2007) Intracellular trafficking of Potato leafroll virus movement protein in transgenic Arabidopsis. Traffic 8: 1205-1214

I.6. Supplementary material

Supplementary figures

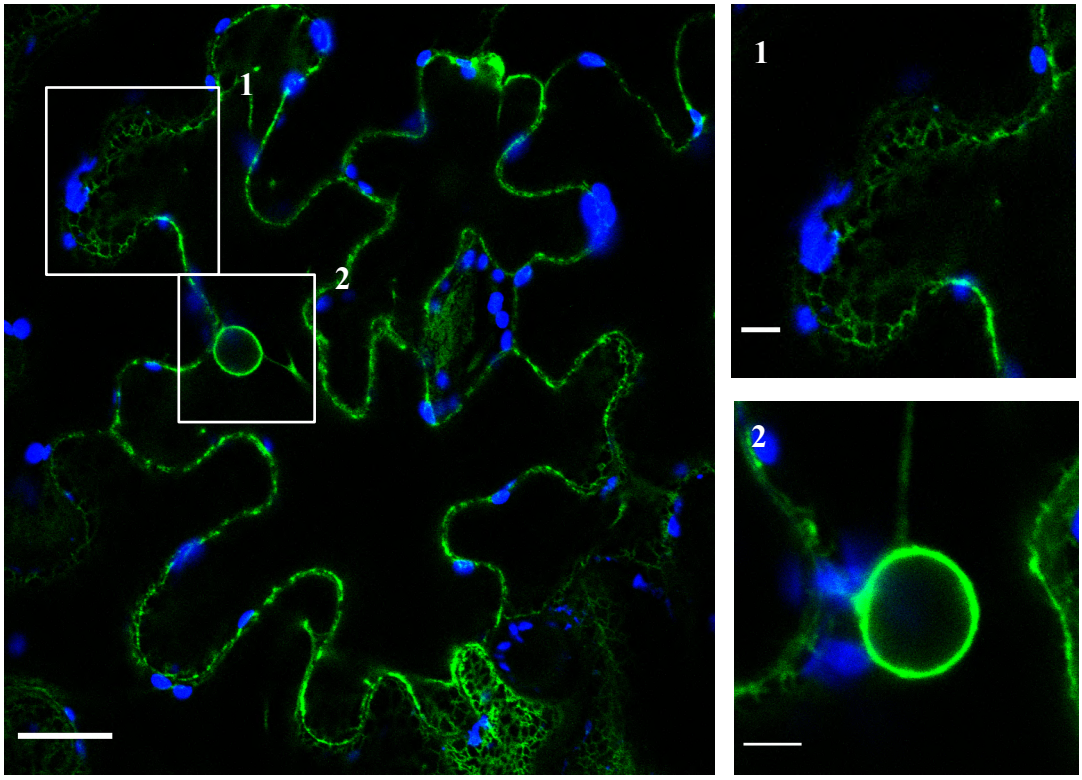

Figure SI.1. Localization of eGFP fluorescence alone in *N. benthamiana* epithelial cells. eGFP is depicted in green while chloroplast autofluorescence is depicted in blue. Image scales from the whole image (left side) correspond to 20 µm and amplified images (right side) scale is 5 µm.

Supplementary tables

Table SI-1. Primers used in this study.

Primer name	Sequence (5' → 3')	Constructs
VPS41 attb4	GGGGACAACTTTGTATAGAAAAGTTGGG TGATCAGTAATGATTTTAACTAGC	CmVPS41-eGFP from cultivars PS, SC, Cabo Verde, I136, C32.
VPS41 attb1	GGGGACAAGTTTGTACAAAAAAGCAGGC TCGATGGCTCCCATTCTATCG	CmVPS41-eGFP from cultivars PS, SC, Cabo Verde, I136, C32.
VPS41 SalI	AGTGAATTCATGGCTCCCATTCTATCGGT A	CmVPS41 PS/SC in pGBKT7.
VPS41 EcoRI	TCGAGCTCGTCAAGTCTTGGAAGCAGCA G	CmVPS41 PS/SC in pGBKT7.
MP BamHI	CATGGAGGCCGAATTCATGGCTTTCCAA GGTACCAGTAGG	MP CMV-LS and CMV-FNY in pGBKT7.
MP EcoRI	GCAGGTCGACGGATCAAGACCGTTAACC ACCTGCGGTCT	MP CMV-LS and CMV-FNY in pGBKT7.

MP attb1	GGGGACAAGTTTGTACAAAAAAGCAGGC TCGATGGCTTTCCAAGGTACC	MP CMV-LS/FNY-RFP.
MP attb4	GGGGACAACTTTGTATAGAAAAGTTGGG TGACCGTTAACCACCTGCGG	MP CMV-LS/FNY-RFP.
L-ascorbate-YC	GGGGACAACTTTTCTATACAAAGTTGTG ATGAGGGAATACAGAGTACTCTGTTCT	L-ascorbate with C-terminal YFP.
L-ascorbate-YC	GGGGACCACTTTGTACAAGAAAGCTGGG TATTAAAGTGGCCTCGTGTGACGT	L-ascorbate with C-terminal YFP.
VPS41-YN	GGGGACAAGTTTGTACAAAAAAGCAGGC TCGATGGCTCCCATTCTATCGGTAAAC	VPS41 PS/SC with N-terminal YFP.
VPS41-YC	GGGGACAACTTTGTATAGAAAAGTTGGG TGCTTGGAAGCAGCAGTAGTACATAA	VPS41 PS/SC with N-terminal YFP.
MP-YC	GGGGACAAGTTTGTACAAAAAAGCAGGC TCGATGGCTTTCCAAGGTACC	MP CMV-LS/FNY with C-terminal YFP.
MP-YC	GGGGACAACTTTGTATAGAAAAGTTGGG TGAAGACCGTTAACCACCTG	MP CMV-LS/FNY with C-terminal YFP.
Syp61 attb1	GGGGACAAGTTTGTACAAAAAAGCAGGC TTCATGTCTTCAGCTCAAGATCCAT	Syp61-RFP.
Syp61 attb2	GGGGACCACTTTGTACAAGAAAGCTGGG TAGGTCAAGAAGACAAGAACGAATAGG	Syp61-RFP.

Table SI-2. Final OD_{600} for infiltration of *A. tumefaciens* cultures in *N. benthamiana* leaves in transient expression experiments.

Construct	**Final OD_{600}**	**Experiment**
CmVPS41 PS-eGFP	0.4	Study localization of CmVPS41 in susceptible versus resistant cultivars, co-localization of CmVPS41 with cellular markers, co-localization with MP-RFP, CMV infection.
CmVPS41 SC-eGFP	0.4	Study localization of CmVPS41 in susceptible versus resistant cultivars, co-localization of CmVPS41 with cellular markers, co-localization with MP-RFP, CMV infection.
CmVPS41 C32-eGFP	0.4	Study localization of CmVPS41 in susceptible versus resistant cultivars.
CmVPS41 I136-eGFP	0.4	Study localization of CmVPS41 in susceptible versus resistant cultivars.
CmVPS41 Cabo Verde-eGFP	0.4	Study localization of CmVPS41 in susceptible versus resistant cultivars.
CmVPS41 PS L348R-eGFP	0.4	Study localization of CmVPS41 in susceptible versus resistant cultivars.
CmVPS41 PS G85E-eGFP	0.4	Study localization of CmVPS41 in susceptible versus resistant cultivars.
MP LS-RFP	0.4	Study effect MPs with CmVPS41s.
MP FNY-RFP	0.4	Study effect MPs with CmVPS41s.
35S:Remorin 1.3-mCherry	0.2	Co-localization of CmVPS41 with cellular markers
35S:HDEL-mCherry	0.4	Co-localization of CmVPS41 with cellular markers.

35S:MAN49-mCherry	0.4	Co-localization of CmVPS41 with cellular markers.
syp21-RFP	0.4	Co-localization of CmVPS41 with cellular markers.
35S:syp61-RFP	0.4	Co-localization of CmVPS41 with cellular markers.
35S:γ-TIP-mCherry	0.4	Co-localization of CmVPS41 with cellular markers.
L-ascorbate oxidase-YN	0.2	BIFC assay.
MP FNY-YC	0.2	BIFC assay.
MP LS-YC	0.2	BIFC assay.
VPS41 PS-YN	0.2	BIFC assay.
VPS41 SC-YN	0.2	BIFC assay.

Chapter II. Searching for interacting proteins of CMV movement protein.

II.1. Introduction

Plant viruses go through several steps to complete their life cycle: uncoating of the viral genome, translation of viral proteins, replication of the genome and encapsidation, movement to neighbour cells (cell-to-cell movement), loading into the vascular system and spreading into new tissues (systemic infection) (Hull, 2002). However, the viral genome is limited, and host factors are required to complete every step and allow a successful infection. For example, several host proteins are required for translation, such as chaperones, RNA-binding proteins, lipids and membrane proteins (Mine and Okuno, 2012). Also, host factors can be involved in resistance. Some host factors protect the host by acting directly against the virus (dominant resistance), while absence of host factors or loss in functionality might also result in resistance (recessive resistance) (Hashimoto et al., 2016b; Palukaitis and Yoon, 2020).

A critical step for most viruses is replication of viral RNAs. Thus, it is no surprise that almost all recessive resistance involve host factors that, in a direct or indirect manner, affect replication (Sanfaçon, 2015). In fact, mutations in different genes coding plant translation initiation factors (eIF) have been involved in natural resistance to most viruses (Hashimoto et al., 2016b). For example, in *Capsicum* species, mutations in *prv1*, which encode an eIF4E, give resistance to *Potato virus Y* (PVY) (Ruffel et al., 2002); or point mutations in *mo1* gene, that encodes an eIF4E, in *Lactuca sativa,* give resistance to *Lettuce mosaic virus* (LMV) (Nicaise et al., 2003), amongst many others (Sanfaçon, 2015). All these deleterious mutations, in the translation initiation factors, impede their interaction with either viral proteins or RNA, and do not allow translation of viral RNAs. In very few cases, resistance has also been related with viral movement, instead of replication (Giner et al., 2017; Michel et al., 2018). In these cases, viruses can replicate but they cannot move either cell-to-cell or systemically. For example, the *mo1* gene reduces LMV accumulation and cell-to-cell movement in lettuce (Nicaise et al., 2003), also loci *bc-1* and *bc-2* , still under gene characterization (Soler-Garzón et al., 2021), were found to affect systemic spread of *Bean common mosaic necrosis virus* (BCMNV) (Feng et al., 2017, 2018). In melon, *cmv1* encodes a Vacuolar Protein Sorting 41 (CmVPS41), which acts as a gatekeeper for resistance to CMV by either restricting the virus in the bundle sheath cells or allowing phloem entry (Guiu-Aragonés et al., 2016).

Plasmodesmata (PD) are connecting channels between neighbour cells that participate in the traffic of molecules and signals. PD inner part consists of a desmotubule, which is an extension of the endoplasmic reticulum that connects neighbour cells (Taliansky et al., 2008; Benitez-Alfonso et al., 2010; Heinlein, 2015b). Moreover, in the surface of both the plasma membrane and the desmotubules there are proteins to regulate the movement of molecules. PD are dynamic and, in normal conditions, allow free movement of relatively small molecules (<1 kDa) (Cilia and Jackson, 2004). However, these channels can also dilate in specific tissues, such as growing tissues or under stress conditions (Burch-Smith et al., 2011; Iswanto et al., 2021), thus, allowing a selective entry of big molecules, such as RNA or proteins. The size exclusion limit (SEL) of plasmodesmata can be modulated by deposition of callose, which has been associated to stress responses of the plant, for example, to limit pathogen transport (Radford et al., 1998; De Storme and Geelen, 2014; Li et al., 2021). However, plant viruses are able to modify plasmodesmata SEL through their MP (Wolf et al., 1989).. Therefore, PD are a regulatory checkpoint in viral movement since they are key for cell-to-cell and long-distance transport.

Movement proteins (MP) are divided into two broad categories depending on the plasmodesmata transport and the changes they induce, as well as, the form the viruses travel through the PD (Taliansky et al., 2008). The first category is formed by the MPs that use the desmotubule to increase SEL to allow movement of an MP-vRNPs aggregate, without further changes in the PD. New vRNAs and the MP form vRNPs complexes that together with replication proteins (Tilsner et al., 2009), are anchored to the desmotubule, formed by ER network, and travel to neighbour cells. In this category MP from TMV is the most studied example. In the second category, the tubule-guided movement category, MPs remove completely the desmotubule and gate the PD to increase SEL and allow free pass of virions (Ritzenthaler and Hofmann, 2007; Amari et al., 2010). This intracellular transport is associated with MP-tubule formation within the plasmodesmata. In this category CaMV is the most studied example (Carluccio et al., 2014). CMV MP categorizes as a tubule-guided movement protein (Canto and Palukaitis, 1999). This MP binds RNA (Andreev et al., 2004) and forms vRNP complexes that travel to the PD, through an unknown mechanism, where the MP increases plasmodesmata SEL and, to do so, requires the actin cytoskeleton (Su et al., 2010). Moreover, CMV-MP alone is not able to perform cell-to-cell movement and it also requires the coat protein (Nagano et al., 2001).

Virus intracellular movement is specific from each virus. In the case of TMV it requires its 126 kDa replicase for movement (Peña and Heinlein, 2012; Heinlein, 2015b). Moreover, replication takes place in viral replication complexes (VRCs) (Tilsner et al., 2009) that are transported through the ER-network to the PD. In *Cauliflower Mosaic Virus* (CaMV), inclusion bodies (IB), where translation occurs, are transported by microfilaments to the PD. In *Melon necrotic spot virus* (MNSV) its two movement proteins (Double Gene Block protein 1 and 2; DGBp1 and DGBp2) use independent pathways to reach the periphery; DGBp1 uses actin microfilaments and moves through mobile granules, while DGBp2 traffics via the COPII-pathway (Genovés et al., 2010; Serra-Soriano et al., 2014; Navarro and Pallás, 2017).

Viruses' movement also requires interaction with host proteins, either through their movement proteins or other viral proteins. In TMV infection, the contractile calcium-binding synaptotagmin SYT1, A, located in the contact sites between the ER and plasma membrane (Yuan et al., 2018) interacts with TMV MP to allow MP trafficking. In the case of CaMV, PD-located protein 1 (PDLP1) recruits and interacts with the CaMV MP at the base of PDs (Thomas et al., 2008). In *N. benthamiana*, Suppressor Of G-two Allele Of Skp1 (SGT1) interacts with *Tomato Spotted Wilt Virus* (TSWV) movement protein NSm for cell-to-cell movement and systemic infection (Noël et al., 2007; Qian et al., 2018b). CMV-MP has one described interactor in *C. sativus*, the ascorbate oxidase, that allows vRNP-MP targeting to the PD (Kumari et al., 2016). In long-distance movement key host proteins are usually host and virus-specific, thus, few have been genetically characterized. For example, in Tobacco, CMV 1a-interacting protein 1 (Tcoi1) interacts with CMV-1a and is required for long-distance movement (Kim et al., 2008a), or in *C. sativus,* P48 is potentially involved in CMV long-distance transport since its interaction with CMV virions facilitates their resistance to RNase A in the phloem (Requena et al., 2006).

Resistance to CMV in SC is recessive and oligogenic (Essafi et al., 2009). The main QTL for systemic resistance corresponds to *cmv1* and encodes the Vacuolar Protein Sorting 41 (CmVPS41), involved in protein transport from the late endosome to the vacuole (Giner et al., 2017). Moreover, CMV-MP is its virulence factor (Guiu-Aragonés et al., 2015). In fact, CmVPS41 from SC is able to restrict movement of strains from subgroup II (like CMV-LS) by blocking the virus in the bundle sheath (BS) cells and impeding phloem entry, but it does not restrict phloem entry of strains from subgroup I (like CMV-FNY) (Guiu-Aragonés et al.,

2016). To overcome the resistance posed by *cmv1*, CMV FNY needs two other QTLs (Guiu-Aragonés et al., 2014). Therefore, to understand how CmVPS41 and CMV-MP communicate at a cellular level, and CmVPS41 allows or blocks CMV transport to the phloem, it is key to study both CmVPS41 and CMV-MP. In the first chapter, the focus has been on CmVPS41 by studying its localization and the possible interaction with CMV-MPs. In this chapter, we have put the focus on CMV-MP. Our approach has been to shed light on MP function through the identification of MP-interacting proteins in susceptible and resistant melon genotypes. This way, it will allow to get a better insight on how CMV moves at cell-to-cell and long-distance levels and its implications on CMV resistance or susceptibility.

II.2. Material and Methods

II.2.1. Growth of plants

Melon seeds were treated with 2,5 g/L Merpan (ADAMA essentials, Spain) for 5 min, rinsed thoroughly and soaked in water overnight. Seeds were pre-germinated for around 3 days in wet plates at 28 ºC with photoperiod of 12 h under light and 12h in the dark. The seedlings were planted in a fitotron (Fitotronic Version2, Inkoa) under long day conditions consisting of 22 ºC for 16 h with light and 18 ºC for 8 h in the dark throughout the whole infection. Zucchini squash (*Cucurbita pepo L.*) Chapin F1 (Semillas Fitó SA, Barcelona, Spain) served as host for viral inocula for melon infections, and it was grown in growth chamber SANYO MLR-350H in long-day conditions consisting of 22 ºC for 16 h with 5,000 lux of light and 18 ºC for 8 h in the dark for all infections.

N. benthamiana plants were grown in the greenhouse under long-day conditions, consisting of 24-28°C with 5000 lux of light for 16 h and 22-24°C 8 h in the dark, and were kept in the same conditions after agroinfiltration.

II.2.2. Viral inoculations

Viral sap from CMV-FNY was freshly prepared from infected zucchini squash (*Cucurbita pepo L.*) Chapin F1 (Semillas Fitó SA) by grinding the new leaves of infected zucchini squash in 0.2% diethyl dithiocaremate of sodium (pH = 7.1-7.2) buffer (DIECA) in the presence of active carbon, to disrupt more efficiently the cells. Cotyledons of 7 to 10 days old melon plants were rub-inoculated with the viral sap.

II.2.3. Agroinfiltration

A. tumefaciens clones of RNA1, RNA2 and RNA3 were cultured, resuspended and agroinfiltrated into the leaf of 2-weeks old *N. benthamiana* plants in a 1:1:1 proportion, as described in M&M from Chapter 1. Agroinfectious clones of CMV-FNY were provided by Prof. Kook- Hyung Kim (Seo et al., 2009) and CMV-LS were developed in our laboratory (unpublished).

II.2.4. RNA isolation

Total RNA was obtained with Spectrum™ Plant Total RNA Kit (Sigma, Saint Louis, USA) following manufacturer's instructions. Quality and quantity of RNA was determined by a 1 % agarose gel electrophoresis and NanoDrop™ ND-1000 Spectrophotometers (Thermo

Fisher Scientific, Waltham, USA). Total RNA was treated with DNase I (Takara, Kyoto, Japan) to eliminate contaminating genomic DNA.

II.2.5. Yeast Two Hybrid Screening

II.2.5.1. Y2H library

Library was nicely provided by Dr. Bin Liu, from our laboratory (unpublished). This library was constructed following the Make Your Own "Mate & Plate" Library System (Takara) using yeast strain Y187 (Takara).

II.2.5.2. Cloning and testing bait for toxicity, autoactivation and expression

Coding sequences of the MP (Guiu-Aragonés et al., 2015) were amplified with primers MP-BamHI-F and MP-EcoRI-R (**Table II-1**) and cloned into plasmid pENTR/D-TOPO (Thermo Fisher Scientific). Digestion of MP FNY and pGBKT7 with *BamHI* (Takara) and *EcoRI* (Takara) was performed following manufacturer's instructions and MP FNY was cloned in pGBKT7 with T4 ligase (Thermo Fisher Scientific) at *BamHI-EcoRI* sites. The correct cloning and insert orientations were confirmed by sequencing. pGBKT7-MP was transformed into *Saccharomyces cereviseae* (*S. cerevisiae*) strain Y2HGold (Takara), using Yeastmaker Yeast Transformation System 2 (Takara). The transformed cells were grown in SD/-Trp plates (Minimal SD Base 26.7 g/l, dropout mix-Trp Clontech 0.69 g/l, agar 2 %, kanamycin 50 µg/ml), at 30ºC for 3-5 days. SD/-Trp medium includes an SD base and a dropout with every essential amino acid except for tryptophan, which is synthesized by the bait vector pGBKT7. To test MP FNY toxicity and autoactivation, pGBKT7-MP and pGBKT7 were separately transformed into Y2HGold (Takara) yeast cells and cultured at 30 ºC for 3-5 days in SD/-Trp, SD/-Leu/X-α-Gal, to select for blue colonies (Minimal SD Base 26.7 g/l, dropout mix-Trp 0.69 g/l, agar 2%, kanamycin 50 µg/ml, X-α-Gal 40 µg/ml) and SD/-Trp/X-α-Gal/AbA (Minimal SD Base/Gal/Raf 37 g/l, dropout mix-Trp 0.69 g/l, agar 2%, kanamycin 50 µg/ml, X-α-Gal 40 µg/ml, Aureobasidin A (AbA) 125 ng/ml) plates following manufacturer's instructions. Both pGBKT7-MP FNY and pGBKT7 were plated in SD/-Trp and SD/-Trp/Gal plates. To test the expression of the MP, MP protein was extracted from a 20 ml yeast pGBKT7-MP FNY Y2HGold culture following the Urea/SDS method (Printen and Sprague, 1994). Western Blot of MP was performed using a specific antibody against CMV MP (1:5000 dilution), following the protocol previously described (Coca et al., 2004).

Table II-1. Primers used in Y2H screening. In bold: *BamHI* (5') and *EcoRI* (3') restriction sites.

Primer name	Sequence (from 5' to 3')
MP-EcoRI-F	CATGGAGGCC**GAATTC**ATGGCTTTCCAAGGTACCAGTAGG
MP-BamHI-R	GCAGGTCGAC**GGATCC**AAGACCGTTAACCACCTGCGGTCT
CMV-2F	TAATACGACTCACTATAGGGC
CMV-2R	AGATGGTGCACGATGCACAG

II.2.5.3.Screening of proteins interacting with CMV-FNY MP

One fresh and large (2-3 mm) Gold strain yeast containing the bait vector pGBKT7-MP FNY and carrying the Gal4 DNA-binding domain was used to prepare a concentrated overnight culture following the manufacturer's instructions. The overnight bait culture was resuspended in SD/-Trp liquid medium to a cell density of > 1 x 10^8 cells per ml. Bait suspension and 1 ml aliquot of prey library carrying the Gal4 activation domain in Y187 strain were combined and cultured overnight following the manufacturer's instructions. After 20 h, zygote presence was determined by epifluorescence microscopy. The mated culture was centrifuged, resuspended, and plated in either viability plates (SD/-Trp, SD/-Leu, SD/-Trp/-Leu; Minimal SD Base 26.7 g/l, dropout mix-Trp 0.69 g/l, dropout mix -Leu 0.64 g/l , agar 2%, kanamycin 50 µg/ml) or mating plates (SD/-Trp/-Leu/X-α-Gal/AbA; Minimal SD Base/Gal/Raf 37 g/l, dropout mix-Trp 0.69 g/l, dropout mix -Leu 0.64 g/l, agar 2%, kanamycin 50 µg/ml, X-α-Gal 40 µg/ml, AbA 125 ng/ml) and grown at 30ºC. After 3 to 5 days viability plates were collected, and the number of total screened clones was >1 million diploid cells (1.3 million estimation from 1/10.000 dilution SD/-Trp/-Leu control plates). After 8 to 10 days, blue colonies from SD/-Trp/-Leu/X-α-Gal/AbA were selected and plated onto more restrictive media SD/-Ade/-His/-Trp/-Leu/X-α-Gal/AbA. Positive colonies were selected as primary interacting proteins for further analysis and then retransferred into SD/-Trp/-Leu liquid medium culturing for 2 days to isolate plasmids using the Easy Yeast Plasmid Isolation Kit (Takara). The constructs isolated were sequenced using CMV-2F and CMV-2R primers (**Table II-1**) and analysed using BLAST from Melonomics (https://www.melonomics.net/melonomics.html#/blast).

II.2.5.4.One-by-one Yeast Two Hybrid

In one-by-one Y2H, previously individually grown colonies from prey (in vector pGADT7) and bait (in vector pGBKT7), following the manufacturer's instructions, were co-cultured with 1 ml of liquid 1XYPDA media with kanamycin (50ug/mL), in 1.5 ml Eppendorf, at 30

ºC with 200 rpm. After 20h, 100 µl from the mating solution are plated in SD/-Trp/-Leu/X-α-Gal agar plates and grown at 30 ºC. After 3-5 days, blue colonies are rescued and plated successively in SD/-Trp/-Leu/X-alpha-Gal/AbA agar plates. Again, if blue colonies appear, they are rescued and plated in the more restrictive media (SD/-Trp/-Leu/X-alpha-Gal/AbA/-Ade/-His agar) plates. Strong or light blue colonies in the more restrictive media are considered true interactors, always comparing with the positive (pGBKT7-53 with pGADT7-T) and negative interaction controls (pGBKT7-Lam with pGADT7-T).

II.2.6. Bimolecular Fluorescence Complementation (BiFC)

For Bimolecular Fluorescence Complementation assay (BIFC), the sequence of *C. melo* Niemann-Pick C1 protein-like interaction domain (MELO3C013507.2.1 or *CmNPC1*) was PCR amplified with the PrimeSTAR® GXL DNA Polymerase (Takara, Japan) using primer combinations NPC1-YC-F with YC-R or NPC1-YN-F with YN-R (**Table II-2**) to introduce NPC1 interaction domain respectively in pDONR P1-P4 or pDONR P4r-P2 by BP reactions and into the expression vector pBAV154 as N-terminal fusion with partial N-terminal YFP (YN) or partial C-terminal (YC) by LR reaction using MultiSite Gateway® Pro (Invitrogen by Thermo Fisher Scientific, Lithuania), resulting in the obtention of constructs CmNPC1-YN and CmNPC1-YC, as previously described in Chapter 1. Both constructs were verified by DNA sequencing and transformed in *A. tumefaciens* GV3101 strain. Combinations of either CmNPC1-YN together with either MP-YC (constructed in Chapter I) or CmNPC1-YC together with CmVPS41-YN (constructed in Chapter I) were agroinfiltrated, as described in Chapter I, and resuspended to a 0.2 OD_{600} value. Also, combination of L-ascorbate oxidase-YN together with MP-YC (both previously constructed in Chapter I, refer to M&M section "Plasmid construction" for more information) were agroinfiltrated in the same conditions as positive control. Transient expression of YFP in *N. benthamiana* was observed 20 h after dexamethasone induction under the confocal microscope.

Table II-2. Primers used for construction of BIFC clones. In bold: attB sequences.

Primer name	Sequence (from 5' to 3')
NPC1-YN-F (attB4r)	**GGGGACAACTTTTCTATACAAAGTTG**CCTATTTTGTTGTGAAGG ATTACAATTA
NPC1-YN-R (attB2)	**GGGGACCACTTTGTACAAGAAAGCTGGGT**ATTTGTAACTTTTAG TGTGTGTGAAA
NPC1-YC-F (attB1)	**GGGGACAAGTTTGTACAAAAAAGCAGGCT**GCATTTTGTTGTGAA GGATTACAATTATAG
NPC1-YC-R (attB4)	**GGGGACAACTTTGTATAGAAAAGTTG**GGTGTTTGTAACTTTTAG TGTGTGTGAAAA

II.2.7. Image capture and analysis

For yeast cells visualization slides were mounted with water solution and DIC (differential interference contrast) images from yeast zygotes were obtained at x200 and x400 magnification (Zeiss Plan-Neofluar 40x/20x, 1.30 numerical aperture, in oil; Oberkochen, Germany). For BIFC assay, Leica TCS-SP5 II confocal microscope (Leica Microsystems, Exton, PA USA) with a 63 x water immersion objective NA 1.2, zoom 1.6 was used. YFP was excited with the blue argon ion laser (514 nm), and emitted light was collected between 530 nm and 630 nm using a HyD detector. Bar scales were set with Fiji (ver 1.52i) software.

II.2.8. Analysis of CmNPC1

The alignment of DNA sequences from CmNPC1 PS interaction domain was performed with Sequencher ® version 5.4.6 DNA sequence analysis software (Gene Codes Corporation, Ann Arbor, MI USA). Sequences were aligned with *CmNPC1 PS* exons and introns. The obtained information was used to reconstruct *CmNPC1* complete interaction domain. Nucleotide coding sequences from *CmNPC1* from PS and SC were obtained from Melonomics database [https://www.melonomics.net, (Ruggieri et al., 2018)] and translated with ExPASy translation tool [http://web.expasy.org/translate/, (Gasteiger et al., 2003)]. CmNPC1 protein sequences from PS and SC cultivars were aligned using ClustalW (Madeira et al., 2019) to find polymorphisms. Effects of the polymorphisms in the CmNPC1 protein from PS versus SC were predicted with Protein Variation Effect Analyzer (PROVEAN) [http://provean. jcvi.org/index.php, (Choi and Chan, 2015)]. Changes were considered deleterious when the predicted PROVEAN score was lower than -2.5. For protein modelling and prediction of transmembrane domain Phyre2 was used [http://www.sbg.bio.ic.ac.uk/~phyre2, (Kelley et al., 2015) in normal mode. To determine whether CmNPC1 interaction domain faced the inside or the outside of the membrane, Transmembrane Helices Hidden Markov Model (TMHMM) v. 2.0 [http://www.cbs.dtu.dk/services/TMHMM/, (Krogh et al., 2001)] and Interpro [https://www.ebi.ac.uk/interpro/, (Hunter et al., 2009)] were used. 3D models of protein CmNPC1 from cultivars PS and SC were carried out with Ezmol [http://www.sbg.bio.ic.ac.uk/ezmol, (Reynolds et al., 2018)].

II.2.8.1.Retrotranscription -Polymerase Chain Reaction (RT-PCR)

From 200 µg of total RNA, Reverse Transcription (RT) reactions were performed using random primer CDSIII/6 (Takara, Mountain View, USA) and Prime Script Reverse

Transcriptase (Takara Biotechnology, Dalian, China) following the manufacturer's instructions. Polymerase Chain Reaction (PCR) reactions were performed with Pfu Taq polymerase (Promega Corporation, Madison, WI) according to manufacturer's instructions. DNA products were electrophoresed in 1.5 % agarose gels.

Table II-3. Primers used in PCRs to amplify introns and exons in CmNPC1 cDNA.

Primer name	Sequence (from 5' to 3')
NPC1-1F	GTTGTGAAGGATTACAATTATAGCTC
NPC1-1R	GTACAATCTCTGCACACTCC
NPC1-2F	GTGTGCAGAGATTGTACAAC
NPC1-2R	GGGTTTTTCACATAAACCTAGTG
NPC1-3R	CCAAATCTGAGTGGCGAAA

II.2.9. Immunoprecipitation

II.2.9.1. Protein extraction and fractionation

Frozen melon leaves were grinded with liquid nitrogen in a mortar. To the finely ground plant material (250 - 300 µl) 500 µl extraction buffer (50mM Tris pH 7.5, 150 mM NaCl, 10% glycerol, 2 mM EDTA, 5 mM DTT, 1 % Triton X-100, plant protease inhibitor protease (Sigma) (10 µl/ml)) was added, samples were mixed and incubated for 30 min at 4 °C. After centrifugation for 15 min (18,000 x g) at 4 °C the supernatant was removed and transferred to a fresh tube and protein concentration was determined using Pierce 660 nm protein assay (Thermo Fisher Scientific).

II.2.9.2. Immunoprecipitation assay

For each immunoprecipitation (IP) 500 µl of protein extract (0.5 mg/ml) were used. In the first IP test, an aliquot of 250 µg protein was diluted with wash buffer (50 mM Tris, pH 7.5, 150 mM NaCl 10% glycerol, 2 mM EDTA). IP was carried out using Dynabeads Protein A (Invitrogen by Thermo Fisher Scientific) modified with anti-MP antibody. Beads were prepared according to the manufacturer's protocol. In brief, per sample 50 µl of beads solution was transferred to a 2 ml tube and placed on a magnetic rack. After removal of the buffer, beads were treated with antibody at dilution 1/300 and incubated for 2 h at 4 °C on a rotator after which, beads were washed once with wash buffer. Next, the beads were treated with 500 µl protein extract (0.5 mg/ml) and incubated for either 2h or overnight on a rotator at 4 ºC. After removal of the supernatant, beads were frozen at -20 °C until the next steps. After thawing, beads were washed 4x with wash buffer. In the second IP test, the IP was

performed as previously described but two different quantities of antibody anti-MP were tested: 1/300 and 1/60. After optimizing the Immunoprecipitation assay, all assays were performed as previously described with 1/300 solution of anti-antibody, and 2h incubation of protein extract with the antibody solution.

II.2.9.3.Peptide digestion

The beads were digested in 25 µl digestion buffer 1 (50 mM Tris pH 7.5, 2M Urea, 1 mM DTT, 5µg/ml Trypsin, Sigma, St. Louis, USA) and incubated in a Thermomixer at 30 ° C with 400 rpm for 30 min. The supernatant was transferred to a fresh tube and the beads were washed again with 50 µl digestion buffer 2 (50 mM Tris pH 7.5, 2M Urea, 5 mM Chloroacetamide), and the supernatant was recovered and combined with the previous one. The total digestion was incubated overnight in a Thermomixer at 32 ° C with 400 rpm until complete digestion of proteins into peptides. After acidification with 2 µl of 50% TFA (trifluoroacetic) samples were desalted using C18 Empore disk membranes (3M, St. Paul, USA) according to the StageTip protocol (Rappsilber et al., 2003). The eluted peptides were dried and then taken up in 10 µl A* buffer (2% acetonitrile or ACN, 0.5% formic acid or FA) and peptide concentration were determined by Nanodrop (Thermo Fisher Scientific).

II.2.9.4.Liquid Chromatography with tandem Mass Spectrometry (LC-MS/MS)

Peptides were analysed using an EASY-nLC 1200 (Thermo Fisher Scientific) coupled to a Q Exactive Plus mass spectrometer (Thermo Fisher Scientific). Peptides were separated on 16 cm frit-less silica emitters (New Objective, 75 µm inner diameter), packed in-house with reversed-phase ReproSil-Pur C18 AQ 1.9 µm resin (Dr. Maisch, Ammerbuch, Germany). Peptides were loaded on the column and eluted for 115 min using a segmented linear gradient of 5% to 95% solvent B (0 min : 5% B; 0-5 min with 5%B; 5-65 min with 20%B; 65-90 min with 35%B; 90-100 min with 55% B; 100-105 min with 95% B, 105-115 min with 95% B) (solvent A is 0% ACN, 0.1% FA; solvent B is 80% ACN, 0.1% FA; Fisher Scientific, Geel, Belgium) at a flow rate of 300 nL/min. Mass spectra were acquired in data-dependent acquisition mode with a TOP15 method. MS spectra were acquired in the Orbitrap analyser with a mass range of 300–1750 m/z at a resolution of 70,000 FWHM and a target value of 3×10^6 ions. Precursors were selected with an isolation window of 1.3 m/z. Higher-energy C-trap dissociation (HCD) fragmentation was performed at a normalized collision energy of 25. MS/MS spectra were acquired with a target value of 10^5 ions at a resolution of 17,500 FWHM, a maximum injection time (max.) of 55 ms and a fixed first mass of m/z 100.

Peptides with a charge of +1, greater than 6, or with unassigned charge state were excluded from fragmentation for MS. Dynamic exclusion for 30 s prevented repeated selection of precursors.

II.2.9.5.Data analysis

Raw data were processed using MaxQuant software (version 1.6.3.4, http://www.maxquant.org/) (Cox and Mann, 2008) with label-free quantification (LFQ) and iBAQ enabled (Tyanova et al., 2016). MS/MS spectra were searched by the Andromeda search engine against a combined database containing the sequences of proteins from *C. melo* version CM4.0 [https://www.melonomics.net, (Ruggieri et al., 2018)] or *Nicotiana benthamiana* genome v1.0.1 [https://solgenomics.net/, (Bombarely et al., 2012)] in the case of IP from tobacco plants, together with movement proteins from CMV-FNY and CMV- LS (Guiu-Aragonés et al., 2015) and sequences of 248 common contaminant proteins and decoy sequences. Trypsin specificity was required and a maximum of two missed cleavages allowed. Minimal peptide length was set to seven amino acids. Carbamidomethylation of cysteine residues was set as fixed, oxidation of methionine and protein N-terminal acetylation were set as variable modifications. The match between runs option was enabled. Peptide-spectrum-matches and proteins were retained if they were below a false discovery rate of 1 % in both cases.

Statistical analysis (Supplementary material 1) of the MaxLFQ values was carried out using Perseus (version 1.5.8.5, http://www.maxquant.org/). Quantified proteins were filtered for reverse hits and hits "only identified by site" and MaxLFQ values were $\log_2$ transformed. After grouping samples by condition, only proteins having three valid values in one of the conditions were retained for the subsequent analysis. Two-sample *t*-tests were performed using a permutation-based FDR of 5 %. Alternatively quantified proteins were grouped by condition and only those hits with four valid values in one of the conditions were retained. Missing values were imputed from a normal distribution, using the default settings in Perseus (1.8 downshift, separately for each column). Volcano plots were generated in Perseus using an FDR of 5%, an $S0 = 2$. Perseus output was exported and further processed using Excel, in which significant proteins, in at least one of the previous test, and with a fold change ($\log_2$ ratio) > 2 were retained for subsequent analysis.

Homologous *A. thaliana* proteins were searched from significant CMV-MP-candidate interactors from either *C. melo* or *Nicotiana benthamiana*. To do so, each *C. melo* or

Nicotiana benthamiana protein sequence was downloaded from Melonomics database ([https://www.melonomics.net, (Ruggieri et al., 2018)] or Solgenomics database ([https://solgenomics.net/, (Bombarely et al., 2012)] accordingly, and BLASTed in TAIR database [BLAST 2.9.0+ (https://www.arabidopsis.org/Blast/)]. Good homology matches were considered with blast hits with an E-value < 0.01 (Wheeler D, 2007).

II.2.9.6. Gene Ontology and pathway enrichment

Candidate interactors from systemic and local *C. melo* CMV infection were separately input into gprofiler2 (version e104_eg51_p15_3922dba) (Kolberg et al., 2020) in R (version 3.6.1), for Gene Ontology (GO) and Kyoto Encyclopaedia of Genes and Genomes (KEGG) classification analysis. The GO enrichment analysis included GO terms into the three major categories (biological process, cellular component, and molecular function). gprofiler2 package function "gost" was used to perform a Fisher's exact test with a p-adjusted value with the Bonferroni correction method (Curtin and Schulz, 1998). Thus, the p-adjusted value corresponds to a p-value for the enriched ontology term adjusted with Bonferroni in which p-adjusted ≦0.05. Enrichment results were graphed in Manhattan plots with "gostplot" function and saved as jpeg files. All R scripts are available in Supplementary material 2B.

Candidate interacting proteins from CMV-infected *N. benthamiana* GO term enrichment analysis was performed with AgriGO 2.0 [http://systemsbiology.cau.edu.cn/agriGOv2/, (Tian et al., 2017)]. The GO enrichment analysis included GO terms into the three major categories and a Singular Enrichment Analysis (SEA) tool was used with the *N. benthamiana* genome v1.0.1 ([https://solgenomics.net/, (Bombarely et al., 2012)] as a reference to perform a Fisher's exact test with a p-adjusted value<0.05 corrected with Bonferroni (Curtin and Schulz, 1998).

II.3. Results

II.3.1. Identification of melon host factors interacting with CMV-MP

In this Chapter, we have tried to get a better insight on the mechanism of infection of CMV by focusing on its virulence factor; the movement protein (MP). For this reason, we have identified melon interactor proteins with the MP to understand how the virulence factor interacts with the host and perpetuates CMV infection. To do so, two different methods were used: Yeast Two Hybrid library screening and Immunoprecipitation of protein complexes coupled to mass spectrometry.

II.3.2. Y2H library screening with CMV-FNY MP

Yeast Two Hybrid screening consists in searching interactors from a library of prey proteins using one protein of interest as bait. In our case, we used as bait the CMV-FNY MP and the library was constructed from CMV-FNY infected PS (Bin Liu, unpublished). Thus, this combination of melon genotype plus CMV strain was chosen, since it would be plausible to have the largest number of MP-interacting-proteins.

II.3.2.1. Bait controls

First, the bait pGBKT7-MPFNY was constructed as explained in M&M section II.2.5.2. Toxicity, autoactivation and expression of this bait were tested before the library screening. The autoactivation test is used to be sure the bait construct does not activate the Gal-responsive genes in the absence of a prey interactor. For this test, Y2H Gold cells were transformed with the bait (pGBKT7-MPFNY) and plated in the presence of X-α-Gal (SD/-Trp/X-α-Gal) or Aureobasidin A (SD/-Trp/X-α-Gal/AbA), two of the inductors of Gal-responsive genes upon interaction. In the case of no interaction, colonies should be able to either: (i) grow but not turn blue (in the presence of X-α-Gal), since MEL1 gene is not expressed and X-α-Gal cannot be processed into α-galactosidase (which has blue colour); or (ii) not be able to grow at all (in the presence of Aureobasidin A), since AUR1-gene is not activated, thus Aureobasidin A, a highly-toxic drug to yeast, cannot be processed by yeast and it produces yeast death. As shown in **Figure II.1**A, the bait grew white in X-α-Gal plates and it did not grow in the presence of Aureobasidin A. Therefore, it is not autoactivated without the presence of a prey. In the toxicity test, the possible toxic effect of the bait protein to yeast was checked. To do so, a comparison between the growth of empty pGBKT7 and pGBKT7-MPFNY was made. As observed in **Figure II.1**A, the growth of pGBKT7-

MPFNY showed a comparable number and size of colonies compared to that of pGBKT7 empty vector; thus, the MP FNY insert in pGBKT7 vector was not toxic for yeast cells. Finally, in the expression test, the correct expression of MP FNY in pGBKT7 was checked through protein extraction from yeast cells and Western Blot, as explained in M&M section II.2.5.2. As observed in the Western Blot (**Figure II.1**B), MP FNY is visualized as a 30.47 KDa band, while in empty pGBKT7 that size band is absent. Therefore, MP FNY, within pGBKT7, was expressed in yeast cells.

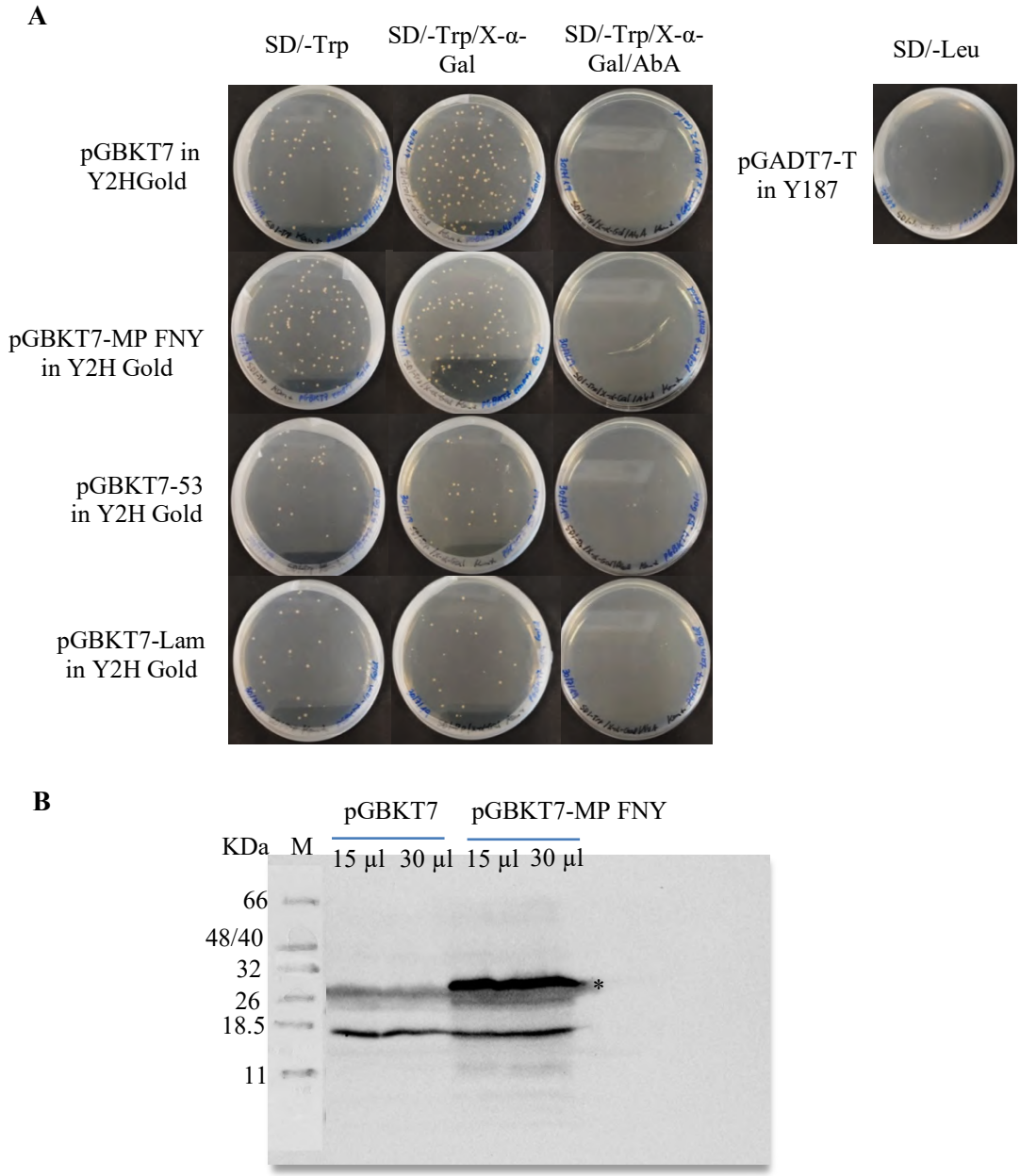

Figure II.1. pGBKT7-MPFNY control experiments in Y2HGold cells. **A**. Toxicity and autoactivation control. SD/-Trp, plates for toxicity control. SD/-Trp/X-α-Gal and SD/-Trp/X-α-Gal/AbA, plates for autoactivation control. pGBKT7-53 and pGBKT7-Lam in Y2HGold with pGADT7-T in Y187 are the positive and negative controls of mating respectively. **B**. Expression control of pGBKT7-MPFNY transformed in Y2H Gold cells. Western Blot with extracted protein from Y2HGold cells transformed with pGBKT7-MPFNY (loading 15 or 30 µl). MP FNY (30.47 KDa) expression is indicated with (*). M indicates the Low Molecular Weight Protein Marker II (by Nzytech).

II.3.2.2.Small-scale mating

To test the system, a small-scale mating control was performed with pGADT7-T, in yeast Y187, grown together with either pGBKT7-Lam (negative control) or pGBKT7-53 (positive control), both in strain Y2HGold, following manufacturer's instructions. This control resulted in the presence of several (> 200) strong blue colonies in the positive control combination, while no colonies could be observed in the negative control combination in the restrictive plates (SD/-Trp/-Leu/AbA/X-alpha-Gal). Therefore, the mating system worked correctly. After passing all the controls, the Y2H library screening was performed.

II.3.2.3.Y2H screening

Y2H library screening was performed as explained in M&M section II.2.5.3. After 20h of mating, yeast diploid cells could be observed in the microscope, with differential interference contrast, indicating a successful mating (**Figure II.2**).

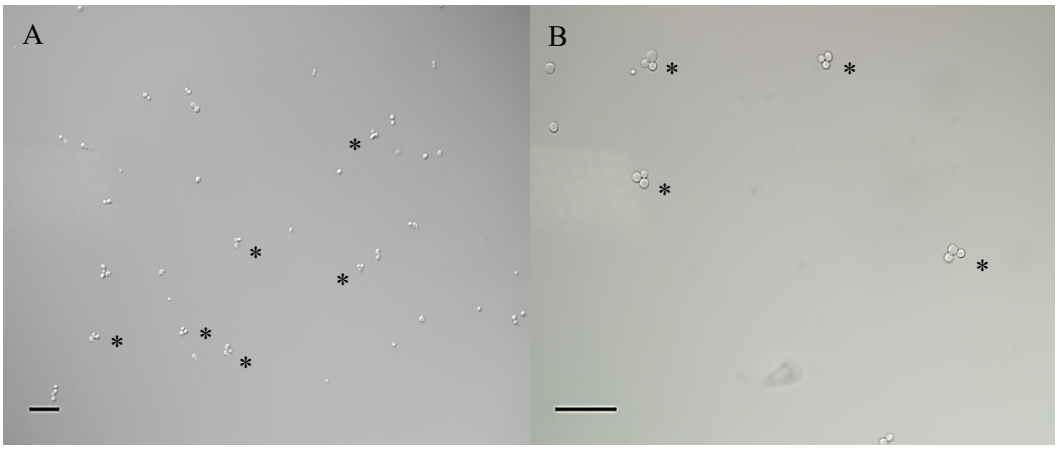

Figure II.2. Yeast diploid cells after 20 h mating. **A**. x200 and **B**. x400 amplification section images. Scale bars correspond to 50 µM. * indicates diploid mating cells.

From the Y2H screening, a total of 180 blue colonies were obtained in SD/-Trp/-Leu/X-alpha-Gal/AbA agar plates and the efficiency of mating was calculated from the control plates. The efficiency of mating was 3.55 %, which is the percentage of total diploid yeast

cells with respect to the total number of cells from the limiting partner, which are the prey library cells in this experiment (**Table II-4**). This efficiency lays within the expected ranges indicated in the manufacturer's protocol (2 – 5 %) (Matchmaker™ Gold Yeast Two-Hybrid System, Clontech by Takara, Japan).

Table II-4. Calculations of mating efficiency in Y2H screening with MP FNY as bait. The number of diploid cells is calculated from control dilution plates as well as prey library cells. Bold: total number of cells used to calculate the efficiency of mating.

Measurements	**Diploid cells in SD/-Trp/-Leu plates**	**Prey library cells (limiting partner) in SD/-Trp/-Leu plates**
Resuspension volume	13 ml	13 ml
Plating volume	100 µl	100 µl
Colonies grown	160	45
Dilution	100	10,000
Total number of cells	2,080,000	58,500,000

From the screening plates (SD/-Trp/-Leu/X-alpha-Gal/AbA), rescue of yeast colonies into successively more restrictive media allowed to reduce false positives. Plating the 180 screened colonies was performed in the following order: (i) first all colonies with either light or dark blue were plated in SD/-Trp/-Leu/X-alpha-Gal agar plates, that resulted in 134 blue colonies (white colonies were not further rescued), which were then plated in (ii) SD/-Trp/-Leu/X-alpha-Gal/AbA agar plates, where 46 blue colonies were selected and plated in (iii) the most restrictive media SD/-Trp/-Leu/X-alpha-Gal/AbA/-His/-Ade that allowed to have a final number of 30 blue colonies (**Figure II.3**). From these final colonies, plasmids were extracted, sequenced and BLASTed against *Cucumis melo L.* CM3.6.1 reference genome [https://www.melonomics.net, (Ruggieri et al., 2018)].

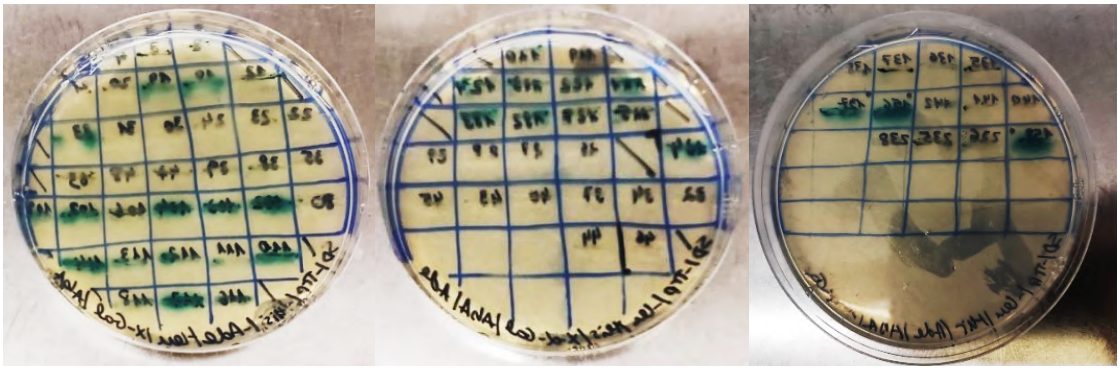

Figure II.3. Final selection of individual yeast colonies in Y2H screening with CMV-FNY MP as bait. All plates contain the most restrictive media (SD/-Trp/-Leu/X-alpha-Gal/AbA/-His/-Ade). True positive interactions of yeast cells grow forming blue colonies.

Finally, out of the 30 final colonies, a total of 6 different genes were identified (**Table II-5**):

(i) MELO3C022246.2.1 (2 colonies with the same sequence), encodes a Cytochrome P450 78A9-like, a monooxygenase that belongs to the cytochrome P450 family (Munro et al., 2007). This family of proteins contains enzymes which oxidize substances using iron. In plants, P450 cytochromes participate in metabolism of phytohormones and secondary metabolites (Mizutani, 2012; Lamb et al., 2019). *A. thaliana* homologous protein CYP78A9 is implicated in reproductive development. However, its specific way of action is still unknown (Sotelo-Silveira et al., 2013).

(ii) MELO3C013507.2.1 (22 colonies with the same sequence), encodes a Niemann-Pick C1 protein-like (CmNPC1) that belongs to the Patched domain-containing family, which is a small but very conserved family of proteins that function in the transport of sterol, sterol-modified proteins and lipids (Zhong et al., 2014). Interestingly, in Y2H screening all 22 colonies from MELO3C013507.2.1 aligned in the same region.

(iii) MELO3C005310.2.1 (3 colonies with the same sequence), encodes a ribose-5-phosophate isomerase A that plays a role in the pentose phosphate pathway and Calvin Cycle (Zhang et al., 2003). Its homologous protein in *A. thaliana* (AT1G71100.1) is involved in the formation of uridine used for the synthesis of UDP-sugars. Mutants of this gene are affected in cellulose biosynthesis (Howles et al., 2006).

(iv) MELO3C022211.2.1 (1 colony), encodes a polyneuridine-aldehyde esterase that catalyses the hydrolysis of methyl esters. Its homologous gene in *A. thaliana* (AT4G09900) encodes a carboxylesterase involved in jasmonic and salicylic acid metabolic processes and it is key to establish systemic spread of CMV in tobacco (Kim et al., 2008b). Moreover, MP from TMV binds a pectin methylesterase which is speculated to participate in cell-to-cell movement of viral ribonucleotide protein (vRNP) complexes (Chen et al., 2000).

(v) MELO3C001175.2.1 (2 colonies with the same sequence), encodes a Gluthation-S-transferase (GST) that belongs to the GST protein family, a large family of genes coding for enzymes well known for their participation in detoxification reactions in

the cell (Strange et al., 2001). In recent years they have been related to multiple roles in plant development, signalling, trafficking and stress (Kumar and Trivedi, 2018).

Table II-5. Y2H screening results. Genes identified after BLASTing the sequences found in the yeast clones. BLAST was performed in Melonomics website (https://www.melonomics.net/) using reference genome assembly CM3.6.1 of *Cucumis melo L.*

Gene Name	Melonomics CM4.0 ID	Position in CM4.0 reference genome	Nº colonies identified	Length of the interaction domain
cytochrome P450 78A9-like	MELO3C022246.2.1	chr11:32115888-32117903 (- strand)	2	327 bp
Niemann-Pick C1 protein-like	MELO3C013507.2.1	chr11:16247002-16290491 (+ strand)	22	1011 bp
Ribose-5-phosphate isomerase A	MELO3C005310.2.1	chr09:20361987.-20363522 (- strand)	3	338 bp
Polyneuridine-aldehyde esterase	MELO3C022211.2.1	chr09:229332-233980 (+ strand)	1	533 bp
Gluthation-S-transferase	MELO3C001175.2.1	chr0: 24168871-24169230 (+strand)	2	373

II.3.2.4.One-by-one Y2H

To confirm these results, one-by-one Y2H experiments were performed by co-culturing one yeast colony from each bait and prey combination and, after mating, plating the resulting culture in SD/-Trp/-Leu/X-α-Gal agar plates. Then, preferably blue colonies were rescued and plated in SD/-Trp/-Leu/X-alpha-Gal/AbA agar plates. In this confirmation, the candidate interacting domains were first confirmed with bait CMV-FNY MP and, if an interaction occurred, the same candidate domain was also tested in another one-by-one Y2H assay with MP from CMV-LS. Finally, only two of the proteins were confirmed: the interaction domain of MELO3C013507.2.1 (or CmNPC1) and the interaction domain of MELO3C005310.2.1 (*Cucumis melo L.* Ribose-5-phosphate isomerase A) (**Figure II.4**). The interaction domain of these two proteins (**Figure II.5**) were able to interact with both MPs (from CMV-FNY and CMV-LS), while the rest of the candidate proteins could not grow blue. Moreover, due to the interaction previously observed (Chapter I) between CMV MP and CmVPS41, we explored the possibility that CmNPC1 was also interacting with CmVPS41. For that purpose, a one-by-one Y2H experiment was performed between CmVPS41 (either from PS or SC) and the previously found CmNPC1 domain. Interestingly, a possible interaction (lighter blue) was found between CmNPC1 domain and CmVPS41s (from both melon cultivars, PS and SC) (**Figure II.4**) compared to the negative control (pGBKT7-Lam with pGADT7-T).

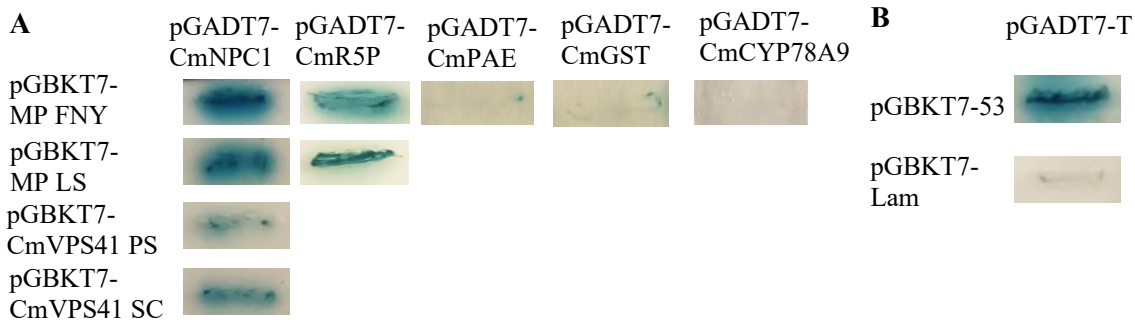

Figure II.4. One-by-one Y2H results. **A**. Y2H one-by-one confirmation of screened interacting protein domains. Each cell shows the results of Y2H interaction combination of prey in vector pGADT7 (column) per bait in vector pGBKT7 (row). Growth of a strong or light blue colony indicates interaction between prey and bait, whilst no growth or white colonies indicate no interaction. **B**. Controls of one-by-one Y2H are pGADT7-T (prey) in combination with either bait pGBKT7-53 (positive interaction) or bait pGBKT7-Lam (no interaction). CmR5P: *C. melo* Ribose-5-phosphate isomerase A, CmPAE: *C. melo* polyneuridine-aldehyde esterase, CmGST: *C. melo* Gluthation-S-transferase, CmCYP78A9: *C. melo* Cytochrome P450 78A9-like.

MELO3C013507.2.1

exon 25 (partial) — exon 26

CCACCATTATATTTTGTTGTGAAGGATTACAATTATAGCTCTAGATCTAGACAGACGAACCAGCTGTGCT
CCATCAGCCATTGTGATTCAAACTCCCTGTTGAATGAGATATCAAGAGCATCATTGACACCAGAGTTGAA — exon 27
CTACATTGCTAAACCAGCAGCATCATGGCTCGATGATTTTCTTGTCTGGTTGTCTCCAGAGGCATTTGGT
TGCTGCCGGAAATTTACAAATGGTTCTTATTGTCCTCCTGATGACCAGGTTTGACTCCATAGGTCTATTTT
CTTTCCTTGCCTATGCTTTATTTTACTACTGATGGTCGCACCTAGTCGTAAACTTCAGATTTTCTGCAAGCT
intron 27-28 CCGACTGTATATTTTCATCTAATACTGAATATAGTTCTTAAATGACCATAATTCTTCTCCATGATTCTATGT
CCCTCTAACATTGGTTGTCTTTTATACAATCGTCCAACCTGACACCACTTCATGATTAATGAAGTATGGCA
ATTTCTTTGTCCAGCCTCCCTGCTGTTTTCCAGATGAAGGTTTCTGTGACTCAAGCGAAGGAGTGTGCAG — exon 28
AGATTGTACAACTGTAAAGTTCTAATTTCTATTACATAGCTTTCAATACTCTAAGGCAGTATTTGGTATGT
GGTATGGTAGGGTAAGAAGCCTGAGAATTGGATAGACAGCTGTGTTTGGTACGTGGGATCAATTCTAA
intron 28-29 (partial) GTGTTTAGATTTCTTTTTATGGTCTATAGTAATCTACTTTTTTTTTTAATATAATAATTATTAAGAAAAGTTT
GCTTAGATTTGTTGGTAATATATAGTTTAATAAGTTGATTCATACTAATTTAAAATAACTATTTTAAGTTA
ATAACAAGTAATTTAATTAAGTAAAATGCACTTTATCCCCTGAGGTTTATAAATGGTTCTTGTTAAACGAT
AAAAAGAAAACACTAGTTTATGTGAAAAACCCTAAAACAA

MELO3C005310.2.1

exon 1

GGGGGAGGAGCCTTATGTCACGGATAATGAGAATTACATAGTGGATTTGTATTTCAAGAAAGATATT
GGCGATTTGAAGATCGCCAGTGATAGAATTTTACGGCTAGCCGGAGTTGTTGAACACGGTATGTTTCT
TGATATGGCTACTACAGTTATTATTGCAGGAGAGTCAGGGATGACAATAAAGAATAAGGAATTAGAA
CAATAACCCATTAAAGGGATGAGCTTAGATTCAATCTAGATATTATAAAATTTTGGTTCCGGAGAAATT
TAGAGATGAAGAAGAAAGAGTTTGGTTTCATAAAATCAAACCCTTTGATTATATAAACACCA

Figure II.5. DNA sequence of confirmed interaction domains found by Y2H. Exons are highlighted in yellow. Introns: not highlighted. Exons 25 and 27 are underlined to differentiate them from exon 26. MELOC013507.2.1 corresponds to CmNPC1. MELO3C005310.2.1 corresponds to CmR5P.

II.3.3. Interaction of CmNPC1 domain with MPs

To confirm *in vivo* the interactions between CmNPC1 domain with MPs and CmVPS41s, a Bimolecular Fluorescence Complementation (BiFC) assay was performed. CmNPC1 fused to the N-terminus of Yellow Fluorescent Protein (YFP) (CmNPC1-YN) was co-expressed in *N. benthamiana* leaves with either MPs (either LS or FNY) fused to the C-terminus of YFP (MP-YC) or CmVPS41 (from PS or SC) fused to C-terminus YFP (CmVPS41-YC), refer to M&M section II.2.6 for more information. After dexamethasone induction, reconstituted YFP could be seen, as a yellow colour, in the combination of CmNPC1-YN with both MP-YC, thus, the interaction between CmNPC1 domain and MPs was confirmed (**Figure II.6**). Moreover, the YFP signal observed resembles the MP location at plasmodesmata, as seen previously in Chapter I, as well as in previous results from this group (Guiu-Aragonés, 2014), which suggests that the interaction between CmNPC1 and MP LS or MP FNY takes place near or at the plasmodesmata (**Figure II.6**) where CMV-MP is localized (Guiu-Aragonés, 2014). However, *N. benthamiana* leaves co-expressing the MP-interacting domain of CmNPC1-YN together with any of the CmVPS41-YC failed to generate YFP signal, indicating that there is no "in vivo" interaction, although they had given a light blue signal in the Y2H experiments. However, given that here we have used only the MP-interacting domain, this does not preclude the possibility that CmVPS41 does interact with another domain of CmNPC1. All tested interactions were compared to the positive control, the interaction of *C. melo* Ascorbate Oxidase 4 (CmAO4-YN) with CMV-LS MP (MP LS-YC). This control was also used in Chapter I since Ascorbate Oxidase 4 from *Cucumis sativus L.* interacts with MP from CMV-SG strain [Accession number HE583224] (Kumari et al., 2016), which has 99 % sequence homology with MP from CMV-LS (both belong to CMV subgroup II). The empty vectors containing exclusively C-terminal YFP (YC) or N-terminal YFP (YN) resulted in the absence of YFP signal (**Figure II.7**), which indicates that reconstitution of YFP signal does not happen in absence of half of YFP sequence.

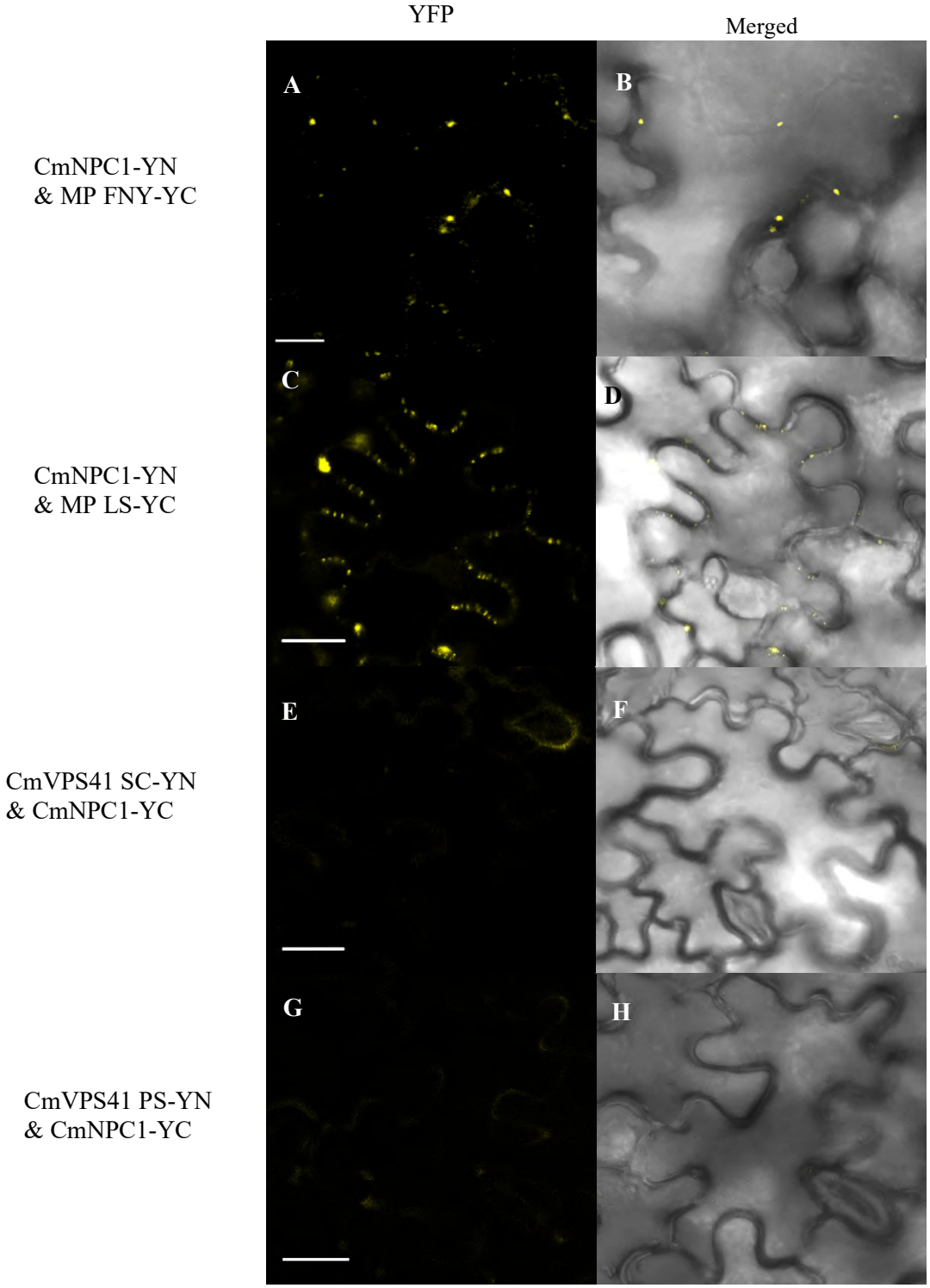

Figure II.6. In planta BIFC assay between CmNPC1 domain and CMV-MPs or CmVPS41s. 'Merged' channel corresponds to YFP and bright field channel merged. All scale bars correspond to 20 µm of length.

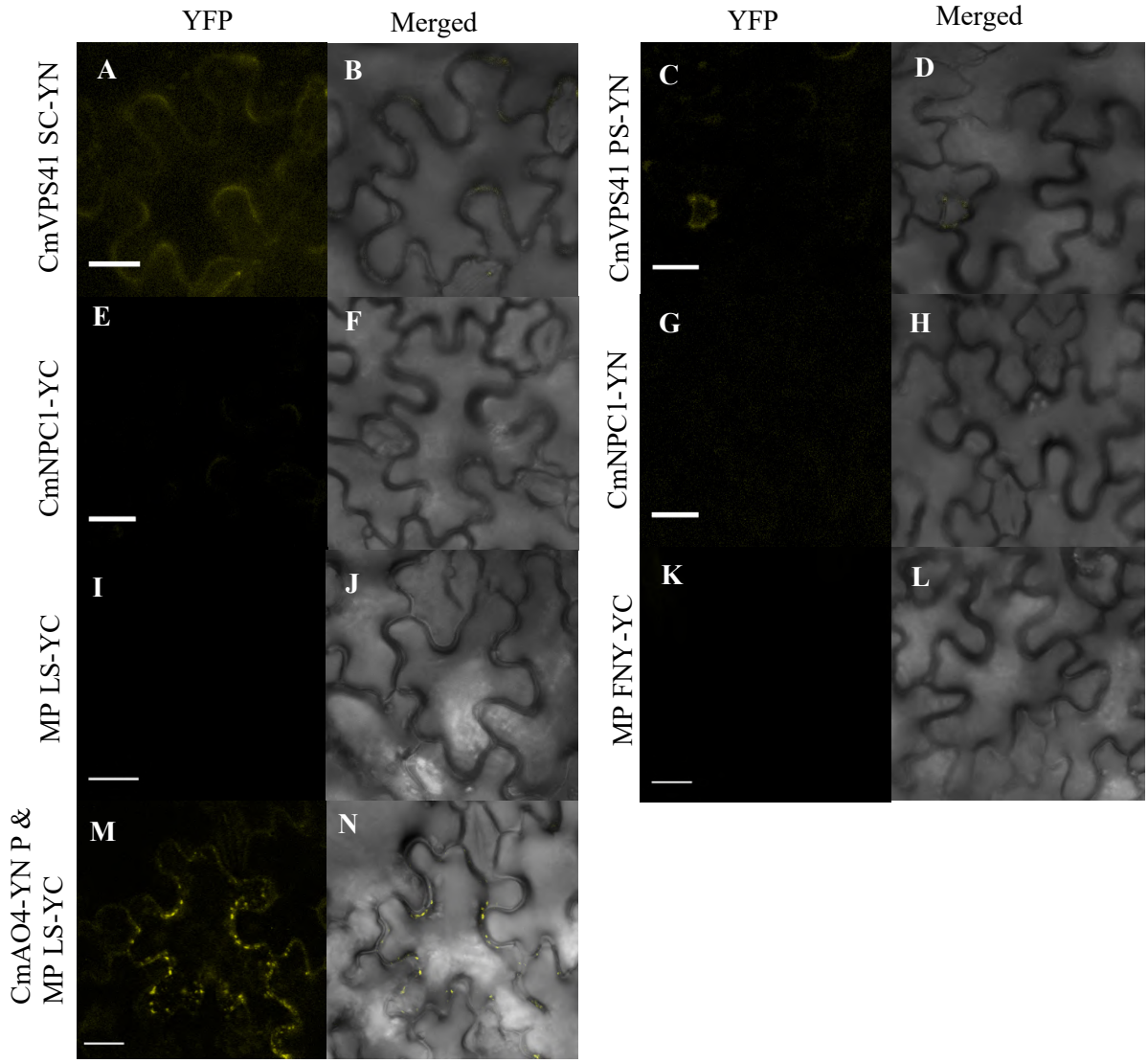

Figure II.7. Visualization of BIFC individual vectors as negative and positive controls. **M-N**. Z-stack of the positive control *Cucumis melo* Ascorbate Oxidase 4 (CmAO4-YN) interacts with MP LS (MP-LS-YC). 'Merged' channel corresponds to YFP and bright field channels merged. All scale bars lengths are 20 µM.

II.3.4. Analysis of CmNPC1 gene and its interaction domain

CmNPC1 (MELO3C013507.2.1, coordinates 16,247,002-16,290,491) maps in chromosome 11. It expands 43.49 Kb encoding a total of 39 exons and produces a coding sequence of 3,933 Kb (https://www.melonomics.net, (Ruggieri et al., 2018)] (**Figure II.8**A). CmNPC1 expression profile shows that, apart from the expression of exons, there are some regions of CmNPC1 gene that exhibit a certain level of expression from introns (arrow in **Figure II.8**B). In fact, both intron regions 26-27 and 27-28 have expression, although at the amplification in **Figure II.8**B only intron 27-28 is visible. CmNPC1 interaction domain was

identified from a PS cDNA library, being PS susceptible to CMV, thus, we searched for differences in CmNPC1 from both melon genotypes (**Figure II.8**C, D). Upon closer look, most of these polymorphisms were observed in intronic regions, therefore, not many differences should be expected at a protein level. Moreover, the reference genome in this region belongs to SC genotype, since no polymorphisms were present between SC and the reference genome. The polymorphisms found in the exons between both variants were further studied to verify their effect at the protein level.

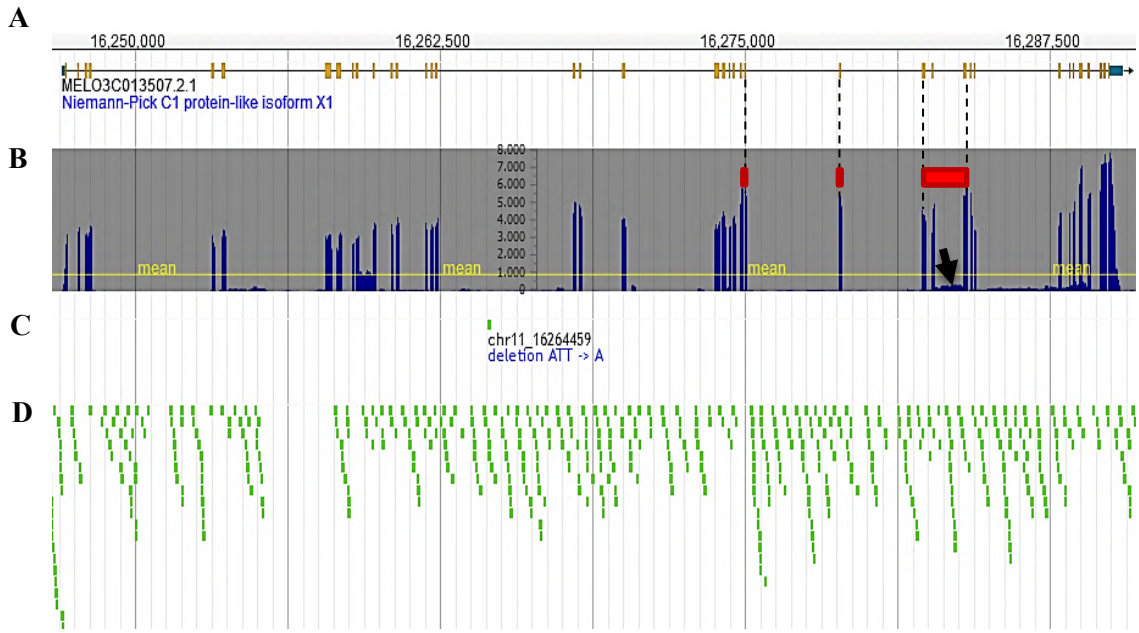

Figure II.8. CmNPC1 genomic region from *C. melo L.* reference genome CM3.6 [https://www.melonomics.net, (Ruggieri et al., 2018)]. **A**. *CmNPC1* genomic representation. Each yellow box represents an exon, each blue box represents a UTR, each black line connecting exons represents an intron **B**. RNA-sequencing data from Melonomics database CMV-MP interaction domain is marked in red boxes and the arrow indicates an intronic region 27-28 (within MP-interacting domain) with expression. Blue peaks represent RNA expression. **C**. *CmNPC1* SC variants compared with the reference genome. **D**. *CmNPC1* PS variants compared with the reference genome. Genomic variants are represented as green boxes.

Thus, to study if these polymorphisms could affect CmNPC1 protein or CmNPC1 interaction domain, both DNA sequences were translated with ExPASy translation tool and the protein sequences were aligned with ClustalW (Madeira et al., 2019). Four aminoacidic changes (F45S, A345T, R838L, G1029E) are found between CmNPC1 PS and SC (**Figure II.9**).

```
PS  1    MFLTRGGWMAFRLRFPISIFLLQMIFLVSMLMGGEALSVPVRSGFTFGERHAAEYCAMYD 60
SC  1    MFLTRGGWMAFRLRFPISIFLLQMIFLVSMLMGGEALSVPVRSGSTFGERHAAEYCAMYD 60

PS  61   ICGTRSDGKVLNCPYGSPSVKPDELFSAKIQSLCPTISGNVCCTEAQFETLRSQVQQAIP 120
SC  61   ICGTRSDGKVLNCPYGSPSVKPDELFSAKIQSLCPTISGNVCCTEAQFETLRSQVQQAIP 120

PS  121  LFVGCPACMRNFLNLFCELSCSPRQSLFINVTSIAEVGGSMTVDGIDYYVTEKFGKGLYD 180
SC  121  LFVGCPACMRNFLNLFCELSCSPRQSLFINVTSIAEVGGSMTVDGIDYYVTEKFGKGLYD 180

PS  181  SCKDVKFGTMNTRAIDFVGGGAKSFEELFAFLGQKVAPGFPGSPYSINFKVNPSKSSQME 240
SC  181  SCKDVKFGTMNTRAIDFVGGGAKSFEELFAFLGQKVAPGFPGSPYSINFKVNPSKSSQME 240

PS  241  LMNVSVYSCGDTSLGCSCGDCPSSPVCSSLEPPSPPKSNACTIKIWSLKISCIDFSITIL 300
SC  241  LMNVSVYSCGDTSLGCSCGDCPSSPVCSSLEPPSPPKSNACTIKIWSLKISCIDFSITIL 300

PS  301  YVIFISSFLGWALFHPTKENRGFSSREEPLLNIGDDGEIKSVNLAENENVTTEEHGVHLT 360
SC  301  YVIFISSFLGWALFHPTKENRGFSSREEPLLNIGDDGEIKSVNLTENENVTTEEHGVHLT 360

PS  361  VRNGVQLSTIQRYISNFYRDYGAWVARNPILVLCMSLSIVLILCVGLVCFKVETRPEKLW 420
SC  361  VRNGVQLSTIQRYISNFYRDYGAWVARNPILVLCMSLSIVLILCVGLVCFKVETRPEKLW 420

PS  421  VGHGSRAAAEKQFFDSNLAPFYRIEQLIIATKPGGKHDRAPRIVTEDNILLLFDIQNKVN 480
SC  421  VGHGSRAAAEKQFFDSNLAPFYRIEQLIIATKPGGKHDRAPRIVTEDNILLLFDIQNKVN 480

PS  481  ELVANYSGSVVSLNDICLKPLGEDCATQSILQYFKMNPENFDDYGGVEHAEYCFQHYTSS 540
SC  481  ELVANYSGSVVSLNDICLKPLGEDCATQSILQYFKMNPENFDDYGGVEHAEYCFQHYTSS 540

PS  541  ETCFSAFKAPLDPSTSLGGFFGSNYSEASAFVITYPVNNAIDAVGNENGKAIAWEKAFVK 600
SC  541  ETCFSAFKAPLDPSTSLGGFFGSNYSEASAFVITYPVNNAIDAVGNENGKAIAWEKAFVK 600

PS  601  LAKEELMPLVHSRNLTLSFSSESSIEEELKRESTADILTIAVSYLVMFAYISVALGDSNI 660
SC  601  LAKEELMPLVHSRNLTLSFSSESSIEEELKRESTADILTIAVSYLVMFAYISVALGDSNI 660

PS  661  SSSFYLSSKVLLGLSGVILVVLSVLGSVGFFSAIGIKSTLIIMEVIPFLVLAVGVDNMCI 720
SC  661  SSSFYLSSKVLLGLSGVILVVLSVLGSVGFFSAIGIKSTLIIMEVIPFLVLAVGVDNMCI 720

PS  721  LVHAVKRQPYELSLEDRISSALVEVGPSITLASLSEILAFAVGTFVPMPACRVFSLFAAL 780
SC  721  LVHAVKRQPYELSLEDRISSALVEVGPSITLASLSEILAFAVGTFVPMPACRVFSLFAAL 780

PS  781  AVLLDFILQLSAFVALIVLDILRAEDHRVDCFPCIKVHPHSDEPNQGFNQGRHGLLSRYM 840
SC  781  AVLLDFILQLSAFVALIVLDILRAEDHRVDCFPCIKVHPHSDEPNQGFNQGRHGLLSLYM 840
```

Figure II.9. ClustalW alignment between CmNPC1 PS and CmNPC1 SC amino acid sequences. Amino acid changes are highlighted in yellow. Amino acids from CmNPC1 interaction domain are highlighted in grey.

The effect of these aminoacidic changes was further analysed with PROVEAN (Choi and Chan, 2015) and the only polymorphism showing a strong deleterious effect was R838L (**Table II-6**). However, R838L appears 68 amino acids before the Y2H interaction domain instead of mapping inside the domain. Consequently, this polymorphism should not play any role in the resistance-susceptibility to CMV. In fact, the coding sequence within CmNPC1 PS interaction domain has the same amino acids in CmNPC1 SC.

Table II-6. CmNPC1 sequence polymorphism analysis using PROVEAN. Cut-off was considered for Provean scores under -2.5.

Amino acid position	Amino acid in CmNPC1 PS	Amino acid in CmNPC1 SC	Provean Score	Prediction (cutoff = -2.5)
45	F	S	0.869	Neutral
345	A	T	0.216	Neutral
838	R	L	-5.111	Deleterious
1029	G	E	2.271	Neutral

To further investigate CmNPC1, Phyre2 tool (Kelley et al., 2015) was used to predict CmNPC1 secondary structure and the three-dimensional prediction was displayed with Ezmol tool (Reynolds et al., 2018). In Phyre2 analysis, 89% of CmNPC1 sequence was modelled with a 100% confidence by the single highest scoring template which is the NPC1-like intracellular cholesterol transporter 1 (NPC1L1) from *Rattus norvegicus* crystallized in a complex with an ezetimibe analogue (6V3H PDB ID). NPC1L1 is a plasma membrane protein with lipid transporter activity and participates in sterol homeostasis (Sané et al., 2006). Additionally, during Phyre2 search for CmNPC1 homologous proteins with an available crystallographic model, we found two highly homologous NPC1 proteins, one from *Saccharomyces cerevisiae* (6r4l PDB ID) and a human NPC1 (3jd8 PDB ID), with a coverage of 84% of CmNPC1 sequence each. However, these models were not used due to their lower coverage rate compared to the crystallographic model from *Rattus norvegicus* (89%). Phyre2 predicted a total of 13 transmembrane helixes in the CmNPC1 protein both from PS and SC, although, these domains did not start nor finish in the same aminoacids. Phyre2 localizes the MP-interacting domain of CmNPC1 as an “extracellular” domain (as

named by the software) of the membrane in question (**Figure II.10**A). In Ezmol visualization CmNPC1 proteins had a very similar conformation (**Figure II.10**C).

TMHMM software (Krogh et al., 2001) was also used to compare with Phyre2 results (See M&M section II.2.8). This algorithm is used to predict transmembrane helices in protein sequences, and it has 97-98% accuracy according to its authors; however, it does not model in three-dimensions. TMHMM showed no major differences with Phyre2. It also predicted that CmNPC1 is part of a membranous organelle (**Figure II.10**B) and that CmNPC1 interaction domain is not part of any transmembrane domain. However, some minor differences should be noted. Whilst in Phyre2 prediction CmNPC1 PS and SC showed different starting amino acids for each transmembrane domain, in the case of TMHMM prediction, these differences were non-existent and both proteins had the same amino acids in each transmembrane domain. Moreover, CmNPC1 interaction domain was predicted to be "extracellular" of the membrane in Phyre2 and "intracellular" of the membrane in TMHMM. Although it is clear that CmNPC1 is in a membrane, none of these software can predict in which membranous organelle it is. CmNPC1 homologous protein in *A. thaliana* (At1g42470) is located in the plasma membrane and tonoplast (Feldman et al., 2015a), whereas human NPC1 is found in late endosome and lysosome membranes (Li et al., 2016; Wang et al., 2016).

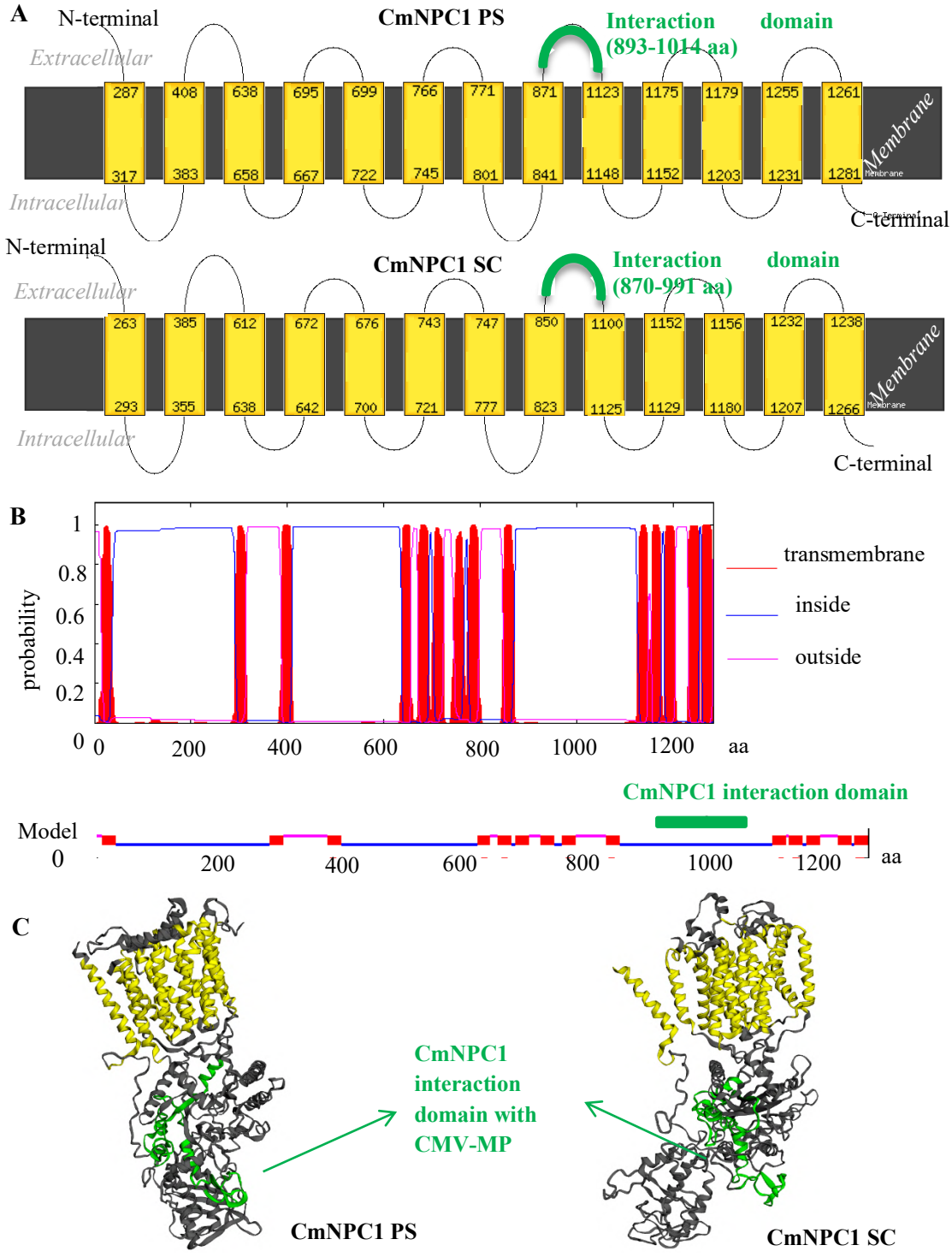

Figure II.10. CmNPC1 secondary structure analysis. **A**. Adapted image from Phyre2 predictions of CmNPC1 PS and SC transmembrane domains (yellow boxes) and the MP-interacting domain of CmNPC1 (green). **B**. Adapted image from TMHMM prediction about CmNPC1 probability of having transmembrane domains (red) or extramembrane domains facing inside (blue) or outside (pink) the membrane. A summary of this transmembrane model from CmNPC1s shows the MPs-interacting domain (green box). **C**. Comparison of CmNPC1 from PS and SC cultivars 3D structure from Phyre2 visualized with Ezmol tool. Transmembrane domains are depicted in yellow and MPs-interacting domain in green.

II.3.5. Alternative splicing in CmNPC1

As previously explained, all CmNPC1 colonies had the same MP-interacting domain. To see exactly the beginning and end of this domain, we did an alignment of the sequences with those of the vector pGADT7-Rec. From the alignment results (**Figure II.5**), we observed that CmNPC1 interacting domain starts in exon 25 (at least nucleotide 40 of that exon onwards) (**Figure II.11**A) and ends at the nucleotide 442 of intron 28-29 (**Figure II.11**B). However, it should be noted that the exact start of the CmNPC1 for now is still unknown since the first codon "CCA" at the start of it is common in pGADT7-Rec and exon 25 (**Figure II.11**A sequence without box). Therefore, CmNPC1 interaction domain includes partial exon 25, whole exons 26 and 27, intron 27-28, exon 28 and the initial 442 bp of intron 28-29.

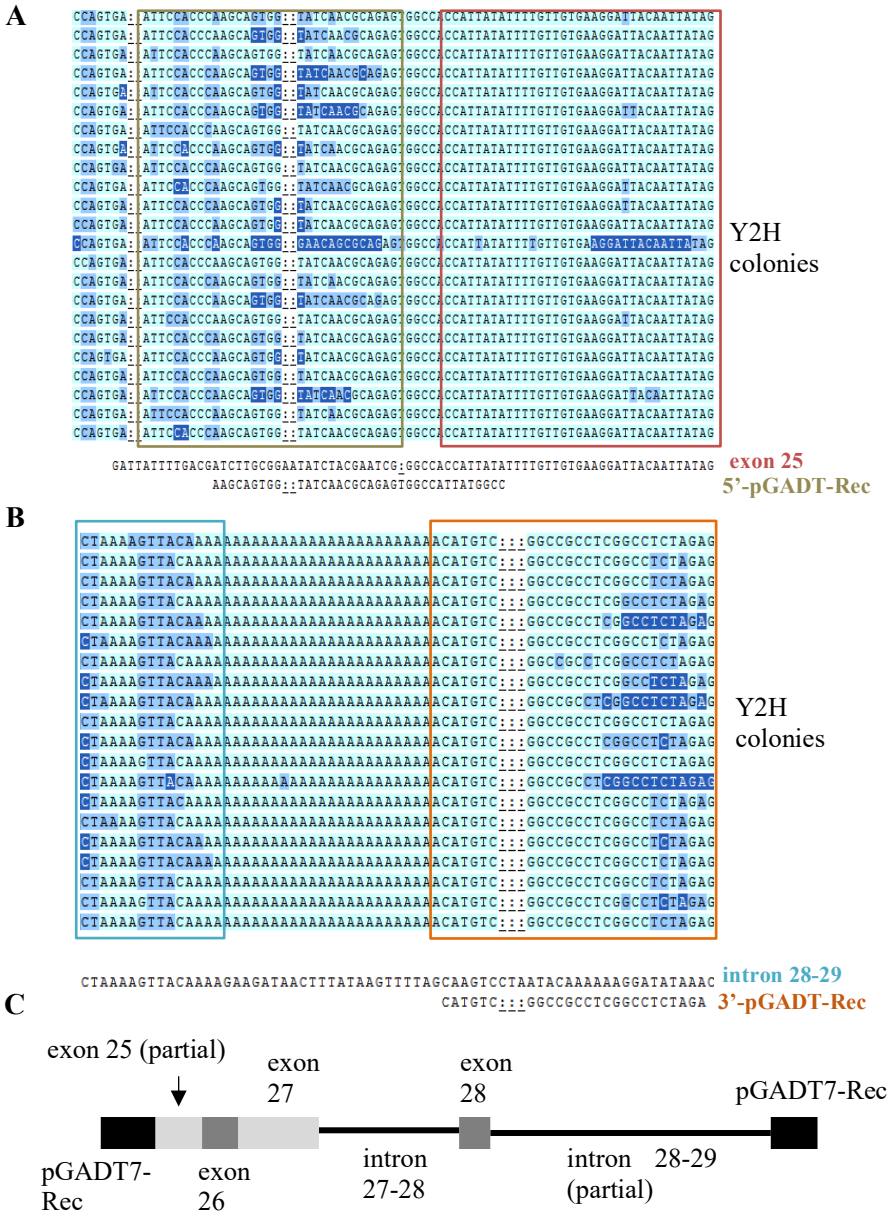

Figure II.11. Flaking regions of CmNPC1 interaction domain with CMV-MP. **A**. Alignment of 5' flanking region of CmNPC1 interaction domain with exon 25 from CmNPC1 and 5' flanking region from pGADT7-Rec. Confidence score of the sequence is indicated in highlighted blue (dark blue corresponds to confidence score <20, medium blue to midrange values and pale blue to confidence score >20 (according to Sequencher ® 5 series manual). **B**. Alignment of 3' flanking region from sequenced colonies with intron 28-29 and 3' flanking region of pGADT7-Rec. **C**. Representation of the interaction domain of CmNPC1. Grey boxes represent exons, black lines connecting exons represent introns and black boxes represent pGADT7 vector.

Analysis of the intron retention

As CmNPC1 interaction domain presents several introns, this suggests that introns could be important for the interaction between CmNPC1 and CMV-MP. However, these introns have stop codons. Therefore, we studied if those introns really exist in the mRNA pool of the infected melon cells. To do so, several PCR amplifications were performed with cDNA from PS, PS infected with CMV-FNY, SC and SC inoculated with CMV-FNY. A total of four PCRs using different primer combinations were used to study intron retention in the whole CmNPC1 RNA encoded in the interacting domain (**Figure II.12**).

A

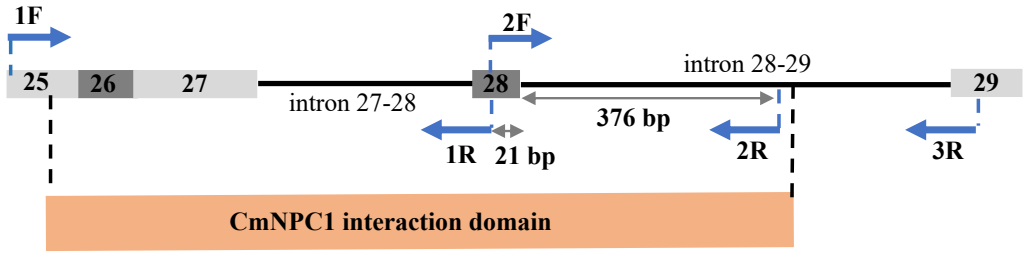

B

Primers	Genomic length	Length exons	Length domain
1F-1R	35,682 bp	317 bp	569 bp
1F – 2R	8,061 bp	-	953 bp
1F – 3R	8,919 bp	339 bp	-
2F– 2R	397 pb	-	397 pb

Figure II.12. PCR details to determine CmNPC1 intron retention. **A**. Representation of CmNPC1 region to be amplified and the primers used. Blue arrows: primers. Orange box: CmNPC1 MP-interaction domain. Grey boxes: exons. Black lines: introns. **B**. Details of the DNA amplification length by each different primer combination. The genomic length (introns plus exons) is shown in the second column. The 3rd column shows the amplified nucleotide if only exons were present in the cDNA, whilst the 4th column shows the length of amplified bp if cDNA was as expected in CmNPC1 interaction domain. If there is no possible amplification is indicated with a hyphen (-).

Combinations of primers 1F-1R, 1F-2R and 2F-2R were used to amplify the two introns within CmNPC1 interaction domain. Amplification with primers 1F and 1R (**Figure II.12**) was designed to amplify intron 27-28. In this case, a band of 569 bp, corresponding to intron 27-28 together with exons 25-28 (until primer 1R), was expected if the intron was retained, whereas a 317 bp band would be observed if the intron was spliced. As observed in **Figure II.13**A, a 569 bp was found in all samples. This indicated that intron 27-28 was present in the RNA pool of the melon plants, both infected or not. As expected, the spliced mRNA (317 bp) was also observed in all samples, which indicates that both forms of the mRNA, spliced and not spliced, are present in melon RNA pool of infected and non-infected melon plants. Also, larger secondary bands were observed, which might correspond to retention of other introns that are not part of CmNPC1 interaction domain with MP, such as intron 25-26 or 26-27 or might be contaminant amplified bands. Amplification with primers 1F and 2R (**Figure II.13**B) attempted to amplify both introns (27-28 and partial intron 28-29). If both introns were present, an expected band of 953 bp should be observed. In fact, a 953 bp band was found in most samples (**Figure II.13**B), which would correspond to retention of intron 27-28 and 376 bp of intron 28-29 (until primer 2R) together with exons 25, 26, 27 and 28 (see **Figure II.12**A). This indicates that, at least partial intron 28-29 is present in the RNA pool of non-infected melon plants, as well as PS CMV-FNY infected plants. However, no amplification could be observed in SC inoculated with CMV-FNY, but this could be a technical problem since for most combinations this sample amplifies weakier than the others. In the same manner, amplification with primers 2F and 2R was used to corroborate the presence of partial intron 28-29. This amplification resulted in the presence of 397 bp which corresponds to end of exon 28 (the last 21 nucleotides) plus partial intron 28-29 (until primer 2R) (**Figure II.13**D). Amplification with primers 1F-3R covers from exon 25 to exon 29, and a 339 bp band should be observed if all introns were spliced (**Figure II.13**C). As expected, a 339 bp band appeared. This indicates that primer 3R was detecting fully spliced CmNPC1 mRNA. As in other amplifications in this case, larger molecular weight bands were also observed, which could indicate retention of some introns of this region of might be unspecific bands. To sum up, introns from CmNPC1 interacting domain are also found usually in melon mRNA pool. Another question would be if these introns do translate. In fact, considering the analysis of CmNPC1 interaction domain clone identified by Y2H, at the end of the interaction domain there is a polyadenylated tail (**Figure II.11**B), which, in theory, would indicate that translation might happen. However, in the first intron there is

already the first stop codon, and a total of 17 stop codons (6 in intron 27-28 and 10 in intron 28-29) are found throughout its sequence. Thus, the implications of these introns and stop codons in CmNPC1 transcripts and their functionality should be investigated in future studies.

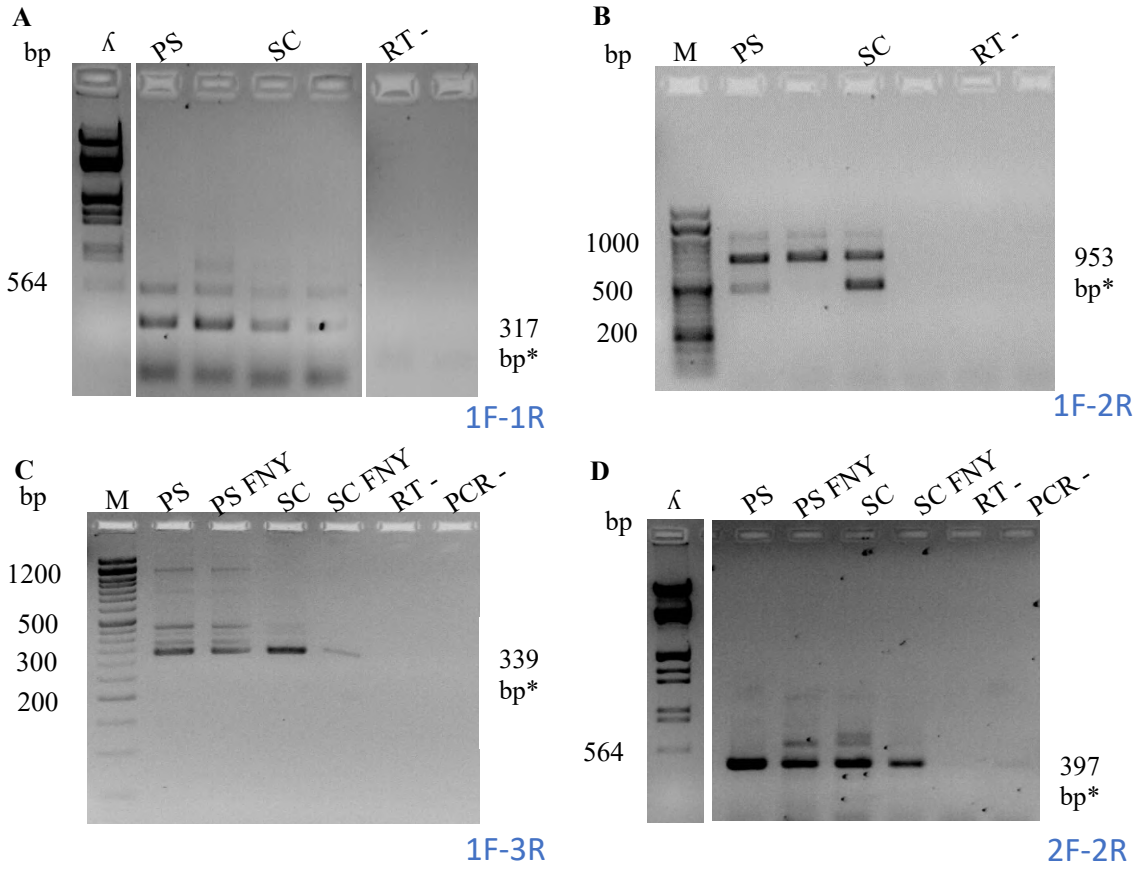

Figure II.13. Amplification of CmNPC1 cDNA to detect intron retention. **A**. cDNA amplification with primers 1F and 1R (exon 25 to exon 28). The three images correspond to the same gel although picture was split. **B**. cDNA amplification using primers 1F and 2R (from exon 25 until intron 28-29). **C**. cDNA amplification with primers 1F and 3R (from exon 25 until exon 29). **D**. cDNA amplification with primers 2F and 2R (from exon 28 until intron 28-29). The two images correspond to the same gel although picture was split. Amplified bands that correspond to exons exclusively are indicated with a star (*). In blue the combination of primers is shown. PS: Piel de Sapo. PS FNY: PS infected with CMV strain FNY. SC: Songwhan Charmi. SC FNY: SC inoculated with CMV FNY. RT - negative control for retro-transcription, without RT. PCR - : negative control for PCR, without Taq polymerase. Molecular weight markers are either *EcoRI-HindIII* digested lambda (λ) DNA or a 50 bp (M) weight marker.

II.3.6. CmNPC1 in the genomic context

The BLAST from Y2H colonies only found one hit for the CmNPC1 interaction domain and it belonged to MELO3C013507.2.1 in chromosome 11 (**Table II-5**). However, there is another CmNPC1 in *C. melo* genome: MELO3C017027.2.1. MELO3C017027.2.1 is found in chromosome 7 (chr07:335,236-350,471) and it expands 15,236 bp. Both proteins have 68% of sequence identity (**Figure II.14**). In the putative interaction domain of CmNPC1 from chromosome 7 the sequence identity of the exons increases to 78 %. However, as expected, the introns are very different in both CmVPS41 (I. Villar, personal communication). Thus, MELO3C017027.2.1 should not interact with CMV MP, since overall, the homology within the interaction domain is very low. At tissue level, expression is also different, while CmNPC1 from chromosome 11 is expressed and in leaves and highly expressed, in mature fruits, CmNPC1 from chromosome 7 is highly expressed mainly in petals [https://melonet-db.dna.affrc.go.jp/ap/mvw, (Yano et al., 2018, 2020)].

A

Score	Expect	Method	Identities	Positives	Gaps
1812 bits(4693)	0.0	Compositional matrix adjust.	882/1289(68%)	1072/1289(83%)	15/1289(1%)

```
Query  9     MAFRLRFPISIFLLQMIFLVSMLMGGEALSVPVRSGSTFGERHAAEYCAMYDICGTRSDG  68
             M  RL F +SI+LLQ++  V +        + + +  T GE+H+  YC MY IC  R DG
Sbjct  1     MRLRLGFILSIYLLQVLCFVLVYAEMSNTRLQLSTNGTSGEKHSEGYCVMYGICAKRPDG  60

Query  69    KVLNCPYGSPSVKPDELFSAKIQSLCPTISGNVCCTEAQFETLRSQVQQAIPLFVGCPAC  128
             K LNCP G+PSV+PD L S+KIQSLCPTI+GNVCCTE QF+TLRSQV QAIP  VGCPAC
Sbjct  61    KALNCPTGAPSVQPDNLLSSKIQSLCPTITGNVCCTEQQFDTLRSQVMQAIPFLVGCPAC  120

Query  129   MRNFLNLFCELSCSPRQSLFINVTSIAEVGGSMTVDGIDYYVTEKFGKGLYDSCKDVKFG  188
             +RNFLNLFCEL+CSP QSLFINVTS+ +V  S+TVD IDYYV + FG+GLY+SCKDVKFG
Sbjct  121   LRNFLNLFCELTCSPNQSLFINVTSVLKVNNSLTVDAIDYYVADAFGEGLYESCKDVKFG  180

Query  189   TMNTRAIDFVGGGAKSFEELFAFLGQKVAPGFPGSPYSINFKVNPSKSSQMELMNVSVYS  248
             TMNTRA+ F+G  AK+F+E FAF+G++  PG PGSPY+I F    S SS M+ MN S YS
Sbjct  181   TMNTRAMQFIGADAKNFKEWFAFIGKQAGPGLPGSPYAIGFPSTVSVSSGMKHMNASAYS  240

Query  249   CGDTSLGCSCGDCPSSPVCSSLEPPSPPKSNACTIKIWSLKISCIDFSITILYVIFISSF  308
             CGDTSLGCSCGDCPS+PVCS+   P   +  +C+++I SLK+ C+DF++ ILY I  S+F
Sbjct  241   CGDTSLGCSCGDCPSAPVCSTTATPVFHRKKSCSVRIGSLKVKCVDFTLCILYFIIASAF  300

Query  309   LGWALFHPTKENRGFSSREEPLLNIGDDGEIKSVNLTENENVTTEEHGVHLTVRNGVQLS  368
             LGW+LF+  K  +  SS  + + NI D G + S    ++E++  +       +R+ +QLS
Sbjct  301   LGWSLFY-RKSQKSLSSGTKTMPNIMDGGSLHSATRQKDESLPMQMLEDAPQIRSRIQLS  359
```

B

Score	Expect	Identities	Gaps	Strand
220 bits(243)	3e-61	227/290(78%)	13/290(4%)	Plus/Plus

```
Query  7     ATCTAGACAGACAAACCAGCTGTGCTCCATCAGCCATTGTGATTCAAACTCCCTGTTGAA  66
             ||| |||||||||||||  | |||||||||| || ||||| ||| |||| || || ||
Sbjct  280   ATCAAGACAGACAAACCAATTATGCTCCATCAGTCAATGTGACTCAGACTCTCTTTTAAA  339

Query  67    TGAGATATCAAGAGCATCATTGACACCAGAGTTGAACTACATTGCTAAACCAGCAGCATC  126
             ||||||  ||| ||| ||| | | |||||||| ||  | |||||| |||||||| || ||
Sbjct  340   TGAGATTGCAAAAGCTTCACTAATACCAGAGTCGAGTTTCATTGCCAAACCAGCTGCTTC  399

Query  127   ATGGCTCGATGATTTTCTTGTCTGGTTGTCTCCAGAGGCATTTGGTTGCTGCCGGAAATT  186
             |||||| ||||||| |||||| ||| | ||||| || |||||||| ||||| ||||| ||
Sbjct  400   ATGGCTTGATGATTATCTTGTGTGGATATCTCCCGAAGCATTTGGATGCTGTCGGAAGTT  459

Query  187   TACAAATGGTTCTTATTGTCCTCCTGATGACCAGCCTCCTTGCTGT-TTTC---CGGATG  242
              ||||||||   |||||| |||||||||||| ||||| |||||||||  |||   ||| ||
Sbjct  460   CACAAATGGGAGTTATTGCCCTCCTGATGATCAGCCCCCTTGCTGTACTTCAAGCGG-TG  518

Query  243   AAGGT--TTC-TGT-GACTCAAGCGAAGGAGTGTGCAGAGATTGTACAAC  288
               |||  ||| ||| | || |    | ||||| |||| ||||||||||||
Sbjct  519   GTGGTGATTCTTGTGGTCTGA----ACGGAGTATGCAAAGATTGTACAAC  564
```

Figure II.14. Identity between both CmNPC1 in the *C. melo* genome. **A**. Whole protein identity. **B**. Nucleotide identity of exons within the interaction domain (without introns). Protein BLAST was performed with blastp. Protein BLAST performed with blastp from NCBI resources (Villar et al., unpublished).

II.3.7. Finding MP interacting proteins using Immunoprecipitation coupled to Mass Spectrometry analysis

An immunoprecipitation (IP) assay coupled to mass spectrometry was also used to find CMV-MP interacting proteins in melon. This is another *in vivo* method to detect Protein-Protein Interactions (PPI) which easily allows to screen different samples.

II.3.7.1. Optimization of Immunoprecipitation

We aimed at optimizing the IP for our non-commercial anti-MP antibody (Guiu-Aragonés, 2014) through testing: (i) different times of incubation of the protein extract with the antibody coupled to the beads, either 2h or overnight, and (ii) different dilutions of anti-MP antibody (Guiu-Aragonés, 2014), either 1/300 or 1/60. Results were visualized through Western Blot using the specific anti-MP antibody (1:5000 dilution). Concerning the incubation time, stronger binding of the antibody to the movement protein was observed with a 2 h incubation, whilst in overnight incubation the binding of the antibody to the beads decreased (**Figure II.15**A). In the antibody dilution, although 1/60 anti-MP dilution in the IP showed higher concentrations of MP, it also carried more contaminant proteins. Conversely, the use of dilution 1/300, allowed less movement protein eluted in the flow-through but retained less contamination (**Figure II.15**B). Finally, after digestion of the immunoprecipitated proteins into peptides, samples from the 1/300 anti-MP dilution had a higher peptide concentration (see table in **Figure II.15**B), which also correlated with the amount of hits (proteins) detected in the mass spectrometer. Thus, for all IPs, 1/300 anti-MP antibody dilution and 2 h incubation with the protein extract were used.

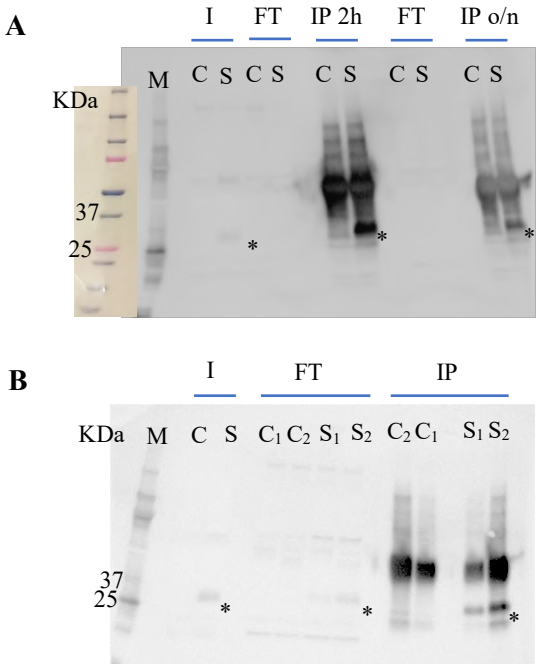

Sample ID	Peptide concentration
C1	0.047 mg/ml
S1	0.057 mg/ml
C2	0.021 mg/ml
S2	0.012 mg/ml

Figure II.15. IP coupled to Western Blot to test antibody incubation time and dilution. Each lane of the blot contains 20 µl of the immunoprecipitated solution. **A**. Western Blot from IP to test antibody incubation time. Protein extracts from PS non-inoculated (C) and CMV-FNY infected PS plant (S) were incubated with the antibody solution either 2 hours (IP 2h) or overnight (IP o/n). **B**. Western Blot from IP and table of peptide concentration after digestion with lysine to test anti-MP antibody dilution. C_1 and S_1: dilution 1/300; S_2 and C_2: dilution 1/60 (Guiu-Aragonés, 2014). Flowthrough (FT); Input (I); molecular weight ladder (M) Precision Plus Protein Dual Xtra Strands (Biorad); Asterik (*) indicates the bands that correspond to CMV-FNY MP (30.47 KDa).

II.3.7.2.Immunoprecipitation screening

To identify MP interacting proteins both at local stage, before reaching the phloem, and at systemic infection stage, plants from three genotypes, PS (susceptible to both strains), SC (resistant to both strains) and the NIL 12-1-99 (resistant to CMV-LS and susceptible to CMV-FNY), were rub-inoculated, at the cotyledon stage, either with CMV FNY, CMV-LS or mock-inoculated. Samples from inoculated cotyledons were taken at 4 dpi to analyse the interacting proteins at the level of local infection, and samples of new leaves, infected or not, were taken at 15 dpi to analyse interacting proteins at systemic infection. For each condition, four biological samples were taken for analysis through IP (**Table II-7**).

Table II-7. *C. melo* IP samples. Sample collection column, local: samples collected at 4 dpi; systemic: samples collected at 15 dpi. Hyphen indicates no data for mock-inoculated samples.

Melon genotype	CMV strain	Local resistance	Systemic resistance	Sample collection
PS	CMV-LS	S	S	local
SC	CMV-LS	S	R	local
NIL12-1-99	CMV-LS	S	R	local
PS	CMV-LS	S	S	systemic
SC	CMV-LS	S	R	systemic
NIL12-1-99	CMV-LS	S	R	systemic
PS	CMV-FNY	S	S	local
SC	CMV-FNY	S	R	local
NIL12-1-99	CMV-FNY	S	S	local
PS	CMV-FNY	S	S	systemic
SC	CMV-FNY	S	R	systemic
NIL12-1-99	CMV-FNY	S	S	systemic
PS	mock	-	-	local
SC	mock	-	-	local
NIL12-1-99	mock	-	-	local
PS	mock	-	-	systemic
SC	mock	-	-	systemic
NIL12-1-99	mock	-	-	systemic

For each sample, four biological replicates were processed and immunoprecipitated with the anti-MP attached beads, as indicated in M&M sections II.2.9.1 and II.2.9.2. The detected interacting proteins were filtered, log2 transformed and considered statistically relevant if they had a log2 value > 2 and were able to overcome at least one of the following statistic tests (refer to M&M section II.2.9.5 for more information): (i) a two-sample t-test with an FDR of 5 %, (ii) a Volcano Plot with FDR of 5 % and an S0=2 or (iii) counted-based test in which the protein was detected in four CMV-inoculated replicates, while absent in the four mock-inoculated replicates. A total of 131 *C. melo* candidate interacting proteins of CMV-MP were obtained: 68 candidate proteins in systemic infection (**Table II-8**) and 61 candidate proteins in local infection (**Table II-9**). At first glance, it can be seen that two candidate interacting proteins were found repeatedly in both infections: MELO3C021648.2.1, a Heat Shock 70 kDa protein, that is later explained into detail in section II.3.7.3, and MELO3C021648.2.1; a Mitochondrial carrier protein, which does not seem to have any relevance to CMV infection, thus, it was not considered for further validation in this thesis.

Table II-8. *C. melo* CMV-MP statistically significant candidate interacting proteins identified in CMV systemic infection. NA indicates no homologous protein was found between *C. melo* protein and *A. thaliana*.

***C. melo* ID**	***C. melo* name**	**E-value BLAST**	***A. thaliana* ID**	**Experiment**					
				PS		**SC**		**NIL12-1-99**	
				LS	**FNY**	**LS**	**FNY**	**LS**	**FNY**
MELO3C009509.2.1	40S ribosomal protein S17-like	3E-78	AT5G04800.1						X
MELO3C009349.2.1	Cell division cycle protein 48 homolog	0	AT3G53230.1						X
MELO3C003119.2.1	Heat shock 70 kDa protein 2	0	AT5G02500.1	X					
MELO3C018459.2.1	40S ribosomal protein S16	9E-92	AT2G09990.1						X
MELO3C015184.2.1	MP domain-containing protein	NA	NA	X	X				X
MELO3C018880.2.1	Glycine-rich protein	NA	NA						X
MELO3C009036.2.1	40S ribosomal protein S25	9E-56	AT2G21580.1						X
MELO3C027652.2.1	30S ribosomal protein S8	6E-30	ATCG00770.1			X			
MELO3C005706.2.1	40S ribosomal protein S10-1	4E-77	AT5G52650.1						X
MELO3C021648.2.1	Heat shock 70 kDa protein	0	AT3G12580.1	X					
MELO3C024461.2.1	Cell division cycle protein 48 homolog	0	AT3G53230.1						X
MELO3C000680.2.1	Tetraspanin family protein	2E-24	AT2G23810.1		X				
MELO3C000003.2.1	Stress-related ozone-induced family protein	4E-40	AT1G01170.1						X
MELO3C014654.2.1	Peroxidase	5E-111	AT5G06720.1	X	X				
MELO3C022303.2.1	Protein curvature Thylakoid 1B	9E-57	AT2G46820.1			X	X		
MELO3C021658.2.1	Heat shock 70 kDa protein	0	AT3G12580.1	X					
MELO3C005446.2.1	60S ribosomal protein L13	9E-120	AT3G49010.1		X				
MELO3C024359.2.1	40S ribosomal S3-like protein	4E-152	AT5G35530.1						X
MELO3C022138.2.1	Protein disulfide isomerase (PDI)-like protein 2	0	AT1G60420.1	X					
MELO3C004955.2.1	4-coumarate:CoA ligase-like protein	0	AT4G05160.1	X					
MELO3C019528.2.1	Glycosyltransferase	0	AT4G34131.1	X					
MELO3C005832.2.1	Cucumisin-like isoform X1	0	AT5G59100.1	X					
MELO3C000108.2.1	50S ribosomal protein L16, chloroplastic	2E-74	ATCG00790.1			X	X		
MELO3C006297.2.1	RNA recognition motif (RRM) containing protein	0	AT3G23900.2						X
MELO3C018796.2.1	Cysteine-rich receptor-kinase-like protein	3E-73	AT3G22060.1		X				X

MELO3C002388.2.1	Calnexin homolog	0	AT5G61790.1							X
MELO3C012008.2.1	Serine/arginine-rich splicing factor RSZ21	1E-56	AT1G23860.1		X					
MELO3C014635.2.1	Lipoxygenase	0	AT3G45140.1	X	X					
MELO3C016378.2.1	Peptidyl-prolyl cis-trans isomerase	3E-69	AT2G18040.1	X						
MELO3C004385.2.1	Pathogenesis-related protein PR-4-like	2E-57	AT3G04720.1	X						
MELO3C023694.2.1	Pathogen-related protein	7E-76	AT1G78780.2	X						
MELO3C005284.2.1	RNA-dependent RNA polymerase	0	AT1G14790.1	X						
MELO3C009383.2.1	Thaumatin-like protein 1a	2E-85	AT1G19320.1	X						
MELO3C024423.2.1	Receptor-like protein kinase	0	AT1G51800.1	X	X					
MELO3C011236.2.1	Peptidyl-prolyl cis-trans isomerase	3E-88	AT4G32420.1			X	X			
MELO3C011393.2.1	Thioredoxin-like protein CITRX	4E-80	AT3G06730.1					X		
MELO3C005257.2.1	RNA-dependent RNA polymerase	0	AT1G14790.1	X						X
MELO3C006032.2.1	Oxygen-evolving enhancer 3-2, chloroplastic-like	3E-69	AT1G14150.1			X	X			
MELO3C019585.2.1	Cytochrome P450 family cinnamate 4-hydroxylase	0	AT2G30490.1							X
MELO3C003985.2.1	30S ribosomal protein S7	1E-24	ATCG01240.1					X		
MELO3C009864.2.1	Cytochrome P450 CYP72A219-like	0	AT3G14610.1							X
MELO3C011498.2.1	Splicing factor u2af large subunit, putative	0	AT4G36690.1			X	X			
MELO3C001113.2.1	U4/U6 small nuclear ribonucleoprotein Prp3	NA	NA		X					
MELO3C024257.2.1	Protein curvature Thylakoid 1C, chloroplastic	9E-45	AT1G52220.1			X	X			
MELO3C014630.2.1	Lipoxygenase	0	AT3G45140.2							X
MELO3C017383.2.1	Strictosidine synthase	0	AT1G08470.1							X
MELO3C016781.2.1	Cysteine proteinase	0	AT1G47128.1	X						
MELO3C022382.2.1	Succinate--CoA ligase [ADP-forming] subunit beta	0	AT2G20420.1	X						
MELO3C016748.2.1	Protein TIC 22	7E-130	AT4G33350.1					X		
MELO3C008800.2.1	Casein kinase	0	AT3G03940.1	X						
MELO3C002447.2.1	L-ascorbate oxidase homolog	0	AT4G22010.1			X				X
MELO3C020966.2.1	Mitochondrial carrier protein, putative	0	AT4G39460.1			X	X			
MELO3C011277.2.1	Flotillin-like protein 1	0	AT5G25250.1							X
MELO3C016002.2.1	Arginine/serine-rich splicing factor	6E-107	AT1G02840.1			X				
MELO3C018517.2.1	Vacuolar-sorting receptor-like protein	0	AT2G14740.1		X					

MELO3C011952.2.1	UDP-galactose:fucoside alpha-3-galactosyltransferase	5E-161	AT1G70630.1			X	X		
MELO3C007358.2.1	Receptor-like protein kinase	0	AT4G21410.1		X				
MELO3C020639.2.1	ATP synthase subunit alpha	8E-50	ATG01190.1				X		
MELO3C004307.2.1	UPF0603 protein	3E-148	AT1G54780.1			X			
MELO3C023630.2.1	ADP-ribosylation factor-like	2E-134	AT1G10630.1						X
MELO3C025065.2.1	Protein TIC 40	4E-124	AT5G16620.1			X			
MELO3C007698.2.1	Serine hydroxymethyltransferase	0	AT4G37930.1				X		
MELO3C017011.2.1	ATP-dependent zinc metalloprotease FTSH, chloroplastic	0	AT1G50250.1				X		
MELO3C021122.2.1	Nucleolar pre-ribosomal-associated protein	0	AT4G27010.2				X		
MELO3C014627.2.1	Lipoxygenase	0	AT3G45140.1			X	X		
MELO3C007483.2.1	ABC transporter family protein	0	AT5G64840.1			X			
MELO3C006948.2.1	Protein SGT1 homolog	2E-159	AT4G11260.1		X				
MELO3C002878.2.1	Elongation factor 1-alpha	0	AT5G60390.1						X

Table II-9. *C. melo* CMV-MP statistically significant candidate interacting proteins in CMV local infection. NA indicates no homologous protein was found between *C. melo* protein and *A. thaliana*.

***C. melo* ID**	***C. melo* name**	**E-value BLAST**	***A. thaliana* ID**	**Experiment**					
				PS		**SC**		**NIL12-1-99**	
				LS	**FNY**	**LS**	**FNY**	**LS**	**FNY**
MELO3C008060.2.1	Photosystem I reaction center subunit N	2.45E-55	AT5G64040.2				X		
MELO3C000173.2.1	Photosystem II CP43 reaction center protein	2.59E-133	ATCG00280.1				X		
MELO3C007091.2.1	Photosystem I reaction center subunit psaK	3.01E-67	AT1G30380.1		X				
MELO3C032881.2.1	Chlorophyll a-b binding protein	3.84E-175	AT2G34430.1		X				
MELO3C008731.2.1	Photosystem I reaction center subunit XI	7.5E-102	AT4G12800.1	X	X				
MELO3C012713.2.1	Zinc finger	5.25E-148	AT1G21580.1				X		
MELO3C023424.2.1	Cucumber peeling cupredoxin-like	6.4E-27	AT5G20230.1						X
MELO3C002030.2.1	Glycine-rich RNA-binding protein	4.86E-43	AT5G61030.1						X
MELO3C002286.2.1	Receptor protein kinase	0.0	AT5G56040.2			X	X		

MELO3C012912.2.1	Chlorophyll a-b binding protein	9.97E-163	AT2G34430.1		X					
MELO3C007438.2.1	Fibrous sheath CABYR-binding protein-like	NA	NA							X
MELO3C023402.2.1	Biotin carboxyl carrier protein of acetyl-CoA carboxylase	3.41E-45	AT3G15690.2		X		X			
MELO3C026955.2.1	Superoxide dismutase [Cu-Zn]	6.72E-107	AT2G28190.1			X	X			
MELO3C022343.2.1	Pyruvate dehydrogenase E1 component subunit beta	0.0	AT5G50850.1							X
MELO3C008191.2.1	50S ribosomal protein L27	3.5E-56	AT5G40950.1				X			
MELO3C016181.2.1	Photosystem II 10 kDa polypeptide	1.88E-43	AT1G79040.1		X					
MELO3C007778.2.1	Peptidylprolyl isomerase	4.12E-97	AT4G39710.1	X	X					
MELO3C021444.2.1	Cytochrome c oxidase	2.17E-26	AT4G21105.1				X			
MELO3C011308.2.1	Membrane steroid-binding protein	2.45E-53	AT2G24940.1		X					
MELO3C024093.2.1	Exocyst complex component SEC5A-like	0.0	AT1G76850.1	X						
MELO3C025164.2.1	Aquaporin	0.0	AT4G00430.1				X			
MELO3C031049.2.1	Peroxidase	2.16E-123	AT5G06730.1					X		X
MELO3C005432.2.1	Rubredoxin family protein	1.84E-132	AT5G17170.1		X					
MELO3C010886.2.1	Succinate dehydrogenase subunit 5	7.49E-87	AT1G47420.1							X
MELO3C020905.2.1	Mitochondrial outer membrane protein porin 2	3.4E-146	AT5G67500.2				X			X
MELO3C024146.2.1	Chalcone-flavonone isomerase family protein	NA	NA					X		X
MELO3C024343.2.1	Proteasome subunit alpha type	9.35E-168	AT5G35590.1				X	X		X
MELO3C020969.2.1	Bifunctional 3-dehydroquinate dehydratase/shikimate dehydrogenase	0.0	AT3G06350.1							X
MELO3C010761.2.1	Far upstream element-binding protein 1	5.67E-122	AT2G25970.1					X		X
MELO3C011483.2.1	Os03g0176600-like protein	1.91E-65	AT2G26340.2					X		X
MELO3C013952.2.1	14 kDa proline-rich protein dc2.15	3.63E-46	AT2G45180.1				X			
MELO3C004590.2.1	Dehydrogenase	1.26E-178	AT4G29120.1					X		X
MELO3C021410.2.1	Peroxiredoxin	8.94E-119	AT3G06050.1					X		
MELO3C023691.2.1	Ureidoglycolate hydrolase	1.07E-72	AT2G35820.1							X
MELO3C004125.2.1	translation initiation factor IF-3	2.52E-80	AT2G24060.1					X		
MELO3C008321.2.1	Biotin carboxyl carrier protein of acetyl-CoA carboxylase	9.72E-79	AT3G56130.1			X	X			
MELO3C017853.2.1	3-isopropylmalate dehydrogenase	0.0	AT1G80560.1							X

MELO3C014321.2.1	2-methyl-6-phytyl-1	0.0	AT3G63410.1	X				
MELO3C003536.2.1	14-3-3 protein	6.68E-154	AT5G65430.3				X	X
MELO3C025609.2.1	30S ribosomal protein S20	8.09E-60	AT3G15190.1				X	
MELO3C006421.2.1	60S ribosomal protein L7	6.23E-155	AT3G13580.3	X				
MELO3C025487.2.1	FKBP-type peptidyl-prolyl cis-trans isomerase	3.46E-56	AT3G12345.1				X	
MELO3C013476.2.1	Phototropin-2	0.0	AT5G58140.2				X	X
MELO3C026800.2.1	Proteasome subunit alpha type	6.93E-151	AT2G27020.1				X	
MELO3C014960.2.1	Cytochrome c1-2	0.0	AT5G40810.1				X	
MELO3C021648.2.1	Heat shock 70 kDa protein	0.0	AT5G02500.1	X				
MELO3C009329.2.1	Peroxidase	0.0	AT2G37130.1		X	X		
MELO3C020966.2.1	Mitochondrial carrier protein	0.0	AT4G39460.1					X
MELO3C024002.2.1	Protein transport protein SEC31 homolog B	0.0	AT3G63460.1	X				
MELO3C020183.2.1	Elongation factor 1-gamma-like	0.0	AT1G09640.1	X				
MELO3C003759.2.1	Protein disulfide-isomerase LQY1	2.6E-80	AT1G75690.1				X	
MELO3C024228.2.1	MAR-binding filament-like protein 1-1	5.49E-175	AT3G16000.1			X		
MELO3C024376.2.1	Eukaryotic initiation factor 4A (ATP-dependent RNA helicase eIF4A)	0.0	AT1G54270.1				X	
MELO3C032583.2.1	Mitochondrial gamma aminobutyrate transaminase 1	3.67E-118	AT3G22200.2				X	
MELO3C004452.2.1	Adenylate kinase	0.0	AT5G35170.1				X	
MELO3C004636.2.1	T-complex protein 1 subunit beta	0.0	AT5G20890.1				X	
MELO3C016021.2.1	Desiccation-related protein PCC13-62	8.62E-108	AT3G62730.1				X	
MELO3C003739.2.1	Zinc finger protein	0.0	AT1G20110.1				X	
MELO3C013153.2.1	Dihydrolipoamide acetyltransferase component of pyruvate dehydrogenase complex	0.0	AT4G26910.1				X	
MELO3C016902.2.1	Nitrilase/cyanide hydratase and apolipoprotein N-acyltransferase family protein	0.0	AT5G12040.1				X	
MELO3C016627.2.1	Potassium/sodium hyperpolarization-activated cyclic nucleotide-gated channel 1	1.39E-84	AT1G51100.1	X				
MELO3C014920.2.1	V-type proton ATPase subunit E	1.97E-126	AT4G11150.1		X	X		

II.3.7.2.1. Functional analysis of candidate interacting proteins

Once all the MP-interacting-proteins were statistically filtered, a functional analysis was performed to obtain information about biological pathways affected by the CMV-MP. For that, a Gene Ontology (GO) and Kyoto Encyclopaedia of Genes and Genomes (KEGG) term enrichment analysis was performed. This analysis allowed to compare the biological processes involved in interacting proteins: (i) in local versus systemic infection, (ii) on different melon genotype, (iii) of different CMV viral strains.

i- Local vs systemic infection.

In Manhattan plot (**Figure II.16**) it can be observed that MP-interacting proteins in local infection were mostly enriched in photosynthesis GO and KEGG terms, such as GO:0009521 photosystem, GO:0015979 photosynthesis, GO:0009507 chloroplast, KEGG:00195 photosynthesis (respectively, 1, 2, 4, 7 in **Figure II.16**A, B) and some in stress responses (i.e. GO: 00019773 proteasome core complex alpha subunit, GO:0016209 antioxidant activity (respectively, 5 and 6 in **Figure II.16**A, B), while in systemic infection, enriched terms were transcription (i.e. GO:0001172 transcription RNA-templated 8, 10 in **Figure II.16**A, B), translation (i.e. GO:0005840 ribosome) protein processing in the endoplasmic reticulum (KEGG:04141) and endocytosis (KEGG:04144). Therefore, in local and systemic samples, CMV-MP interacts with proteins involved in different biological processes.

A

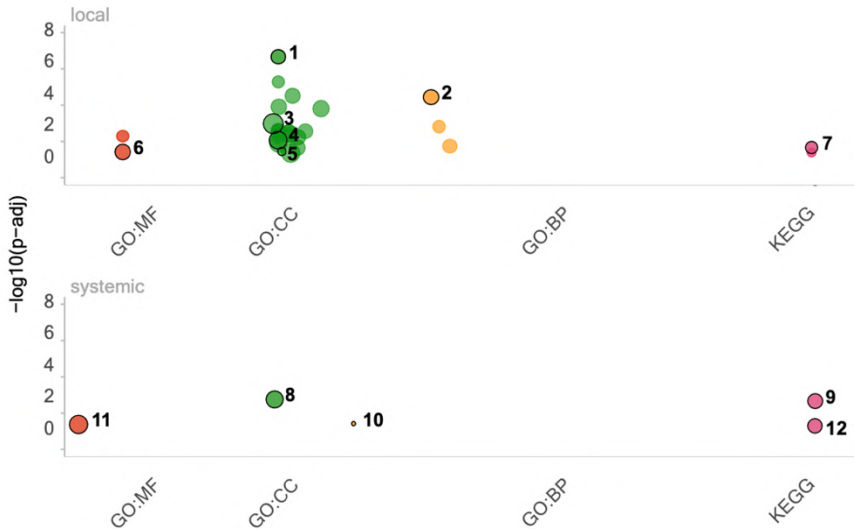

(figure continued on the next page)

B

id	source	term id	term name	term size	p-adj local	p-adj systemic
1	GO:CC	GO:0009521	photosystem	67	2.3e−07*	1
2	GO:BP	GO:0015979	photosynthesis	134	3.8e−05*	1
3	GO:CC	GO:0005737	cytoplasm	2323	1.1e−03*	1
4	GO:CC	GO:0009507	chloroplast	562	8.8e−03*	1
5	GO:CC	GO:0019773	proteasome core complex, alpha−subunit complex	9	3.7e−02*	1
6	GO:MF	GO:0016209	antioxidant activity	128	3.8e−02*	1
7	KEGG	KEGG:00195	Photosynthesis	30	2.2e−02*	1
8	GO:CC	GO:0005840	ribosome	352	1	1.8e−03*
9	KEGG	KEGG:04141	Protein processing in endoplasmic reticulum	105	1	2.3e−03*
10	GO:BP	GO:0001172	transcription, RNA−templated	6	1	3.9e−02*
11	GO:MF	GO:0003723	RNA binding	743	1	4.3e−02*
12	KEGG	KEGG:04144	Endocytosis	75	1	5.0e−02

Figure II.16. Functional enrichment analysis of candidate CMV-MP-interacting proteins comparing local and systemic infection of *C. melo*. Only combinations of >10 proteins in each group were considered for GO enrichment analysis. **A.** Representation of the enrichment results. The y-axis shows the adjusted enrichment significant p-values (p-adj < 0.05), with Bonferroni correction, in negative log10 scale. The location of each term on the x-axis is fixed and terms from the same GO subtree are located closer to each other. The circles represent significant terms and circle size is in accordance with term size. Representative terms are numbered. GO: MF is GO term under Molecular Function category. GO:BP is GO term under the Biological Process category. GO:CC is GO term under the Cellular Component category. **B**. Enrichment analysis table. Every id in the table corresponds to a representative GO significantly enriched (*) in at least one Manhattan plot.

ii- Melon genotypes

As just explained, MP-interacting proteins participate in different biological processes in local and systemic infection. However, are these same processes also enriched independently of the melon genotype or does MP interact with proteins involved in different biological processes depending on the melon genotype? To answer this question, another functional enrichment was performed by separating interacting proteins by melon genotype within each type of infection (local or systemic). In local infection, interacting proteins in PS-infected plants were exclusively enriched by representative terms of photosynthesis, while the NIL was the only cultivar enriched by proteolysis (GO:0019773 proteasome core complex, alpha sub-unit, 4 **Figure II.17**A). In systemic infection, MP-interacting proteins in cultivar PS were enriched by RNA processing (such as GO:0001172 transcription RNA-templated or KEGG:03040 spliceosome, 7 and 9 in **Figure II.17**A, B) and endocytosis (KEGG:04144, 8 in **Figure II.17**A, B). Interestingly, performing a functional enrichment analysis separating by melon genotypes, allowed us to find enriched terms that had been previously masked in the comparison of all interacting proteins together in systemically infected tissues. These enriched terms are

related to endocytosis and are only present in the systemically samples from PS previously CMV-FNY inoculated (such as GO:0005901 caveola or GO:0044853 plasma membrane raft, 10 and 11 in **Figure II.17**A, B). Finally, in MP-interacting proteins within SC, there was no enrichment of GO or KEGG terms and no resulting Manhattan plot, as expected, since SC is resistant to systemic infection. To sum up, there is certain a genotype-specific enrichment of MP-candidate interacting proteins.

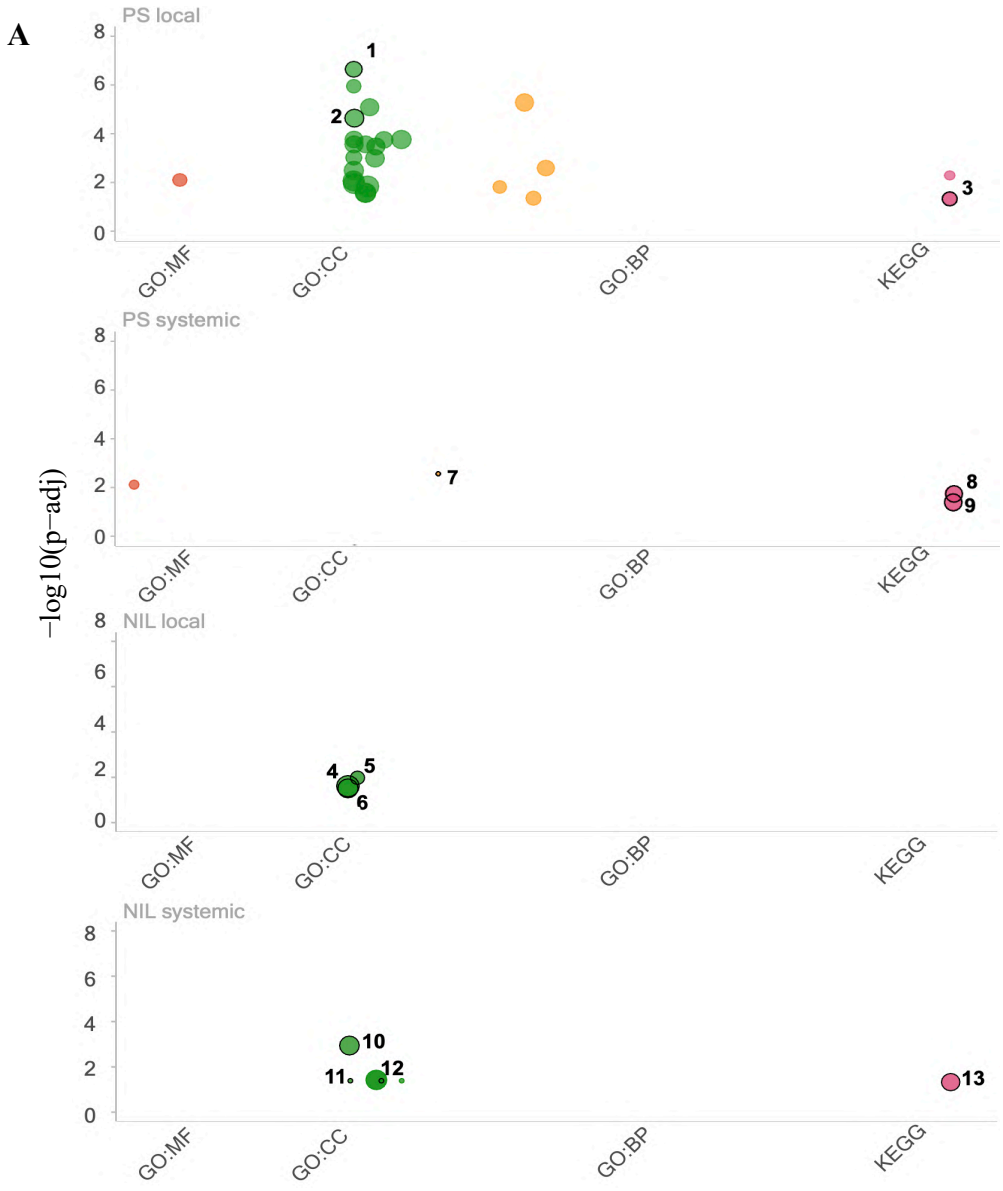

(figure continued on the next page)

B

id	source	term id	term name	term size	p-adj PS local	p-adj NIL local	p-adj SC local	p-adj PS systemic	p-adj NIL systemic	p-adj SC systemic
1	GO:CC	GO:0009521	photosystem	67	2.2e−07*	1	1.3e−01	1	1	1.8e−01
2	GO:CC	GO:0009579	thylakoid	167	2.2e−05*	1	7.4e−01	1	1	6.3e−02
3	KEGG	KEGG:00195	Photosynthesis	30	4.7e−02*	1	4.0e−01	1	1	2.7e−01
4	GO:CC	GO:0019773	proteasome core complex, alpha−subunit complex	9	1	1.1e−02*	5.3e−01	1	1	1
5	GO:CC	GO:0005737	cytoplasm	2323	1.9e−01	2.5e−02*	1	1	1	1
6	GO:CC	GO:0005739	mitochondrion	334	1	3.2e−02*	1	1	1	1
7	GO:BP	GO:0001172	transcription, RNA−templated	6	1	1	1	2.8e−03*	1	1
8	KEGG	KEGG:04144	Endocytosis	75	1	1	1	1.9e−02*	1	1
9	KEGG	KEGG:03040	Spliceosome	98	1	1	1	4.1e−02*	1	8.4e−01
10	GO:CC	GO:0005840	ribosome	352	1	1	1	1	1.1e−03*	1
11	GO:CC	GO:0005901	caveola	1	1	1	1	1	4.2e−02*	1
12	GO:CC	GO:0044853	plasma membrane raft	1	1.	1	1	1	4.2e−02*	1
13	KEGG	KEGG:04141	Protein processing in endoplasmic reticulum	105	5.2e−01	1	1	5.0e−02	4.6e−02*	1

Figure II.17. Functional enrichment analysis of candidate CMV-MP-interacting proteins comparing melon genotypes of *C. melo*. Only combinations of >10 proteins in each group were considered for GO enrichment analysis. **A.** Representation of the enrichment results. The y-axis shows the adjusted enrichment significant p-values (p-adj < 0.05), with Bonferroni correction, in negative log10 scale. The term location on the x-axis is fixed and terms from the same GO subtree are located closer to each other. The circles represent significant terms and circle size is in accordance with term size. Representative terms are numbered. GO: MF is GO term under Molecular Function category. GO:BP is GO term under the Biological Process category. GO:CC is GO term under the Cellular Component category. **B**. Enrichment analysis table. Every id in the table corresponds to a representative GO significantly enriched (*) in at least one Manhattan plot.

iii- CMV-LS vs CMV-FNY

A last enrichment analysis was attempted to find if there were differences of MP-interacting proteins depending on the CMV strain (CMV-LS or CMV-FNY). However, this comparison was only possible with SC cultivar, since these were the only comparisons that had enough MP-interacting proteins within the same genotype and stage of infection to perform a KEGG and GO enrichment analysis (minimum 10 proteins). However, after analysis there was no enrichment in local infection. In the case of systemic infection there was some common enrichment of thylakoid for both strains in SC cultivar (GO:0009579 thylakoid, 2 in **Figure II.18**A, B) and CMV-LS-specific enrichment of rRNA binding (GO:0019843 rRNA binding, 1 in **Figure II.18**A, B). However, SC is a resistant cultivar. Therefore, MP-interacting proteins enrichment in systemic infection are most probably artifacts since CMV is not present in those leaves.

A

B

id	source	term id	term name	p-adj SC LS systemic	p-adj SC FNY systemic
1	GO:CC	GO:0009579	thylakoid	3.55E-02*	2.52E-02*
2	GO:MF	GO:0019843	rRNA binding	4.93E-02*	1

Figure II.18. Functional enrichment analysis of candidate CMV-MP-interacting proteins in systemic infection to compare viral strains effect. Only combinations of >10 proteins in each group were considered for GO enrichment analysis. **A.** Representation of the enrichment results. The y-axis shows the adjusted enrichment significant p-values (p-adj < 0.05), with Bonferroni correction, in negative log10 scale. The term location on the x-axis is fixed and terms from the same GO subtree are located closer to each other. The circles represent significant terms and circle size is in accordance with term size. Representative terms are numbered. GO: MF is GO term under Molecular Function category. GO:BP is GO term under the Biological Process category. GO:CC is GO term under the Cellular Component category. **B**. Enrichment analysis table. Every id in the table corresponds to a representative GO significantly enriched (*) in at least one Manhattan plot.

II.3.7.3. Candidate interactor proteins selected for further validation

Selection of *C. melo* candidate CMV-MP-interacting proteins for further validation was performed using a second criterion after statistical analysis. Suitable protein-interacting candidates were considered if a possible connection with CmVPS41 or viral infection, regarding biological process, function or location could be found either in the candidate itself or in its homologous protein from Arabidopsis. After filtering, a total of 18 genes (12 found in systemic infection and 6 from local infection) were selected for further analysis (**Table II-10**).

Table II-10. *C. melo L.* candidate proteins from the Immunoprecipitation assay selected for further validation.

***C. melo* ID**	***C. melo* name**	**Infection**	**Possible connection with CmVPS41**	**Possible connection with CMV**
MELO3C02 4093.2.1	exocyst complex component SEC5A-like	local	Predicted to function in the trans-Golgi network.	Predicted location in plasmodesmata.
MELO3C02 4002.2.1	Protein transport protein SEC31 homolog B	local	Predicted function in the trans-Golgi network.	Predicted location plasmodesma.
MELO3C00 3739.2.1	Zinc finger protein	local	Arabidopsis homologous protein is required for endosomal sorting and in the late endosome.	-
MELO3C00 3759.2.1	Protein disulfide isomerase (PDI) LQY1	local	-	Several PDIs mutants are involved in resistance to *Bymoviruses*.
MELO3C01 1308.2.1	Membrane steroid-binding protein	local	-	Protein involved in steroid transport, like CmNPC1 which interacts with CMV-MP.
MELO3C02 4343.2.1 and MELO3C02 6800.2.1	proteasome subunit alpha type	local	-	Interacts with HcPro of *Potato virus Y* and *Lettuce mosaic virus*. It also has RNAse activity.
MELO3C02 2138.2.1	Protein disulfide isomerase (PDI)-like protein 2	systemic	-	Several PDIs mutants are involved in resistance to *Bymoviruses*.
MELO3C00 3119.2.1	Heat shock 70 kDa protein	systemic	-	Involved in several plant viral infections.
MELO3C00 6948.2.1	Protein SGT1 homolog	systemic	-	Homologous genes in other species regulate innate immune response.
MELO3C00 9349.2.1 or MELO3C02 4461.2.1	cell division cycle protein 48 homolog	systemic	Mediates membrane fusion of proteasome with HOPS complex in yeast.	Interacts with and directs TMV movement protein.
MELO3C00 2388.2.1	calnexin homolog	systemic	Participates in unfolding proteins in ER-mediated phagocytosis.	Arabidopsis homologous protein is predicted to be in the plasmodesma.

MELO3C006297.2.1	RNA recognition motif (RRM) containing protein	systemic	-	Arabidopsis homologous protein participates in splicing of defence proteins.
MELO3C004385.2.1	pathogenesis-related protein PR-4-like	systemic	Predicted location in the secretory pathway.	Triggered in immune responses.
MELO3C005257.2.1	RNA-dependent RNA polymerase	systemic	-	Arabidopsis homologous protein involved in viral siRNAs production that confers viral resistance.
MELO3C009864.2.1	cytochrome P450 CYP72A219-like	systemic	-	Involved in synthesis of defensive compounds. Similar protein detected by Y2H.
MELO3C018517.2.1	Vacuolar-sorting receptor-like protein	systemic	Arabidopsis homologous gene functions in vacuolar sorting.	-
MELO3C005832.2.1	cucumisin-like isoform X1	systemic	-	Associated with plant immunity.
MELO3C002878.2.1	elongation factor 1-alpha	systemic	-	Participates in the movement of several viruses.
MELO3C009383.2.1	Thaumatin-like protein 1a	systemic	-	PR-5 family proteins. In Nicotiana, the homologous protein interacts with protein 1a, MP and coat protein from CMV-Kor.
MELO3C023630.2.1	ADP-ribosylation factor-like	systemic	Involved in vesicle coating and uncoating in the secretory pathway.	Interacts with p27 of *Red clover necrotic mosaic* .

From local CMV infection in melon, six proteins were selected for further study:

(i) MELO3C024093.2.1, named exocyst complex component SEC5A-like protein, is predicted to be in a protein complex associated with the plasma membrane that determines where vesicles dock and fuse (GO:0000145), and would be involved in the transport from the trans-Golgi network to the plasma membrane (GO:0006893) [https://www.melonomics.net; (Ruggieri et al., 2018)]. Moreover, its homologous protein in *A. thaliana* (AT1G76850.1) is

also involved in tethering vesicles to the plasma membrane and it is located in the plasmodesmata (GO:0009506), were CMV-MP is found (Vukašinovic and Žárský, 2016). So, a possible connection with both CmVPS41 and CMV could be possible.

(ii) MELO3C024002.2.1, named protein transport SEC31 homolog B, is predicted to be part of various organelles related to vesicle transport in the trans-Golgi network (GO:0005783 endoplasmic reticulum, GO:0005794 Golgi apparatus and GO:0005829 cytosol) and plasmodesmata (GO:0009506) [https://www.melonomics.net; (Ruggieri et al., 2018)]. Interestingly, its homologous protein in *A. thaliana* is SEC31B (AT3G63460.1), a component of the coat protein complex (COP II) (Berardini et al., 2015). COPII vesicles are involved in the vesicle budding and cargo export in the trans-Golgi network from the endoplasmic reticulum (ER) to the Golgi apparatus (Marti et al., 2010). Thus, this protein could be related to CmVPS41, which also functions in the transport of cargo proteins (in this case from the late endosome to the vacuole).

(iii) MELO3C003739.2.1, named zinc finger protein, is involved in metal ion binding. Its homologous protein in *A. thaliana* (AT1G20110.1) is named Fyve domain protein, required for endosomal sorting 1 (FREE1) and it is located in the late endosome (Gao et al., 2014; Kwon et al., 2018), which is one of the locations of CmVPS41, as demonstrated in Chapter I. Moreover, AT1G20110.1 is a key component of Endosomal Sorting Complex Required for Transport (ESCRT) machinery which, together with VPS23A, plays a role in Multi Vesicular Body (MVB) protein transport and autophagy (Gao et al., 2015). ESCRT targets cargo proteins to the membrane, which, as previously explained for SEC31 homolog B protein, could also relate this protein with CmVPS41, both functioning in the secretory pathway.

(iv) MELO3C011308.2.1, named Membrane steroid-binding protein, gained interest because of its relationship to NPC1, an interactor of CMV MP which is also involved in steroid signalling. Moreover, its Arabidopsis homologous protein is a membrane-associated progesterone binging protein 2 (AT2G24940.1). This progesterone binding protein is active in the endomembrane system (Mi et al., 2021) and located at the cytosol (Aryal et

al., 2014) and vacuole (McBride et al., 2017) which is related to CmVPS41 location.

(v) MELO3C024343.2.1 and MELO3C026800.2.1, named proteasome subunit alpha type, are part of the proteasome. Interactions of Arabidopsis proteasome subunits and HcPro protein from the potyvirus PVY (Jin et al., 2007), and LMV have been observed. Precisely, the alpha subunit of the proteasome shows RNAse activity during LMV infection (Dielen et al., 2011). As a protein involved in defence response to other viruses, it becomes interesting for validation.

(vi) MELO3C003759.2.1, named protein disulfide isomerase LQY1 (PDI), usually participates in the ubiquitin proteasome system (UPS) machinery (Sun and Brodsky, 2019) as an identifier of malformed proteins from the ER to repair or eliminate them (Matsusaki et al., 2020). The proteasome has been implicated with several plant viral infections (Verchot, 2016; Sun and Brodsky, 2019), thus, it could be involved in CMV infection as well. Moreover, a mutant in a protein disulfide isomerase (PDI) was identified as the resistance factor to multiple strains of *Bymoviruses* in barley(Yang et al., 2014). Thus, PDI could be an interesting candidate for validation.

From all proteins identified in CMV systemic infection in melon, 14 were selected for further validation:

(i) MELO3C022138.2.1, named protein disulfide isomerase (PDI), is another PDI, thus, it was selected for its involvement as a resistance factor in some viral infections, as previously explained for MELO3C003759.2.1.

(ii) MELO3C003119.2.1, named Heat shock 70 kDa protein (Hsp70), is a chaperone that participates in the ER-associated degradation (ERAD) mechanism impeding protein aggregation and facilitating the association between E3 ubiquitin ligase and ERAD-C substrate (Nakatsukasa et al., 2008). Hsp70 participates in several viral infections at multiple levels. For example, it can interact with *Tombusvirus* replicase (Serva and Nagy, 2006) or with the coat protein of *Potyvirus* (Hafrén et al., 2010). Also, it is involved in the assembly of the replicase complex in *Red cloved necrotic mosaic virus* (Mine et al., 2012) and it allows *Tomato yellow leaf curl virus* (TYLCV) to stablish

an infection in plants (Gorovits et al., 2013). This versatility in participating in different moments of the virus cycle makes it a very interesting candidate interactor of CMV-MP.

(iii) MELO3C006948.2.1, named suppressor of the G2 allele of skp1 (SGT1) homolog, is a co-chaperone known to form a complex together with Hsp70 that regulates innate immune response in *A. thaliana* (Noël et al., 2007). Also, SGT1 in *N. benthamiana* is critical for cell-to-cell movement and systemic infection of *Tomato Spotted Wilt virus* (Qian et al., 2018b). SGT1 also forms a complex with Hsp90 to mediate resistance to TMV (Qian et al., 2018a). For all the mentioned above, SGT1 is a good candidate to participate in CMV resistance.

(iv) MELO3C009349.2.1, named cell division cycle protein 48 homolog (CDC48), is a chaperone that directs substrates to the proteasome after ubiquitination (Nakatsukasa et al., 2008). In yeast, the ubiquitin-proteasome system regulates membrane fusion in the vacuole, where the HOPS complex is found (Kleijnen et al., 2007). In *A. thaliana,* CDC48 is induced upon infection and interacts with TMV movement protein to promote its degradation (Niehl et al., 2012). Thus, several relationships are found with CmVPS41 and CMV.

(v) MELO3C002388.2.1, named calnexin homolog, is another chaperon involved in protein folding of unfolded proteins in ER-mediated phagocytosis (Liu et al., 2017). In *C. melo* it is predicted to locate in the ER (GO: GO:0005783 endoplasmic reticulum), where is also located its *A. thaliana* homologous protein (AT5G61790.1). Moreover, this protein participates in some viral infections in humans; it interacts with the glycoprotein of *Rubivirus rubellae* (Nakhasi et al., 2001), as well as with the Nef protein of *Human immunodeficiency virus 1* (HIV-1) (Jennelle et al., 2014). Therefore, it is worth investigating if a possible connection is also found with CMV-MP.

(vi) MELO3C006297.2.1, named RNA recognition motif (RRM) containing protein, is predicted to bind nucleic acids (GO:0003676) or metal ions (GO:0046872). Its homologous protein in *A. thaliana* (AT3G23900.2) promotes splicing of transcripts of defense proteins, including the Calcium dependent Protein Kinase 28 (CPK28), a key negative regulator of pattern recognition receptor complexes in immune response (Dressano et al., 2020).

(vii) MELO3C004385.2.1, named pathogenesis-related protein PR-4-like, is predicted to be a protein from the Pathogenesis-related (PR) family of proteins, which are key components of the innate immune system of plants. *C. melo* PR-4-like protein is predicted to participate in reactions triggered in response to the presence of bacteria, in which PR-4-like acts to protect the cell or organism (GO:0042742) and in response to fungi (GO:0050832) [https://www.melonomics.net; (Ruggieri et al., 2018)]. Thus, it would not be unexpected to participate in other resistances, such as to CMV. Moreover, its homologous protein in *A. thaliana* (AT3G04720.1) is located in the apoplast and in vesicles of the secretory pathway (Berardini et al., 2015), where VPS41 is found. For that reason, connections to CmVPS41 should be further studied.

(viii) MELO3C005257.2.1, named RNA-dependent RNA polymerase, has an homologous protein in *A. thaliana* (AT1G14790.1) that synthesizes dsRNAs, which in turn, are digested to produce viral siRNAs that confer viral resistance through RNA silencing (Diaz-Pendon et al., 2007). Therefore, it would be expected a participation during CMV infection, although maybe restricted to silencing and not movement.

(ix) MELO3C009864.2.1, named cytochrome P450 CYP72A219-like, is another protein from the cytochrome P450 family. As previously explained, cytochromes P450 are enzymes that play essential roles in synthesis of sterols, secondary metabolites, such as fatty acids, and defensive compounds, among others (Pinot and Beisson, 2011). Thus, its relationship to both sterols and defense could relate it to CmNPC1 and CMV.

(x) MELO3C018517.2.1, named Vacuolar-sorting receptor-like protein, is predicted as an integral component of the membrane (GO:0016021) that binds calcium ion (Ca^{2+}) (GO:0005509) [https://www.melonomics.net]. Its homologous protein in *A. thaliana* (AT2G14740.1) is a vacuolar-sorting receptor (VSR) involved in clathrin-coated vesicle sorting from the Golgi apparatus to the vacuoles (Zouhar et al., 2010). Thus, a clear relationship with CmVPS41 is found, at least regarding to cellular localization.

(xi) MELO3C005832.2.1, named cucumisin-like isoform X1, is predicted to have serine-type endopeptidase activity (GO:0004252) and to be involved in proteolysis (GO:0006508) [https://www.melonomics.net]. This protein belongs to the subtilisin-like proteases family, a very diverse serine-peptidase

family that has been associated with pathogen resistance and plant immunity (Figueiredo et al., 2018). Then, it could participate as well in CMV resistance.

(xii) MELO3C002878.2.1, named elongation factor 1-alpha, belongs to the family of Eukaryotic Elongation Factors in plants, a well-known family of proteins involved in translation elongation (Mateyak and Kinzy, 2010; Sasikumar et al., 2012). During viral infection, these proteins participate in RNA viral multiplication and spread (Li et al., 2013a). For example, eEFBβ proteins are involved in replication and movement of TMV (Yamaji et al., 2010) and facilitate infection of *Potato Virus X* (Hwang et al., 2015). Also, eEFBβ is targeted by *Soybean Mosaic Virus* (SMV) protein P3, to promote ER-stress response of unfolded proteins (Luan et al., 2016). Then, it has a possible link with the MP.

(xiii) MELO3C009383.2.1, named Thaumatin-like protein 1a, belongs to the family of Pathogenesis-Related 5 proteins (PR-5). As previously explained, PR proteins and induced after pathogen attack by accumulating hormones associated with plant defence (de Jesús-Pires et al., 2020). Interestingly, Thaumatin-like protein from *N. benthamiana* interacts with the CMV-Kor strain proteins 1a, MP and coat protein (Kim et al., 2005).

(xiv) MELO3C023630.2.1, named ADP-ribosylation factor-like, has an Arabidopsis homologue (AT1G10630.1) essential for vesicle coating and uncoating and acts in the secretory pathway (Bassham et al., 2008), where VPS41 is also found. Moreover, ADP-ribosylation factor 1 play an essential role in the replication of *Red clover necrotic mosaic virus* (RCNMV) by interacting with the viral p27 protein. This interaction is essential for the correct functioning of the viral replicase complex (Hyodo et al., 2013). Thus, this protein could also be interacting with CMV-MP in CMV infection.

On another note, two other candidate MP-interacting proteins were interesting because they mapped inside the two QTL intervals (QTLIII and QTLX), which are involved in resistance to CMV SG I strains. Both candidates were found in SC cultivar infected with CMV-FNY. The candidates are:

(i) MELO3C008321.2.1 (chr03:3,631,881..3,640,515), named Biotin carboxyl carrier protein of acetyl-CoA carboxylase, is located inside QTL III interval (chr03:2,804,514..23,616,908). Its *A. thaliana* homologous protein

(AT3G56130.1) is a negative regulator of fatty acid biosynthetic process (Salie et al., 2016). However, only some SNPs between cultivars PS and SC are found in the promotor of this gene and none in the coding sequence.

(ii) MELO3C011952.2.1 (chr10:3661607..3677971), named UDP-galactose:fucoside alpha-3-galactosyltransferase, is located inside QTL X interval (chr10:1,122,396..4,747,687). This protein is predicted to be implicated in cell wall biogenesis (GO: GO:0042546) and to be in the Golgi apparatus (GO:0005794), chloroplast (GO:0009507) and cytoplasm (GO:0005737) [https://www.melonomics.net; (Ruggieri et al., 2018)]. Interestingly, MELO3C011952.2.1 homologous gene in tomato Twi1 plays a role in defence against virus (Campos et al., 2019). Also, this gene has several SNPs and insertion–deletion mutations between the coding sequence of PS and SC.

Due to the lack of time, none of the candidate genes has been validated yet.

II.3.7.4.MP interacting proteins in N. benthamiana

To find CMV-MP-interacting-proteins across species, an Immunoprecipitation coupled to Mass Spectrometry was performed in *N. benthamiana*. This approach would help to find some common candidate CMV-MP-interacting proteins.

For this purpose, *N. benthamiana* plants were agroinfiltrated, as indicated in M&M from Chapter I section "Transient expression in *Nicotiana benthamiana*", either with the three constructs encoding the CMV-FNY RNAs or the three constructs encoding the three CMV-LS RNAs. Samples were taken from the infiltrated leaves (3 dpi) to find MP-interacting proteins in local infection, and from systemically infected leaves (15 dpi) to find MP-interacting proteins at the level of systemic infection. For each condition, four biological replicates were taken for analysis. The whole immunoprecipitation coupled to LC-MS/MS was performed as previously described for *C. melo* (M&M section II.2.9) and MS/MS spectra was searched against a combined database containing the sequences of proteins from *Nicotiana benthamiana* genome v1.0.1 ([https://solgenomics.net/, (Bombarely et al., 2012)] and also the MP sequences from CMV-FNY and CMV-LS (Guiu-Aragonés, 2015). Arabidopsis homologous proteins were searched through a BLAST, as explained in M&M II.2.9.5, to gain information about the candidate interacting proteins and compare them with those obtained in *C. melo* (**Table II-8** and **Table II-9**).

Table II-11. *N. benthamiana* candidate CMV-MP-interacting proteins in local and systemic infection and their homologous proteins in *A. thaliana*. E-value are from the BLAST in *A. thaliana*.

***N. benthamiana* ID**	***N. benthamiana* name**	**E-value BLAST**	***A. thaliana* ID**	**Experiment**			
				local		**systemic**	
				LS	FNY	LS	FNY
Niben101Scf00369g19019.1	Protein of unknown function (DUF1399)	2E-23	AT1G56230.1	X	X		
Niben101Scf14996g00009.1	Catalase	2E-179	AT1G20630.1	X	X		X
Niben101Scf10986g00001.1	Cysteine-rich repeat secretory protein 55	2E-23	AT5G48540.1	X	X		
Niben101Scf00360g05009.1	Cyclic nucleotide-gated channel 14	5E-98	AT2G24610.1	X	X		
Niben101Scf01001g00005.1;Niben101Scf01001g00004.1; Niben101Scf01001g00003.1;Niben101Ctg13736g00004.1	Glucan endo-1 3-beta-glucosidase	2E-15	AT3G57270.1	X	X		
Niben101Scf03768g03011.1;Niben101Scf01656g00009.1	Membrane protease subunit stomatin/prohibitin-like protein	4E-37	AT4G27585.1	X			
Niben101Scf08478g00016.1	RNA-binding protein 4.1	2E-60	AT3G23900.1	X			
Niben101Scf03759g01001.1;Niben101Scf08206g02027.1	BnaA03g12140D	5E-14	AT5G53620.1	X	X		
Niben101Scf02069g02008.1;Niben101Scf03985g02025.1	COP1-interactive protein 1	3E-24	AT5G41790.1	X			
Niben101Scf00653g00002.1;Niben101Scf04375g08004.1; Niben101Scf32212g00014.1;Niben101Scf01791g03001.1	T-complex protein 1 subunit eta	1E-31	AT5G26360.1	X			
Niben101Scf02104g00001.1;Niben101Scf01212g01017.1	Photosystem Q(B) protein	0	ATCG00020.1	X	X		
Niben101Scf14210g00021.1	Late embryogenesis abundant protein	2E-68	AT2G44060.1	X	X		
Niben101Scf06091g00010.1;Niben101Scf06976g03021.1; Niben101Scf06976g03021.1	Stromal cell-derived factor 2-like protein precursor	7E-16	AT2G25110.1	X			
Niben101Scf21110g00005.1;Niben101Scf06506g00001.1	Fatty acid oxidation complex subunit alpha;	1E-17	AT4G29010.1	X			
Niben101Scf03711g01021.1;Niben101Ctg14629g00001.1	Peroxiredoxin-2B	1E-44	AT1G65980.1	X			
Niben101Scf05890g02025.1;Niben101Scf04560g03018.1	T-complex protein 1 subunit beta (Fragments)	8E-130	AT5G20890.1	X			

Niben101Scf03572g02005.1	T-complex protein 1 subunit theta	8E-11	AT3G45900.1	X			
Niben101Scf02982g01007.1	RNA-binding protein 4.1	2E-178	AT3G23900.1	X			
Niben101Scf00369g09017.1;Niben101Scf03643g09015.1; Niben101Scf04300g05005.1;Niben101Scf04432g00008.1	26S protease regulatory subunit 4 homolog	0	AT3G05530.1	X			
Niben101Scf02240g02008.1;Niben101Scf32453g00005.1	Acyl-CoA-binding protein	5E-26	AT3G45900.1		X		
Niben101Scf01596g12004.1	Calnexin homolog	0	AT5G61790.1		X		
Niben101Scf16915g00006.1;Niben101Scf03923g14010.1	Ubiquinone/menaquinone biosynthesis C-methyltransferase UbiE	1,00E-57	AT3G63410.1	X	X		
Niben101Scf04331g09018.1;Niben101Scf00837g11004.1; Niben101Scf27914g00006.1	Chaperone protein htpG family protein	0	AT4G24190.1		X		
Niben101Scf06545g00010.1;Niben101Scf01945g01009.1; Niben101Scf00272g11021.1;Niben101Scf01945g01012.1; Niben101Scf05229g04025.1;Niben101Ctg11463g00002.1; Niben101Scf05229g04013.1	30S ribosomal protein S4	2E-89	AT5G39850.1		X		
Niben101Scf01498g11008.1	Phosphoinositide phosphatase family protein	3E-53	AT1G22620.1		X		
Niben101Scf00614g00023.1;Niben101Scf01072g03005.1	ATP-dependent Clp protease proteolytic subunit	1E-52	AT4G17040.1		X		
Niben101Scf12383g01002.1;Niben101Scf03066g02005.1	RNA-binding protein 25	3E-54	AT1G60200.1			X	
Niben101Scf00397g00001.1	T-complex protein 1 alpha subunit	0.0	AT3G20050.1			X	
Niben101Scf06823g02004.1	SWIB/MDM2 domain superfamily protein	3E-16	AT4G34290.1			X	

To functionally characterize *N. benthamiana* MP-interacting proteins, a GO enrichment of these candidates was performed with an exact Fisher's test with Bonferroni correction (p-adjusted<0.05), as explained in M&M section II.2.9.6. This time, no KEGG enrichment was performed due to the too little enrichment already obtained during GO analysis. KEGG pathways have even fewer terms annotated, thus a KEGG analysis was not performed. Moreover, GO enrichment in systemic infection could not be performed neither with CMV-FNY nor CMV-LS MP-interacting proteins, due to the small number of proteins found. According to AgriGO, the minimum number of proteins to perform a GO enrichment analysis is 10. Specifically, only one candidate MP-interacting-protein was found in systemic infection of CMV-FNY and three for CMV-LS (**Table II-11**). From the functional enrichment results, our results show that there was no enrichment of MP-FNY-interacting proteins in local infection, while MP-LS-interacting proteins had two enriched terms, both related to protein folding (**Table II-12**). Therefore, the already selected protein folding related proteins in *Cucumis melo* could be more important than initially speculated.

Table II-12. Functional enrichment analysis of candidate CMV-MP-interacting proteins in local infection of *N. benthamiana*. Adjusted enrichment significant p-values (p-adj < 0.05) with Bonferroni correction are indicated (*).

Term id	Source	Term name	p-adj CMV-LS	p-adj CMV-FNY
GO:0006457	GO:BP	protein folding	1.1E-04*	1
GO:0051082	GO:MF	unfolded protein binding	4.8E-06*	1

As previously performed for melon candidate MP-interacting proteins, a bibliographic search was made to gain insight on CMV infection and allow to find the most promising candidate interacting proteins for validation. These proteins were:

(i) Niben101Scf01001g00005.1, named Glucan endo-1 3-beta-glucosidase (GLU I), is involved in callose deposition. Mutants in this protein have higher callose deposition and reduced plasmodesmata SEL, which can impair cell-to-cell movement and delay local infection of some plant viruses, including CMV in tobacco plants as well as Arabidopsis (Iglesias and Meins, 2000; Zavaliev et al., 2013). In fact, CMV-MP cell-to-cell traffic is restricted in GLU I-deficient mutants in tobacco (Iglesias and Meins, 2000).

(ii) Niben101Scf08478g00016.1, as well as Niben101Scf12383g01002.1 are RNA-binding proteins (RBPs). RBPs have many diverse roles in RNA

activity, transport (Pallas and Gómez, 2013) and plant defence (Woloshen et al., 2011). For example, its homologous protein in Arabidopsis (AT3G23900.1) interacts with TSWV movement protein (von Bargen et al., 2001) and it is part of a family of proteins that participate in cell-to-cell trafficking (Paape et al., 2006).

(iii) Niben101Scf05890g02025.1, named T-complex protein 1 subunit beta, is a protein part of the T-complex that appears associated with some animal viruses, such as mammalian reovirus, where it participates in late events during replication (Knowlton et al., 2018) or in the egress of *Epstein-Barr virus* (EBV) (Kashuba et al., 1999). In our experiment, we have also found several other subunits from this complex (β, θ and η) as interactors of CMV-MP, which increases their relevance.

(iv) Niben101Scf01498g11008.1, named phosphoinositide phosphatase family protein, is a key protein involved in vacuolar trafficking and morphology (Nováková et al., 2014). Phosphoinositides control the localization of VPS41 (Brillada et al., 2018) and are also related to NPC1. NPC1 regulates the location of phosphatidylinositol kinases in membrane contact sites of Golgi and lysosomes (Kutchukian et al., 2021). Therefore, this could be a very interesting protein due to its relationship to both VPS41 and NPC1.

Another comparison was performed between interacting-proteins in *C. melo* (from Y2H and IP) and *N. benthamiana* (IP) to see if any protein was common in different assays. This would highlight some proteins important for the infection in both species (**Figure II.19**). Three common proteins were found between IP in *C. melo* and *N. benthamiana*. Two of them are chaperones involved in protein folding; Chaperonin Containing T-complex-beta (AT5G20890.1) and calnexin homolog 1 (AT5G61790.1) (Liu et al., 2017; Ahn et al., 2019). The third one is the 2-methyl-6-phytyl-1,4-hydroquinone methyltransferase (AT3G63410.1) involved in the key methylation step of tocopherols (vitamin E) and plastoquinone synthesis in the chloroplast (Cheng et al., 2003). Thus, calnexin homolog and T-complex proteins gained importance, not only because all their previously mentioned links to CMV, but also for being identified in both *C. melo* and *N. benthamiana* CMV infection, implying that they are not host specific and thus, could be acting in the core of the CMV transport pathway.

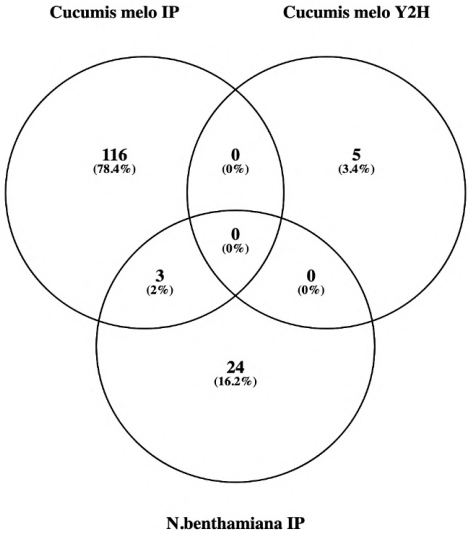

Figure II.19. Venn diagram of candidate CMV-interacting proteins from *N. benthamiana* and *C. melo* with Venny 2.1 tool (Oliveros, 2008).

II.3.8. Validation of candidate interacting proteins by Y2H

Due to lack of time, only three candidate interacting proteins from the IP could be investigated by one-by -one Y2H assay. This Y2H assays were performed with both CMV-LS and CMV-FNY MPs and as previously described, for Y2H candidate interactors confirmation. The proteins investigated were: protein SGT1 homolog (MELO3C006948.2.1), elongation factor 1-alpha (MELO3C002878.2.1) and pathogenesis-related protein PR-4-like (MELO3C004385.2.1). However, no interaction could be observed in this assay (**Figure II.20**). From these results, the direct interaction of these proteins with CMV-MP should be discarded or at least proven with another PPI method, such as BIFC. In any case, the rest of relevant MP-candidate interactors should be validated in the future.

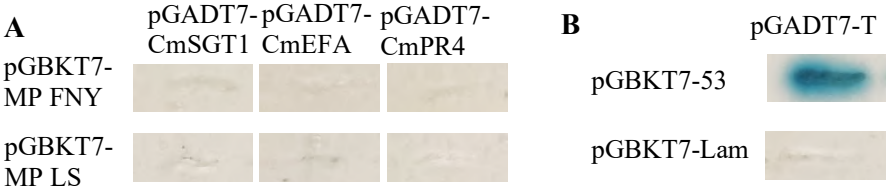

Figure II.20. One-by-one Y2H results of previously detected candidate interacting proteins by IP. **A.** Y2H one-by-one confirmation of IP interacting protein combination of prey (pGADT7) and bait (pGKBT7). Strong or light blue colonies indicates interaction **B.** Controls of one-by-one Y2H are pGADT7-T (prey) in combination with either bait pGBKT7-53 (positive interaction) or bait pGBKT7-Lam (no interaction). CmSGT1: *C. melo* SGT1 homolog. CmEFA: *C. melo* elongation factor 1-alpha. CmPR4: *C. melo* pathogenesis-related protein PR-4-like.

II.4. Discussion

In this Chapter, several candidate interacting proteins of CMV-MP were found through different protein-protein interaction (PPI) methods. There are many methods that allow to study PPIs, such as one-by-one Y2H, Co-IP followed by western blotting, among others. These methods work testing already suspected interactions and need previous knowledge about the interaction partners to test. In our case, Y2H screening and IP coupled to LC-MS assay do not need previous knowledge about the possible partners of the protein of interest, and they are complementary methods. On one hand, Y2H screening allows to detect direct, binary interactions *in vivo* and it also helps to elucidate weak and transient PPIs. Also, construction of the cDNA library by random amplification of RNA allows to detect: (i) fragments of interacting domains that might fail to be captured when the whole protein is present (maybe due to the conformation or even the size) or (ii) proteins (or protein domains) bound to a membranous organelle. However, Y2H does not give information about the physiological state of the samples due to the yeast environment and forced co-expression of proteins, which in turn, provides a limited understanding of PPI dynamics (Makuch et al., 2014). On the other hand, IP coupled to AP-MS is an *in vitro* assay that detects protein complexes and delivers information about the conditions in which the interaction takes place, but usually does not allow transient or weak PPIs, which are often lost during lysis and purification steps. Nevertheless, all candidate interactors must always be further validated with another assay (Struk et al., 2019).

In the case of Y2H screening, five candidate interactors were finally obtained and one of them (CmNPC1) was further validated with BIFC due to its more obvious connection with both CmVPS41 and CMV. However, 5-ribose-isomerase was also a positive interactor in one-by-one Y2H assay. This protein was observed to be in higher amounts in BS cells compared to the mesophyll in maize and common millet (Edwards and Gutierrez, 1972; Kanai and Edwards, 1973). BS are the cells where the resistance take place in melon. However, a possible location at the site of resistance does not necessarily mean a direct link with CMV infection. Thus, lack of time and a not clear connection between 5-ribose-isomerase and CmVPS41 or CMV, impede its validation with other PPI techniques, such as BIFC. However, it could still be an important component of CMV infection.

C. melo NPC1 has an sterol-sensing domain (SSD) and is predicted to have lipid transporter activity (GO:0005319). From BIFC results, it seems that CmNPC1 interacts with CMV-MP at the plasmodesmata, where the MP localizes (see Chapter I). In fact, NPC1 homologous proteins in *A. thaliana* are located in the plasma membrane (At1g42470) (Mitra et al., 2009; Zhang and Peck, 2011; Feldman et al., 2015b) or both the plasma membrane and other membranes such as the tonoplast (Feldman et al., 2015b) (At4g38350) (Shimaoka et al., 2004; Szponarski et al., 2004; Jaquinod et al., 2007). The misexpression of these homologous proteins has been implicated in an increase of fatty acid content in the Arabidopsis cell, specifically affecting sphingolipids but not sterols (Feldman et al., 2015b). In *S. cerevisiae*, the NPC1 homologue (Ncr1p) is located in the vacuolar membrane and this location is impaired by mutations in proteins working in the Vacuolar protein sorting (VPS) pathway, such as proteins pep12, vps45, vps1 and vps27 (Zhang et al., 2004). This can relate this protein to VPS41, that also participates in vacuolar protein sorting towards the vacuole. Human NPC1 is located in the late-endosomal and lysosome membranes (Higgins et al., 1999) and works in cholesterol trafficking in the cholesterol uptake pathway (Carstea et al., 1997). HsNPC1 is also implicated in several viral infections, such as *Zaire ebolavirus* (EboV), *Marburgvirus* (MARV), HIV-1 and *Hepatitis C virus* (HCV) (Tang et al., 2009b; Carette et al., 2011a; Hunt et al., 2012; King et al., 2018; Stoeck et al., 2018). In fact, EboV entry is strictly dependent on HsNPC1, which is the receptor that interacts with the cleaved glycoprotein 1 subunit (GP_1) viral protein and allows viral membrane fusion (Carette et al., 2011a; Côté et al., 2011). During HIV-1 infection, deficiency of HsNPC1 results in a suppression of viral replication (Tang et al., 2009b). HIV-1 entry and exit happens through lipid rafts (Nguyen and Hildreth, 2000; Carter et al., 2009), which were among the enriched GO terms found in candidate interacting-proteins in the MP FNY-infected NIL in systemic infection. Moreover, efficient EboV GP-mediated binding to NPC1, is its filoviral receptor, requires the expression of the homotypic fusion and protein sorting (HOPS) tethering complex (Bo et al., 2020); where VPS41 is found. Also, NPC1 has a di-leucine motif at the C-terminus of its cytosolic tail (LLNF) required to mediate sorting of cargo proteins by binding to membrane lipids and target proteins (Poirier et al., 2013). VPS41 also mediates sorting of cargo proteins as part of the HOPS complex, by two ways, either via late endosomes or via AP3 pathway, the late one transporting proteins in vesicles towards the vacuole, (Rehling et al., 1999; Asensio et al., 2013a). Thus, NPC1 could be also related to CMV viral entry, endocytosis and VPS41.

From CmNPC1 conformational predictions, CmNPC1 showed 89 % of sequence homology with a NPC1-like intracellular cholesterol transporter 1 (NPC1L1) in complex with an ezetimibe analogue, a cholesterol absorption inhibitor, from *Rattus norvegicus* (Wang et al., 2020b). NPC1L1 sequence shares 42 % identity and 51 % similarity with human NPC1 (Davies et al., 2000). In mammals, NPC1L1 is abundantly located in the apical membrane of enterocytes in the intestine (Sané et al., 2006) and it mediates intestinal cholesterol absorption though clathrin-mediated endocytosis (Ge et al., 2008; Betters and Yu, 2010; Wei et al., 2014). Moreover, in humans, NPC1L1 is essential for intestinal absorption of plant sterols (Tang et al., 2009a; Jia et al., 2011). CmNPC1 was predicted as part of a membranous organelle, with the interacting domain facing the external part of the organelle according to Phyre2 but facing the internal part according to TMHMM. However, it should be considered that if, as it seems from BIFC results, this membranous organelle is the plasma membrane, the interaction domain should be facing the cytoplasm and not in the extra membranous space, as Phyre2 predicted, since the MP is inside the cell.

Focusing on CmNPC1 interaction domain, it could be that only part of it is interacting with CMV-MP, especially considering the two introns present in this sequence and that both have stop codons within their sequence. At the same time, we have seen that the CMV-MP-FNY interacts with both CmVPS41 SC and PS but not the MP from CMV-LS (Chapter I). Taking this into account it seems CMV-MP-FNY would recruit both CmNPC1 and CmVPS41 for targeting and movement through the PD in PS and NIL plants, while in SC plants although this interaction would happen, the two other QTLs would still impede PD movement. In the case of CMV-LS it would be reasonable to think another pathway to reach the PD is needed in which CmNPC1 might participate or not in PD targeting and somehow CmVPS41 would not interact directly to CMV-MP but its resistance mutation would affect CMV movement as well. Also, CmNPC1 could still be interacting with CmVPS41 through another CmNPC1 domain and this would create even more combinations of interactions to allow or impede recruitment to the PD, since, according to our BIFC assays, the interaction between CmNPC1 domain and MP seems to happen at the PDs. Nevertheless, CmNPC1 could also have more locations apart from this one. As mentioned before, within CmNPC1 interaction domain, there were two introns suggesting that there could be some alternative splicing (AS) leading to the retention of these two introns in some mRNA CmNPC1 molecules. In this scenario, the virus could eventually, use the product of these AS RNAs to bind the truncated CmNPC1 protein and be transported to the PDs. AS has been observed and even increased

during stress and, although its implications in the proteome remains still unknown, Chaudary et al., 2019, proposed that under stress, plants use AS to decrease the translation of a significant portion of the transcriptome to influence proteome composition at the same time that metabolic cost is reduced (by decreasing translation of transcripts) (Chaudhary et al., 2019). In our case, these transcripts are found in both, infected and non-infected melon plants. Thus, it does not appear to be a response to infection. In the interaction domain, there are several termination codons in the first intron, thus, a shorter CmNPC1 protein would be expected. Alternatively, a readthrough event would allow to avoid the stop codons and result in a CmNPC1 protein not only shorter than the native one, but with a different amino acid sequence in its C-terminal end, putatively providing the real interacting domain for the viral MP, which would not be able to bind the native NPC1.

Looking at the IP assay in *C. melo*, we found 131 candidate interactors, most of which remain to be confirmed. One interesting aspect of this whole assay was the statistic and biologic filtering criteria of MP-candidate interacting proteins. First, our statistical approach consisted on more than one method to try to not exclude any potential interactors. In the end, statistics play with probability and sticking only to one statistical method had the risk to lose interesting interactors just by a statistical criterion. Therefore, we used more than one method and in a non-exclusive manner. Then, a complementary biological criterion was used to reduce the candidate list for validation and focused on the more interesting candidates based on their putative biological relationship to either CmVPS41 or CMV. In any case, it should be clear that all candidates that passed any of the statistical analysis, could still be interactors of CMV-MPs or implicated in CMV infection through protein-complexes. Also, the three MP-candidate interacting proteins, SGT1 homolog, elongation factor 1-alpha and pathogenesis-related protein PR-4-like, that were not finally confirmed through one-by-one Y2H assay, could still be part of protein complexes that interact indirectly with CMV-MP through another protein. In the case of PR-4-like protein, as well as RRM containing protein it would be more reasonable that their mechanism of action would be working in a dominant resistance manner through another pathway independently of *cmv1*. In this putative alternative mechanism both proteins would be able to detect the virulence factor, in this case the MP, instead of being a cellular factor necessary for CMV infection, as it happens in recessive resistance.

The use of *N. benthamiana*, another susceptible plant, to study general CMV-MP candidates allowed to find some interesting trans-species candidate interactors of CMV-MP. Compared to *C. melo*, not many candidates were obtained. However, three candidate proteins were homologous to candidate proteins in *C. melo*. In fact, two of them were involved in protein folding, which was not a surprise considering the big number of chaperons that were found among the candidates. One of these two proteins is the subunit beta of the T-complex, that is part of the chaperonin-containing T-complex (TRiC), a molecular chaperon complex involved in folding of proteins and has 8 subunits (α, β, γ, δ, ε, ζ, η and θ) (Wang et al., 2020a). In fact, in melon only the subunit beta was found with the IP, while in *N. benthamiana* several subunits of the T-complex were found (η, β, θ and α). T-complex has been associated to several animal infections. Several interactions of T-complex (CCT) have been reported with animal viruses, such as: interaction with Epstein Barr Virus (EBV) EBNA-3 protein (Kashuba et al., 1999), interaction with *Influenza A virus* (FLUAV) RNA polymerase subunit PB2 (Fislová et al., 2010) or with *Mason-Pfizer monkey virus* (M-PMV) Gag polyprotein (Hong et al., 2001). Moreover, the T-complex has also been implied in selective transport through the PD of knotted1 (KN1) homeobox (KNOX) family transcription factors in Arabidopsis (Xu et al., 2011). According to these results, it seems that protein folding might play a common role in CMV infection across species. The third protein, named 2-methyl-6-phytyl-1,4-hydroquinone methyltransferase, is involved in the methylation of tocopherols and plastoquinone. Tocopherols are lipid-soluble antioxidants that play a role in immunity to bacterial infection, possibly at a basal level by protecting oxidation of fatty acid-containing lipids (Stahl et al., 2019). Plastoquinone is involved in plant response to stress in abiotic and also biotic stress acting as an antioxidant and preventing lipid peroxidation, protein oxidation and DNA damage (Liu and Lu, 2016). Thus, it could also be involved in plant biotic stress, especially after finding it is a common protein candidate to interact with CMV-MP in both *N. benthamiana* and *C. melo*.

Finally, when speculating on how these candidate proteins could participate in CMV infection we hypothesize CMV-MP would target CmNPC1 in the intron region and then use this protein to target itself to the PD. Another candidate interactor that could participate in the fate of CMV-MP is CDC48 that has been previously demonstrated to interact and direct the fate of TMV-MP (Niehl et al., 2012). The rest of interactors we hypothesize would be needed for viral protein processing or intracellular transport of CMV. For example, viral proteins need to be processed and folded, through the endoplasmic reticulum in which

several chaperons and folding proteins are needed. In this sense, calnexin-homolog protein or Hsp70 that are key chaperons could participate (Nakatsukasa et al., 2008). For intracellular transport of vRNP-MP complexes, other proteins could be implicated, such as transport protein SEC31 homolog B that is a component of the COPII vesicles, the vacuolar-sorting receptor-like protein that participates in vesicle transport from the Golgi apparatus to the vacuoles (Pols et al., 2013), or the exocyst complex component SEC5A-like protein that in yeast participates in docking of exocytic vesicles with fusion sites on the plasma membrane (Novick et al., 1980; TerBush et al., 1996; Vukašinovic and Žárský, 2016). However, there is a low level of applicability of other long-distance host proteins restricting phloem movement since they are usually host-specific, thus, new hypothesis will probably emerge after validation of candidates (Hipper et al., 2013).

Chapter III. Proteomic analysis in *C. melo* and *N. benthamiana* in response to *Cucumber mosaic virus*.

III.1. Introduction

Plant viruses are obligate parasites and only encode a few proteins, thus, need the host machinery to complete every step of the viral cycle. After viral entry, viruses remove the capsid and release the viral genome for translation of the viral proteins. For translation, viruses recruit host ribosomes and other translation-required components, such as the eukaryotic translation elongation factor 1A (eEF1A), that participate in a variety of mechanisms in several organisms (Li et al., 2013b), as well as chaperones and helicases that allow folding of viral proteins. For viral replication, viral (+)RNA templates are recruited by specific host membranes and the viral replication complexes (VRCs) are established there. Host RNA-binding proteins facilitate transport of viral proteins and RNA to specific membranes. For example, *Tomato bushy stunt virus* (TBSV) p33 protein has a peroxisomal targeting signal and it interacts with host protein PEX19 that acts as a transporter to peroxisomal membranes (Pathak et al., 2008). After translation and replication, viruses travel to neighbour cells through plasmodesmata (PD). To reach the periphery from the site of replication, viruses use transport route/s (the endomembrane system, secretory pathway, or cytoskeleton) to deliver the viral MPs, vRNPs or virions to the PD (Harries et al., 2010). For example, *Tobacco Mosaic Virus* (TMV) MP uses microtubules and other motor proteins (Heinlein, 2015a). In the PD, tubule-movement viruses use PD-located (PDLPs) host proteins to assemble the MP-tubule in the PD (den Hollander et al., 2016), and other host proteins, such as pectin methylesterase and glucanases, facilitate PD opening (De Storme and Geelen, 2014; Lionetti et al., 2014). Finally, most viruses use the phloem to transport themselves to new tissues. From the epidermis, plant viruses move through different cells types (epidermis, mesophyll, bundle sheath, phloem parenchyma and companion cells) to reach the phloem sieve elements (Hipper et al., 2013). Once in the sieve elements viruses use the source-to-sink flow of photoassimilates as passive transport to reach upper parts of the plant. Little is known about the exact mechanism and roles of the host factors in the phloem, although some have been identified. These include pectin methylesterases for TMV exit and transport through the vascular system in tobacco (Chen and Citovsky, 2003), IP-L protein from tobacco for *Tomato Mosaic Virus* (ToMV) phloem transport (Li et al., 2005), TCOI1 for CMV 1a

interaction that is necessary for systemic transport in tobacco (Kim et al., 2008a), amongst others.

The recruitment of host proteins by the virus and the host defence against it, may result in the disturbance of host physiology causing disease symptoms. Host immune responses result in symptomatic manifestation such as chlorotic lesions or spots, ringspots and necrotic lesions in infected cells (Mandadi and Scholthof, 2013). Viral factors affect several processes as well. Plant hormone signalling affections are related to developmental abnormalities such as stunting and leaf curling (Culver and Padmanabhan, 2007). At a molecular level, physiological processes affected upon viral infection are: (i) photosynthesis and photorespiration, which might be a direct effect of the viruses or a result of infection due to chloroplast damage, as chlorosis is a very common symptom observed in infected plant (Bhattacharyya and Chakraborty, 2018), (ii) stress responses such as the production of reaction oxygen species (ROS) that are accumulated and directly participate in cell death pathways (Kuźniak and Kopczewski, 2020), (iii) carbohydrate and aminoacid biosynthesis that might be upregulated or downregulated depending on the virus and even protein within this process (Rojas et al., 2014), (iv) protein folding proteins are frequently enriched (Verchot, 2012) and (v) pathogen defence proteins, such as pathogenesis-related proteins, chitinases, peroxidases, among others (Alexander and Cilia, 2016).

All molecules within the cell (proteins, nucleic acids, and others) form a dense network of molecular interactions. The architecture of molecular networks can reveal principles regarding organization and function of molecules within the cell, similarly as when protein structure tells us about the function and organization of a protein. High-throughput data provides maps of diverse networks as metabolic, protein-protein, protein-DNA. In a graphical representation of a network of co-abundant proteins, proteins are presented as nodes of the network and co-abundant proteins as undirected edges (Spirin and Mirny, 2003). Sets of proteins that are more connected with one another might work in the same function or biological pathway. Thus, identifying most connected sets of proteins, called modules, is key to understand biological pathways happening (Rives and Galitski, 2003). To do so, several algorithms cluster proteins together into modules that have more edges (interactions) within themselves and fewer with the rest of the network. At the same time, a high-connected

node is called ‘hub’ and it can be determined within each module. Hubs tend to essential and summarize the function/s of a module (Vandereyken et al., 2018).

CMV has the highest host range within plant viruses, and it is also well distributed throughout the globe, colonizing both temperate and tropical plant species (Palukaitis and García-Arenal, 2003). Its ability to adapt to new environments and hosts is also palpable with the variable symptoms that it can cause in different hosts. CMV symptoms range from mosaic and distortion of the leaves to fruit lesions, including as well chlorosis, severe mosaic, leaf deformation and dwarfism depending on the host and viral strain (Palukaitis et al., 1992). In *Cucumis melo* susceptible varieties, CMV can cause mosaic in the leaves, severely stunted growing tips, and although fruit may not show symptoms they are of poor quality (Palukaitis and García-Arenal, 2003). However, some melon genotypes have resistance to CMV (Karchi et al., 1975; Risser, 1977; Diaz et al., 2003; Dhillon et al., 2009; Daryono et al., 2010; Fergany et al., 2011; Malik et al., 2014). In the case of resistant melon variety ‘Songwhan Charmi’ (SC), the resistance to CMV is oligogenic (Karchi et al., 1975) and quantitative and it has a major QTL in chromosome XII (Dogimont et al., 2000; Essafi et al., 2009) that encodes *cmv1*. *cmv1* by itself can confer total resistant to CMV subgroup I strains, while at least three minor QTLs are involved in resistance to subgroup II strains (Guiu-Aragonés et al., 2014). *cmv1* encodes a vacuolar protein sorting 41 (CmVPS41) (Giner et al., 2017) that allows CMV-LS, from CMV subgroup II, replication and cell-to-cell movement but it impedes reaching the phloem and stops the virus at the bundle sheath (Guiu-Aragonés et al., 2016). However, the molecular mechanism by which CmVPS41, together with other host proteins, impedes movement of CMV subgroup strains II is still unknown.

This is the reason why in this Chapter a proteome network of co-abundant proteins was performed to get a better insight on CMV challenge at a protein level and study the biological pathways involved in compatible and incompatible plant-virus interactions in melon.

III.2. Material and Methods

III.2.1. Growth of plants, viral inoculations and agroinfiltration

In melon, plant growth and viral inoculations, with either CMV-LS and CMV-FNY sap, were performed as previously described in Chapter II sections II.2.1 and II.2.2 respectively.

In *N. benthamiana*, plant growth and agroinfiltrations with clones of RNA1, RNA2 and RNA3 from CMV-LS and CMV-FNY RNA, were performed as previously described in Chapter II sections II.2.1 and II.2.2 respectively.

III.2.2. Total proteome analysis

III.2.2.1. Protein extraction, fractionation and digestion

Frozen melon leaves were grinded with liquid nitrogen in a mortar. To the finely ground plant material (50 µL) 200 µL urea/DTT extraction buffer (8M urea, 5mM DTT, 100mM Tris, pH 8.5 (Carl Roth), protease inhibitor cocktail 2 and 3 (20 µL/mL) (Sigma)) was added, samples were mixed and incubated for 30 min at room temperature (RT). After centrifugation for 10 min (10k x g) at RT, the supernatant was removed and transferred to a fresh tube, this procedure was repeated up to 3 times, until no visible pellet was retained. Protein concentration was determined using Pierce 660 nm protein assay (Thermo Fisher Scientific). For digestion, samples were alkylated in 14 mM chloroacetamide (Sigma) for 30 min at RT in the dark, after which, an aliquot corresponding to 50 µg total protein was subjected to in-solution digestion. In brief, samples were diluted with 50 µL of 100mM Tris, pH 8.5, 1mM $CaCl_2$ and then 0.5 µg Lys-C (WAKO, Neuss, Germany) was added. Samples were incubated for 4h at 37 °C with shaking (200 rpm). Then 300 µL of 100mM Tris, pH 8.5 and 0.5 µg trypsin were added followed by incubation o/n at 37 °C with shaking. Samples were acidified with 20 µL of 50% TFA and split up for single BoxCar samples and library samples. For the library samples, 90 µL of each condition per replicate were mixed and submitted to Strong cation exchange or SCX fractionation. To this end, StageTips were prepared using 6 layers of Solid Phase Extraction (SPE) disk (Empore Cation 2251 material by 3M, St. Paul, USA,) activated with acetonitrile and 100 µl each StageTip of 1% TFA (Sigma, St. Louis, USA) and washed with 100 µl of buffer A (water, 0.2% TFA) by spinning 5 min (1.5k x g), samples were acidified to 1 % TFA, loaded by centrifugation (10 min, 800 x g) and washed with 100

µl buffer A (5 min, 1.5k x g). Fractionation was carried out using an ammonium acetate gradient (20% acetonitrile (ACN), 0.5 % formic acid (FA)) starting from 25 mM to 500 mM for 9 fractions and two final elution steps using 1% ammonium acetate (Sigma), 80% ACN and finally 5% ammonium acetate, 80% ACN (Fisher Scientific). All fractions were eluted by centrifugation (5 min, 500 x g) using 2 x 30 µL eluent. The fractions were dried and resuspended in 10 µL buffer A*. For measurement, library samples were diluted 1:10. For the BoxCar analysis, the remaining samples were desalted with C18 Empore disk membranes according to the StageTip protocol (Rappsilber et al., 2003). The eluted peptides were dried and then resuspended in 10 µl buffer A*. Peptide concentration was determined by Nanodrop and samples were diluted to 0.1 µg/µl for identification of peptides in the liquid chromatography with tandem Mass Spectrometry.

III.2.2.2. Liquid Chromatography with tandem Mass Spectrometry (LC-MS/MS)

Library samples were analysed, and mass spectra were acquired as described in Chapter II M&M section II.2.9.4.

For BoxCar samples EASY-nLC 1200 (Thermo Fisher) coupled to a Q Exactive Plus mass spectrometer (Thermo Fisher) was used and peptides were separated, loaded on the column, and eluted as previously described in Chapter II except for mass spectra acquisition. For BoxCar samples, mass spectra were acquired in a data-independent manner using the MaxQuant. Live application (Wichmann et al., 2019). The acquisition was initiated using the "magic scan" protocol and consisted of one full MS scan with a mass range of 300–1650 m/z at a resolution of 140,000 FWHM, a target value of 3×10^6 ions and a maximum injection time of 20 ms. This was followed by two BoxCar scans, each consisting of 10 boxes with 1 Da overlap and a scan range from 400-1200 m/z. The maximum injection time for a BoxCar scan was set to 250 ms, with a resolution of 140,000 FWHM, a target value of 5×10^5 ions. The 5 most abundant ions from each BoxCar scan were selected for HCD fragmentation at a normalized collision energy of 27. Precursors were selected with an isolation window of 1.4 m/z. MS/MS spectra were acquired with a target value of 10^5 ions at a resolution of 17,500 FWHM, a maximum injection time (max.) of 28 ms and a fixed first mass of m/z 50. Peptides with a charge of +1, greater than 5 or with unassigned charge state were excluded from fragmentation for MS, dynamic exclusion for 30s prevented repeated selection of precursors.

III.2.2.3. Data analysis

Raw data were processed using MaxQuant software (version 1.6.3.4, http://www.maxquant.org/) (Cox and Mann, 2008) with label-free quantification (LFQ) and iBAQ enabled (Tyanova et al., 2016). Library samples and BoxCar samples were grouped into separate parameter groups. In the group specific parameters, library samples were set to "Standard" type and BoxCar samples to "BoxCar" type, in the Misc. setting the Match type for library samples was set to "match from" and for BoxCar to "match from and to". MS/MS spectra were searched by the Andromeda search engine, as previously described in Chapter II M&M section II.2.9.5.

Statistical analysis of the MaxLFQ values was carried out using Perseus (version 1.5.8.5, http://www.maxquant.org/). Quantified proteins were filtered for reverse hits and hits "only identified by site" and MaxLFQ values were log2 transformed. After grouping samples by condition, only those proteins that had three valid values in one of the conditions were retained for subsequent analysis. Then, two subsets were generated depending on the origin of the missing data. Missing at random (MAR) subset was created by filtering proteins for 1 valid value in each condition, the proteins filtered out were kept in a separate matrix and this matrix was the Missing Not At Random (MNAR) subset. Imputations of missing values was performed for each set: (i) the MAR dataset missing values were imputed with knn (nearest neighbor) imputation method with 4 nearest neighbours (Beretta and Santaniello, 2016), (ii) the MNAR dataset missing values were imputed with minProb method with the default parameters (q = 0.01) (Lazar et al., 2016). After imputation, the two subsets were merged again, and the rest of the analysis was performed on the whole set. Two-sample *t*-tests were performed using a permutation-based FDR of 5 % and significant proteins were filtered by fold change ($\log_2$ ratio) $\geqq$ 1 or fold change $\leqq$ -1. Perseus output was exported to Excel. The imputed dataset with all proteins was exported to R to continue network analysis.

A matrix of medians was generated within each treatment using the MaxLFQ of each replicate in Excel and imported to R (version 4.1.0). Volcano plots were generated with 'ggplot2' package, with S0 = 1 and FDR 0.05. Heatmaps were generated with 'pheatmap' package, with hierarchical clustering, according to the WardD2 method (Murtagh and Legendre, 2014), of Z-means of the median MaxLFQ for each protein.

III.2.3. Network of co-abundant proteins

Central networks were constructed in R (version 4.0.1) from the imputed datasets of relative intensity abundance of all detected proteins in LC-MS/MS (MaxLFQ). Co-abundance matrices were computed with values for controls and each of the treatments according to pairwise Pearson correlations, with adjusted p≦0.05, FDR correction according to the Benjamini-Hochberg method (Benjamini and Hochberg, 1995) to define node connectivity in each network with 'Hmisc' package. The correlation coefficient (r) cut-off was established with a density graph at the saturation of the network (Borate et al., 2009) that was used to create the co-abundance network with 'lgraph' package. Networks were exported to Cytoscape, version 3.8.2 (Shannon et al., 2003) for visualization and further analysis. From 'Analyze network' tool degree from all proteins was obtained and hubs from each module were characterized. To characterize hubs within each module, a distribution of the number of connections per each protein of that module was used to choose the hub or hubs in comparison to the rest. To see the distribution graphs refer to Supplementary material 3D "Analysis of modules and hubs". Network modularity was conducted either with: (i) Fast Greedy method (Clauset et al., 2004) 'lgraph' package for networks >500 nodes or with (ii) Cytoscape software Clustermaker app with 'Community Cluster' option which corresponds to a Fast Greedy algorithm combined with a Fruchterman-Reingold layout for networks <500 nodes (Shannon et al., 2003). To extract subnetwork of co-abundant proteins, one-way ANOVA (P≦0.05) was employed to exclude molecules that did not change under any of the conditions tested with package 'agricolae'. The significant proteins were retained, the matrix of co-abundant proteins, the corresponding subnetworks and modules were generated as previously described.

III.2.3.1. Gene Ontology and pathway enrichment

Module functional enrichment analysis was performed as previously described in Chapter II M&M section II.2.9.6 for *C. melo* and *N. benthamiana*.

III.2.3.2. Finding homologous hubs

Homologous *N. benthamiana* hubs were searched in *C. melo* to find their homologous proteins in melon. To do so, coding sequences from *N. benthamiana* genes were downloaded from Solgenomics database ([https://solgenomics.net/, (Bombarely et al., 2012)] and

BLASTed in Melonomics database with its BLAST tool ([https://www.melonomics.net, (Ruggieri et al., 2018)]. Good homology matches were considered with blast hits with an E-value < 0.01 (Wheeler, 2007).

III.3. Results

In this chapter, a proteome approach was used to have a better knowledge of molecular virus-host interaction during susceptibility and resistance scenarios. Three different melon genotypes with different responses to CMV challenge were tested. The proteome was prepared from all melon genotypes (PS, SC, NIL12-1-99), at either local or systemic stages of infection (4 dpi or 15 dpi) after CMV or mock-inoculation. The relative intensity values from the detected proteins were processed to generate a matrix of protein intensity across all treatments per each protein.

III.3.1. CMV causes great proteome perturbations in melon

Our approach provided a coverage of approximately 5,000 proteins in systemic infection and 5,600 in local infection. To investigate if there are disturbances in the proteome of CMV versus mock-inoculated melon plants two heatmaps were generated, for either local or systemic infection, with the Z-scores from relative intensity values of each protein and hierarchical clustering, to determine which treatments have the most similar protein intensity values across all detected proteins (for more information refer to M&M section III.2.2.3). As observed in the local infection heatmap, clustering per treatments shows two main clusters of treatments showing similar proteomes (indicated above the heatmap, **Figure III.1**A). One cluster includes the resistant SC plants and the second includes NIL and PS plants. This is, at local level, the proteome depends more on the genotype than on the virus inoculated. Thus, at early stages of infection, SC plants, either mock or CMV-inoculated, have a more similar proteome between them than compared to both NIL or PS plants. These results are not strange since at early stages of infection the melon response is starting, and NIL has a similar genome to PS. Then, it is expected that most of the proteome of the NIL at those stages is more like PS rather than like SC, from which, it only shares the 2.2 cM introgression that contains *cmv1* (Essafi et al., 2009). In the heatmap corresponding to the systemic infection, there are also two big clusters (indicated above the heatmap, **Figure III.1**B); one with all susceptible combinations (PS CMV-FNY, PS CMV-LS and NIL CMV-FNY), and the second with all resistant combinations and mock-inoculated plants. Thus, in systemic infection, the melon proteome is more similar in resistant and mock-inoculated plants than in the susceptible

infected melons. As a result, the NIL shows a different proteome at systemic infection depending on the CMV strain (LS or FNY) used for inoculation. NIL CMV-FNY-infected plants have a proteome more similar to PS CMV-infected plants, while NIL CMV-LS-inoculated plants have a proteome more like SC and mock-inoculated plants. This correlates with previous results, since after the phloem barrier, only the NIL infected with CMV-FNY can suffer a systemic infection, with the virus reaching upper leaves, while the NIL inoculated with CMV-LS restricts the virus to the bundle sheath cells, preventing systemic infection. Overall, CMV disturbs the melon proteome response, and it affects the proteome differently in local and systemic infection.

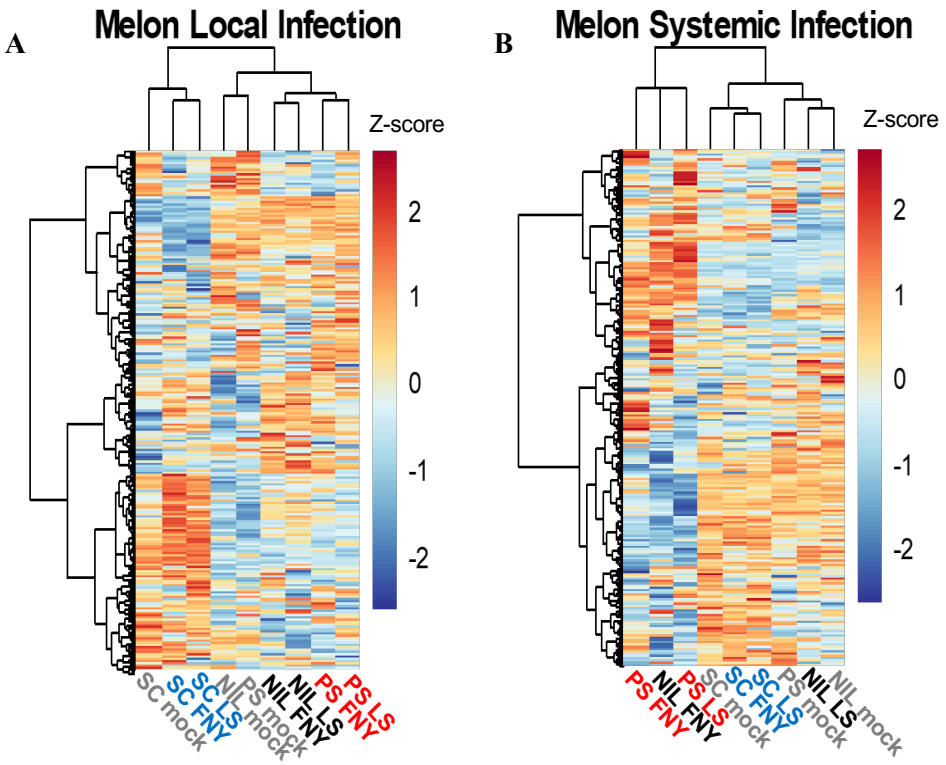

Figure III.1. Proteome disturbances in melon as a response to CMV infection. **A**. Heatmap of melon proteome response to CMV local infection (cotyledons). **B**. Heatmap of melon proteome response to CMV systemically infected leaves. Clusters per treatment are indicated above with tree structure, and protein clusters are indicated on the left side of the heatmap. Hierarchical clustering was performed according to the WardD2 method with Z-means of the relative intensity abundance values of each protein (liquid chromatography-tandem mass spectrometry peak intensity) per treatment. SC mock: SC mock-inoculated. SC FNY: SC CMV-FNY-inoculated. SC LS: SC CMV-LS-inoculated. NIL mock: NIL mock-inoculated. PS mock: PS mock-inoculated. NIL FNY: NIL CMV-FNY-inoculated. NIL LS: NIL CMV-LS-inoculated. PS FNY: PS CMV-FNY-inoculated. PS LS: PS CMV-LS-inoculated. Gray: mock-inoculated plants. Red: susceptible inoculated melon plants. Blue: resistant inoculated melon plants.

After the first observation that NIL CMV-FNY and NIL CMV-LS have either similar or distant proteomes depending on the stage of infection, we wanted to exactly see to which extennt these differences occurred. To do so, volcano plots (log2 fold-change ≧ 1; FDR 0.05) were generated to compare NIL CMV-FNY and NIL CMV-LS inoculated plants in either local or systemic infection. As observed in **Figure III.2**A, at local infection, there were only three proteins significantly enriched in NIL CMV-FNY plants and one significantly enriched in NIL CMV-LS, while at systemic infection stage, (**Figure III.2**B) many proteins were significantly enriched or decreased between both NIL CMV-inoculated plants.

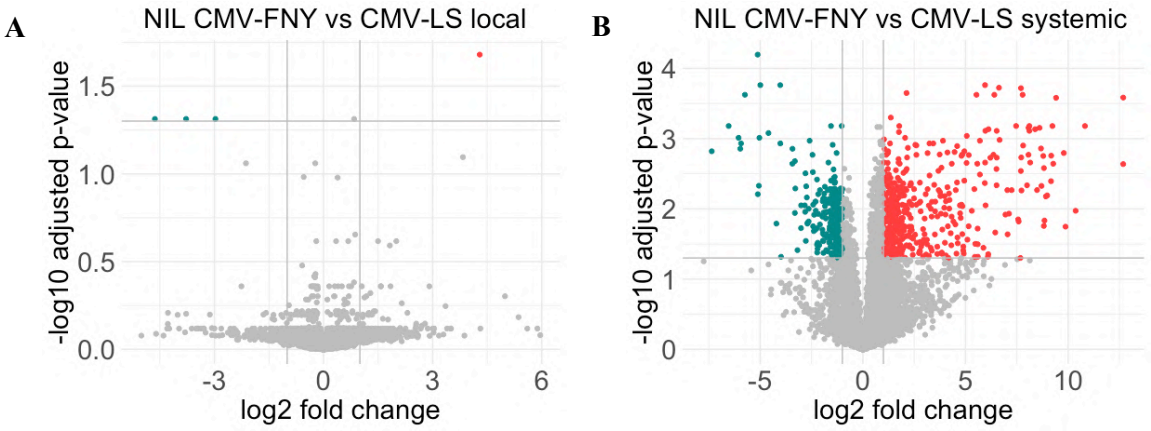

Figure III.2. Significantly enriched and depleted proteins in NIL CMV-FNY compared to NIL CMV-LS inoculated plants at different stages of infection. Local: local infection. Systemic: systemic infection. Volcano plots were generated with an absolute log2 in fold-change of ≧1 and FDR of 0.05 according to the Benjamini-Hochberg method.

The proteins with significant differences in NIL CMV-FNY versus NIL CMV-LS inoculations in local infection are:

(i) MELO3C010810.2.1, named Sigma factor sigb regulation protein rsbq, which is the only significantly enriched protein in NIL CMV-FNY compared to NIL CMV-LS. This protein is predicted to be a hydrolase (Hunter et al., 2009) that participates in axillary shoot meristem initiation (GO:00100223) and strigolactone biosynthetic process (GO:1901601) [https://www.melonomics.net, (Ruggieri et al., 2018)]. Its homologous protein in *Arabidopsis* (AT3G03990.1) encodes a hydrolase essential for strigolactone signalling, and is transported through the phloem to work as a signalling

molecule (Kameoka et al., 2016) and is also involved in secondary shoot formation (Beveridge and Kyozuka, 2010).

(ii) MELO3C026885.2.1, named Adenylyl-sulphate kinase, is increased in CMV-LS local infection. It is predicted to participate in sulphate assimilation (GO:0000103) and to have nucleotide binding (GO:0000166) and adenylylsulphate kinase activity (GO:0004020) [https://www.melonomics.net, (Hunter et al., 2009; Ruggieri et al., 2018)]. Its homologous protein in *Arabidopsis* (AT3G03900.1), named adenosine-5'-phosphosulfate kinase 3, provides an activated sulphate for the sulfation of secondary metabolites, including glycosynolates (Mugford et al., 2010).

(iii) MELO3C015851.2.1, named R3H domain-containing protein 4, is increased in CMV-LS inoculated NIL. It is an uncharacterized protein that is predicted to have nucleic acid binding activity (GO:0003676) [https://www.melonomics.net, (Ruggieri et al., 2018)]. Its homologous protein in *Arabidopsis* (AT1G03250.2) has an R3H domain involved in ribosome biogenesis (Cheong et al., 2021).

(iv) MELO3C011773.2.1, named oxidoreductase/transition metal ion-binding protein (DUF3531), also increased in CMV-LS locally infected NIL, is a protein of unknown function, like its homologous in *Arabidopsis* (AT5G08400.1).

In principle, looking at the bibliography, these differently abundant proteins found in local infection do not have a connection with CMV infection. However, they should not be underestimated.

In the case of systemic infection, there are many differentially abundant proteins between NIL CMV-FNY and NIL CMV-LS that will not be described one by one. Instead, this will be further investigated in section III.3.2, that will summarize global responses of CMV infection in all cultivars, taking a deeper look into this comparison as well. Moreover, in this first look at the proteins found in the proteome, some proteins belonging to HOPS complex were detected during CMV-FNY and CMV-LS systemic NIL infection, although no significant differences were observed in mock versus CMV-inoculated samples (**Table III-1**), meaning that these proteins are present but not enriched in one treatment compared to the other. Thus, this indicates that the presence of CmVPS41 and the other components of the HOPS complex are constitutively expressed independently of the infection.

Table III-1. HOPS proteins detected in systemic infection. T-test, FDR ≤ 0.05 (*), log_2 ratio for NIL CMV-FNY (NIL FNY), NIL CMV-LS (NIL LS) and NIL mock-inoculated (NIL-mock).

Name	log2 ratio NIL FNY vs NIL mock	p-value NIL FNY vs NIL mock	log2 ratio NIL LS vs NIL mock	p-value NIL LS vs NIL mock
Vacuolar protein sorting-associated protein 16-like protein	0.45	0.58	-0.99	0.28
Vacuolar protein sorting-associated protein 18-like	0.34	0.31	-0.37	0.38
Vacuolar protein sorting-associated protein 41 homolog	0.34	0.40	-0.49	0.27
Vacuolar protein-sorting-associated protein 11 homolog	0.31	0.32	-0.51	0.20

III.3.2. Network of co-abundant proteins during CMV infection in melon

After observing the differences in local and systemic proteomes, we aimed at providing a holistic interpretation of the reconfiguration of proteomes that capture the different biological processes in which these proteins are involved. To do so, local and systemic networks of co-abundant proteins were constructed from the matrixes of relative intensity values of proteins. First, the matrix of proteins across treatments was filtered to exclude proteins that did not change under any of the treatments tested (one-way ANOVA, $P \leq 0.05$). Then, pair-wise Pearson correlations (r) were computed to find the correlated abundance (co-abundance) between proteins across all treatments. To determine a cut-off for r in each network that preserves a significant number of connections (edges) while avoiding saturation, the evolution of network parameter density according to the absolute value of r was monitored with a resolution of 0.01 for each network. Density determines the real connections happening in a network compared to the hypothetic fully connected network (network where all proteins are interconnected). Thus, by increasing the absolute value of r, the density drops due to removal in connections (edges) and proteins (nodes) from the network, until a value for r (cut-off) where density rises again since the minimum number of nodes present in the network are well interconnected in the network (**Figure III.3**). Systemic infection showed the minimum number of connections with a higher correlation ($r \geq 0.94$) compared to local infection ($r \geq 0.90$).

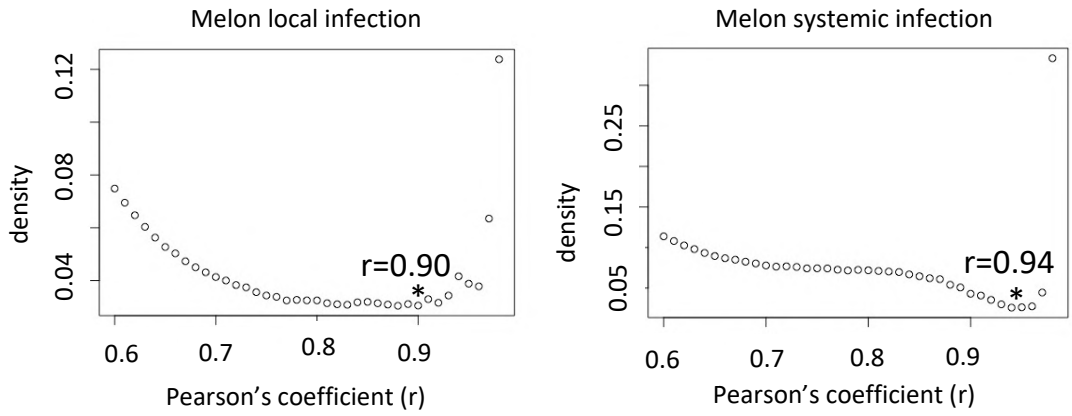

Figure III.3. Density of the main networks of co-abundant proteins in *C. melo* for local and systemic stages of CMV infection. Dot plots represent the density (portion of real connections out of all possible connections in a network) depending on the Pearson's coefficient (r). The r value cut-off (*) is the maximum correlation (r) per minimum density of connections of the network.

Networks of co-abundant proteins were constructed in which co-abundant proteins called 'nodes' in the network (black disks in **Figure III.4**) are connected by 'edges' (lines in **Figure III.4**) to other nodes. Each edge has a co-abundance value (r) associated per each two proteins connected with edges, $r \geq x$ depending on network. Communities of more than 10 co-abundant proteins were identified with the Fast Greedy algorithm (Clauset et al., 2004) and clustered in 'modules' (indicated in **Figure III.4**). For more information, refer to M&M section III.2.3.

Systemic and local networks of co-abundant proteins showed the same scale (408 nodes in the local network and 242 nodes in the systemic one) but differed in connectivity (2,535 edges in local network while 756 edges in systemic). This correlated with the average number of neighbours, which in the local network is 14.12 per protein against 6.7 neighbours in the systemic network. Thus, both networks have a similar number of proteins but, in local infection proteins are more connected, this is, there are more co-abundant proteins. Network modularity measures the strength of division of a network into modules, that are groups of proteins more connected (co-abundant) with one another than with the rest of proteins. In our case, modularity has intermediate values in both networks (0.51 in local infection and 0.53 in systemic infection) which means that there are groups of proteins highly connected (modules) within them, but these proteins are not exclusively connected with proteins of their module but have some minoritarian connections with proteins from other modules. Thus, for

each module, proteins that are found always in the same conditions most probably participate in the same biological processes. For this reason, finding modules helps to determine biological processes in a network and observe how this biological process interact with others (different modules). In our case, modularity is not equally distributed in local infection, in which module 3 is isolated from the rest (**Figure III.4**). Thus, the proteins within that module have no co-abundant proteins with proteins belonging to other modules, and the biological processes in which these proteins participate, which are gene expression and translation, seem to be more independent from the rest. Conversely, modules 1, 2 and 4 from local infection are densely connected outside their module, thus, their biological processes are highly related with one another, these processes are photosynthesis, sugar metabolism and biosynthesis of secondary metabolites and oxidation-reduction processes.

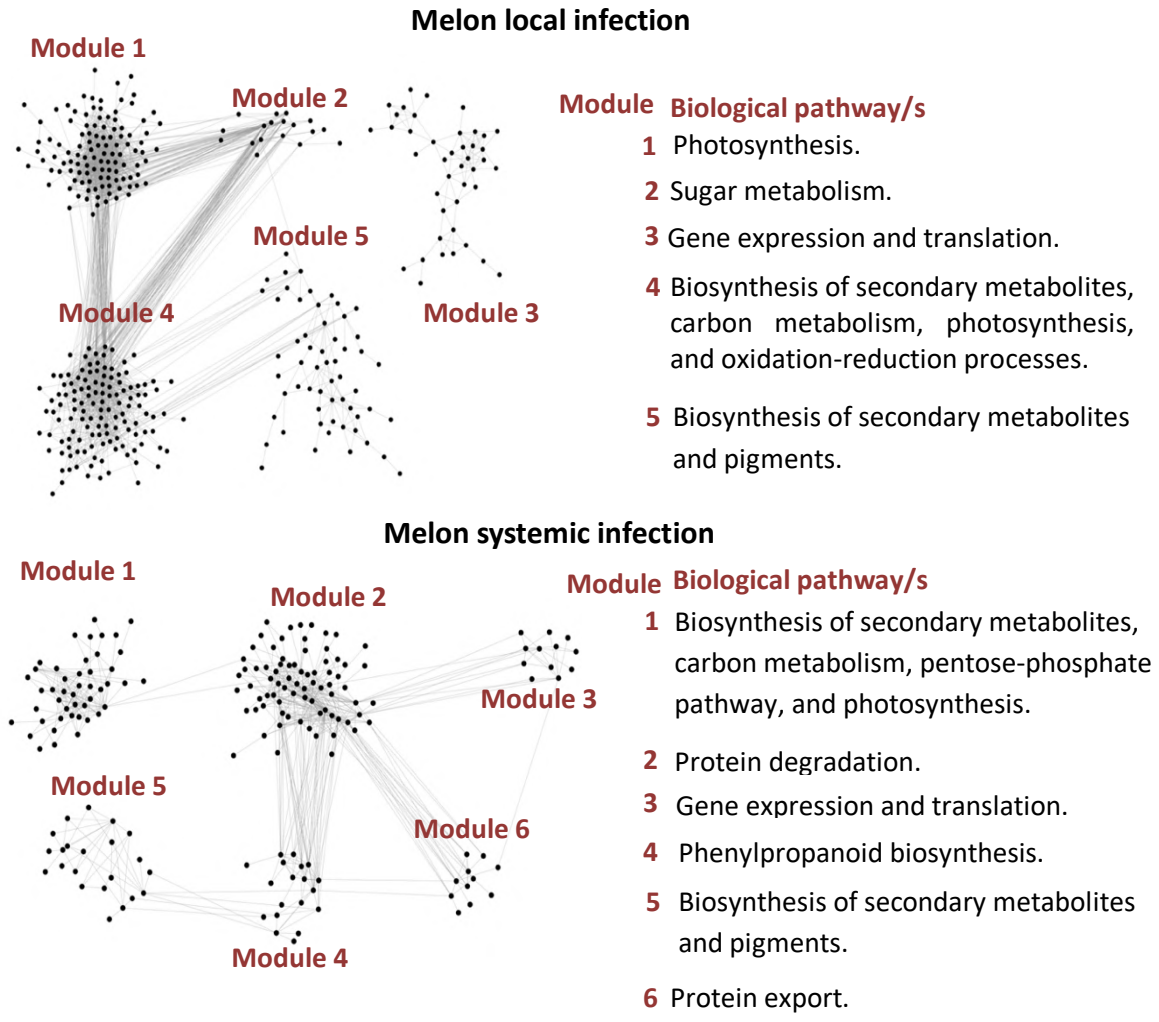

Figure III.4. Network of co-abundant proteins in systemic and local infection of CMV in melon. Circles represent proteins (nodes) and co-abundant proteins are connected with lines (edges). Each top-ranked significant GO terms and KEGG pathways (Fisher test; adjusted $p<0.05$) in each module are on the right for each network.

After seeing the structure of both networks and to investigate which biological processes are happening, a functional annotation of each module, using all the proteins within each module separately, was conducted with a Gene Ontology (GO) term and Kyoto Encyclopaedia of Genes and Genomes (KEGG) enrichment of no-redundant GO terms. The highest significant GO terms were used to annotate each module. As depicted in **Table III-2**, which contains the functional characterization of each module, gene expression, photosynthesis and biosynthesis of secondary metabolites and pigments were enriched in both local and systemic networks. Some biological processes were exclusive of each network; sugar metabolism (module 2), response to toxic substance and nitrogen metabolism (module 4) and oxidation-reduction processes (modules 1, 2, 4) were only present in the local network, while protein degradation (module 2), phenylpropanoid biosynthesis (module 4) and protein export (module 6) were exclusive of the systemic network. For detailed information of specific GO terms and adjusted p-values, refer to Supplementary material 3D "Analysis of modules and hubs". Taking together the functional characterization and the network organization, it can be seen that in local infection, biosynthesis of secondary metabolites (module 4) had several proteins co-abundant with other modules participating in gene expression (module 5), photosynthesis (module 1 and module 2), reduction-oxidation processes (module 1) and carbon metabolism (module 2), while in systemic infection, protein degradation (module 2) was most connected with the other modules, except for biosynthesis of secondary metabolites and pigments (module 5) (**Figure III.4**). Therefore, network organization and the biological pathways are connected to one another differently, also each network has specific biological processes happening.

Table III-2. Functional characterization of each module for local and systemic networks using a GO and KEGG enrichment (Fisher test; adjusted p<= 0.05). Enriched biological processes are orange coloured. The numbering of the modules is as in **Figure III.4**. Local modules: 1- photosynthesis, 2- sugar metabolism, 3- gene expression and translation, 4- biosynthesis of secondary metabolites, carbon metabolism, photosynthesis, and oxidation-reduction processes, 5- biosynthesis of secondary metabolites and pigments. Systemic modules: 1- biosynthesis of secondary metabolites, carbon metabolism, pentose-phosphate pathway, and photosynthesis, 2- protein degradation, 3- gene expression and translation, 4- phenylpropanoid biosynthesis, 5- biosynthesis of secondary metabolites and pigments, 6- protein export.

	LOCAL MODULES					SYSTEMIC MODULES					
Biological Process	**1**	**2**	**3**	**4**	**5**	**1**	**2**	**3**	**4**	**5**	**6**
Aminoacid metabolism											
Carbon fixation											
Gene expression											
Generation of precursor metabolites and energy											
Glycolysis											
Glyoxylate and dicarboxylate metabolism											
Sugar metabolism											
Nitrogen metabolism											
Nucleotide synthesis											
Oxidation-reduction process											
Oxoacid metabolism											
Pentose-phosphate pathway											
Photosynthesis											
Phenylpropanoid biosynthesis											
Pigment biosynthesis											
Protein degradation											
Protein export											
Protein folding											
Protein modification											
Response to toxic substance											
RNA binding											
Sulphur metabolism											
Synthesis of secondary metabolites											
Translation											

III.3.2.1. Biological processes affected upon CMV-inoculation

After characterizing the different biological processes in the two proteomic networks, we aimed at finding if some of these modules had proteins with increased or decreased abundance upon CMV infection. To do so, several pair-wise comparisons were performed between CMV versus mock-inoculated melon plants (T-test; FDR ≤ 0.05) and the differentially abundant proteins were coloured in the filtered network. In this section all comparisons are between CMV and mock-inoculated plants from the same cultivars. Thus, in the text it will not be specified each time that the specific CMV-inoculated plant is compared with its corresponding mock.

III.3.2.1.1. Biological changes in local infection of CMV in melon

In local infection, NIL and SC inoculated with either CMV-LS or CMV-FNY, present a large decrease in abundance of proteins (blue coloured nodes in **Figure III.5**A, C, D, F) within modules 3 and module 5, compared to their respective mock-inoculated plants. Module 3 participates in translation and gene expression, while module 5 is involved in biosynthesis of secondary metabolites and pigments. In other modules, such as module 1 and 4, there are only a few proteins with differences in abundance in NIL and SC CMV-inoculated plants. In PS there are no changes in abundance after CMV-LS inoculation (**Figure III.5**B), however, after CMV-FNY challenge a few depleted proteins are found in modules 3 and 5 (**Figure III.5**E). Therefore, in early stages of CMV-infection, susceptible PS plants present very little perturbances in the proteome, while in NIL and SC there are several changes focused on decreasing translation and secondary metabolism. These changes in protein abundance are independent on CMV strain in the case of SC and NIL genotypes, while in PS CMV-FNY is able to induce more changes in protein abundance than CMV-LS, although still fewer than those observed in SC and NIL plants.

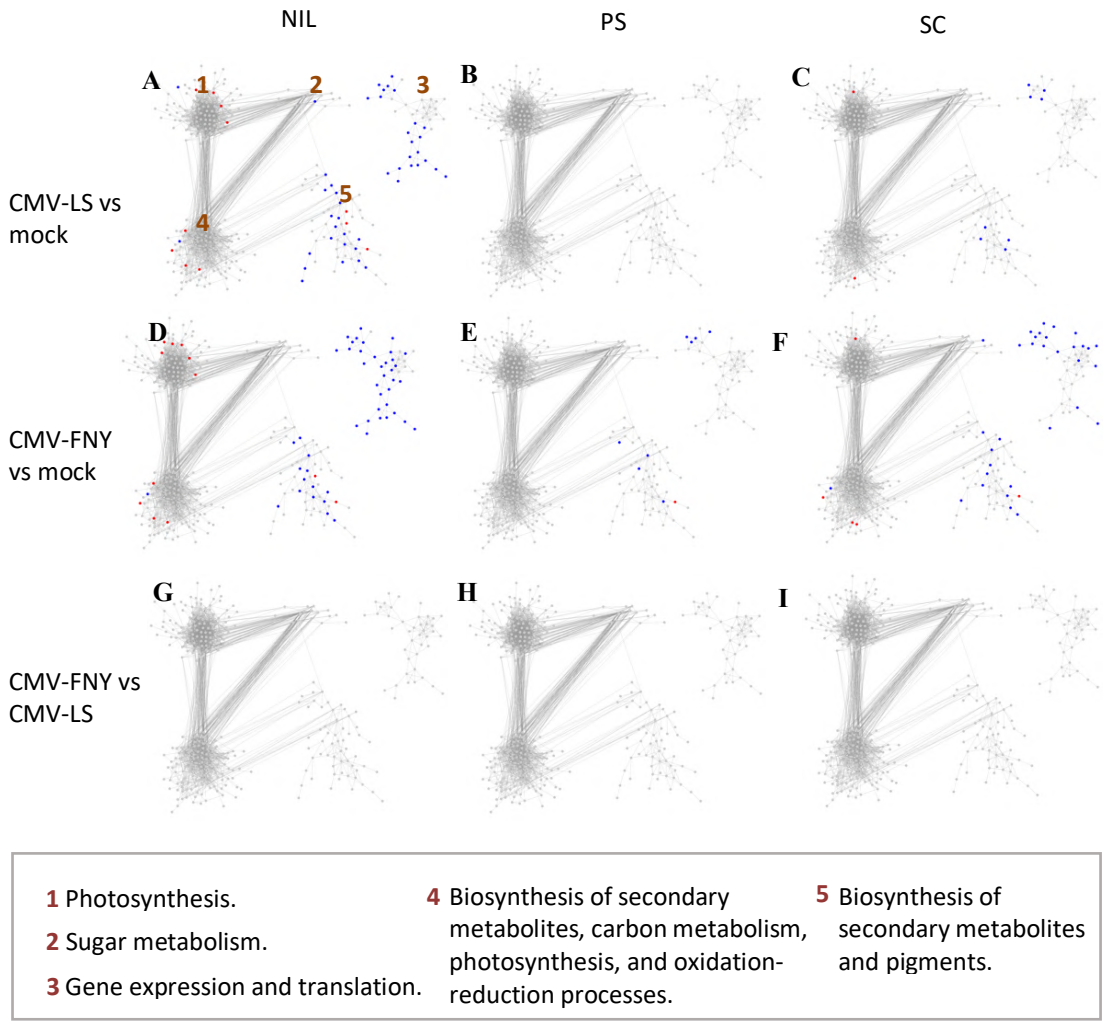

Figure III.5. Differentially abundant proteins upon CMV inoculation in local infection. Pair-wise comparisons with CMV compared to mock-inoculated plants (rows) within the same cultivar (NIL, PS or SC) (columns). Changes in protein abundance of each protein (node) are coloured: increased (red), decreased (blue), no changes (grey). The numbers to indicate each module are shown once but are the same in all the sub-networks. The legend box contains the biological characterization of each module.

i. Local sub-networks during CMV-inoculation

In local infection, modules 3 and 5 were re-investigated due to their high number of proteins with less abundance upon CMV inoculation in resistant genotypes. To do so, GO and KEGG terms enrichment analyses (Fisher test; $p<=0.05$ adjusted by Bonferroni correction) were performed as in previous comparisons. However, this time only proteins with less abundance in CMV-inoculated plants (within each module) were analysed, instead of using all proteins.

Nevertheless, SC CMV-LS analysis of less abundant proteins could not be performed due to the low number of proteins (minimum 10 needed).

As observed in **Table III-3**, GO and KEGG analysis of the proteins within module 3 that are less abundant upon CMV inoculation, show that these proteins are enriched by GO terms of translation (GO:0006412) and Coatomer protein I (COPI) (GO:0030663). Translation was already enriched in the previous terms analysis that considered all proteins of module 3, independently if they were more or less abundant. However, COPI vesicles enrichment appears exclusively for less abundant proteins upon CMV inoculation in resistant melons. Thus, it seems upon CMV inoculation there is both decrease in translation as well as in COPI vesicles in resistant genotypes. COPI vesicles are involved in retrograde transport of cargo from the Golgi apparatus to the endoplasmic reticulum (Guo et al., 2014).

Table III-3. GO and KEGG enriched terms in proteins with less abundance upon CMV inoculation in module 3 local infection. Fisher test; p-value<=0.05 adjusted by Bonferroni correction (p-adj) are considered significant (*).

Term name	**Term ID**	**p-adj NIL FNY vs NIL mock**	**p-adj NIL LS vs NIL mock**	**p-adj SC FNY vs SC mock**
Structural constituent of ribosome	GO:0003735	4.50E-18*	4.80E-05*	3.64E-07*
RNA binding	GO:0003723	4.44E-05*	0.006*	1
Unfolded protein binding	GO:0051082	0.005*	0.057	0.001*
mRNA binding	GO:0003729	0.033*	1	1
Translation	GO:0006412	1.22E-15*	3.78E-05*	1.08E-08*
Peptide biosynthetic process	GO:0043043	1.58E-15*	4.23E-05*	3.74E-07*
Gene expression	GO:0010467	1.64E-05*	0.665	0.033*
Protein metabolic process	GO:0019538	0.001*	1	1
Ribosome	GO:0005840	1.05E-16*	0.001*	1.82E-08*
Ribonucleoprotein complex	GO:1990904	3.78E-05*	0.172	1
Nascent polypeptide-associated complex	GO:0005854	0.003*	0.001*	1
COPI-coated vesicle membrane	GO:0030663	0.036*	0.011*	0.01*
Ribosome	KEGG:03010	3.36E-10*	1.19E-04*	2.39E-04*

In module 5, GO and KEGG term enrichment analysis (**Table III-4**) of proteins with decreased abundance upon CMV inoculation in resistant genotypes, showed an enrichment of GO and KEGG terms related to pigment biosynthesis in both NIL-CMV-inoculated plants, but not in SC CMV-FNY-inoculated plants, thus the decrease in pigment biosynthesis might be specific of NIL plants upon CMV inoculation. Also, other terms were enriched. This is the case for cytoskeleton proteins that were enriched in all resistant genotypes upon CMV inoculation. Thus, it would be expected that a decrease in abundance of proteins related to the cytoskeleton, that happens in all resistant genotypes upon CMV inoculation, might somehow be related to *cmv1*-controlled resistance. Moreover, proteins with lower abundance in CMV-LS-inoculated NIL plants had enriched GO and KEGG terms of carboxylic acid biosynthesis (GO:0046394) and biosynthesis of unsaturated fatty acids (KEGG:01040), while none of the CMV-FNY comparisons showed them. Thus, depletion of carboxylic acid and fatty acid biosynthesis could be specific to CMV-LS. Also, GTPase activity (GO:0003924) and phagosome (KEGG:04145) terms appear enriched exclusively in proteins with decreased abundance in CMV-FNY-inoculated plants (both NIL and SC) but not in the CMV-LS-inoculated NIL.

Table III-4. GO and KEGG terms enriched in proteins from module 5 local network with decreased abundance. Fisher test; p-value<=0.05 adjusted by Bonferroni correction (p-adj) are considered significant (*).

Term name	Term ID	p-adj NIL FNY vs NIL mock	p-adj NIL LS vs NIL mock	p-adj SC FNY vs SC mock
Structural constituent of cytoskeleton	GO:0005200	0.005*	0.013*	0.003*
GTPase activity	GO:0003924	0.032*	0.110	0.013*
Carboxylic acid biosynthesis	GO:0046394	1	0.003*	1
Chlorophyll biosynthesis	GO:0015995	0.010*	0.031*	1
Porphyrin-containing compound biosynthesis	GO:0006779	0.038*	0.113	1
Cytoplasm	GO:0005737	0.115	0.013*	1
Fatty acid metabolism	KEGG:01212	1	0.006*	1
Biosynthesis of unsaturated fatty acids	KEGG:01040	1	0.014*	1
Linoleic acid metabolism	KEGG:00591	0.296	1	1
Phagosome	KEGG:04145	0.030*	0.291	0.018*

In local infection, PS plants do not present major disturbances upon CMV inoculation, but NIL and SC plants have a decrease in translation, cytoskeleton and COPI vesicles. Moreover, in both CMV-inoculated NIL plants there is also a decrease in chlorophyll biosynthesis. Also, in CMV-LS-inoculated NIL plants, gene expression does not change and there is a depletion of biosynthesis of unsaturated fatty acid and carboxylic acid, which should be studied.

III.3.2.1.2. Biological changes in systemic infection of CMV in melon

In systemic infection, neither CMV-LS-inoculated NIL, nor CMV-inoculated SC plants presented changes in abundance compared to their respective mock-inoculated plants (**Figure III.6**A, C, F). In fact, these are the resistant combinations of plants, in which, although locally inoculated with CMV, at later stages CMV has not reached new leaves. In the susceptible combinations, NIL CMV-FNY, PS CMV-LS and PS CMV-FNY-inoculated plants (**Figure III.6**D, B, E), there are large perturbations through the whole proteomic network.

CMV-FNY-infected PS plants (**Figure III.6**E) present the least changes in protein abundance compared to the rest of susceptible combinations. Almost all disturbances belong to module 2, which was previously shown to be enriched by protein folding and protein degradation (**Table III-2**). Then, module 4, involved in phenylpropanoid biosynthesis, had also some protein abundance changes, but fewer than PS CMV-LS and NIL CMV-FNY had. Module 3 (translation) showed no changes, whereas modules 1, 5 and 6 had also little changes. CMV-LS-infected PS plants (**Figure III.6**B) presented many proteins with increased abundance in module 2 (protein degradation). Module 3 (translation) and module 5 (biosynthesis of secondary metabolites and pigments) presented several proteins with depleted abundance, and so do some proteins in module 1 (biosynthesis of secondary metabolites, pentose-phosphate pathway, and photosynthesis). In module 4 (phenylpropanoid biosynthesis) and 6 (protein export) most proteins have abundance changes, some increase and some decrease their abundance compared with mock plants. CMV-FNY infected NIL plants, compared to their mock-inoculated plants, presented an enriched module 2 (protein degradation), depleted both module 1 and module 3 (translation), and enriched and depleted proteins in both module 4 (phenylpropanoid biosynthesis) and module 6 (protein export) as had also been observed

in CMV-LS-inoculated PS. Therefore, at late stages of CMV infection protein folding and degradation was enriched (module 2 in **Figure III.6**D, B, E) in all melon susceptible plants and in the combinations PS-CMV-LS and NIL-CMV-FNY, translation was depleted. In the remaining modules there was no clear trend of enrichment/depletion in any susceptible genotype.

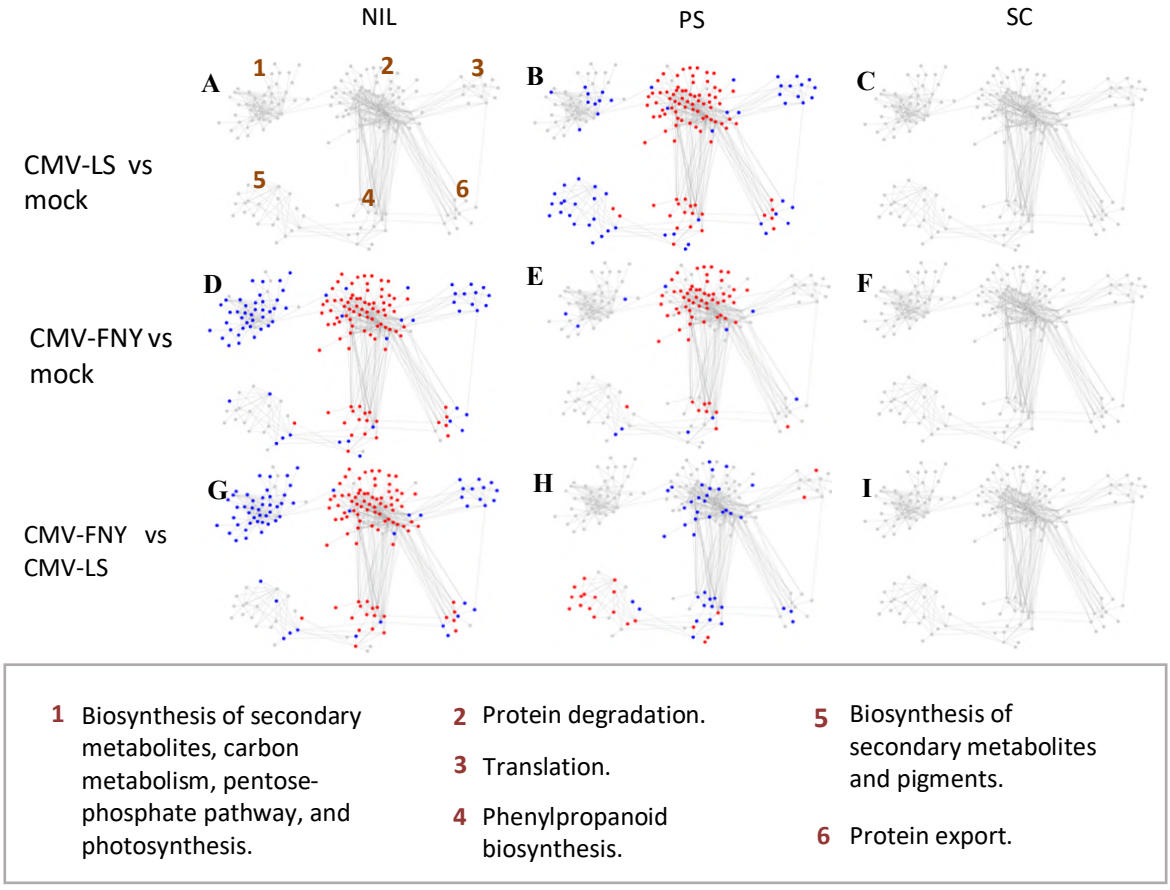

Figure III.6. Differentially abundant proteins upon CMV inoculation during systemic infection. Pair-wise comparisons with CMV compared to mock-inoculated plants (rows) within the same cultivar (NIL, PS or SC) (columns). Red nodes: significantly enriched proteins. Blue nodes: significantly depleted proteins. Gray nodes: proteins with no significant changes in abundance. The numbers indicate the module, which are shown once but are the same in all the sub-networks. The box contains a legend with the biological characterization summary of each module.

Looking at the most similar proteomes within susceptible networks, it can be observed that the combinations PS CMV-LS and NIL CMV-FNY presented the most similar proteome. Both combinations, showed a decrease in photosynthesis and carbon metabolism (module 1) and translation and gene expression (module 3 in **Figure III.6**B, D), while in PS CMV-FNY

these biological processes do not change. It seems that, at late stages of infection, in PS CMV-FNY plants there was no decrease in the generation of precursor metabolites, energy, and translation and little increase of phenylpropanoid biosynthesis, while there was an extreme depletion of energy, precursor metabolites and translation in PS CMV-LS infected plants. Moreover, biosynthesis of secondary metabolites and pigments (module 5) was depleted only in PS CMV-LS plants. Finally, phenylpropanoid biosynthesis (module 4) and protein export (module 6) were quite affected, including both enriched and depleted proteins in PS-CMV-LS and NIL CMV-FNY plants.

Systemic sub-networks during CMV-inoculation

After the analysis of susceptible genotypes in systemic infection, it was clear that some modules needed re-investigation to get a better knowledge of the effect of the increase or decrease of protein abundance in that module. We are referring to modules 4 and 6. Both modules present several proteins with changes in abundance which leaves unclear in which direction the biological processes of the module are affected. To understand the participation of these proteins in each module, these modules were re-investigated, if possible, through a GO and KEGG terms enrichment analysis (Fisher test; $p<=0.05$ adjusted by Bonferroni correction) of either enriched or depleted proteins separately. For fewer than 10 proteins within a comparison, bibliography was searched to know more about these proteins.

As observed in **Table III-5**, in module 4, in both PS CMV-LS and NIL CMV-FNY, the terms involved in biosynthesis of phenylpropanoid and secondary metabolites, as well as extracellular region and catalytic activity were enriched in abundance. Proteins with depleted abundance in module 4 (**Table III-6**) participate in the biosynthesis of nucleotides, aminoacid biosynthesis, translation, and chlorophyll biosynthesis, which agrees with previous results in (module 1 and 3 in **Figure III.6**B, D), that showed a decrease in translation, gene expression and photosynthesis in PS CMV-LS and NIL CMV-FNY plants.

Table III-5. GO and KEGG enriched terms in proteins that increase their abundance upon CMV inoculation in module 5 of systemic infection. Fisher test; p-value<=0.05 adjusted by Bonferroni correction (p-adj) are considered significant (*).

Term name	Term ID	p-adj value PS CMV-LS vs PS mock	p-adj value NIL CMV-FNY vs NIL mock
Catalytic activity	GO:0003824	0.011*	0.011*
Extracellular region	GO:0005576	0.004*	0.004*
Phenylpropanoid biosynthesis	KEGG:00940	0.004*	0.004*
Biosynthesis of secondary metabolites	KEGG:01110	0.047*	0.047*

Table III-6. Proteins with decreased abundance (blue) in module 5 during CMV systemic infection in both PS CMV-LS and NIL CMV-FNY plants. Their homologous proteins in *A. thaliana* and a bibliographical summary of the proteins are shown.

C. melo ID	*C. melo* Name	*A. thaliana* ID and name	Description *A. thaliana*
MELO3C020563.2.1	ATP-dependent zinc metalloprote-ase FTSH	AT2G29630.2; Pyrimidine requiring Thiamine C	Involved in thiamine biosynthesis. Protein of the iron-sulfur cluster. A severe reduction of 4-amino-2-methyl-5-hydroxymethylpyrimidine phosphate synthase (THIC) levels decreases vitamin B1 (Raschke et al., 2007; Wachter et al., 2007; Kong et al., 2008).
MELO3C025408.2.1	thiamine thiazole synthase	AT5G54770.1; Thiamine 4	Encodes a thiamine biosynthetic gene that has a dual function in thiamine biosynthesis and mitochondrial DNA damage tolerance. It appears to be involved in producing the thiazole portion of thiamine (vitamin B1) (Rapala-Kozik et al., 2012; Garcia et al., 2014).
MELO3C010552.2.1	translation initiation factor IF-2	AT1G17220.1; Fug1	Encodes a chloroplast localized protein with similarity to translation initiation factor 2. Suggested as a translation initiation factor *in vivo* (Miura et al., 2007).
MELO3C016714.2.1	Protochloro-phyllide reductase	AT4G27440.1: Protochloro-phyllide oxidoreductase B	Light-dependent NADPH:protochlorophyllide oxidoreductase B involved in chlorophyll biosynthetic process and response to ethylene (Zhong et al., 2009; Buhr et al., 2017).
MELO3C018695.2.1	Ketol-acid reductoisome-rase	AT3G58610.; ketol-acid reductoisome-rase	Predicted to be involved in aminoacid biosynthesis (isoleucine and valine) (Gaudet et al., 2011).

Module 6 was previously characterized as to participate in protein export and modification, (**Table III-2**). However, in PS CMV-LS and NIL CMV-FNY comparison with their respective mock plants, half of the proteins had increased abundance and the rest, decreased. Thus, it was not clear which biological processes were affected in the module. To get a better idea, a bibliographical search was done for each protein to determine the module affection in these comparisons. As observed in **Table III-7**, the proteins with enriched abundance (in red) are three protein disulfide isomerase-like (PDIL) proteins and two heat shock proteins. These proteins are highly connected with proteins from module 2 (protein degradation). On the other hand, depleted proteins (in blue) have different functions, such as biosynthesis of secondary metabolites, generation of energy, photosynthesis, and translation, which were already observed in other modules as depleted, so it is not unexpected. Overall, it seems that protein export and modification are enriched in the combinations PS CMV-LS and NIL CMV-FNY and this is highly connected with protein degradation.

Table III-7. Bibliographical summary of proteins of module 6 from systemic infection. Proteins with enriched abundance are in red and proteins with depleted abundance are in blue.

***C. melo* ID**	**Name *C. melo***	***A. thaliana* ID and name**	**Description *A. thaliana***
MELO3C006552.2.1	Glucose-1-phosphate adenylyltrans-ferase	AT5G19220.1; Glucose pyrophospho-rylase 2	It catalyzes the first step in starch biosynthesis (Streb and Zeeman, 2012).
MELO3C005568.2.1	Adenosine tRNA methylthiotrans-ferase MiaB	AT1G62780.1; dimethylallyl, adenosine tRNA methylthio-transferase	It is predicted to be involved in flavonoid biosynthesis and cold response (Depuydt and Vandepoele, 2021).
MELO3C024010.2.1	Porphobilino-gen deaminase	AT5G08280.1; Hydroxymethyb ilane synthease	Involved in chlorophyll biosynthesis and chloroplast RNA modification. In the absence of pathogen attack mutants develop chlorotic leaf lesions (Lim et al., 1994; Huang et al., 2017).
MELO3C005462.2.1	Transcriptional coactivator in dehydratase	AT5G51110.1; Rubisco assembly factor 2	It participates in Rubisco assembly that mediates abscisic acid-dependent stress response (Zhang et al., 2015). It also participates in the ribulose biphosphate carboxylase complex assembly (Fristedt et al., 2018).

MELO3C003811.2.1	50S ribosomal protein l31	AT1G75350.1; Embryo defective 2184	This protein encodes a ribosomal protein L31 that supports translation under stress (Pulido et al., 2018).
MELO3C024550.2.1	Signal recognition particle 54 kDa protein	AT5G03940.1; Chloroplast signal recognition particle 54 Kda subunit	It participates in protein import into the chloroplast thylakoid membrane (High et al., 1997).
MELO3C010625.2.1	Protein disulfide-isomerase-like	AT1G21750.1; Protein disulfide isomerase 5	It encodes a protein disulfide isomerase-like (PDIL) protein that is up-regulated in response to Endoplasmic Reticulum (ER) stress (Lu and Christopher, 2008).
MELO3C015939.2.1	Protein disulfide isomerase	AT2G47470.1; Protein disulfide isomerase 11	It encodes a PDIL that is also induced by three different chemicals of ER stress (Lu and Christopher, 2008).
MELO3C026855.2.1	Protein disulfide-isomerase	AT5G60640.1; Protein disulfide isomerase 2	Encodes a PDIL but unlike other PDI family members, transcript levels for this gene are not up-regulated in response inducers of ER stress (Cho et al., 2011).
MELO3C026399.2.1	Heat shock 70 kDa protein	AT4G16660.1; Heat shock protein 70 (Hsp70)	As previously explained in Chapter II, Hsp70 acts in response to ERAD mechanism (Nakatsukasa et al., 2008) and participates in several viral infections at multiple levels (Mine et al., 2012; Gorovits et al., 2013; Molho et al., 2021).
MELO3C005757.2.1	Luminal binding heat shock protein 70	AT5G28540.1; BIP1	Encodes the ER luminal binding protein BiP, member of the HSP70 family that binds improperly or incompletely folded proteins (GO:0051787) in the ubiquitin-dependent ERAD pathway (GO:0030433) (Lu and Christopher, 2008). It also participates in polar nuclei fusion and gametogenesis (Maruyama et al., 2010, 2014).

III.3.2.2. Biological processes different between melon genotypes

The same network approach was used to seek differences between melon genotypes, although this is a secondary objective of the proteome study. Pair-wise comparisons of the melon genotypes were performed, following the same methods as in CMV comparisons, and the differentially abundant proteins were coloured in the filtered network. In this section the only variable will be the melon genotype, while CMV inoculation will be with the same strain or mock-inoculated plant.

III.3.2.2.1. Local network differences depending on melon genotype

In the local network, PS compared to SC, either CMV or mock-inoculated, had most differences in module 1, with most proteins of the module with increased or decreased abundance (**Figure III.7** A, B, C). Thus, photosynthesis and carbon metabolism (module 1) seem to be very different in PS and SC plants. Also in module 2, that participates in sugar metabolism and oxidation-reduction processes, there were several proteins with changes in abundance in PS versus SC comparison, whereas in module 4 (biosynthesis of secondary metabolites) fewer proteins presented changes in abundance. In the case of NIL plants compared to SC, (**Figure III.7** D, E, F) almost the same changes than in the PS versus SC comparison were found, with most changes happening in module 1 and 2. This is not unexpected, since the NIL has mostly PS genome, except for the *cmv1*-containing introgression from SC. However, when comparing CMV-FNY-inoculated NIL and SC, module 3 was enriched. This module was associated to several processes including translation and protein folding. Thus, in early stages of CMV-FNY infection the NIL, which is susceptible to CMV-FNY, shows more abundance of proteins related to translation than in SC, which is the other resistant combination. In PS compared to NIL plants (CMV or mock-inoculated) (**Figure III.7** G, H, I) there are no changes in abundance, which again, is expected since their genome is mostly the same. These results correlate with the local infection heatmap (**Figure III.1**A) where two main clusters were observed: one with SC and a second one with PS and the NIL.

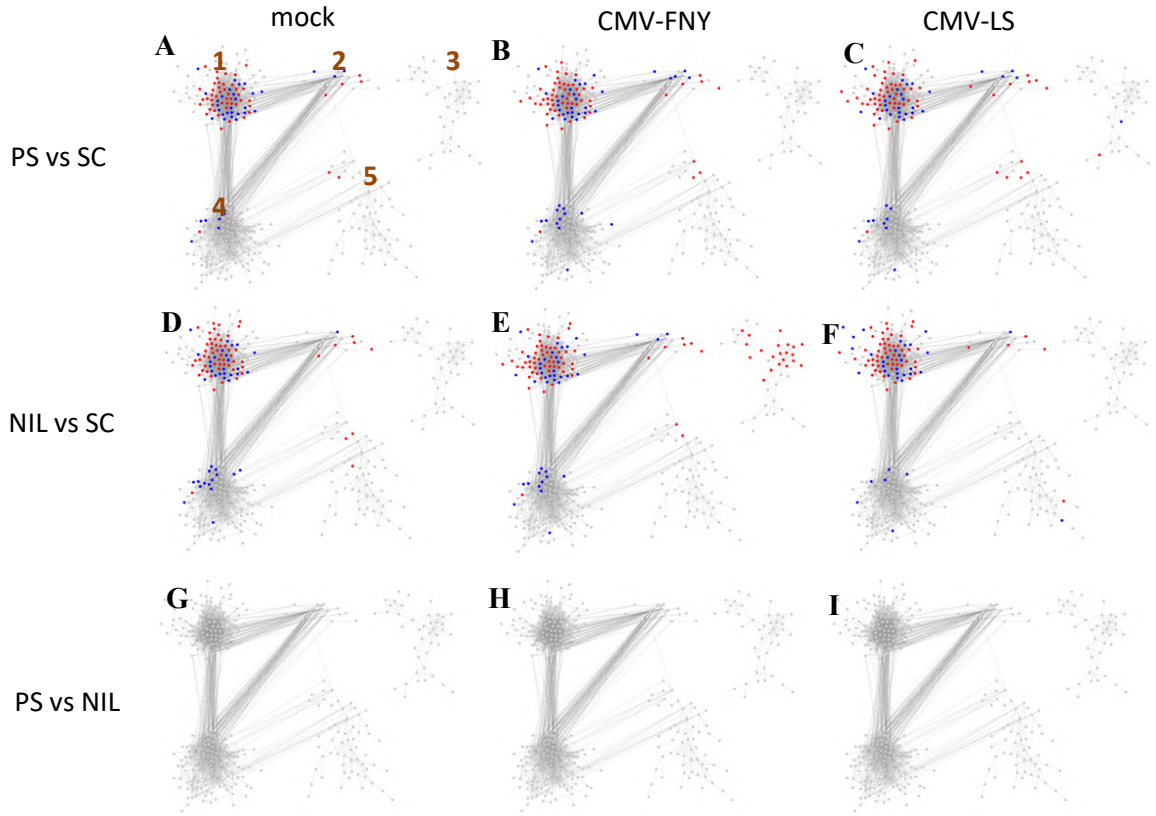

Figure III.7. Comparisons of local networks from melon genotypes (PS vs SC, NIL vs SC and PS vs NIL) (rows) between mock, CMV-FNY or CMV-LS inoculated plants (columns). Red nodes: significantly enriched proteins. Blue nodes: significantly depleted proteins. Gray nodes: proteins with no significant changes in abundance. The box contains a legend with the biological characterization summary of each module.

Local sub-networks to compare melon genotypes

To understand better the differences in locally inoculated leaves between PS and SC, we re-investigated module 1, since it has most changes in protein abundance. To do so, a GO and KEGG enrichment analysis was performed separating proteins with increased and decreased abundance upon pair-wise comparisons of PS genotype and SC with the same inoculation status As observed in **Table III-8**, PS seems to be enriched in inhibitors of protein degradation (GO:0004866, endopeptidase inhibitor activity) while proteins with decreased

abundance include those that participate in photosynthetic processes (GO:0016168, chlorophyll binding). Thus, PS would be expected to have less photosynthetic activity and stronger inhibition of protein degradation than SC, both in normal conditions as well as during CMV inoculation. Also, the comparison between CMV-FNY-inoculated PS vs SC, showed enrichment in cell wall proteins (GO:0005618). However, it is unknown if this could play any role in CMV-FNY infection compared to that of CMV-LS.

Table III-8. GO and KEGG enriched terms in module 1 for PS compared to SC genotypes. Enrichment analysis was performed separately for proteins with increased (red) or decreased (blue) abundance. Fisher test; p-value<=0.05 adjusted by Bonferroni correction (p-adj) are considered significant (*).

Term name	Term ID	p-adj PS CMV-FNY vs SC CMV-FNY		p-adj PS CMV-LS vs SC CMV-LS		p-adj PS mock vs SC mock	
Chlorophyll binding	GO:0016168	1	0.043*	1	3.26E-04*	1	0.048*
Endopeptidase inhibitor activity	GO:0004866	0.032*	1	0.032*	1	0.021*	1
Oxidoreductase activity	GO:0016491	0.107	1	0.498	1	0.039	0.544
Photosystem I	GO:0009522	1	0.009*	1	4.36E-05*	1	0.009*
Photosystem II	GO:0009523	1	0.023*	1	2.01E-04*	1	0.023*
Thylakoid membrane	GO:0042651	1	0.138	1	0.003*	1	0.138
Cell wall	GO:0005618	0.027*	1	0.359	1	0.254	1
Photosynthesis (antenna proteins)	KEGG:00196	1	0.002*	1	5,05E-06*	1	0.001*

Comparisons of PS and NIL with SC, gave very similar abundance changes, except for the enrichment of several proteins in module 3 when both NIL and SC were CMV-FNY inoculated (**Figure III.7**E). To get a better understanding of these differences, a GO and KEGG enrichment analysis was performed only for proteins with increased abundance in module 3 in the mentioned comparison. NIL proteins in module 3 compared to SC, both upon CMV-FNY inoculation (**Table III-9**), showed an enrichment of ribosome proteins and translation related terms. It seems that in the NIL, CMV-FNY can enhance the translation

machinery, while in SC it cannot do that, which could be related to the susceptibility of the NIL to CMV-FNY.

Table III-9. GO and KEGG analysis in module 3 for proteins with enriched abundance in NIL vs SC genotypes. Fisher test; p-value<=0.05 adjusted by Bonferroni correction (p-adj) are considered significant (*).

Term name	Term ID	adj p-value NIL CMV-FNY vs SC CMV-FNY	adj p-value NIL mock vs SC mock	adj p-value NIL CMV-LS vs SC CMV-LS
Structural constituent of ribosome	GO:0003735	1.01E-07*	1	1
RNA binding	GO:0003723	0.003*	1	1
Translation	GO:0006412	2.88E-05*	1	1
Peptide biosynthetic process	GO:0043043	3.76E-04*	1	1
Gene expression	GO:0010467	1.18E-07*	1	1
Ribosome	GO:0005840	1.47E-07*	1	1
Large ribosomal subunit	GO:0015934	8.28E-08*	1	1
Ribonucleoprotein complex	GO:1990904	4.07E-05*	1	1
Ribosome	KEGG:03010	4.42E-04*	1	1

III.3.2.2.2. Systemic network differences depending on the melon genotype

In systemic infection, the largest abundance differences between melon genotypes are found when comparing resistant or mock-inoculated plants with susceptible CMV-inoculated plants, this is, the combinations PS CMV-FNY, PS CMV-LS, NIL CMV-FNY with SC CMV-LS, SC CMV-FNY, NIL CMV-LS or mock-inoculated plants (**Figure III.8**). This was already observed in previous CMV comparisons (**Figure III.6**), as well as in the first heatmap based in the systemic infection (**Figure III.1**B). Again, the same modules are enriched or depleted during systemic infection in susceptible CMV-inoculated plants, that were already inspected in depth in section III.3.2.1.2.

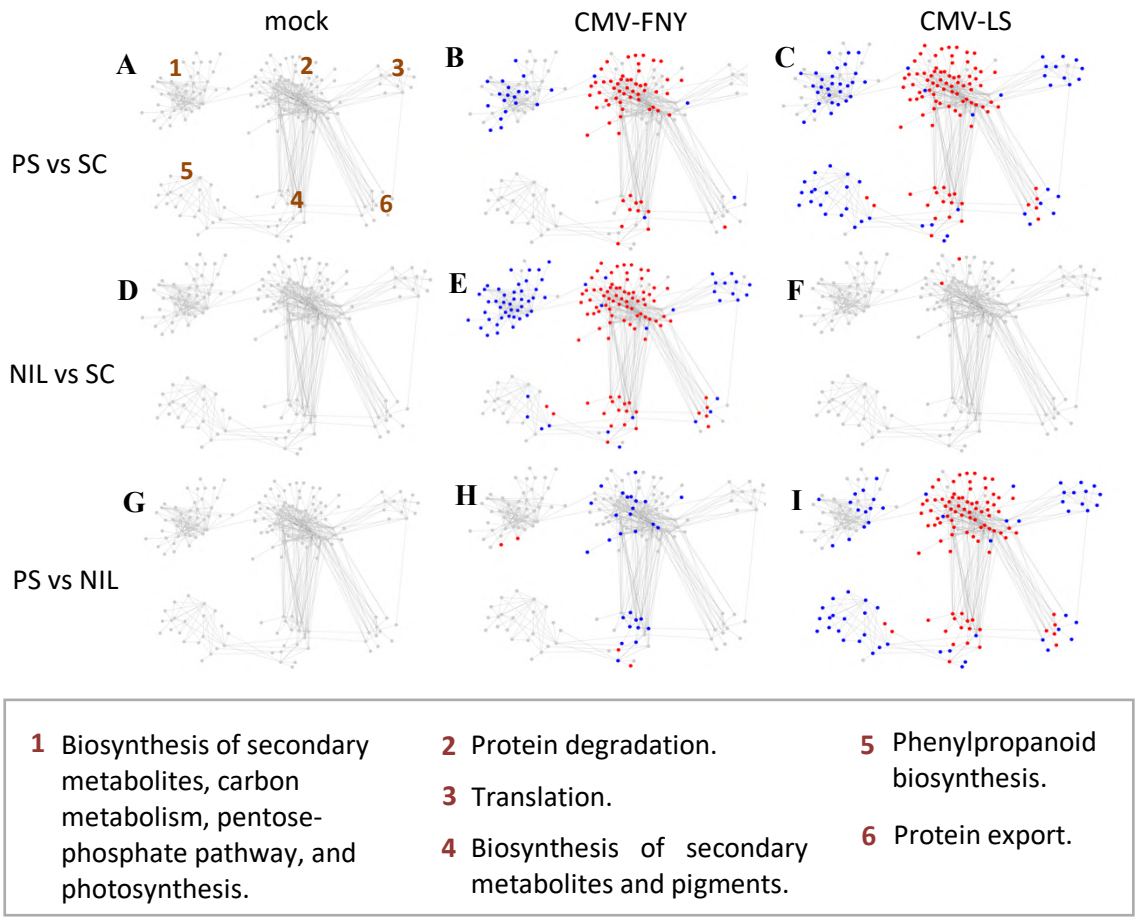

Figure III.8. Network of systemic infections comparing melon genotypes (PS vs SC and NIL vs SC) (rows) between mock, CMV-FNY or CMV-LS inoculated plants (columns). Red nodes: significantly enriched proteins. Blue nodes: significantly depleted proteins. Gray nodes: proteins with no significant changes in abundance. The legend (box) contains the biological characterization of each module.

III.3.2.3. Hubs in local and systemic C. melo networks

After observing the main biological processes governing CMV infection, we aim to identify the central components of CMV response in melon. For this reason, 'hub' proteins were determined in each module. Hubs are highly connected nodes that exceed the average, providing information about sets of co-abundant nodes (proteins), and therefore, coordinated proteomic changes (Berlingerio et al., 2011). As explained in M&M section III.2.3.2, hubs were determined by using a distribution graph of the number of edges or connections (degree) per nodes of all proteins within a module and choosing the nodes (proteins) with the highest connections independently of the degree of nodes from other modules.

In the local network, CMV infection is governed by hubs from modules 3 and 5, as these modules are the ones with most changes in protein abundance upon CMV infection, (**Figure III.5**). As observed in the degree distribution graph (**Figure III.9**A, marked with an asterisk), in module 3 there is one main hub: MELO3C022485.2.1, a 50S ribosomal protein L3 which participates in ribosome biogenesis (Popescu and Tumer, 2004). This correlates with the previous analysis in which module 3 proteins were enriched by translation GO and KEGG terms (**Table III-2**). In module 5 there are three main hubs (**Figure III.9**B): (i) MELO3C007233.2.1, a Mg-protoporphyrin IX chelatase, is involved in chlorophyll biosynthesis (Willows, 2003), (ii) MELO3C018025.2.1, a tubulin alpha chain protein, is the major constituent of microtubules (Gadadhar et al., 2017), and (iii) MELO3C016068.2.1, an UDP-glucose 6-dehydrogenase, is a key enzyme for generation of polysaccharides of the cell wall (Klinghammer and Tenhaken, 2007). Thus, although the characterization of module 5 suggested that these proteins participate in biosynthesis of secondary metabolites and pigments, it seems, that the cytoskeleton is also key for CMV local infection.

A

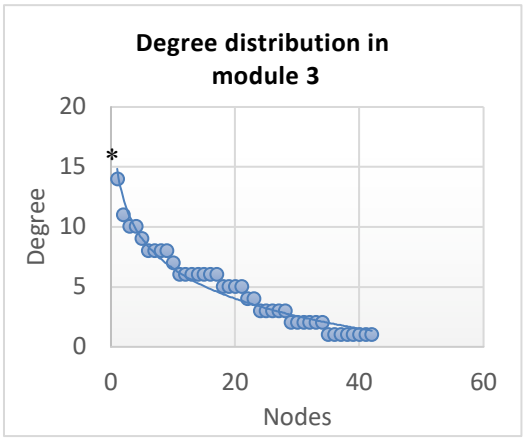

B

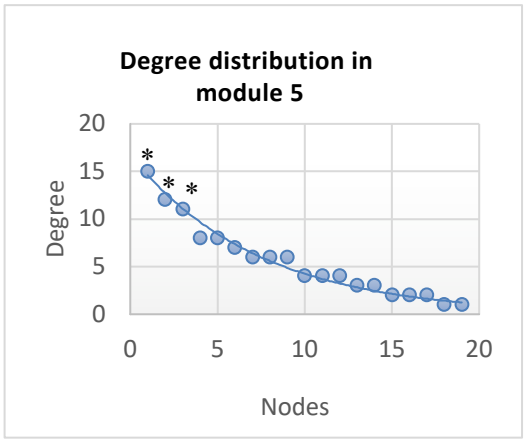

C

Hub	Name ID	M	NIL FNY vs NIL mock	NIL LS vs NIL mock	SC FNY vs SC mock	SC vs SC mock	LS vs LS mock	PS vs PS mock	PS vs PS mock	FNY
MELO3C022485.2.1	50S ribosomal protein L3	3								
MELO3C007233.2.1	Mg-protoporphy-rin IX chelatase	5								
MELO3C018025.2.1	Tubulin alpha chain	5								
MELO3C016068.2.1	UDP-glucose 6-dehydrogenase	5								

Figure III.9. Hubs in melon local infection. **A**. Distribution graph of the degree (number of edges or connections with other nodes) in all nodes from module 3. **B**. Distribution graph of the degree of all proteins within module 5. Hubs are indicated with an asterisk (*) and correspond to the nodes with higher degree (number of edges) with other proteins of the module. **C**. Hub summary with depletion (blue) or no change (white) of protein abundance in each comparison. M: network module.

In the systemic network, CMV infection affects only networks of susceptible interactions (NIL CMV-FNY, PS CMV-FNY, PS CMV-LS inoculated plants). Modules 2 and 4 present protein abundance changes in all susceptible genotypes upon CMV challenge (**Figure III.6**B, D, E). In module 2, two hubs were found (**Figure III.10**A): (i) MELO3C009453.2.1 is a monodehydroascorbate reductase that participates in oxidoreductase activity (GO:0016491), whose homologous protein in Arabidopsis acts in response to zinc ion (Fukao et al., 2009) and (ii) MELO3C011416.2.1, or alpha-1, is a 4-glucan-protein synthase UDP-forming which is probably involved in the biosynthesis of cell wall non-cellulosic polysaccharides (UniProt Consortium, 2021). These two proteins were not expected since GO and KEGG term enrichment analysis of all proteins within module 2 had pointed to biological processes related to protein degradation and folding. In module 4 three hubs were found (**Figure III.10**B): (i) MELO3C020563.2.1 is an ATP-dependent zinc metalloprotease FTSH. Its homologous protein in Arabidopsis is an iron-sulfur cluster protein that participates in thiamine biosynthesis and has a riboswitch in the 3'UTR that affects alternative splicing (Raschke et al., 2007; Kong et al., 2008). (ii) MELO3C005643.2.1, named Thaumatin-like protein, is predicted to participate in defence response (GO:0006952). Its homologous protein in Arabidopsis regulates the generation of Abscisic Acid (ABA) responses and is also involved in defence response (Capelli et al., 1997). (iii) MELO3C009826.2.1, a Carboxypeptidase, is predicted to participate in proteolysis (GO:0006508) and its homologous protein in Arabidopsis is located in the cell wall and plasmodesmata (Bayer et al., 2006; Aryal et al., 2014). Hubs from module 5 showed that, in fact, the most connected proteins within this module had decreased abundance upon CMV inoculation and were related to proteolysis and defence response, specifically to thiamine biosynthesis, while proteins with increased abundance were related to phenylpropanoid biosynthesis, as already observed in the previous GO and KEGG term analysis of enriched proteins within module 5 (**Table III-5**).

Overall, these results indicate that the key proteins of CMV systemic infection have increased abundance in susceptible cultivars, while resistant ones do not change protein abundance (**Figure III.10**C). In module 2, the key proteins participated in oxidation reduction and cell wall biosynthesis processes while in module 4, as expected from the network results, some proteins were enriched and participate in defence response and proteolysis processes while others had depleted abundance and participate in thiamine biosynthesis.

A

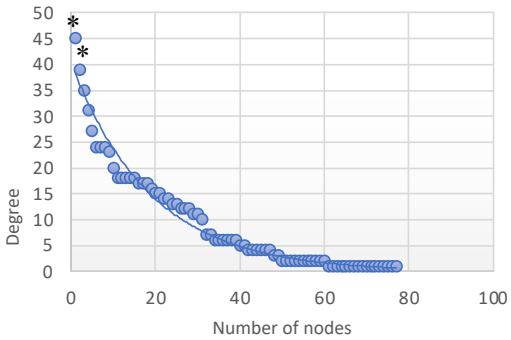

B

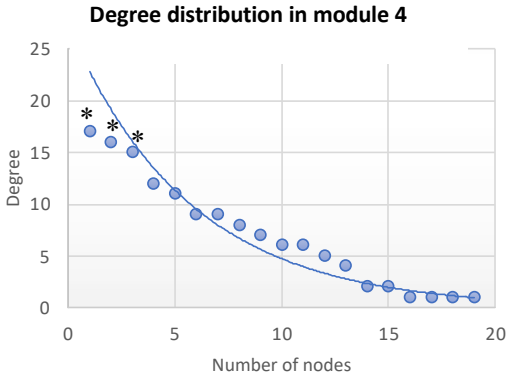

C

Hub	Name melonomics	M	NIL FNY vs NIL mock	PS FNY vs PS mock	PS LS vs PS mock	R
MELO3C009453.2.1	Monodehydroascorbate reductase	2				
MELO3C011416.2.1	alpha-1	2				
MELO3C020563.2.1	ATP-dependent zinc metalloprotease FTSH	5				
MELO3C005643.2.1	Thaumatin-like protein	5				
MELO3C009826.2.1	Carboxypeptidase	5				

Figure III.10. Protein hubs in modules 2 and 4 in melon systemic network. **A**. Distribution graph of degree per nodes in module 2. **B**. Distribution graph of degree per nodes in module 4. Hubs are indicated (*). **C**. Hub summary. R column represents all resistant comparisons between mock and CMV inoculated plants (NIL CMV-LS, SC CMV-LS, SC CMV-FNY inoculated plants compared with their respective mock-inoculated plants). M column indicated network module. Changes in protein abundance: significantly decreased (blue), significantly increased (red), no changes in abundance (grey).

As previously explained in the systemic network (**Figure III.6**), NIL CMV-FNY and PS CMV-LS have protein abundance differences in all modules. In modules 2 and 4, these differences were also common to PS CMV-FNY. For this reason, the rest of hubs of the systemic network were also investigated (**Figure III.11**). In module 1, three hubs were found: (i) MELO3C019634.2.1 is a phosphoglycerate kinase predicted to be involved in the glycolytic process (GO:006096). (ii) MELO3C017044.2.1, named Glyceraldehyde-3-phosphate dehydrogenase, participates in the reductive pentose-phosphate cycle of the Calvin cycle (cmo_M00165) (Marri et al., 2005). (iii) MELO3C027174.2.1 is an ATP synthase subunit beta that synthesizes ATP from ADP in the thylakoids. Its homologous protein in Arabidopsis also acts in response to cold (Goulas et al., 2006). All these hubs were expected, since glycolysis, pentose-phosphate pathway and generation of energy were enriched in the functional analysis of module 1 (**Table III-2**). In module 3 the three hubs found are related to ribosome biogenesis (MELO3C006733.2.1, MELO3C006733.2.1 and MELO3C022485.2.1), which makes sense, since module 3 was functionally characterized as involved in translation. In module 4 the most connected protein is MELO3C007233.2.1; a Mg-protoporphyrin IX chelatase which, as a magnesium chelatase, participates in chlorophyll biosynthesis, like its homologous protein in Arabidopsis (Rissler et al., 2002). Again, this hub has an expected function since module 4 was functionally characterized as a pigment biosynthesis module (**Table III-2**). In module 6 there was one hub which is MELO3C005757.2.1, the Luminal binding heat shock protein 70, which was previously mentioned (**Table III-7**) and participates in protein folding and response to endoplasmic reticulum stress (Lu and Christopher, 2008). Functional characterization of module 6 had determined its involvement in protein modification and export (**Table III-2**). Thus, it is expected that this hub would participate in a process related to protein folding and response to stress in the endoplasmic reticulum, which is tightly related with protein modification and export.

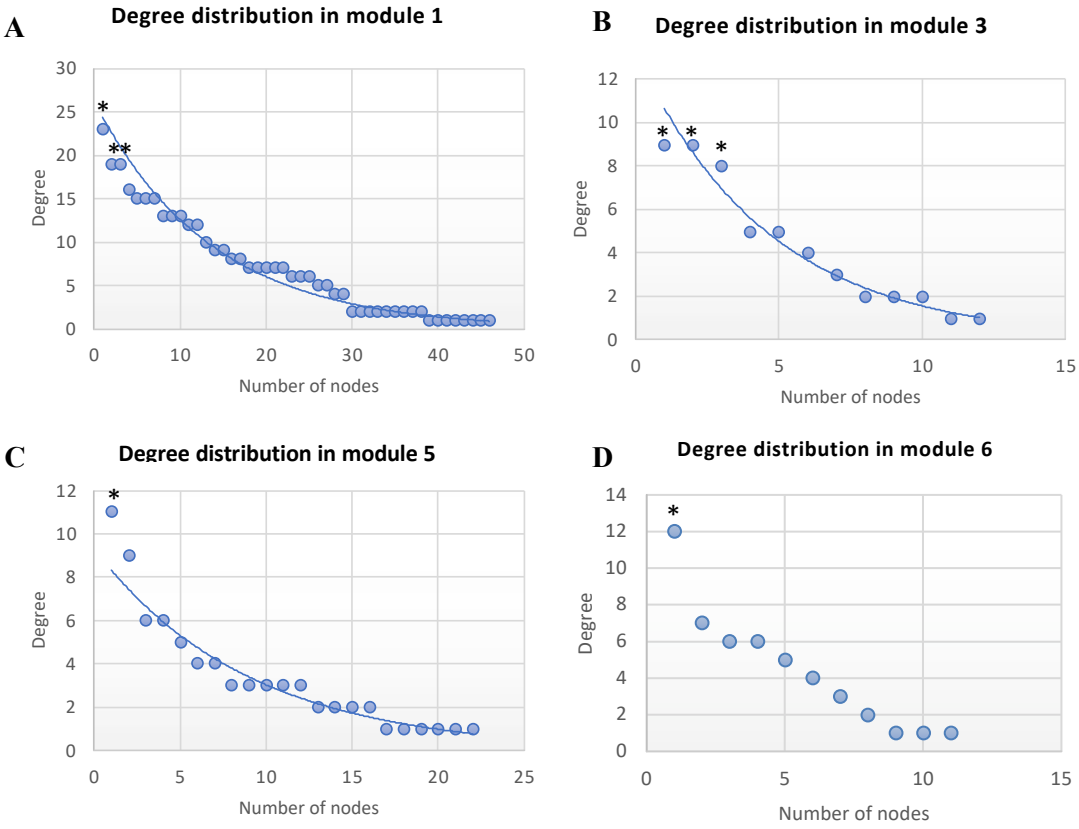

E

Hub	Name melonomics	M	NIL FNY vs NIL mock	PS FNY vs PS mock	PS LS vs PS mock	R
MELO3C019634.2.1	Phosphoglycerate kinase	1				
MELO3C017044.2.1	Glyceraldehyde-3-phosphate dehydrogenase	1				
MELO3C027174.2.1	ATP synthase subunit beta	1				
MELO3C006733.2.1	30S ribosomal protein S1	3				
MELO3C006088.2.1	50S ribosomal protein L5	3				
MELO3C022485.2.1	50S ribosomal protein L3	3				
MELO3C007233.2.1	Mg-protoporphyrin IX chelatase	4				
MELO3C005757.2.1	Luminal binding heat shock protein 70	6				

Figure III.11. Protein hubs in melon systemic network enriched or depleted in NIL CMV-FNY and PS CMV-LS inoculated plants in comparison to their mock-inoculated plants. **A**. Distribution graph of degrees per node in module 1. Hubs are indicated (*). **B**. Distribution graph of degrees per node in module 3. **C**. Distribution graph of degrees per node in module 5. **D**. Distribution graph of degrees per node in module 6. **E**. Hub summary. R column indicates all CMV-inoculated resistant combinations (SC CMV-LS, SC CMV-FNY, NIL CMV-LS compared with respective mock plant). Protein abundance changes: depletion (blue), no change (grey), enrichment (red).

III.3.3. CMV proteome in Nicotiana benthamiana

To study if there is a common response to CMV infection in other susceptible organisms, the proteome of *N. benthamiana* plants was studied after CMV-inoculation. The *N. benthamiana* proteome was prepared from either CMV-FNY, CMV-LS or mock-inoculated plants at local or systemic stages of infection (3 dpi or 15 dpi) as described in M&M sections III.2.2.1 and III.2.2.2. The relative intensity values from the detected proteins were processed to generate a matrix of protein intensity across all treatments per each protein. For more information refer to M&M section III.2.2.3. In this case, heatmaps were not generated, since only 3 treatments were available, which is not enough to perform a heatmap (minimum of 6 comparisons). Proteome co-abundance networks were generated for either local or systemic infection, as explained in M&M section III.2.3. Density graphs were performed as previously shown in *C. melo* and are available in Supplementary material 3D "Density graphs of *N. benthamiana*".

III.3.3.1. Protein abundance networks in Nicotiana benthamiana

To investigate if there were disturbances in the proteome of *N. benthamiana* plants upon CMV challenge compared to the mock-inoculated plants, proteins increased or decreased in their abundance (T-test; FDR ≤ 0.05) were plotted in the co-abundant networks. As observed in **Figure III.12**, at early stages of infection (local infection), both CMV-inoculated *N. benthamiana* plants have several protein abundance changes compared to their respective mock-inoculated plants. Later in infection (systemic infection), very few proteins have those changes. In local infection of *N. benthamiana*, there were five modules, all of them with many proteins affected in abundance, while in systemic infection there were 7 modules, with fewer proteins affected. The differences in abundance were almost exclusively in module 4, upon both CMV infection, and module 7, after CMV-LS infection. This is the opposite of what we observed in melon PS, where there were little disturbances in the local network (**Figure III.5**) whereas there was a more significant proteome disturbance in its systemic network (**Figure III.6)**. This is the first difference in the proteome response of the susceptible *N. benthamiana* and melon cultivar PS.

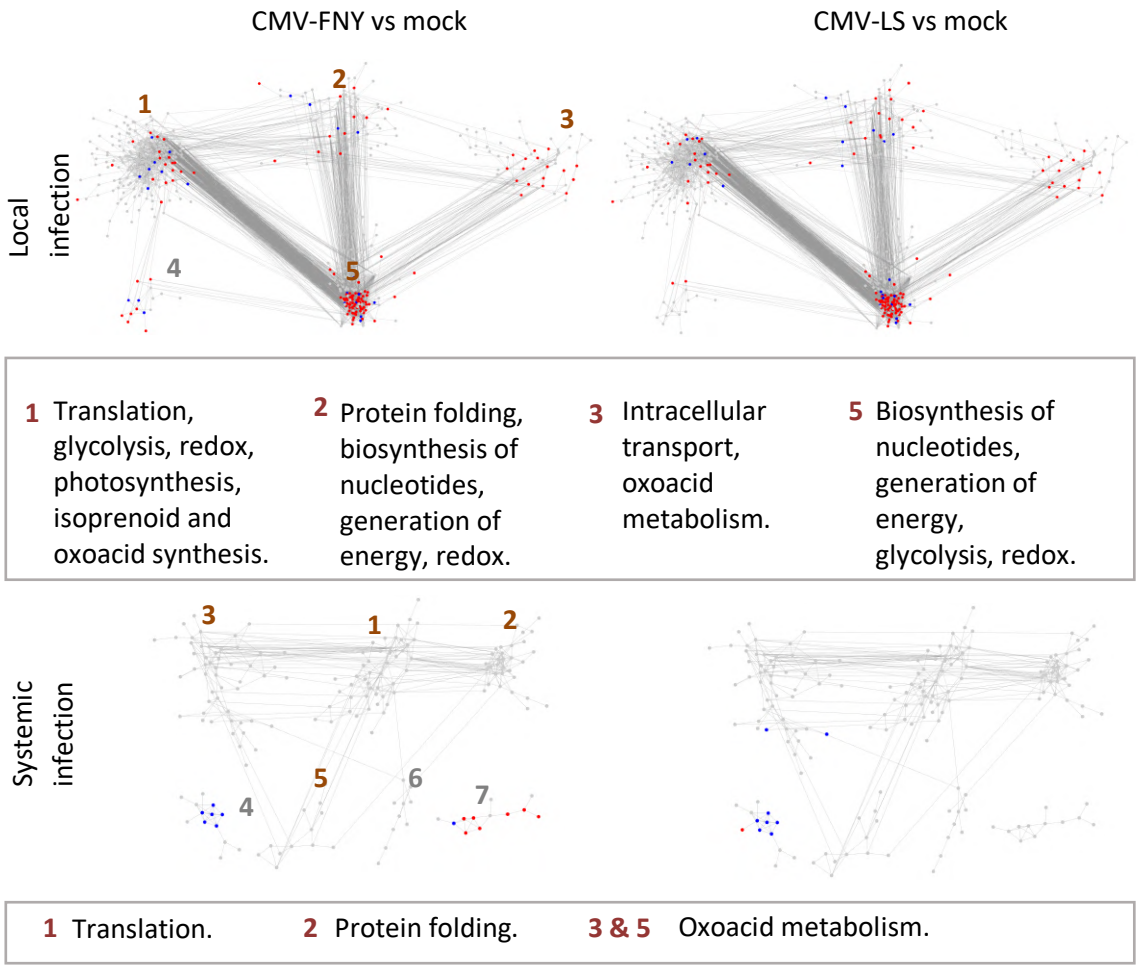

Figure III.12. *N. benthamiana* networks of co-abundant proteins. Circles represent proteins (nodes) and co-abundant proteins are connected with lines (edges). Red nodes: significantly enriched proteins. Blue nodes: significantly depleted proteins. Gray nodes: proteins with no significant changes in abundance. Modules with grey numbering could not be functionally characterized by a biological process and do not appear in the legend.

After observing the disturbances in *N. benthamiana* networks, we aimed at biologically characterizing each module to see if the processes of the network (either with protein abundance changes or not) were similar to those observed in the susceptible melon PS. To do so, a GO term enrichment analysis was performed for all the proteins in each module (Fisher test; p-value <0.05 with Bonferroni correction). In the modules identified in local infection (**Table III-10**) biological processes after the GO term analysis included: pigment biosynthesis (module 1), glycolysis, (module 1 and 5), oxidation-reduction processes (module 1, 2, 5), protein folding (modules 1, 2, 5), translation (module 1), photosynthesis (module 1), isoprenoid biosynthesis (module 1), oxoacid biosynthesis (module 1, 2, 3, 5),

nucleotide biosynthesis (module 2) and intracellular transport (module 3). However, module 4 was not enriched by any GO term, and could not be functionally characterized. In the modules of the systemic infection network the processes enriched were: oxoacid metabolism (module 3 and 5), translation (module 1) and protein folding (module 2). Also in this network some modules (4, 6, 7) had no GO term enrichment impeding its functional characterization. Thus, in *N. benthamiana* networks the biological processes affected were the same than those previously observed in *C. melo*, except for intracellular transport, only present in local *N. benthamiana* network (module 3 in **Figure III.12** and protein degradation which is exclusive of *C. melo* systemic network (module 2 in **Figure III.6**).

Table III-10. GO and KEGG term enrichment and functional characterization of each module for local and systemic networks of *N. benthamiana* (Fisher test; adjusted p<= 0.05). Enriched biological processes are orange coloured.

Biological Process	**LOCAL MODULES**					**SYSTEMIC MODULES**						
	1	2	3	4	5	1	2	3	4	5	6	7
Biosynthesis of nucleotides		■			■							
Generation of energy		■			■							
Glycolysis	■				■							
Intracellular transport			■									
Isoprenoid biosynthesis	■											
Oxidation-reduction process	■	■			■							
Oxoacid metabolic process	■		■					■		■		
Photosynthesis	■											
Pigment biosynthesis	■											
Protein folding		■					■					
Translation	■					■						

To re-investigate the similarities and differences between PS and *N. benthamiana* proteomes in local infection, a second GO term analysis was performed but this time only enriched or depleted proteins were used. As observed in **Table III-11**, both CMV-inoculated *N. benthamiana* plants showed a depletion of proteins related to carbohydrate metabolic process and an increase of redox processes and oxoacid metabolism, compared to the mock-inoculated plants. In addition, CMV-LS-inoculated compared with mock-inoculated *N. benthamiana* plants were also significantly enriched in terms related to response to stress, binding to unfolded proteins and peptidase activity (Fisher test; p-value <0.05 with

Bonferroni correction). Conversely, during early stages of infection in PS there was very little proteome perturbances and the few proteins with decreased abundance were related to translation, pigment biosynthesis and synthesis of secondary metabolites. Thus, at early stages of infection PS does not present changes similar to those of *N. benthamiana*, neither in the number of changes nor in the biological processes affected. In systemic infection of *N. benthamiana* there were not enough proteins to perform a GO term enrichment analysis, whereas in PS at this timepoint there were many disturbances, affecting several biological processes as well.

Table III-11. GO and KEGG enrichment analysis for either enriched (red) or depleted (blue) proteins in *N. benthamiana* local infection. Separated analysis for enriched and depleted proteins were performed and the results were merged in this table. Fisher test; p-value<=0.05 adjusted (p-adj) by Bonferroni correction.

Term name	Term ID	p-adj CMV-FNY vs mock	p-adj CMV-LS vs mock
Carbohydrate metabolic process	GO:0005975	0.018*	0.013*
Carboxylic acid metabolic process	GO:0019752	0.007*	0.0023*
Oxoacid metabolic process	GO:0043436	0.007*	0.0023*
Oxidation-reduction process	GO:0055114	0.00022*	0.00013*
Response to stress	GO:0006950	1	0.025*
Binding to an unfolded protein	GO:0051082	1	0.0047*
Cysteine-type peptidase activity	GO:0008234	1	0.032*

III.3.4. General hubs of CMV infection

To find inter-species key proteins for CMV infection, hub proteins from *N. benthamiana* modules were determined and blasted with *C. melo* reference genome (Ruggieri et al., 2018) to find their respective homologous melon proteins, either as hub proteins or other proteins present in the network, as explained in M&M section III.2.3.2. As observed in **Table III-12**, eight hub proteins from *N. benthamiana* were also found as proteins in *C. melo* network, although only two of them were also hubs in the *C. melo* network (alpha-1 and 6-phosphogluconate dehydrogenase decarboxylating 3 in **Table III-12**).

The common proteins are:

(i) Niben101Scf01209g04002.1, named Magnesium-chelatase subunit ChlI homolog. This protein is predicted to participate in chlorophyll biosynthesis (GO:0015995) and photosynthesis (GO:0015979) [https://solgenomics.net/, (Fernandez-Pozo et al., 2015)]. The *C. melo* hub from module 4 in systemic infection was another chelatase, although different from this one.

(ii) Niben101Scf05414g00004.1, named Alpha-1, is a 4-glucan-protein synthase UDP-forming protein that participates in biosynthesis of cellulose (GO:0030244) both in *C. melo* and *N. benthamiana*. This protein is also a hub in module 2 of the systemic network in *C. melo*.

(iii) Niben101Scf04347g00001.1, named Dynamin-related protein 5A, is predicted to participate in mitochondrial fission (GO:0000266) in both *C. melo* and *N. benthamiana* and it has microtubule binding activity (GO:0008017) (Gaudet et al., 2011). Its homologous protein in Arabidopsis (AT5G42080.1) functions in vascular patterning, embryogenesis, trichome branching, and endocytosis due to clathrin-coated vesicle formation in post Golgi trafficking (Collings et al., 2008; Fujimoto et al., 2010; Yoshinari et al., 2016).

(iv) Niben101Scf18107g00014.1, named D-glycerate 3-kinase, encodes a protein predicted to participate in photorespiration in the C2 cycle, like its homologous protein in Arabidopsis (Boldt et al., 2005).

(v) Niben101Scf08127g08009.1, named 6-phosphogluconate dehydrogenase decarboxylating 3. Both in *C. melo* and *N. benthamiana,* is predicted to participate in the pentose-phosphate pathway (GO:0006098), like their homologous protein in Arabidopsis (AT3G02360.2), which is involved in the pentose-phosphate shunt and D-gluconate catabolic process.

(vi) Niben101Scf08898g00002.1 and Niben101Scf09363g00018.1 are both named 60 kDa chaperonin and 60 kDa chaperonin 2. In *C. melo,* their homologous protein is the ruBisCO large subunit-binding protein subunit beta. Both participate in protein folding (GO:0006457) and refolding (GO:0042026).

(vii) Niben101Scf01982g00002.1, named PsbP-like protein 2, is part of an extrinsic subunit of photosystem II (GO:009523). Its homologous protein in Arabidopsis

is also a part of PsbP II and works in photosynthesis, where is required for the accumulation of the NADH dehydrogenase-like complex (Ishihara et al., 2007).

(viii) Niben101Scf04198g01001.1, named Ferredoxin-dependent glutamate synthase, is involved in photorespiration and nitrogen assimilation, specifically in the glutamate biosynthesis (GO:0006537). Its homologous protein in Arabidopsis is involved in iron-deficiency response and long-distance transportation of iron (Cui et al., 2020).

Table III-12. Hubs identified in *N. benthamiana* infection that have a homologous protein in *C. melo* networks. L: local infection. S: systemic infection. Red: protein with enriched abundance in CMV- compared to mock-inoculated plants. N: network. M: module from either *N. benthamiana* or melon as indicated in the heading column.

N. benthamiana				***C. melo***			
Hub ID	**N**	**M**	**Name**	**ID**	**N**	**M**	**Name**
Niben101Scf01209g04002.1	L	1	Magnesium-chelatase subunit ChlI homolog	MELO3C014571.2.1	L S	3 4	Mg-protoporphyrin IX chelatase
Niben101Scf05414g00004.1	L	2	Alpha-1	MELO3C002047.2.1	S	2	Alpha-1
Niben101Scf04347g00001.1	L	2	Dynamin-related protein 5A	MELO3C016301.2.1	L	1	Dynamin-like family protein
Niben101Scf18107g00014.1	L	3	D-glycerate 3-kinase chloroplastic	MELO3C023371.2.1	L	4	D-glycerate 3-kinase
Niben101Scf08127g08009.1	L	5	6-phosphoglu-conate dehydroge-nase decarboxylating 3	MELO3C022063.2.1	S	2	6-phospho-gluconate dehydrogenase
Niben101Scf08898g00002.1; Niben101Scf09363g00018.1	S	3	60 kDa chaperonin; 60 kDa chaperonin 2	MELO3C015568.2.1	L S	5 4	ruBisCO large subunit-binding protein subunit beta
Niben101Scf01982g00002.1	S	5	PsbP-like protein 2	MELO3C025467.2.1	L	4	Photosynthetic NDH subunit of lumenal location 1
Niben101Scf04198g01001.1	S	6	Ferredoxin-dependent glutamate synthase	MELO3C009759.2.1	L	4	Glutamate synthase

Several hubs from *N. benthamiana* are also present in *C. melo* network, either as hub or not. These proteins participate in different pathways, such as photosynthesis, cell wall construction, intracellular transport, carbon metabolism, nitrogen assimilation and stress. Although in *N. benthamiana* most changes happened at local stages of infection and in melon it was the opposite, many of the same biological processes are affected in both plants. Thus, these proteins could be key components of CMV infection.

III.4. Discussion

In the past ten years, functional genomics has been focused in the transcriptomic area and, in proportion, less work has been done in proteomics. However, the emergence of newer quantitative approaches has led to more powerful proteomics tools. Until now, most publications on plant-virus proteomics have used the so-called "second generation" proteomic tools which used 2-dimension electrophoresis (2D) difference in gel electrophoresis (2D DIGE) to visualize proteins. Using these techniques, complexes have been purified, and individual gel bands identified. In our case we have used "third generation" or high-throughput proteomics, where the whole proteome was extracted and digested with trypsin to obtain peptides that were analysed with liquid chromatography coupled to tandem mass spectrometry (LC-MS/MS) (Di Carli et al., 2012; Keilhauer et al., 2015). In this approach there is no attempt to purify complexes. Instead, analysis methods are used to find background binders in control samples for normalization. Moreover, a relative label-free quantification (LFQ) strategy intensity-based is cost-effective and MaxQuant software integrates normalization algorithms specifically developed for high-resolution quantitative MS data to maximize accuracy and robustness (Cox and Mann, 2008).

Our networks of co-abundant proteins has allowed to summarize high-throughput proteomics data in a visual manner and identify CMV-associated modules, as well as hub proteins (Bensimon et al., 2012), that represent molecular targets that can be used in the future to understand CMV infection. To date, this is the first proteomic work in melon plants infected with CMV that includes high-throughput data of the whole proteome and network analysis. Previous work includes a melon phloem-sap from CMV-infected plants, using 2D gel electrophoresis to excise proteins that were later analysed by MS (Malter and Wolf, 2011). In this study only five proteins were differentially increased in CMV-infected melons in comparison to the control.

Upon CMV inoculation, the melon network of resistant cultivar SC shows a local response in the inoculated leaves, while the susceptible cultivar PS has little disturbance at this point. Interestingly, NIL12-1-99, an introgression line carrying the parental genome of PS and an introgression including *cmv1* resistance gene from SC, has an early response as well (**Figure III.5**). Both SC and NIL have decreased abundance of proteins that participate in proteosynthesis, as well as intracellular transport, specifically COPI and cytoskeleton

proteins. COPI is involved in retrograde transport vesicle formation from the Golgi Apparatus (GA) to the ER and some viruses, as the bipartite *Red clover necrotic mosaic virus* (RCNMV), family *Tombusviridae*, use these vesicles for their transport to the ER membrane for replication (Turner et al., 2004). CMV replication complexes machinery localizes in the tonoplast (Cillo et al., 2002). Given our results, it is feasible that CMV would also use COPI to transport the replication machinery to the tonoplast or the vRNP-MP complexes to the PD. However, in the resistant melons, in which COPI vesicles abundance decreases, and we speculate that CMV would not able to use this route of transport anymore. Also, at early stages of infection in resistant melon combinations, the cytoskeleton proteins abundance decreased. We looked which specific proteins we had under the GO term of cytoskeleton proteins, and we observed these were actin proteins. Actin proteins have been described to participate in transport or as surface receptors (Walsh and Naghavi, 2019). Moreover, CMV-MP severs actins microfilaments (Su et al., 2010). Thus, in susceptible cultivars we speculate the MP could use these proteins to transport itself or vRNP-MP complexes intracellularly. In NIL CMV-inoculated plants there was also a decrease in abundance of proteins related to chlorophyll biosynthesis. In fact, reduced chlorophyll has been linked with chlorotic symptoms in the past (Balachandran et al., 1994). Thus, it could be that, in NIL CMV-inoculated plants, chlorotic symptoms are caused from the reduced chlorophyll content to some extent. Either way, measurement of chlorophyll content would be useful to validate these results.

Later, after CMV inoculation, new upper leaves from resistant genotypes (SC and NIL CMV-LS plants) had no proteomic changes compared to their mock-inoculated plants. These results are no surprise since in new leaves from these genotypes the virus is not present, since it was stopped before entering to the phloem (Guiu-Aragonés et al., 2016). However, in the case of susceptible genotypes (PS and NIL CMV-FNY plants) CMV did infect systemically, and it caused massive perturbations. The strong proteome changes in susceptible melon plants were expected, since the virus is present in new leaves, replicating, with high titter, and using the host machinery in its own benefit. In all susceptible CMV-infected melon plants there was an increase of abundance in proteins that participate in protein folding and degradation (module 2) and phenylpropanoid biosynthesis (module 4) (**Figure III.6**). The ER associated degradation (ERAD) pathway has been linked to virus replication and infection in the past. Several viruses use this mechanism for different purposes, TBSV and *Cymbidium ringspot virus* (CymRSV) use it for replication, *Turnip yellow mosaic virus*

(TYMV) uses it to target specific proteins (Verchot, 2016). In Chapter II, we also detected several candidate interactors of CMV-MP that participate in this pathway. Thus, it seems very plausible that CMV uses the ERAD pathway for replication or it could also be that CMV-MP is targeted to the proteasome at later stages of infection since CDC48, a candidate interactor found in Chapter II targets TMV-MP to the proteasome in TMV infection (Niehl et al., 2012). As for the increase in phenylpropanoid synthesis, it is also no surprise. Phenylpropanoids have been described in several plant-pathogen interactions. In some cases, accumulation of phenylpropanoids has been paralleled to virus susceptibility and increase of symptoms. For example, in a study that used *Prunus necrotic ringspot virus* (PNRSV) infected *Cucumis sativus* plants and MNSV-infected melon plants, these had enriched phenylpropanoids correlating in time with the development and severity of symptoms (Bellés et al., 2008). The same was observed in a study of tomato leaves systemically infected with *Tomato Mosaic Virus* (López-Gresa et al., 2012). However, in other studies, phenylpropanoids have been associated with milder symptoms and even resistance (Kandan et al., 2002; Shadle et al., 2003). This was the case in a proteomic study of *C. sativus*, in which the resistant variety had a 3-fold increase of a protein related to phenylpropanoid biosynthesis in comparison with the susceptible *C. sativus* plant, both CMV-inoculated (Nováková et al., 2020). Another example can be found in tobacco resistant plants to TMV where an increase of phenylpropanoids was observed upon inoculation (Choi et al., 2006) and even in potato inoculated with a mild isolate from *Potato virus Y* (PVY) in which milder symptomatology was observed and correlated to a phenylpropanoid increase (Kogovšek et al., 2016). In our case, since all susceptible plants present an increase of phenylpropanoids at later stages of infection as well as severe symptoms, it would seem plausible to think that an increase in phenylpropanoid synthesis is at least partially related to the symptoms observed in systemically infected susceptible plants.

Looking at the systemic PS infection with CMV-LS, there was a decrease of abundance in proteins participating in biosynthesis of metabolites and pigments (module 5) (**Figure III.6**B). Specifically, the detailed terms enrichment of this module (Supplementary Material 3D "Analysis of modules and hubs") included the KEGG term "porphyrin and chlorophyll metabolism" (KEGG:00860) and even two hubs, one in systemic and another in the local network, were protoporphyrin chelatases. A CMV strain (CMV-Y) targets a protoporphyrin protein through host RNA silencing machinery and decreases the levels of these proteins (Shimura et al., 2011). Thus, we thought CMV might target protoporphyrin proteins as well.

However, this article also mentions that because of diminished protoporphyrin there were more severe symptoms, which in our case we did not have since all susceptible plants had severe but similar symptomatology.

Looking at PS CMV-FNY systemically infected plants at 15 dpi, there is no decrease in abundance of proteins related to translation (**Figure III.6** E module 3), but there is a decrease of abundance of those proteins in NIL CMV-FNY and PS CMV-LS. Likewise, in a study in *C. sativus* long-term CMV infection (33 dpi) there was a decrease in translation in susceptible cultivars (Nováková et al., 2020). The authors hypothesized that translation was impaired due to an advanced infection or because the specific ribosomal proteins had an antiviral function, that was already reported either inhibiting directly transcription or translation or activating the immune response (Li, 2019). In our case, looking at the proteins within module 3 (gene expression and translation), we found out that all are ribosomal proteins, thus both scenarios could apply. It would be interesting to see if there is a decrease of translation in PS CMV-FNY after a longer period (30 dpi) than that reported in our experiments (15 dpi). Moreover, several ribosomal proteins are hubs in both local and systemic infection and are either decreased in resistant cultivars right after inoculation or decreased in susceptible cultivars during systemic infection. Thus, it seems that these proteins might have a big importance in CMV infection. Overall, CMV-FNY seems to be able to cause less stress in PS in newly infected leaves, as we saw by the fewer changes of protein abundance throughout the systemic network. It would seem reasonable to think that the fewer proteome changes would propitiate a better environment for viral infection, with less stress from the plant, to allow even a more rapid and stable infection over time.

Comparison of melon cultivars showed that most differences between inoculated melon genotypes are found in local infection, while in systemically infected leaves there are no differences between the mock-inoculated plants from different genotypes. Interestingly, in local inoculation, CMV-FNY has differentially increased abundance in translation in NIL compared to SC (module 3 in **Figure III.7**E and **Table III-9** GO:0006412 terms) which could be related to the susceptibility of the NIL to CMV-FNY. Moreover, most differences between susceptible and resistant melons come from photosynthesis and protein degradation; susceptible melon PS has a decrease in proteins that participate in photosynthetic activity and increased abundance of inhibitors of protein degradation compared to SC (module 1 in **Figure III.7** A and **Table III-8** GO:0016168 and GO:0004866

terms respectively). Similar results were obtained in tomato plants, where most differences between resistant transgenic tomato plants to CMV compared to their susceptible wildtype counterparts were due to photosynthesis (Di Carli et al., 2010) and that, like in our case, resistant plants had enriched photosynthesis proteins compared to the wildtype plants. In the case of the NIL there are no changes in the proteome compared to PS, which is expected as they share most of their genome.

Concerning the hubs found in melon, glyceraldehyde-3-phosphate dehydrogenase was down-regulated in susceptible NIL CMV-FNY and PS CMV-LS systemic leaves. A similar phenotype had already been observed in a proteome analysis in tomato in which this protein was also down-regulated in wildtype symptomatic CMV-inoculated tomato leaves (Di Carli et al., 2010). In *C. sativus* this tendency was also observed, when Glyceraldehyde-3-phosphate dehydrogenase was depleted in susceptible Vanda cultivar in comparison to the resistant cultivar Heliana (both CMV inoculated) (Nováková et al., 2020). Thaumatin-like proteins are other hubs found enriched in systemically infected susceptible melon plants. Thaumatin-like proteins (TLPs) are a family of proteins associated to defence and development. The TLPs proteins are diverse and classified as a Pathogenesis Related-5 (PR-5) proteins since they participate in many responses to biotic and abiotic stresses (de Jesús-Pires et al., 2020). In fact, a thaumatin-like protein was also found enriched in *C. sativus* susceptible cultivars upon CMV inoculation. (Nováková et al, 2020). Also, in another melon phloem-sap study, this case inoculated with *Melon necrotic spot virus* (MNSV), Thaumatin-like proteins were accumulated in infected plants (Serra-Soriano et al., 2015). Many other studies also detected thaumatin proteins as a defence response against several fungi (Mahdavi et al., 2012; Misra et al., 2016; Lambertucci et al., 2019; Liu et al., 2019b; Zhang et al., 2021; Anisimova et al., 2022), some yeast and viruses (Cornelissen et al., 1986; Van der Maelen et al., 2019) or even in response to wounding (Dafoe et al., 2009; Kang et al., 2021).

From *N. benthamiana* networks, our results show an early response, compared to melon, correlating with those of a transcriptome study in *N. tabacum* (Liu et al., 2019a). In this study, tobacco response presented most changes at a very early stage. In fact, most DEGs were found at 1 dpi, and they decreased with time (until 5 dpi). This agrees with our proteome results, that showed almost no differences in the proteome between infected and non-infected plants at 14 dpi, but several protein abundance changes were found at early

stages of infection (3 dpi). As for biological processes, in the susceptible tobacco some of them were in common with our results. Specifically, carbohydrate and carbon metabolism, photosynthesis, nucleotide biosynthesis and pigment biosynthesis correlate with our *N. benthamiana* enrichment analysis at early stages of infection (**Table III-11**). For example, magnesium protoporphyrin IX methyltransferase activity was also enriched after CMV inoculation of susceptible tobacco plants, which corresponds to one of the hubs found in our proteome analysis of local infection in *N. benthamiana*. As already mentioned, this protein was present in the melon networks, thus it could be a key protein involved in pivotal roles in response to CMV infection.

In general, some hub proteins in *N. benthamiana* were also common in melon PS, which again shows that although the proteome response happens later in time, most of the biological processes affected by CMV infection are the same in both species. One interesting protein is the Dynamin-related protein 5A (Niben101Scf04347g00001.1) whose homologous is Dynamin-related protein 1A (DRP1A). This protein accumulates in sterol-enriched membranes (Frescatada-Rosa et al., 2014) and has several roles in growth and development as well as in clathrin-mediated endocytosis. For example, it mediates bacterial flagellin or flg22-peptide internalization from the plasma membrane, acting as a ligand (Ekanayake et al., 2021). In Chapter II, we validated the interaction domain of CmNPC1 with CMV-MP. NPC1 is a transporter of cholesterol, a type of sterol (Pfeffer, 2019). Thus, it would seem an interesting protein that CMV could use together with CmNPC1 in its infection mechanism. In any case, all hubs should be confirmed in the future to determine its real implication and or use as targets of CMV infection.

General discussion

C. melo Vacuolar Protein Sorting 41 (CmVPS41) was identified as the protein encoded by *cmv1* (Giner et al., 2017), a gene for resistance to CMV in melon accession 'Songwhan Charmi' (SC) (Karchi et al., 1975). In Chapter I, we have characterized CmVPS41 cellular location in susceptible and resistant varieties and shown that it localizes to differential structures. One of them are the trans-vacuolar strands (TVS) that are present in susceptible genotypes. TVS were already described in the past as mobile structures dependent on actin microfilaments (Uemura et al., 2002). CMV-MP severs acting microfilaments (Su et al., 2010). Thus, CmVPS41 TVS could work in targeting the virus towards the plasmodesma (PD), while its absence seems to correlate with resistance. Moreover, specific structures of CmVPS41 co-localize with late endosomes (LE). Thus, TVS could participate in CMV transport to the PD through the endosomal network.

The movement protein (MP) was described as the virulence factor of CMV (Guiu-Aragonés et al., 2015). However, a connection between CmVPS41 and CMV-MP could not be found in the past. In this thesis, we found *in vivo* interaction between the MP of CMV-FNY and CmVPS41 both from both PS and SC at the PD. The Homotypic Fusion and Protein Sorting (HOPS) complex, where CmVPS41 is found and works as the effector subunit (Price et al., 2000), regulates cell trafficking. Thus, this *in vivo* interaction between the MP of CMV-FNY and CmVPS41 could affect CMV intracellular transport to the PD. In the case of the MP of CMV-LS, there was no interaction with CmVPS41 in any of the approaches used (Yeast Two Hybrid and Bimolecular Fluorescence complementation assays). Either way, the interaction between MP-FNY and CmVPS41s should be further validated with a complementary protein-protein interaction method, such as co-Immunoprecipitation.

To travel within the cell, CMV-MP must also need other host factors. In this thesis, we found several candidates that, together with CmVPS41, could work in the transport mechanism of vRNP and the MP to the PD. One of them is *C. melo* Niemman-Pick C1 protein-like (CmNPC1). CmNPC1 interacts with the MP from both CMV-FNY and CMV-LS, *in vitro* and *in vivo*, in this last case it interacts at the PD, where the MP localizes (Guiu-Aragonés, 2014). In humans, HsNPC1 participates in several viruses' infection, such as those caused by *Zaire ebolavirus* (EboV), *Human immunodeficiency virus type 1* (HIV-1), *Marburgvirus* (MARV) and *Hepatitis virus C* (HCV) (Tang et al., 2009b; Carette et al., 2011a; Hunt et al., 2012; King et al., 2018; Stoeck et al., 2018). During EboV infection, glycoprotein 1 subunit (GP_1) viral protein needs to interact with HsNPC1 to allow viral membrane fusion with the

LE (Carette et al., 2011a; Côté et al., 2011). EboV GP_1 also requires the HOPS complex subunits, where CmVPS41 is found, to bind efficiently NPC1 (Bo et al., 2020). Thus, CmNPC1 seems a very promising candidate to participate together with CmVPS41 in CMV infection mechanism in *C. melo*.

Based on our results, neither CmVPS41 from PS nor SC can interact with CMV-LS. However, the fact that CmNPC1 does interact with the MP from CMV-LS makes possible to think that CMV-LS uses a slightly different mechanism than CMV-FNY to reach the PD. CMV resistance takes place at the bundle sheath (BS) cells before entering the phloem (Guiu-Aragonés et al., 2016). However, in the resistance mechanism the cellular processes and pathways happening within the BS cells are not known. For this reason, we used a proteomic approach to investigate local and systemic responses to CMV challenge. Upon local entry, CMV replicates and travels through different cell types, from the epidermis until it arrives to the BS cells (Guiu-Aragonés et al., 2016). Taking together the CmVPS41 localization studies, network results and the candidate CMV-MP interacting proteins, we propose a model of CMV intracellular transport at the BS cells.

Once in the BS cells, CMV would translate its viral proteins in the cytoplasm and start its intracellular transport of (+)ssRNA and replication proteins (governed by 1a and 2a proteins) to the tonoplast, as this organelle co-localizes with CMV replication machinery in *C. sativus* and *N. benthamiana* (Cillo et al., 2002). In the BS cells of CMV-FNY-infected PS plants (**Figure GD.1**A), we propose that the MP interacts with both CmVPS41 and CmNPC1. This association would allow the transport, of (+)ssRNA templates and replication machinery, together with MP, to the trans-golgi network (TGN), and from there, to the vacuolar membrane. In Chapter II, a vacuolar sorting receptor (VSR) was found as a candidate interactor of CMV-MP. VSRs are believed to bind their ligands at the TGN and target them to the vacuoles (Kang and Hwang, 2014; Künzl et al., 2016). Thus, we propose (+)ssRNA templates, replication machinery (1a and 2a CMV proteins) and the MP could travel to the TGN, and there, the MP could interact with the VSR. MP-VSR interaction would allow the delivery of all these proteins and vRNA to the tonoplast. In the tonoplast the viral replication complexes (VRC) would form. CmVPS41 TVS were present in susceptible plants (Chapter I). CMV-MP is involved in severing actin microfilaments (Su et al., 2010). And TVS are dependent on actin microfilaments (Uemura et al., 2002). Thus, we propose that vRNP-MP complexes could travel from the tonoplast using TVS and actin microfilaments to the PD.

As observed in Chapter II, CMV-MP had also candidate interacting proteins that are constituents of Coatomer Protein I (COPI) vesicles. However, in the resistant CMV-inoculated plants COPI proteins and the cytoskeleton were decreased in comparison to non-inoculated resistant plants (see Chapter III). Considering these results, we propose that the CMV-MP could use another route to target itself to the PD and form the MP-tubule channel. We propose that after translation, one part of CMV-MP molecules could travel from the Golgi apparatus (GA) and use COPI vesicles to arrive to the ER. The PD channel is formed by desmotubule, a continuation of the ER (Heinlein, 2015b). Thus, once in the ER we propose that the MP would travel to the PD. In the PD, the MP would form the MP-tubule channel to allow vRNP traffic to the neighbour cell, which are the companion cells (CC), that in cucurbits are called intermediary cells. Again, CMV would infect these neighbour cells and transport itself to the sieve elements (SE). From the SE, CMV would travel through the phloem to reach upper leaves. Several candidate CMV-MP interacting proteins participate in the proteasome degradation pathway, including the proteasome subunit alpha itself, ADP-ribosylation factor, Hsp70 and CDC48. In *Tobacco mosaic virus* (TMV) infection, CDC48 targets TMV-MP to the proteasome (Niehl et al., 2012). We propose that later in infection, CMV-MP is targeted to the proteasome for degradation. First, the MP would be ubiquitinated, using MP-candidate interactors such as the ADP-ribosylation factor or Hsp70, and ubiquitinated MP complexes would be directed by CDC48 to the proteasome for degradation. Chloroplast components are targeted by several viruses to enhance virus replication (Zhao et al., 2016). For example, photosystem II is able to decrease virus replication in TMV infection (Abbink et al., 2002). Modification of photosynthesis can cause chloroplast damage and reduce chlorophyll content, that in turn, causes chlorosis (Balachandran et al., 1994; Bhattacharyya and Chakraborty, 2018). In tobacco plants, Tsip1, a chloroplast protein, interacts with CMV proteins 1a and 2a, and the chlorophyll mRNA is targeted by a 22-nt vsiRNA from CMV Y-satellite RNA and induces yellowing of leaves (Huh et al., 2011; Shimura et al., 2011). In Chapter II, several candidate interactor proteins of CMV-MP were chloroplast components, such as photosystems I, II subunits and a chlorophyll binding protein. We propose that these components would be targets of CMV-MP but would not participate in the intracellular transport route of vRNP-MP. As a result, photosynthesis decreases, and we observe chlorosis symptoms in infected plants.

In the susceptible plant NIL12-1-99 inoculated with CMV-FNY (**Figure GD.1**A), we propose that CMV would use the same intracellular transport as previously explained for PS

CMV-FNY inoculated plants. In this case CMV-MP would be able to interact with CmVPS41 SC, but this would not change the intracellular transport. Again, replication would happen in the tonoplast, vRNP-MP would reach the PD using TVS, later in infection the MP would be degraded in the proteasome, and CMV-MP would target chloroplast components which would result in yellowing of the leaves. In these plants, COPI decreases as well although it does not impede CMV transport to the intermediary cells.

In the case of susceptible PS upon CMV-LS inoculation (**Figure GD.1**B), we propose that CMV-LS would transport itself through the endosomes due to its interaction with CmNPC1, although without a direct interaction with CmVPS41. Possibly, another mechanism involving CmVPS41 would still be able to transport the replication machinery and the MP to the tonoplast, as well as the MP to the PD. Afterwards, vRNP-MP complexes would follow the same pathway to the PD, and again the MP would transport itself to the PD through the alternative pathway from the ER. The MP would also affect chloroplast components, and later it would be degraded in the proteasome.

In resistant SC plants inoculated with CMV-FNY (**Figure GD.1**C), the endosomal entry would occur, HOPS and CmNPC1 would interact with CMV-MP, and replication of CMV would occur in the tonoplast as well. In Chapter I, in the resistant plants TVS are fewer, if not absent, compared to the susceptible plants. Thus, as there are not TVS, this pathway would not be available. We propose the two QTLs of resistance would impede TVS forming. In Chapter III, we observed in resistant cultivars a decrease of COPI vesicles and cytoskeleton. The decrease of COPI vesicles would impede that CMV-MP reaches the PD and in turn, the transport of vRNP-MP complexes to the intermediary cells would not happen. Thus, SE would not be reached, and phloem transport would be impaired. The proteasome machinery would again work in degrading the MP at later stages of inoculation.

In resistant NIL and SC plants upon CMV-LS inoculation (**Figure GD.1**D), CMV-LS would reach the LE and bind CmNPC1 but not CmVPS41 SC. Again, VRC would form in the tonoplast, but *cmv1* alone would impede TVS formation and transport of vRNP-MP complexes to the PD. Thus, *cmv1* would act independently of the presence (in SC plants) or not (in NIL plants) of two other QTLs of resistance. Again, vRNP-MP complexes would not be transported to neighbour cells and CMV would not arrive to the phloem. Also, COPI and cytoskeleton proteins would decrease, which might impede the MP alternative route to the PD. Again, CMV-MP would target the chloroplast and later CMV-MP would be degraded.

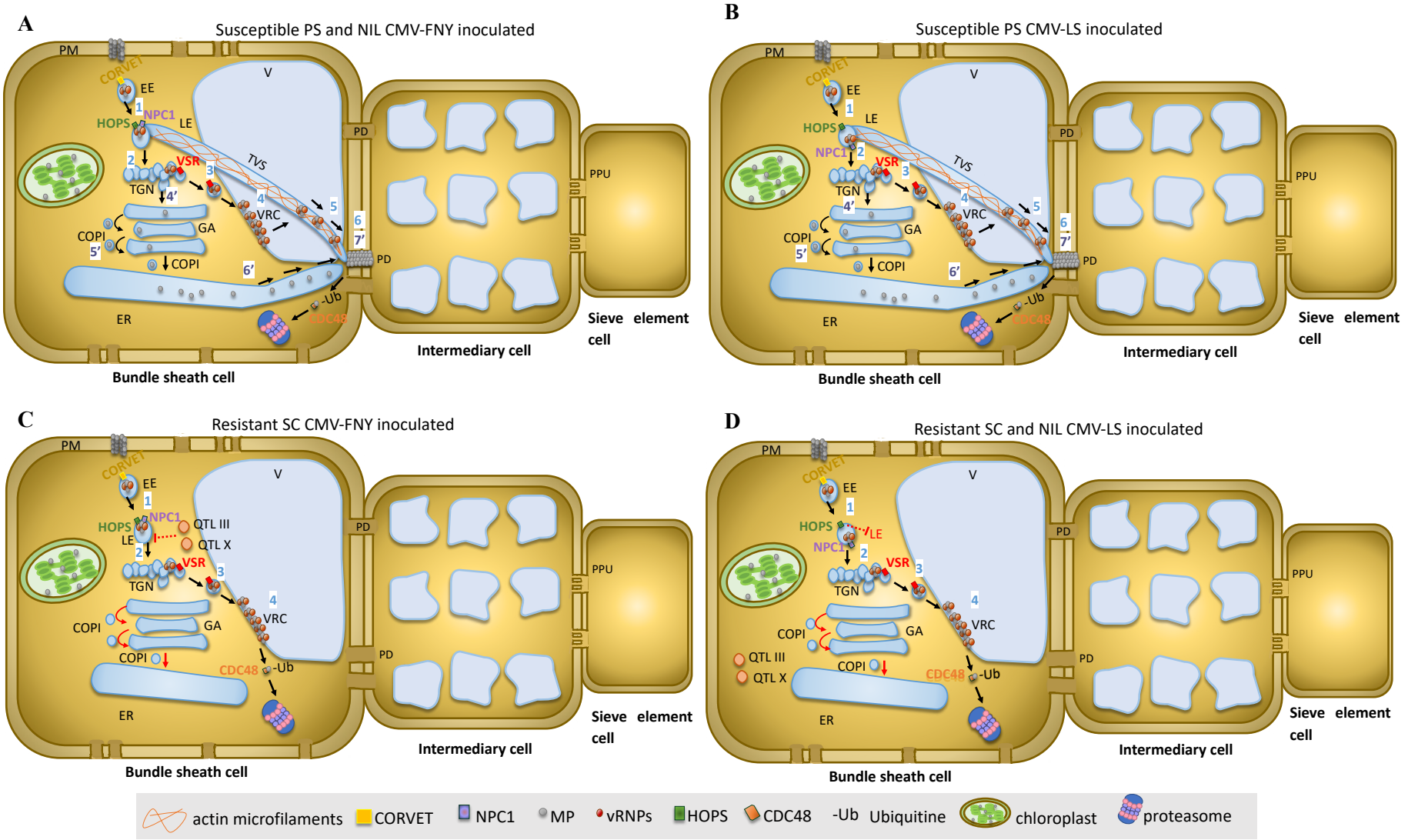
A
Susceptible PS and NIL CMV-FNY inoculated
B
Susceptible PS CMV-LS inoculated
C
Resistant SC CMV-FNY inoculated
D
Resistant SC and NIL CMV-LS inoculated
PM
CORVET
EE
LE
HOPS
NPC1
VSR
TVS
TGN
GA
COPI
VRC
CDC48
-Ub
ER
V
PD
PPU
QTL III
QTL X
Bundle sheath cell
Intermediary cell
Sieve element cell
actin microfilaments
CORVET
NPC1
MP
vRNPs
HOPS
CDC48
-Ub Ubiquitine
chloroplast
proteasome

Figure GD.1. Model for CMV resistance mechanism in the bundle sheath cells. **A**. Bundle sheath (BS) cells of PS and NIL inoculated with CMV-FNY. After translation of CMV proteins in the cytoplasm, (1) the replication machinery, (+)ssRNA and the MP would travel from the early endosomes (EE) to the late endosomes (LE) (2) in the LE the movement protein (MP) would interact with CmVPS41, a HOPS subunit, as well as with CmNPC1, and the replication components (ssRNA, CMV proteins 1a and 2a) and the MP would be transported to the trans-golgi network (TGN). In the TGN, (3) a vacuolar sorting receptor (VSR) could bind the MP and transport it together with the replication components and vRNA to the vacuolar membrane (tonoplast). (4) The viral replication complexes (VRC) would be formed within the tonoplast and virions would be generated. (5) In parallel (or not) to replication, vRNP-MP complexes would use the LE trans-vacuolar strands (TVS) to reach the plasmodesma (PD) together with actin filaments (6). The MP would use a second route to arrive to the PD. From the TGN network, it would travel to the golgi apparatus (GA) (4') and use the COPI vesicles to reach the ER (5'). From the ER, CMV-MP would transport itself within the ER to the PD (6'). At the PD, the MP increases the size exclusion limit (SEL) of the PD and generates the MP-tubules for the transport of vRNP-MP complexes (7'). CMV-MP would also target chloroplast components. Later in infection, we propose the MP is degraded through ubiquitin binding and CDC48 assisted transport of ubiquitinated MP to the proteasome. **B**. BS cells of PS inoculated with CMV-LS. In this infection, there would be the same steps as in route A, however, in the LE (2) CmVPS41 does not interact with the MP. **C**. BS cells of SC and NIL inoculated with CMV-FNY. The initial steps (1-4) are the same as in route A, however, in the LE (2) the two other QTLs for resistance would impede the formation of TVS and the cytoskeleton proteins would decrease. Thus, VRC would form but then vRNP-MP could not be transported to the PD. Also, COPI proteins decrease, and this could impede or decrease MP and vRNP-MP complexes transport to the PD. **D**. BS cells of NIL and SC upon CMV-LS inoculation. In this case, the same scenario as in route C would happen. However, (2) at the LE *cmv1* alone can stop TVS from forming. Again, there is replication at the tonoplast, although vRNP-MP complexes cannot travel to the PD and COPI and cytoskeleton proteins decrease. CDC48: cell division cycle protein 48 homolog. CmNPC1: *C. melo* Niemann-Pick C1 protein-like. COPI (Coatomer Protein 1) vesicles. CORVET (class C core vacuole/endosome tethering factor) complex. EE: early endosome. GA: Golgi Apparatus. HOPS (Homotypic Fusion and Protein Sorting) complex. PM: plasma membrane. PPU: plasmodesmata-pore unit. QTL III: quantitative trait locus from QTL in Linkage group (LG) III, either resistant or susceptible alleles depending on the cultivar. QTL X: quantitative trait locus from QTL in LG X, , either resistant or susceptible alleles depending on the cultivar. V: vacuole.

We propose this model since it would be the most similar mechanism to the one that other viruses that interact with NPC1 use (Tang et al., 2009b; Stoeck et al., 2018; Bo et al., 2020). However, we need to consider all these viruses (HIV-1, EboV, HCV) infect mammal cells, thus this mechanism might not work in plants. This model also correlates, to some degree, with the proteomic data in resistant cultivars. If, as proposed by the model, CMV-MP is stopped at LE interphase and it does not reach the PD, COPI vesicles and cytoskeleton proteins might be reduced in comparison to mock plants. This is in fact the case observed in proteomic data of resistant cultivars. In the NIL CMV-FNY inoculated plants, COPI vesicles and the cytoskeleton are also decreased compared to the respective mock-inoculated plants, which in theory would not be expected in our model. However, NIL12-1-99 carry the gene *cmv1* (CmVPS41 SC). Even though *cmv1* alone is not able to stop infection, it might decrease, to some degree the abundance of COPI and cytoskeleton proteins and delay, but

not stop CMV-MP transport to the PD. Indeed, CMV FNY infection is delayed in melon plants carrying either *cmv1* alone and combinations of *cmv1* with QTLs III and X (Yan, 2018).

Another option would be that replication happens first in the tonoplast. Then, through the TGN network vRNP-MP complexes would be transported to the PD through the TVS. In this mechanism, the tonoplast would be the first step in CMV replication, that would happen in both resistant and susceptible melon plants. Later, vRNP-MP complexes might travel to the TGN and to the endosomes where resistant plants would stop its further transport. In susceptible plants vRNP-MP would travel to the PD from the LE using TVS. This option was discarded because it does not correlate with any previous models in plant or animal viruses nor follows the usual order in the TGN-endosomes network. In fact, proteins can go from the PM to the endosomes or from the TGN/EE network to the PM, but travelling from the LE to the PM is quite rare and used for recycling proteins (Naslavsky and Caplan, 2018).

In new melon leaves, CMV is not present in the resistant combinations, thus, there are no differences in the proteome of previously inoculated resistant plants and their mock counterparts. In susceptible plants, CMV has performed a systemic infection and reached new leaves. Based on our network approach, systemically infected leaves of susceptible cultivars seem to have an increase in their proteosynthesis and would cause ER stress, that in turn, increases abundance of protein disulfide isomerase-like (PDIL) and other proteins, that are known to activate the ER associated degradation pathway (Nakatsukasa et al., 2008; Sun and Brodsky, 2019). One candidate interactor of the MP of CMV-LS is a 4-coumarate:CoA ligase-like protein, one of the first proteins in the initial steps of phenylpropanoid synthesis (Bauters et al., 2021). Phenylpropanoid synthesis increases as the infection develops and it correlates with severity of symptoms in other studies (Bellés et al., 2008; López-Gresa et al., 2012). Also, several phenylpropanoids compounds function in plant defence (Dixon et al., 2002; Naoumkina et al., 2010). Therefore, we propose that during a systemic infection, melon plants would try to increase their phenylpropanoid compounds and CMV might be targeting the first steps of phenylpropanoid biosynthesis to reduce the amount of defence metabolites and facilitate infection.

In *N. benthamiana* CMV infection it seems that, independently of the timepoint of infection, most of the same biological pathways participate in CMV challenge. Interestingly, eight hubs from *N. benthamiana* shared homologous proteins within the curated network of *C.*

melo, and even two of them were also hubs in the *C. melo* network. Thus, it could be that in different susceptible hosts CMV would target common biological pathways. Moreover, the common hubs between *N. benthamiana* and *C. melo*, Alpha-1 and 6-phosphogluconate dehydrogenase decarboxylating 3, could be key proteins that govern the global response to CMV in different plants and should be further studied as potential targets against CMV infection.

Conclusions

1- CmVPS41 from susceptible cultivar PS and resistant cultivar SC associates *in vivo* with the movement protein of CMV-FNY in *N. benthamiana* leaves, through BIFC assay. The movement protein of CMV-LS does not interact with CmVPS41 from PS nor SC.
2- CmVPS41 localizes in differential structures in susceptible and resistant genotypes and co-localizes with the late endosomes.
3- CmVPS41 localization in susceptible plants consisted of strong spots in the plasma membrane or tonoplast, nuclear speckles, and several trans-vacuolar strands. CmVPS41 from resistant accessions showed no membrane spots, smooth expression in the nucleus and cytoplasm, and several tonoplast invaginations towards the vacuole.
4- The presence of the causal resistance mutations (L348R and G85E) induces a change in CmVPS41 localization decreasing the number of trans-vacuolar strands.
5- The different distribution of CmVPS41 PS and SC does not change with the co-expression with CMV-MP.
6- CmVPS41 distinctive structures re-localize during CMV infection in *N. benthamiana* cells. In CmVPS41SC expressing cells, nuclear localization and the number of tonoplast invaginations decreased, and the number of cells with membrane spots increased, with respect to non-infected plants. In CmVPS41PS expressing cells, trans-vacuolar strands decreased significantly during viral infection.
7- Y2H screening found 6 candidate interacting proteins with CMV-MP. Two candidate interactors were confirmed by one-by-one Y2H assay: Ribose-5-phosphate isomerase A and Niemann-Pick C1 protein-like.
8- A total of 136 *C. melo* candidate MP-interacting proteins were obtained through Y2H and IP screenings.
9- The CmNPC1 interacting domain, interacts with both FNY-MP and LS-MP through BIFC assay and it consists of partial exon 25, exon 26, exon 27, intron 27-28, exon 28, partial intron 28-29. Introns within the CmNPC1 MP-interaction domain are present in the RNA pool of infected and non-infected PS and SC melon plants.
10- A total of 20 candidate interactor proteins from the IP (14 in systemic infection and 6 in local infection) are closely related to either VPS41 or CMV infection in bibliography.

11- CMV causes great proteome perturbations in *C. melo*. Proteomic data from CMV infection allowed to generate the first network of co-abundant proteins in *C. melo*.

12- Upon CMV inoculation, the local response of the resistant cultivar SC consists of a decrease of proteosynthesis and intracellular transport, while the susceptible cultivar PS shows almost no disturbances in the network of co-abundant proteins.

13- In new leaves, all susceptible CMV-infected plants displayed an increase of protein folding and degradation, and phenylpropanoid biosynthesis.

14- Systemically infected leaves of NIL CMV-FNY and PS CMV-LS presented a decrease in translation, while those of PS CMV-FNY presented a decrease of biosynthesis of metabolites and pigments.

15- At early stages of infection, *N. benthamiana* CMV-inoculated plants showed a depletion of proteins related to carbohydrate metabolic process and an increase of redox processes and oxoacid metabolism, while PS presented very few changes.

16- In systemically infected leaves, *N. benthamiana* had few proteins with changes in abundance, whereas in PS at this timepoint there were many disturbances.

17- We have found two common hubs in *C. melo* and *N. benthamiana*: 6-phosphogluconate dehydrogenase decarboxylating 3 and Alpha-1 proteins.

Bibliography

Abad-Zapatero, C., Abdel-Meguid, S. S., Johnson, J. E., Leslie, A. G., Rayment, I., Rossmann, M. G., et al. (1980). Structure of southern bean mosaic virus at 2.8 A resolution. Nature 286, 33–39. doi: 10.1038/286033a0.

Abbink, T. E. M., Peart, J. R., Mos, T. N. M., Baulcombe, D. C., Bol, J. F., and Linthorst, H. J. M. (2002). Silencing of a gene encoding a protein component of the oxygen-evolving complex of photosystem II enhances virus replication in plants. Virology 295, 307–319. doi: 10.1006/viro.2002.1332.

Agrios, G. N. (2005). Plant Pathology. 5th ed. , ed. A. Press doi: https://doi.org/10.1016/C2009-0-02037-6.

Ahn, H.-K., Yoon, J.-T., Choi, I., Kim, S., Lee, H.-S., and Pai, H.-S. (2019). Functional characterization of chaperonin containing T-complex polypeptide-1 and its conserved and novel substrates in Arabidopsis. J. Exp. Bot. 70, 2741–2757. doi: 10.1093/jxb/erz099.

Albert, M. (2013). Peptides as triggers of plant defence. J. Exp. Bot. 64, 5269–5279. doi: 10.1093/jxb/ert275.

Alcaide-Loridan, C., and Jupin, I. (2012). Ubiquitin and plant viruses, let's play together! Plant Physiol. 160, 72–82.

Alexander, M. M., and Cilia, M. (2016). A molecular tug-of-war: Global plant proteome changes during viral infection. Curr. Plant Biol. 5, 13–24. doi: https://doi.org/10.1016/j.cpb.2015.10.003.

Amano, M., Mochizuki, A., Kawagoe, Y., Iwahori, K., Niwa, K., Svoboda, J., et al. (2013). High-resolution mapping of zym, a recessive gene for Zucchini yellow mosaic virus resistance in cucumber. Theor. Appl. Genet. 126, 2983–2993. doi: 10.1007/s00122-013-2187-5.

Amari, K., Boutant, E., Hofmann, C., Schmitt-Keichinger, C., Fernandez-Calvino, L., Didier, P., et al. (2010). A family of plasmodesmal proteins with receptor-like properties for plant viral movement proteins. PLoS Pathog. 6, e1001119. doi: 10.1371/journal.ppat.1001119.

An, C. H., Kim, Y. R., Kim, H. S., Kim, S. S., Yoo, N. J., and Lee, S. H. (2012). Frameshift mutations of vacuolar protein sorting genes in gastric and colorectal cancers with

microsatellite instability. Hum. Pathol. 43, 40–47.

Anderson, B. J., Boyce, P. M., and Blanchard, C. L. (1995). RNA 4 sequences from cucumber mosaic virus subgroups I and II. Gene 161, 293–294. doi: 10.1016/0378-1119(95)00276-c.

Andika, I. B., Wei, S., Cao, C., Salaipeth, L., Kondo, H., and Sun, L. (2017). Phytopathogenic fungus hosts a plant virus: A naturally occurring cross-kingdom viral infection. Proc. Natl. Acad. Sci. 114, 12267 LP – 12272. doi: 10.1073/pnas.1714916114.

Andreev, I. A., Hyon Kim, S., Kalinina, N. O., Rakitina, D. V, Fitzgerald, A. G., Palukaitis, P., et al. (2004). Molecular interactions between a plant virus movement protein and RNA: force spectroscopy investigation. J. Mol. Biol. 339, 1041–1047. doi: 10.1016/j.jmb.2004.04.013.

Anisimova, O. K., Kochieva, E. Z., Shchennikova, A. V, and Filyushin, M. A. (2022). Thaumatin-like Protein (TLP) Genes in Garlic (Allium sativum L.): Genome-Wide Identification, Characterization, and Expression in Response to Fusarium proliferatum Infection. Plants (Basel, Switzerland) 11. doi: 10.3390/plants11060748.

Arakel, E. C., and Schwappach, B. (2018). Formation of COPI-coated vesicles at a glance. J. Cell Sci. 131. doi: 10.1242/jcs.209890.

Argyris, J. M., Pujol, M., Martín-Hernández, A. M., and Garcia-Mas, J. (2015). Combined use of genetic and genomics resources to understand virus resistance and fruit quality traits in melon. Physiol. Plant. 155, 4–11.

Aryal, U. K., Xiong, Y., McBride, Z., Kihara, D., Xie, J., Hall, M. C., et al. (2014). A Proteomic Strategy for Global Analysis of Plant Protein Complexes. Plant Cell 26, 3867–3882. doi: 10.1105/tpc.114.127563.

Asensio, C. S., Sirkis, D. W., Maas, J. W., Egami, K., To, T. L., Brodsky, F. M., et al. (2013a). Self-Assembly of VPS41 Promotes Sorting Required for Biogenesis of the Regulated Secretory Pathway. Dev. Cell 27, 425–437. doi: 10.1016/j.devcel.2013.10.007.

Asensio, C. S., Sirkis, D. W., Maas, J. W. J., Egami, K., To, T.-L., Brodsky, F. M., et al. (2013b). Self-assembly of VPS41 promotes sorting required for biogenesis of the

regulated secretory pathway. Dev. Cell 27, 425–437. doi: 10.1016/j.devcel.2013.10.007.

Ashby, J., Boutant, E., Seemanpillai, M., Groner, A., Sambade, A., Ritzenthaler, C., et al. (2006). Tobacco mosaic virus movement protein functions as a structural microtubule-associated protein. J. Virol. 80, 8329–8344. doi: 10.1128/JVI.00540-06.

Asurmendi, S., Berg, R. H., Koo, J. C., and Beachy, R. N. (2004). Coat protein regulates formation of replication complexes during tobacco mosaic virus infection. Proc. Natl. Acad. Sci. U. S. A. 101, 1415–1420. doi: 10.1073/pnas.0307778101.

Balachandran, S., Osmond, C. B., and Daley, P. F. (1994). Diagnosis of the earliest strain-specific interactions between tobacco mosaic virus and chloroplasts of tobacco leaves in vivo by means of chlorophyll fluorescence imaging. Plant Physiol. 104, 1059–1065.

Balderhaar, H. J. kleine, and Ungermann, C. (2013). CORVET and HOPS tethering complexes - coordinators of endosome and lysosome fusion. J. Cell Sci. 126, 1307–1316. doi: 10.1242/jcs.107805.

Barlowe, C. K., and Miller, E. A. (2013). Secretory protein biogenesis and traffic in the early secretory pathway. Genetics 193, 383–410.

Bassham, D. C., Brandizzi, F., Otegui, M. S., and Sanderfoot, A. A. (2008). The secretory system of Arabidopsis. Arab. B. 6, e0116. doi: 10.1199/tab.0116.

Bauters, L., Stojilković, B., and Gheysen, G. (2021). Pathogens pulling the strings: Effectors manipulating salicylic acid and phenylpropanoid biosynthesis in plants. Mol. Plant Pathol. 22, 1436–1448. doi: https://doi.org/10.1111/mpp.13123.

Bayer, E. M., Bottrill, A. R., Walshaw, J., Vigouroux, M., Naldrett, M. J., Thomas, C. L., et al. (2006). Arabidopsis cell wall proteome defined using multidimensional protein identification technology. Proteomics 6, 301–311. doi: https://doi.org/10.1002/pmic.200500046.

Beijerinck, W. M. (1898). Ueber ein contagium vivum fluidum als Ursache der Fleckenkrankheit der Tabaksblatter. Verh. Kon. Akad. Wetensch. 5, 3–21.

Bellés, J. M., López-Gresa, M. P., Fayos, J., Pallás, V., Rodrigo, I., and Conejero, V. (2008). Induction of cinnamate 4-hydroxylase and phenylpropanoids in virus-infected cucumber and melon plants. Plant Sci. 174, 524–533. doi:

https://doi.org/10.1016/j.plantsci.2008.02.008.

Bendahmane, A., Kanyuka, K., and Baulcombe, D. C. (1999). The Rx gene from potato controls separate virus resistance and cell death responses. Plant Cell 11, 781–792. doi: 10.1105/tpc.11.5.781.

Benitez-Alfonso, Y., Faulkner, C., Ritzenthaler, C., and Maule, A. J. (2010). Plasmodesmata: gateways to local and systemic virus infection. Mol. Plant. Microbe. Interact. 23, 1403–1412. doi: 10.1094/MPMI-05-10-0116.

Benjamini, Y., and Hochberg, Y. (1995). Controlling the False Discovery Rate: A Practical and Powerful Approach to Multiple Testing. J. R. Stat. Soc. Ser. B 57, 289–300. Available at: http://www.jstor.org/stable/2346101.

Bensimon, A., Heck, A. J. R., and Aebersold, R. (2012). Mass spectrometry-based proteomics and network biology. Annu. Rev. Biochem. 81, 379–405. doi: 10.1146/annurev-biochem-072909-100424.

Berardini, T. Z., Reiser, L., Li, D., Mezheritsky, Y., Muller, R., Strait, E., et al. (2015). The Arabidopsis information resource: Making and mining the "gold standard" annotated reference plant genome. Genesis 53, 474–485. doi: 10.1002/dvg.22877.

Beretta, L., and Santaniello, A. (2016). Nearest neighbor imputation algorithms: a critical evaluation. BMC Med. Inform. Decis. Mak. 16, 74. doi: 10.1186/s12911-016-0318-z.

Berlingerio, M., Coscia, M., Giannotti, F., Monreale, A., and Pedreschi, D. (2011). The pursuit of hubbiness: Analysis of hubs in large multidimensional networks. J. Comput. Sci. 2, 223–237. doi: https://doi.org/10.1016/j.jocs.2011.05.009.

Bernal, J. D., and Fankuchen, I. (1937). Structure Types of Protein Crystals from Virus-infected Plants. Nature 139, 923–924. doi: 10.1038/139923a0.

Betters, J. L., and Yu, L. (2010). NPC1L1 and cholesterol transport. FEBS Lett. 584, 2740–2747. doi: 10.1016/j.febslet.2010.03.030.

Beveridge, C. A., and Kyozuka, J. (2010). New genes in the strigolactone-related shoot branching pathway. Curr. Opin. Plant Biol. 13, 34–39. doi: https://doi.org/10.1016/j.pbi.2009.10.003.

Bhattacharyya, D., and Chakraborty, S. (2018). Chloroplast: the Trojan horse in plant-virus interaction. Mol. Plant Pathol. 19, 504–518. doi: 10.1111/mpp.12533.

Bigeard, J., Colcombet, J., and Hirt, H. (2015). Signaling mechanisms in pattern-triggered immunity (PTI). Mol. Plant 8, 521–539. doi: 10.1016/j.molp.2014.12.022.

Bin, L., Domingo, M. S., Mayobre, C., Martín-Hernández, A. M., Pujol, M., and Garcia-Mas, J. (2022). Knock-out of CmNAC-NOR affects melon climacteric fruit ripening. bioRxiv, 2022.02.02.478821. doi: 10.1101/2022.02.02.478821.

Blackman, L. M., Boevink, P., Cruz, S. S., Palukaitis, P., and Oparka, K. J. (1998). The movement protein of cucumber mosaic virus traffics into sieve elements in minor veins of nicotiana clevelandii. Plant Cell 10, 525–538. doi: 10.1105/tpc.10.4.525.

Bo, Y., Qiu, S., Mulloy, R. P., and Côté, M. (2020). Filoviruses Use the HOPS Complex and UVRAG To Traffic to Niemann-Pick C1 Compartments during Viral Entry. J. Virol. 94. doi: 10.1128/JVI.01002-20.

Boccard, F., and Baulcombe, D. (1993). Mutational analysis of cis-acting sequences and gene function in RNA3 of cucumber mosaic virus. Virology 193, 563–578. doi: 10.1006/viro.1993.1165.

Boldt, R., Edner, C., Kolukisaoglu, U., Hagemann, M., Weckwerth, W., Wienkoop, S., et al. (2005). D-GLYCERATE 3-KINASE, the last unknown enzyme in the photorespiratory cycle in Arabidopsis, belongs to a novel kinase family. Plant Cell 17, 2413–2420. doi: 10.1105/tpc.105.033993.

Bombarely, A., Rosli, H. G., Vrebalov, J., Moffett, P., Mueller, L. A., and Martin, G. B. (2012). A draft genome sequence of Nicotiana benthamiana to enhance molecular plant-microbe biology research. Mol. Plant. Microbe. Interact. 25, 1523–1530. doi: 10.1094/MPMI-06-12-0148-TA.

Borate, B. R., Chesler, E. J., Langston, M. A., Saxton, A. M., and Voy, B. H. (2009). Comparison of threshold selection methods for microarray gene co-expression matrices. BMC Res. Notes 2, 240. doi: 10.1186/1756-0500-2-240.

Boutrot, F., and Zipfel, C. (2017). Function, Discovery, and Exploitation of Plant Pattern Recognition Receptors for Broad-Spectrum Disease Resistance. Annu. Rev. Phytopathol. 55, 257–286. doi: 10.1146/annurev-phyto-080614-120106.

Boyko, V., Hu, Q., Seemanpillai, M., Ashby, J., and Heinlein, M. (2007). Validation of

microtubule-associated Tobacco mosaic virus RNA movement and involvement of microtubule-aligned particle trafficking. Plant J. 51, 589–603. doi: https://doi.org/10.1111/j.1365-313X.2007.03163.x.

Brenner, S., and Horne, R. W. (1959). A negative staining method for high resolution electron microscopy of viruses. Biochim. Biophys. Acta 34, 103–110. doi: 10.1016/0006-3002(59)90237-9.

Brigneti, G., Voinnet, O., Li, W. X., Ji, L. H., Ding, S. W., and Baulcombe, D. C. (1998). Viral pathogenicity determinants are suppressors of transgene silencing in Nicotiana benthamiana. EMBO J. 17, 6739–6746. doi: 10.1093/emboj/17.22.6739.

Brillada, C., Zheng, J., Krüger, F., Rovira-Diaz, E., Askani, J. C., Schumacher, K., et al. (2018). Phosphoinositides control the localization of HOPS subunit VPS41, which together with VPS33 mediates vacuole fusion in plants. Proc. Natl. Acad. Sci. U. S. A. 115, E8305–E8314. doi: 10.1073/pnas.1807763115.

Buhr, F., Lahroussi, A., Springer, A., Rustgi, S., von Wettstein, D., Reinbothe, C., et al. (2017). NADPH:protochlorophyllide oxidoreductase B (PORB) action in Arabidopsis thaliana revisited through transgenic expression of engineered barley PORB mutant proteins. Plant Mol. Biol. 94, 45–59. doi: 10.1007/s11103-017-0592-x.

Bujarski, J. J. (2021). Bromoviruses (Bromoviridae). Encycl. Virol., 260–267. doi: 10.1016/B978-0-12-809633-8.21563-X.

Burch-Smith, T. M., Stonebloom, S., Xu, M., and Zambryski, P. C. (2011). Plasmodesmata during development: re-examination of the importance of primary, secondary, and branched plasmodesmata structure versus function. Protoplasma 248, 61–74. doi: 10.1007/s00709-010-0252-3.

Burns, C. H., Yau, B., Rodriguez, A., Triplett, J., Maslar, D., An, Y. S., et al. (2021). Pancreatic β-Cell-Specific Deletion of VPS41 Causes Diabetes Due to Defects in Insulin Secretion. Diabetes 70, 436–448. doi: 10.2337/db20-0454.

Callaway, A., Giesman-Cookmeyer, D., Gillock, E. T., Sit, T. L., and Lommel, S. A. (2001). The multifunctional capsid proteins of plant RNA viruses. Annu. Rev. Phytopathol. 39, 419–460. doi: 10.1146/annurev.phyto.39.1.419.

Campos, L., López-Gresa, M. P., Fuertes, D., Bellés, J. M., Rodrigo, I., and Lisón, P. (2019).

Tomato glycosyltransferase Twi1 plays a role in flavonoid glycosylation and defence against virus. BMC Plant Biol. 19, 450. doi: 10.1186/s12870-019-2063-9.

Canto, T., and Palukaitis, P. (1999). Are Tubules Generated by the 3a Protein Necessary for Cucumber Mosaic Virus Movement? Mol. Plant-Microbe Interact. 12, 985–993. doi: 10.1094/MPMI.1999.12.11.985.

Capelli, N., Diogon, T., Greppin, H., and Simon, P. (1997). Isolation and characterization of a cDNA clone encoding an osmotin-like protein from Arabidopsis thaliana. Gene 191, 51–56. doi: https://doi.org/10.1016/S0378-1119(97)00029-2.

Caranta, C., Pflieger, S., Lefebvre, V., Daubèze, A. M., Thabuis, A., and Palloix, A. (2002). QTLs involved in the restriction of cucumber mosaic virus (CMV) long-distance movement in pepper. Theor. Appl. Genet. 104, 586–591. doi: 10.1007/s001220100753.

Carette, J. E., Raaben, M., Wong, A. C., Herbert, A. S., Obernosterer, G., Mulherkar, N., et al. (2011a). Ebola virus entry requires the cholesterol transporter Niemann-Pick C1. Nature 477, 340–343. doi: 10.1038/nature10348.

Carette, J. E., Raaben, M., Wong, A. C., Herbert, A. S., Obernosterer, G., Mulherkar, N., et al. (2011b). Ebola virus entry requires the cholesterol transporter Niemann-Pick C1. Nature 477, 340–343. doi: 10.1038/nature10348.

Carluccio, A. V., Zicca, S., and Stavolone, L. (2014). Hitching a ride on vesicles: cauliflower mosaic virus movement protein trafficking in the endomembrane system. Plant Physiol. 164, 1261–1270. doi: 10.1104/pp.113.234534.

Carrington, J. C., Kasschau, K. D., Mahajan, S. K., and Schaad, M. C. (1996). Cell-to-Cell and Long-Distance Transport of Viruses in Plants. Plant Cell 8, 1669–1681. doi: 10.1105/tpc.8.10.1669.

Carstea, E. D., Morris, J. A., Coleman, K. G., Loftus, S. K., Zhang, D., Cummings, C., et al. (1997). Niemann-Pick C1 disease gene: homology to mediators of cholesterol homeostasis. Science 277, 228–231. doi: 10.1126/science.277.5323.228.

Carter, G. C., Bernstone, L., Sangani, D., Bee, J. W., Harder, T., and James, W. (2009). HIV entry in macrophages is dependent on intact lipid rafts. Virology 386, 192–202. doi: 10.1016/j.virol.2008.12.031.

Castanera, R., Ruggieri, V., Pujol, M., Garcia-Mas, J., and Casacuberta, J. M. (2020). An

Improved Melon Reference Genome With Single-Molecule Sequencing Uncovers a Recent Burst of Transposable Elements With Potential Impact on Genes. Front. Plant Sci. 10, 1815. doi: 10.3389/fpls.2019.01815.

Chang, C.-L., Chen, Y.-J., and Liou, J. (2017). ER-plasma membrane junctions: Why and how do we study them? Biochim. Biophys. acta. Mol. cell Res. 1864, 1494–1506. doi: 10.1016/j.bbamcr.2017.05.018.

Chaudhary, S., Jabre, I., Reddy, A. S. N., Staiger, D., and Syed, N. H. (2019). Perspective on Alternative Splicing and Proteome Complexity in Plants. Trends Plant Sci. 24, 496–506. doi: 10.1016/j.tplants.2019.02.006.

Chen, M.-H., and Citovsky, V. (2003). Systemic movement of a tobamovirus requires host cell pectin methylesterase. Plant J. 35, 386–392. doi: 10.1046/j.1365-313x.2003.01818.x.

Chen, M. H., Sheng, J., Hind, G., Handa, A. K., and Citovsky, V. (2000). Interaction between the tobacco mosaic virus movement protein and host cell pectin methylesterases is required for viral cell-to-cell movement. EMBO J. 19, 913–920. doi: 10.1093/emboj/19.5.913.

Cheng, Z., Sattler, S., Maeda, H., Sakuragi, Y., Bryant, D. A., and DellaPenna, D. (2003). Highly Divergent Methyltransferases Catalyze a Conserved Reaction in Tocopherol and Plastoquinone Synthesis in Cyanobacteria and Photosynthetic Eukaryotes . Plant Cell 15, 2343–2356. doi: 10.1105/tpc.013656.

Cheong, B. E., Beine-Golovchuk, O., Gorka, M., Ho, W. W. H., Martinez-Seidel, F., Firmino, A. A. P., et al. (2021). Arabidopsis REI-LIKE proteins activate ribosome biogenesis during cold acclimation. Sci. Rep. 11, 2410. doi: 10.1038/s41598-021-81610-z.

Cho, E. J., Yuen, C. Y. L., Kang, B.-H., Ondzighi, C. A., Staehelin, L. A., and Christopher, D. A. (2011). Protein disulfide isomerase-2 of Arabidopsis mediates protein folding and localizes to both the secretory pathway and nucleus, where it interacts with maternal effect embryo arrest factor. Mol. Cells 32, 459–475. doi: 10.1007/s10059-011-0150-3.

Choi, S., Lee, J.-H., Kang, W.-H., Kim, J., Huy, H. N., Park, S.-W., et al. (2018). Identification of Cucumber mosaic resistance 2 (cmr2) That Confers Resistance to a New Cucumber mosaic virus Isolate P1 (CMV-P1) in Pepper (Capsicum spp.). Front.

Plant Sci., 1106.

Choi, Y., and Chan, A. P. (2015). PROVEAN web server: A tool to predict the functional effect of amino acid substitutions and indels. Bioinformatics 31, 2745–2747. doi: 10.1093/bioinformatics/btv195.

Choi, Y. H., Kim, H. K., Linthorst, H. J. M., Hollander, J. G., Lefeber, A. W. M., Erkelens, C., et al. (2006). NMR Metabolomics to Revisit the Tobacco Mosaic Virus Infection in Nicotiana tabacum Leaves. J. Nat. Prod. 69, 742–748. doi: 10.1021/np050535b.

Chomicki, G., Schaefer, H., and Renner, S. S. (2020). Origin and domestication of Cucurbitaceae crops: insights from phylogenies, genomics and archaeology. New Phytol. 226, 1240–1255. doi: https://doi.org/10.1111/nph.16015.

Christensen, N., Tilsner, J., Bell, K., Hammann, P., Parton, R., Lacomme, C., et al. (2009). The 5' cap of tobacco mosaic virus (TMV) is required for virion attachment to the actin/endoplasmic reticulum network during early infection. Traffic 10, 536–551. doi: 10.1111/j.1600-0854.2009.00889.x.

Cilia, M. L., and Jackson, D. (2004). Plasmodesmata form and function. Curr. Opin. Cell Biol. 16, 500–506. doi: 10.1016/j.ceb.2004.08.002.

Cillo, F., Roberts, I. M., and Palukaitis, P. (2002). In situ localization and tissue distribution of the replication-associated proteins of Cucumber mosaic virus in tobacco and cucumber. J. Virol. 76, 10654–10664. doi: 10.1128/jvi.76.21.10654-10664.2002.

Citovsky, V., Knorr, D., Schuster, G., and Zambryski, P. (1990). The P30 movement protein of tobacco mosaic virus is a single-strand nucleic acid binding protein. Cell 60, 637–647. doi: 10.1016/0092-8674(90)90667-4.

Citovsky, V., Wong, M. L., Shaw, A. L., Prasad, B. V, and Zambryski, P. (1992). Visualization and characterization of tobacco mosaic virus movement protein binding to single-stranded nucleic acids. Plant Cell 4, 397–411. doi: 10.1105/tpc.4.4.397.

Claessen, J. H. L., Kundrat, L., and Ploegh, H. L. (2012). Protein quality control in the ER: balancing the ubiquitin checkbook. Trends Cell Biol. 22, 22–32.

Clauset, A., Newman, M. E. J., and Moore, C. (2004). Finding community structure in very large networks. Phys. Rev. E. Stat. Nonlin. Soft Matter Phys. 70, 66111. doi: 10.1103/PhysRevE.70.066111.

Coca, M., Bortolotti, C., Rufat, M., Peñas, G., Eritja, R., Tharreau, D., et al. (2004). Transgenic rice plants expressing the antifungal AFP protein from Aspergillus giganteus show enhanced resistance to the rice blast fungus Magnaporthe grisea. Plant Mol. Biol. 54, 245–259. doi: 10.1023/B:PLAN.0000028791.34706.80.

Collings, D. A., Gebbie, L. K., Howles, P. A., Hurley, U. A., Birch, R. J., Cork, A. H., et al. (2008). Arabidopsis dynamin-like protein DRP1A: a null mutant with widespread defects in endocytosis, cellulose synthesis, cytokinesis, and cell expansion. J. Exp. Bot. 59, 361–376. doi: 10.1093/jxb/erm324.

Connerly, P. L. (2010). How do proteins move through the golgi apparatus. Nat. Educ. 3, 60.

Cornelissen, B. J., Hooft van Huijsduijnen, R. A., and Bol, J. F. (1986). A tobacco mosaic virus-induced tobacco protein is homologous to the sweet-tasting protein thaumatin. Nature 321, 531–532. doi: 10.1038/321531a0.

Côté, M., Misasi, J., Ren, T., Bruchez, A., Lee, K., Filone, C. M., et al. (2011). Small molecule inhibitors reveal Niemann-Pick C1 is essential for Ebola virus infection. Nature 477, 344–348. doi: 10.1038/nature10380.

Cox, J., and Mann, M. (2008). MaxQuant enables high peptide identification rates, individualized p.p.b.-range mass accuracies and proteome-wide protein quantification. Nat. Biotechnol. 26, 1367–1372. doi: 10.1038/nbt.1511.

Crick, F. H. C., and Watson, J. D. (1956). Structure of small viruses. Nature 177, 473–475.

Cui, M., Gu, M., Lu, Y., Zhang, Y., Chen, C., Ling, H.-Q., et al. (2020). Glutamate synthase 1 is involved in iron-deficiency response and long-distance transportation in Arabidopsis. J. Integr. Plant Biol. 62, 1925–1941. doi: https://doi.org/10.1111/jipb.12985.

Cui, W., and Lee, J.-Y. (2016). Arabidopsis callose synthases CalS1/8 regulate plasmodesmal permeability during stress. Nat. plants 2, 16034. doi: 10.1038/nplants.2016.34.

Culver, J. N., and Padmanabhan, M. S. (2007). Virus-Induced Disease: Altering Host Physiology One Interaction at a Time. Annu. Rev. Phytopathol. 45, 221–243. doi: 10.1146/annurev.phyto.45.062806.094422.

Curtin, F., and Schulz, P. (1998). Multiple correlations and Bonferroni's correction. Biol. Psychiatry 44, 775–777. doi: 10.1016/s0006-3223(98)00043-2.

Dafoe, N. J., Zamani, A., Ekramoddoullah, A. K. M., Lippert, D., Bohlmann, J., and Constabel, C. P. (2009). Analysis of the Poplar Phloem Proteome and Its Response to Leaf Wounding. J. Proteome Res. 8, 2341–2350. doi: 10.1021/pr800968r.

Dahmani-Mardas, F., Troadec, C., Boualem, A., Leveˆque, S., Alsadon, A. A., Aldoss, A. A., et al. (2010). Engineering melon plants with improved fruit shelf life using the TILLING approach. PLoS One 5, e15776.

Daniëlle O. Kisluk-Grosheide (1991). Tulips in Dutch seventeenth century decorative arts. Mag. Antiq., 740–741.

Daryono, B. S., Wakui, K., and Natsuaki, K. T. (2010). Linkage analysis and mapping of SCAR markers linked to CMV-B2 resistance gene in melon. Sabrao J Breed Genet 42, 35–45.

Davies, J. P., Levy, B., and Ioannou, Y. A. (2000). Evidence for a Niemann-pick C (NPC) gene family: identification and characterization of NPC1L1. Genomics 65, 137–145. doi: 10.1006/geno.2000.6151.

Davis, G. N. (1962). Cucurbits: Botany Cultivation & Utilization.

de Jesús-Pires, C., Ferreira-Neto, J. R. C., Pacifico Bezerra-Neto, J., Kido, E. A., de Oliveira Silva, R. L., Pandolfi, V., et al. (2020). Plant Thaumatin-like Proteins: Function, Evolution and Biotechnological Applications. Curr. Protein Pept. Sci. 21, 36–51. doi: 10.2174/1389203720666190318164905.

De Marcos Lousa, C., Gershlick, D. C., and Denecke, J. (2012). Mechanisms and concepts paving the way towards a complete transport cycle of plant vacuolar sorting receptors. Plant Cell 24, 1714–1732.

De Storme, N., and Geelen, D. (2014). Callose homeostasis at plasmodesmata: molecular regulators and developmental relevance . Front. Plant Sci. 5, 138. Available at: https://www.frontiersin.org/article/10.3389/fpls.2014.00138.

den Hollander, P. W., Kieper, S. N., Borst, J. W., and van Lent, J. W. M. (2016). The role of plasmodesma-located proteins in tubule-guided virus transport is limited to the plasmodesmata. Arch. Virol. 161, 2431–2440. doi: 10.1007/s00705-016-2936-2.

Depuydt, T., and Vandepoele, K. (2021). Multi-omics network-based functional annotation of unknown Arabidopsis genes. Plant J. 108, 1193–1212. doi: https://doi.org/10.1111/tpj.15507.

Dhillon, N. P. S., Ranjana, R., Singh, K., Eduardo, I., Monforte, A. J., Pitrat, M., et al. (2007). Diversity among landraces of Indian snapmelon (Cucumis melo var. momordica). Genet. Resour. Crop Evol. 54, 1267–1283.

Dhillon, N. P. S., Singh, J., Fergany, M., Monforte, A. J., and Sureja, A. K. (2009). Phenotypic and molecular diversity among landraces of snapmelon (Cucumis melo var. momordica) adapted to the hot and humid tropics of eastern India. Plant Genet. Resour. 7, 291–300.

Di Carli, M., Benvenuto, E., and Donini, M. (2012). Recent insights into plant-virus interactions through proteomic analysis. J. Proteome Res. 11, 4765–4780. doi: 10.1021/pr300494e.

Di Carli, M., Villani, M. E., Bianco, L., Lombardi, R., Perrotta, G., Benvenuto, E., et al. (2010). Proteomic analysis of the plant-virus interaction in cucumber mosaic virus (CMV) resistant transgenic tomato. J. Proteome Res. 9, 5684–5697. doi: 10.1021/pr100487x.

Diaz-Pendon, J. A., Li, F., Li, W.-X., and Ding, S.-W. (2007). Suppression of Antiviral Silencing by Cucumber Mosaic Virus 2b Protein in Arabidopsis Is Associated with Drastically Reduced Accumulation of Three Classes of Viral Small Interfering RNAs. Plant Cell 19, 2053–2063. doi: 10.1105/tpc.106.047449.

Diaz, A., Fergany, M., Formisano, G., Ziarsolo, P., Blanca, J., Fei, Z., et al. (2011). A consensus linkage map for molecular markers and quantitative trait loci associated with economically important traits in melon (Cucumis melo L.). BMC Plant Biol. 11, 1–14.

Diaz, J. A., Mallor, C., Soria, C., Camero, R., Garzo, E., Fereres, A., et al. (2003). Potential sources of resistance for melon to nonpersistently aphid-borne viruses. Plant Dis. 87, 960–964.

Dielen, A.-S., Sassaki, F. T., Walter, J., Michon, T., Ménard, G., Pagny, G., et al. (2011). The 20S proteasome α5 subunit of Arabidopsis thaliana carries an RNase activity and interacts in planta with the lettuce mosaic potyvirus HcPro protein. Mol. Plant Pathol. 12, 137–150. doi: 10.1111/j.1364-3703.2010.00654.x.

Dixon, R. A., Achnine, L., Kota, P., Liu, C.-J., Reddy, M. S. S., and Wang, L. (2002). The phenylpropanoid pathway and plant defence-a genomics perspective. Mol. Plant Pathol. 3, 371–390. doi: 10.1046/j.1364-3703.2002.00131.x.

Dogimont, C., Leconte, L., Périn, C., Thabuis, A., Lecoq, H., and Pitrat, M. (2000). Identification of QTLs contributing to resistance to different strains of cucumber mosaic cucumovirus in melon. in VII Eucarpia Meeting on Cucurbit Genetics and Breeding 510, 391–398.

Dressano, K., Weckwerth, P. R., Poretsky, E., Takahashi, Y., Villarreal, C., Shen, Z., et al. (2020). Dynamic regulation of Pep-induced immunity through post-translational control of defence transcript splicing. Nat. Plants 6, 1008–1019. doi: 10.1038/s41477-020-0724-1.

Drugeon, G., and Jupin, I. (2002). Stability in vitro of the 69K movement protein of Turnip yellow mosaic virus is regulated by the ubiquitin-mediated proteasome pathway. J. Gen. Virol. 83, 3187–3197.

Du, Z., Chen, F., Zhao, Z., Liao, Q., Palukaitis, P., and Chen, J. (2008). The 2b protein and the C-terminus of the 2a protein of cucumber mosaic virus subgroup I strains both play a role in viral RNA accumulation and induction of symptoms. Virology 380, 363–370. doi: https://doi.org/10.1016/j.virol.2008.07.036.

Duan, C.-G., Fang, Y.-Y., Zhou, B.-J., Zhao, J.-H., Hou, W.-N., Zhu, H., et al. (2012). Suppression of Arabidopsis ARGONAUTE1-Mediated Slicing, Transgene-Induced RNA Silencing, and DNA Methylation by Distinct Domains of the Cucumber mosaic virus 2b Protein. Plant Cell 24, 259–274. doi: 10.1105/tpc.111.092718.

Eduardo, I., Arús, P., and Monforte, A. J. (2005). Development of a genomic library of near isogenic lines (NILs) in melon (Cucumis melo L.) from the exotic accession PI161375. Theor. Appl. Genet. 112, 139–148. doi: 10.1007/s00122-005-0116-y.

Edwards, G. E., and Gutierrez, M. (1972). Metabolic Activities in Extracts of Mesophyll and Bundle Sheath Cells of Panicum miliaceum (L.) in Relation to the C4 Dicarboxylic Acid Pathway of Photosynthesis 1. Plant Physiol. 50, 728–732. doi: 10.1104/pp.50.6.728.

Edwardson, J. R., and Christie, R. G. (1991). Cucumoviruses. CRC Handb. viruses Infect. Legum., 293–319.

Edwardson, J. R., and Christie, R. G. (2018). CRC handbook of viruses infecting legumes. CRC Press.

Ekanayake, G., Smith, J. M., Jones, K. B., Stiers, H. M., Robinson, S. J., LaMontagne, E. D., et al. (2021). DYNAMIN-RELATED PROTEIN DRP1A functions with DRP2B in plant growth, flg22-immune responses, and endocytosis. Plant Physiol. 185, 1986–2002. doi: 10.1093/plphys/kiab024.

El Hadidi, M. N., Fahmy, A. G., and Willerding, U. (1996). The paleoethnobotany of locality 11c, Hierakonpolis (3880–3500 BC), Egypt 1. Cultivated crops and wild plants of potential value. Taekholmia 16, 31–44.

Ellgaard, L., and Helenius, A. (2003). Quality control in the endoplasmic reticulum. Nat. Rev. Mol. cell Biol. 4, 181–191.

Endl, J., Achigan-Dako, E. G., Pandey, A. K., Monforte, A. J., Pico, B., and Schaefer, H. (2018). Repeated domestication of melon (Cucumis melo) in Africa and Asia and a new close relative from India. Am. J. Bot. 105, 1662–1671.

Escriu, F., Perry, K. L., and García-Arenal, F. (2000). Transmissibility of Cucumber mosaic virus by Aphis gossypii Correlates with Viral Accumulation and Is Affected by the Presence of Its Satellite RNA. Phytopathology® 90, 1068–1072. doi: 10.1094/PHYTO.2000.90.10.1068.

Essafi, A., Díaz-Pendón, J. A., Moriones, E., Monforte, A. J., Garcia-Mas, J., and Martín-Hernández, A. M. (2009). Dissection of the oligogenic resistance to Cucumber mosaic virus in the melon accession PI 161375. Theor. Appl. Genet. 118, 275–284. doi: 10.1007/s00122-008-0897-x.

Eun, M. H., Han, J.-H., Yoon, J. B., and Lee, J. (2016). QTL mapping of resistance to the Cucumber mosaic virus P1 strain in pepper using a genotyping-by-sequencing analysis. Hortic. Environ. Biotechnol. 57, 589–597.

FAOSTAT, R. (2017). FAOSTAT database. Food Agric. Organ. UN.

Feldman, M. J., Poirier, B. C., and Lange, B. M. (2015a). Misexpression of the Niemann-Pick disease type C1 (NPC1)-like protein in Arabidopsis causes sphingolipid accumulation and reproductive defects. Planta 242, 921–933. doi: 10.1007/s00425-015-2322-4.

Feldman, M. J., Poirier, B. C., and Lange, B. M. (2015b). Misexpression of the Niemann-Pick disease type C1 (NPC1)-like protein in Arabidopsis causes sphingolipid accumulation and reproductive defects. Planta 242, 921–933. doi: 10.1007/s00425-015-2322-4.

Feng, X., Guzmán, P., Myers, J. R., and Karasev, A. V (2017). Resistance to Bean common mosaic necrosis virus Conferred by the bc-1 Gene Affects Systemic Spread of the Virus in Common Bean. Phytopathology 107, 893–900. doi: 10.1094/PHYTO-01-17-0013-R.

Feng, X., Orellana, G. E., Myers, J. R., and Karasev, A. V (2018). Recessive Resistance to Bean common mosaic virus Conferred by the bc-1 and bc-2 Genes in Common Bean (Phaseolus vulgaris) Affects Long-Distance Movement of the Virus. Phytopathology 108, 1011–1018. doi: 10.1094/PHYTO-01-18-0021-R.

Fergany, M., Kaur, B., Monforte, A. J., Pitrat, M., Rys, C., Lecoq, H., et al. (2011). Variation in melon (Cucumis melo) landraces adapted to the humid tropics of southern India. Genet. Resour. Crop Evol. 58, 225–243.

Fernandez-Pozo, N., Menda, N., Edwards, J. D., Saha, S., Tecle, I. Y., Strickler, S. R., et al. (2015). The Sol Genomics Network (SGN)--from genotype to phenotype to breeding. Nucleic Acids Res. 43, D1036-41. doi: 10.1093/nar/gku1195.

Figueiredo, J., Silva, M. S., and Figueiredo, A. (2018). Subtilisin-like proteases in plant defence: the past, the present and beyond. Mol. Plant Pathol. 19, 1017–1028. doi: 10.1111/MPP.12567.

Fislová, T., Thomas, B., Graef, K. M., and Fodor, E. (2010). Association of the influenza virus RNA polymerase subunit PB2 with the host chaperonin CCT. J. Virol. 84, 8691–8699. doi: 10.1128/JVI.00813-10.

Folimonova, S. Y., and Tilsner, J. (2018). Hitchhikers, highway tolls and roadworks: the interactions of plant viruses with the phloem. Curr. Opin. Plant Biol. 43, 82–88. doi: 10.1016/j.pbi.2018.02.001.

Frescatada-Rosa, M., Stanislas, T., Backues, S. K., Reichardt, I., Men, S., Boutte, Y., et al. (2014). High lipid order of Arabidopsis cell-plate membranes mediated by sterol and DYNAMIN-RELATED PROTEIN1A function. Plant J. 80, 745–757.

Fristedt, R., Hu, C., Wheatley, N., Roy, L. M., Wachter, R. M., Savage, L., et al. (2018). RAF2 is a RuBisCO assembly factor in Arabidopsis thaliana. Plant J. 94, 146–156. doi: https://doi.org/10.1111/tpj.13849.

Fu, Z. Q., and Dong, X. (2013). Systemic acquired resistance: turning local infection into global defense. Annu. Rev. Plant Biol. 64, 839–863. doi: 10.1146/annurev-arplant-042811-105606.

Fujimoto, M., Arimura, S., Ueda, T., Takanashi, H., Hayashi, Y., Nakano, A., et al. (2010). Arabidopsis dynamin-related proteins DRP2B and DRP1A participate together in clathrin-coated vesicle formation during endocytosis. Proc. Natl. Acad. Sci. 107, 6094 LP – 6099. doi: 10.1073/pnas.0913562107.

Fukao, Y., Ferjani, A., Fujiwara, M., Nishimori, Y., and Ohtsu, I. (2009). Identification of Zinc-Responsive Proteins in the Roots of Arabidopsis thaliana Using a Highly Improved Method of Two-Dimensional Electrophoresis. Plant Cell Physiol. 50, 2234–2239. doi: 10.1093/pcp/pcp154.

Gadadhar, S., Bodakuntla, S., Natarajan, K., and Janke, C. (2017). The tubulin code at a glance. J. Cell Sci. 130, 1347–1353. doi: 10.1242/jcs.199471.

Gao, C., Luo, M., Zhao, Q., Yang, R., Cui, Y., Zeng, Y., et al. (2014). A Unique plant ESCRT component, FREE1, regulates multivesicular body protein sorting and plant growth. Curr. Biol. 24, 2556–2563. doi: 10.1016/j.cub.2014.09.014.

Gao, C., Zhuang, X., Cui, Y., Fu, X., He, Y., Zhao, Q., et al. (2015). Dual roles of an Arabidopsis ESCRT component FREE1 in regulating vacuolar protein transport and autophagic degradation. Proc. Natl. Acad. Sci. U. S. A. 112, 1886–1891. doi: 10.1073/pnas.1421271112.

Garcia-Mas, J., Benjak, A., Sanseverino, W., Bourgeois, M., Mir, G., González, M. V., et al. (2012). The genome of melon (Cucumis melo L.). Proc. Natl. Acad. Sci. 109, 11872–11877. doi: 10.1073/pnas.1205415109.

Garcia-Mas, J., Oliver, M., Gomez-Paniagua, H., and De Vicente, M. C. (2000). Comparing AFLP, RAPD and RFLP markers for measuring genetic diversity in melon. Theor. Appl. Genet. 101, 860–864.

Garcia-Ruiz, H. (2019). Host factors against plant viruses. Mol. Plant Pathol. 20, 1588–1601.

doi: https://doi.org/10.1111/mpp.12851.

Garcia, A. F., Dyszy, F., Munte, C. E., DeMarco, R., Beltramini, L. M., Oliva, G., et al. (2014). THI1, a protein involved in the biosynthesis of thiamin in Arabidopsis thaliana: Structural analysis of THI1(A140V) mutant. Biochim. Biophys. Acta - Proteins Proteomics 1844, 1094–1103. doi: https://doi.org/10.1016/j.bbapap.2014.03.005.

Garg, S., Sharma, M., Ung, C., Tuli, A., Barral, D. C., Hava, D. L., et al. (2011). Lysosomal trafficking, antigen presentation, and microbial killing are controlled by the Arf-like GTPase Arl8b. Immunity 35, 182–193.

Gasteiger, E., Gattiker, A., Hoogland, C., Ivanyi, I., Appel, R. D., and Bairoch, A. (2003). ExPASy: The proteomics server for in-depth protein knowledge and analysis. Nucleic Acids Res. 31, 3784–3788. doi: 10.1093/nar/gkg563.

Gaudet, P., Livstone, M. S., Lewis, S. E., and Thomas, P. D. (2011). Phylogenetic-based propagation of functional annotations within the Gene Ontology consortium. Brief. Bioinform. 12, 449–462. doi: 10.1093/bib/bbr042.

Ge, L., Wang, J., Qi, W., Miao, H.-H., Cao, J., Qu, Y.-X., et al. (2008). The Cholesterol Absorption Inhibitor Ezetimibe Acts by Blocking the Sterol-Induced Internalization of NPC1L1. Cell Metab. 7, 508–519. doi: https://doi.org/10.1016/j.cmet.2008.04.001.

Genovés, A., Navarro, J. A., and Pallás, V. (2010). The Intra- and intercellular movement of Melon necrotic spot virus (MNSV) depends on an active secretory pathway. Mol. Plant. Microbe. Interact. 23, 263–272. doi: 10.1094/MPMI-23-3-0263.

Giner, A., Pascual, L., Bourgeois, M., Gyetvai, G., Rios, P., Picó, B., et al. (2017). A mutation in the melon Vacuolar Protein Sorting 41prevents systemic infection of Cucumber mosaic virus. Sci. Rep. 7, 10471. doi: 10.1038/s41598-017-10783-3.

Giordano, A., Domingo, M. S., Quadrana, L., Pujol, M., Martín-Hernández, A. M., and Garcia-Mas, J. (2022). CRISPR/Cas9 gene editing uncovers the role of CTR1 and ROS1 in melon fruit ripening and epigenetic regulation. J. Exp. Bot., erac148. doi: 10.1093/jxb/erac148.

Gonzalez-Ibeas, D., Blanca, J., Roig, C., González-To, M., Picó, B., Truniger, V., et al. (2007). MELOGEN: an EST database for melon functional genomics. BMC Genomics 8, 306. doi: 10.1186/1471-2164-8-306.

González, I., Martínez, L., Rakitina, D. V, Lewsey, M. G., Atencio, F. A., Llave, C., et al. (2010). Cucumber mosaic virus 2b protein subcellular targets and interactions: their significance to RNA silencing suppressor activity. Mol. Plant. Microbe. Interact. 23, 294–303. doi: 10.1094/MPMI-23-3-0294.

González, M., Xu, M., Esteras, C., Roig, C., Monforte, A. J., Troadec, C., et al. (2011). Towards a TILLING platform for functional genomics in Piel de Sapo melons. BMC Res. Notes 4, 1–11.

Gonzalo, M. J., Claveria, E., Monforte, A. J., and Dolcet-Sanjuan, R. (2011). Parthenogenic haploids in melon: generation and molecular characterization of a doubled haploid line population. J. Am. Soc. Hortic. Sci. 136, 145–154.

Gorovits, R., Moshe, A., Ghanim, M., and Czosnek, H. (2013). Recruitment of the host plant heat shock protein 70 by Tomato yellow leaf curl virus coat protein is required for virus infection. PLoS One 8, e70280. doi: 10.1371/journal.pone.0070280.

Goto, K., Kobori, T., Kosaka, Y., Natsuaki, T., and Masuta, C. (2007). Characterization of Silencing Suppressor 2b of Cucumber Mosaic Virus Based on Examination of its Small RNA-Binding Abilities. Plant Cell Physiol. 48, 1050–1060. doi: 10.1093/pcp/pcm074.

Goulas, E., Schubert, M., Kieselbach, T., Kleczkowski, L. A., Gardeström, P., Schröder, W., et al. (2006). The chloroplast lumen and stromal proteomes of Arabidopsis thaliana show differential sensitivity to short- and long-term exposure to low temperature. Plant J. 47, 720–734. doi: https://doi.org/10.1111/j.1365-313X.2006.02821.x.

Gouveia, B. C., Calil, I. P., Machado, J. P. B., Santos, A. A., and Fontes, E. P. B. (2016). Immune Receptors and Co-receptors in Antiviral Innate Immunity in Plants. Front. Microbiol. 7, 2139. doi: 10.3389/fmicb.2016.02139.

Grube, R. C., Zhang, Y., Murphy, J. F., Loaiza-Figueroa, F., Lackney, V. K., Provvidenti, R., et al. (2000). New Source of Resistance to Cucumber mosaic virus in Capsicum frutescens. Plant Dis. 84, 885–891. doi: 10.1094/PDIS.2000.84.8.885.

Gu, Y., and Innes, R. W. (2011). The KEEP ON GOING protein of Arabidopsis recruits the ENHANCED DISEASE RESISTANCE1 protein to trans-Golgi network/early endosome vesicles. Plant Physiol. 155, 1827–1838.

Guenoune-Gelbart, D., Elbaum, M., Sagi, G., Levy, A., and Epel, B. L. (2008). Tobacco

mosaic virus (TMV) Replicase and Movement Protein Function Synergistically in Facilitating TMV Spread by Lateral Diffusion in the Plasmodesmal Desmotubule of Nicotiana benthamiana. Mol. Plant-Microbe Interact. 21, 335–345. doi: 10.1094/MPMI-21-3-0335.

Guiu-Aragonés, C. (2014). Study of Cucumber mosaic virus infection in the resistant melon accession PI 161375.

Guiu-Aragonés, C., Díaz-Pendón, J. A., and Martín-Hernández, A. M. (2015). Four sequence positions of the movement protein of Cucumber mosaic virus determine the virulence against cmv1-mediated resistance in melon. Mol. Plant Pathol. 16, 675–684. doi: 10.1111/mpp.12225.

Guiu-Aragonés, C., Monforte, A. J., Saladié, M., Corrêa, R., García-Mas, J., and Martín-Hernández, A. M. (2014). The complex resistance to cucumber mosaic cucumovirus (CMV) in the melon accession PI161375 is governed by one gene and at least two quantitative trait loci. doi: doi:10.1007/s11032-014-0038-y.

Guiu-Aragonés, C., Sánchez-Pina, M. A., Díaz-Pendón, J. A., Peña, E. J., Heinlein, M., and Martín-Hernández, A. M. (2016). cmv1 is a gate for Cucumber mosaic virus transport from bundle sheath cells to phloem in melon. Mol. Plant Pathol. 17, 973–984. doi: 10.1111/mpp.12351.

Guiu-Aragonés, C., Díaz-Pendón, J. A., and Martín-Hernández, A. M. (2015). Four sequence positions of the movement protein of C ucumber mosaic virus determine the virulence against cmv1-mediated resistance in melon. Mol. Plant Pathol. 16, 675–684.

Guiu-Aragonés, C., Sánchez-Pina, M. A., Díaz-Pendón, J. A., Peña, E. J., Heinlein, M., and Martín-Hernández, A. M. (2016). cmv1 is a gate for Cucumber mosaic virus transport from bundle sheath cells to phloem in melon. Mol. Plant Pathol. 17, 973–984.

Guo, G., Wang, S., Liu, J., Pan, B., Diao, W., Ge, W., et al. (2017). Rapid identification of QTLs underlying resistance to Cucumber mosaic virus in pepper (Capsicum frutescens). Theor. Appl. Genet. 130, 41–52. doi: 10.1007/s00122-016-2790-3.

Guo, Y., Sirkis, D. W., and Schekman, R. (2014). Protein sorting at the trans-Golgi network. Annu. Rev. Cell Dev. Biol. 30, 169–206. doi: 10.1146/annurev-cellbio-100913-013012.

Habili, N., and Francki, R. I. (1974). Comparative studies on tomato aspermy and cucumber mosaic viruses. II. Virus stability. Virology 60, 29–36. doi: 10.1016/0042-6822(74)90362-6.

Hafrén, A., Hofius, D., Rönnholm, G., Sonnewald, U., and Mäkinen, K. (2010). HSP70 and its cochaperone CPIP promote potyvirus infection in Nicotiana benthamiana by regulating viral coat protein functions. Plant Cell 22, 523–535. doi: 10.1105/tpc.109.072413.

Hamera, S., Song, X., Su, L., Chen, X., and Fang, R. (2012). Cucumber mosaic virus suppressor 2b binds to AGO4-related small RNAs and impairs AGO4 activities. Plant J. 69, 104–115. doi: https://doi.org/10.1111/j.1365-313X.2011.04774.x.

Hao, L., Liu, J., Zhong, S., Gu, H., and Qu, L. J. (2016). AtVPS41-mediated endocytic pathway is essential for pollen tube-stigma interaction in Arabidopsis. Proc. Natl. Acad. Sci. U. S. A. 113, 6307–6312. doi: 10.1073/pnas.1602757113.

Hara-Nishimura, I., Nishimura, M., and Akazawa, T. (1985). Biosynthesis and intracellular transport of 11S globulin in developing pumpkin cotyledons. Plant Physiol. 77, 747–752.

Hara-Nishimura, I., Shimada, T., Hatano, K., Takeuchi, Y., and Nishimura, M. (1998). Transport of storage proteins to protein storage vacuoles is mediated by large precursor-accumulating vesicles. Plant Cell 10, 825–836.

Harries, P. A., Palanichelvam, K., Yu, W., Schoelz, J. E., and Nelson, R. S. (2009). The cauliflower mosaic virus protein P6 forms motile inclusions that traffic along actin microfilaments and stabilize microtubules. Plant Physiol. 149, 1005–1016. doi: 10.1104/pp.108.131755.

Harries, P. A., Schoelz, J. E., and Nelson, R. S. (2010). Intracellular transport of viruses and their components: utilizing the cytoskeleton and membrane highways. Mol. Plant. Microbe. Interact. 23, 1381–1393. doi: 10.1094/MPMI-05-10-0121.

Hashimoto, M., Neriya, Y., Yamaji, Y., and Namba, S. (2016a). Recessive Resistance to Plant Viruses: Potential Resistance Genes Beyond Translation Initiation Factors. Front. Microbiol. 7, 1695. doi: 10.3389/fmicb.2016.01695.

Hashimoto, M., Neriya, Y., Yamaji, Y., and Namba, S. (2016b). Recessive resistance to plant

viruses: Potential resistance genes beyond translation initiation factors. Front. Microbiol. 7, 1695. doi: 10.3389/fmicb.2016.01695.

Hebert, D. N., and Molinari, M. (2007). In and out of the ER: protein folding, quality control, degradation, and related human diseases. Physiol. Rev. 87, 1377–1408.

Heinlein, M. (2015a). Plant virus replication and movement. Virology 479–480, 657–671. doi: 10.1016/j.virol.2015.01.025.

Heinlein, M. (2015b). Plasmodesmata: channels for viruses on the move. Methods Mol. Biol. 1217, 25–52. doi: 10.1007/978-1-4939-1523-1_2.

Higgins, M. E., Davies, J. P., Chen, F. W., and Ioannou, Y. A. (1999). Niemann-Pick C1 is a late endosome-resident protein that transiently associates with lysosomes and the trans-Golgi network. Mol. Genet. Metab. 68, 1–13. doi: 10.1006/mgme.1999.2882.

High, S., Henry, R., Mould, R. M., Valent, Q., Meacock, S., Cline, K., et al. (1997). Chloroplast SRP54 interacts with a specific subset of thylakoid precursor proteins. J. Biol. Chem. 272, 11622–11628. doi: 10.1074/jbc.272.17.11622.

Hily, J. M., García, A., Moreno, A., Plaza, M., Wilkinson, M. D., Fereres, A., et al. (2014). The relationship between host lifespan and pathogen reservoir potential: an analysis in the system Arabidopsis thaliana--cucumber mosaic virus. PLoS Pathog. 10, e1004492. doi: 10.1371/journal.ppat.1004492.

Hipper, C., Brault, V., Ziegler-Graff, V., and Revers, F. (2013). Viral and cellular factors involved in Phloem transport of plant viruses. Front. Plant Sci. 4, 154. doi: 10.3389/fpls.2013.00154.

Höfte, H., and Voxeur, A. (2017). Plant cell walls. Curr. Biol. 27, R865–R870. doi: 10.1016/j.cub.2017.05.025.

Holmes, K. C., & Franklin, R. E. (1958). The radial density distribution in some strains of tobacco mosaic virus. Virology 6, 328–336.

Hong, J.-S., and Ju, H.-J. (2017). The Plant Cellular Systems for Plant Virus Movement. plant Pathol. J. 33, 213–228. doi: 10.5423/PPJ.RW.09.2016.0198.

Hong, J. S., Ohnishi, S., Masuta, C., Choi, J. K., and Ryu, K. H. (2007). Infection of soybean by Cucumber mosaic virus as determined by viral movement protein. Arch. Virol. 152, 321–328.

Hong, S., Choi, G., Park, S., Chung, A. S., Hunter, E., and Rhee, S. S. (2001). Type D retrovirus Gag polyprotein interacts with the cytosolic chaperonin TRiC. J. Virol. 75, 2526–2534. doi: 10.1128/JVI.75.6.2526-2534.2001.

Howles, P. A., Birch, R. J., Collings, D. A., Gebbie, L. K., Hurley, U. A., Hocart, C. H., et al. (2006). A mutation in an Arabidopsis ribose 5-phosphate isomerase reduces cellulose synthesis and is rescued by exogenous uridine. Plant J. 48, 606–618. doi: 10.1111/J.1365-313X.2006.02902.X.

Huang, C., Yu, Q.-B., Li, Z.-R., Ye, L.-S., Xu, L., and Yang, Z.-N. (2017). Porphobilinogen deaminase HEMC interacts with the PPR-protein AtECB2 for chloroplast RNA editing. Plant J. 92, 546–556. doi: https://doi.org/10.1111/tpj.13672.

Huh, S. U., Kim, M. J., Ham, B.-K., and Paek, K.-H. (2011). A zinc finger protein Tsip1 controls Cucumber mosaic virus infection by interacting with the replication complex on vacuolar membranes of the tobacco plant. New Phytol. 191, 746–762. doi: 10.1111/j.1469-8137.2011.03717.x.

Hull, R. (2002). Matthews' Plant Virology. 4rd ed. Academic Press doi: https://doi.org/10.1016/B978-0-12-361160-4.X5050-6.

Hunt, C. L., Lennemann, N. J., and Maury, W. (2012). Filovirus entry: A novelty in the viral fusion world. Viruses 4, 258–275. doi: 10.3390/v4020258.

Hunter, P. R., Craddock, C. P., Di Benedetto, S., Roberts, L. M., and Frigerio, L. (2007). Fluorescent reporter proteins for the tonoplast and the vacuolar lumen identify a single vacuolar compartment in Arabidopsis cells. Plant Physiol. 145, 1371–1382.

Hunter, S., Apweiler, R., Attwood, T. K., Bairoch, A., Bateman, A., Binns, D., et al. (2009). InterPro: The integrative protein signature database. Nucleic Acids Res. 37. doi: 10.1093/nar/gkn785.

Hwang, J., Lee, S., Lee, J.-H., Kang, W.-H., Kang, J.-H., Kang, M.-Y., et al. (2015). Plant Translation Elongation Factor 1Bβ Facilitates Potato Virus X (PVX) Infection and Interacts with PVX Triple Gene Block Protein 1. PLoS One 10, e0128014. doi: 10.1371/JOURNAL.PONE.0128014.

Hwang, M. S., Kim, K. N., Lee, J. H., and Park, Y. I. (2007). Identification of amino acid sequences determining interaction between the cucumber mosaic virus-encoded 2a

polymerase and 3a movement proteins. J. Gen. Virol. 88, 3445–3451. doi: 10.1099/vir.0.83207-0.

Hwang, M. S., Kim, S. H., Lee, J. H., Bae, J. M., Paek, K. H., and Park, Y. I. (2005). Evidence for interaction between the 2a polymerase protein and the 3a movement protein of Cucumber mosaic virus. J. Gen. Virol. 86, 3171–3177. doi: 10.1099/vir.0.81139-0.

Hyodo, K., Mine, A., Taniguchi, T., Kaido, M., Mise, K., Taniguchi, H., et al. (2013). ADP Ribosylation Factor 1 Plays an Essential Role in the Replication of a Plant RNA Virus. J. Virol. 87, 163 LP – 176. doi: 10.1128/JVI.02383-12.

Iglesias, V. A., and Meins, F. J. (2000). Movement of plant viruses is delayed in a beta-1,3-glucanase-deficient mutant showing a reduced plasmodesmatal size exclusion limit and enhanced callose deposition. Plant J. 21, 157–166. doi: 10.1046/j.1365-313x.2000.00658.x.

Ishibashi, K., and Ishikawa, M. (2013). The resistance protein Tm-1 inhibits formation of a tomato mosaic virus replication protein-host membrane protein complex. J. Virol. 87, 7933–7939.

Ishibashi, K., and Ishikawa, M. (2014). Mechanisms of tomato mosaic virus RNA replication and its inhibition by the host resistance factor Tm-1. Curr. Opin. Virol. 9, 8–13.

Ishihama, A., and Barbier, P. (1994). Molecular anatomy of viral RNA-directed RNA polymerases. Arch. Virol. 134, 235–258. doi: 10.1007/BF01310564.

Ishihara, S., Takabayashi, A., Ido, K., Endo, T., Ifuku, K., and Sato, F. (2007). Distinct Functions for the Two PsbP-Like Proteins PPL1 and PPL2 in the Chloroplast Thylakoid Lumen of Arabidopsis. Plant Physiol. 145, 668–679. doi: 10.1104/pp.107.105866.

Iswanto, A. B. B., Vu, M. H., Pike, S., Lee, J., Kang, H., Son, G. H., et al. (2021). Pathogen effectors: What do they do at plasmodesmata? Mol. Plant Pathol. doi: 10.1111/mpp.13142.

Ivanowski, D. (1892). Ueber die Mosaikkrankheit der Tabakspflanze. Bull. Acad. Imp. Sci. 35, 67–70.

Jacquemond, M. (2012). “Chapter 13 - Cucumber Mosaic Virus,” in Viruses and Virus Diseases of Vegetables in the Mediterranean Basin, eds. G. Loebenstein and H. B. T.-

A. in V. R. Lecoq (Academic Press), 439–504. doi: https://doi.org/10.1016/B978-0-12-394314-9.00013-0.

Jacquemond, M., and Tepfer, M. (1998). Satellite RNA-mediated resistance to plant viruses: are the ecological risks well assessed?

Jaquinod, M., Villiers, F., Kieffer-Jaquinod, S., Hugouvieux, V., Bruley, C., Garin, J., et al. (2007). A proteomics dissection of Arabidopsis thaliana vacuoles isolated from cell culture. Mol. Cell. Proteomics 6, 394–412. doi: 10.1074/mcp.M600250-MCP200.

Jennelle, L., Hunegnaw, R., Dubrovsky, L., Pushkarsky, T., Fitzgerald, M. L., Sviridov, D., et al. (2014). HIV-1 protein Nef inhibits activity of ATP-binding cassette transporter A1 by targeting endoplasmic reticulum chaperone calnexin. J. Biol. Chem. 289, 28870–28884. doi: 10.1074/jbc.M114.583591.

Jia, L., Betters, J. L., and Yu, L. (2011). Niemann-pick C1-like 1 (NPC1L1) protein in intestinal and hepatic cholesterol transport. Annu. Rev. Physiol. 73, 239–259. doi: 10.1146/annurev-physiol-012110-142233.

Jin, Y., Ma, D., Dong, J., Jin, J., Li, D., Deng, C., et al. (2007). HC-Pro protein of Potato virus Y can interact with three Arabidopsis 20S proteasome subunits in planta. J. Virol. 81, 12881–12888. doi: 10.1128/JVI.00913-07.

Joklik, W. K., and Grossberg, S. E. (2006). How the American Society for Virology was founded. Virology 344, 250–257. doi: 10.1016/j.virol.2005.09.022.

Ju, H.-J., Ye, C.-M., and Verchot-Lubicz, J. (2008). Mutational analysis of PVX TGBp3 links subcellular accumulation and protein turnover. Virology 375, 103–117.

Jürgens, G. (2004). Membrane trafficking in plants. Annu. Rev. Cell Dev. Biol. 20, 481–504.

Kameoka, H., Dun, E. A., Lopez-Obando, M., Brewer, P. B., de Saint Germain, A., Rameau, C., et al. (2016). Phloem Transport of the Receptor DWARF14 Protein Is Required for Full Function of Strigolactones. Plant Physiol. 172, 1844–1852. doi: 10.1104/pp.16.01212.

Kanai, R., and Edwards, G. E. (1973). Separation of mesophyll protoplasts and bundle sheath cells from maize leaves for photosynthetic studies. Plant Physiol. 51, 1133–1137. doi: 10.1104/pp.51.6.1133.

Kanazawa, A., Inaba, J., Shimura, H., Otagaki, S., Tsukahara, S., Matsuzawa, A., et al. (2011). Virus-mediated efficient induction of epigenetic modifications of endogenous genes with phenotypic changes in plants. Plant J. 65, 156–168. doi: https://doi.org/10.1111/j.1365-313X.2010.04401.x.

Kandan, A., Commare, R. R., Nandakumar, R., Ramiah, M., Raguchander, T., and Samiyappan, R. (2002). Induction of phenylpropanoid metabolism byPseudomonas fluorescens against tomato spotted wilt virus in tomato. Folia Microbiol. (Praha). 47, 121–129. doi: 10.1007/BF02817669.

Kang, B.-C., Yeam, I., and Jahn, M. M. (2005). Genetics of plant virus resistance. Annu. Rev. Phytopathol. 43, 581–621.

Kang, H., and Hwang, I. (2014). Vacuolar Sorting Receptor-Mediated Trafficking of Soluble Vacuolar Proteins in Plant Cells. Plants (Basel, Switzerland) 3, 392–408. doi: 10.3390/plants3030392.

Kang, J.-N., Lee, W.-H., Won, S. Y., Chang, S., Hong, J.-P., Oh, T.-J., et al. (2021). Systemic Expression of Genes Involved in the Plant Defense Response Induced by Wounding in Senna tora. Int. J. Mol. Sci. 22. doi: 10.3390/ijms221810073.

Kang, W.-H., Hoang, N. H., Yang, H.-B., Kwon, J.-K., Jo, S.-H., Seo, J.-K., et al. (2010). Molecular mapping and characterization of a single dominant gene controlling CMV resistance in peppers (Capsicum annuum L.). Theor. Appl. Genet. 120, 1587–1596. doi: 10.1007/s00122-010-1278-9.

Kanyuka, K., Druka, A., Caldwell, D. G., Tymon, A., McCallum, N., Waugh, R., et al. (2005). Evidence that the recessive bymovirus resistance locus rym4 in barley corresponds to the eukaryotic translation initiation factor 4E gene. Mol. Plant Pathol. 6, 449–458.

Karchi, Z., Cohen, S., and Govers, A. (1975). Inheritance of resistance to cucumber mosaic virus in melons. Phytopathology.

Karimi, M., Inzé, D., and Depicker, A. (2002). GATEWAYTM vectors for Agrobacterium-mediated plant transformation. Trends Plant Sci. 7, 193–195.

Kashuba, E., Pokrovskaja, K., Klein, G., and Szekely, L. (1999). Epstein-Barr virus-encoded nuclear protein EBNA-3 interacts with the epsilon-subunit of the T-complex protein 1

chaperonin complex. J. Hum. Virol. 2, 33–37.

Kasteel, D., Wellink, J., Verver, J., van Lent, J., Goldbach, R., and van Kammen, A. (1993). The involvement of cowpea mosaic virus M RNA-encoded proteins in tubule formation. J. Gen. Virol. 74 (Pt 8), 1721–1724. doi: 10.1099/0022-1317-74-8-1721.

Keilhauer, E. C., Hein, M. Y., and Mann, M. (2015). Accurate protein complex retrieval by affinity enrichment mass spectrometry (AE-MS) rather than affinity purification mass spectrometry (AP-MS). Mol. Cell. Proteomics 14, 120–135. doi: 10.1074/mcp.M114.041012.

Kelley, L. A., Mezulis, S., Yates, C. M., Wass, M. N., and Sternberg, M. J. E. (2015). The Phyre2 web portal for protein modeling, prediction and analysis. Nat. Protoc. 10, 845–858. doi: 10.1038/nprot.2015.053.

Kim, J.-Y. (2018). Symplasmic Intercellular Communication through Plasmodesmata. Plants (Basel, Switzerland) 7. doi: 10.3390/plants7010023.

Kim, M. J., Ham, B.-K., Kim, H. R., Lee, I.-J., Kim, Y. J., Ryu, K. H., et al. (2005). In vitro and in planta interaction evidence between Nicotiana tabacum thaumatin-like protein 1 (TLP1) and cucumber mosaic virus proteins. Plant Mol. Biol. 59, 981–994. doi: 10.1007/s11103-005-2619-y.

Kim, M. J., Huh, S. U., Ham, B.-K., and Paek, K.-H. (2008a). A novel methyltransferase methylates Cucumber mosaic virus 1a protein and promotes systemic spread. J. Virol. 82, 4823–4833. doi: 10.1128/JVI.02518-07.

Kim, M. J., Huh, S. U., Ham, B.-K., and Paek, K.-H. (2008b). A Novel Methyltransferase Methylates Cucumber Mosaic Virus 1a Protein and Promotes Systemic Spread. J. Virol. 82, 4823–4833. doi: 10.1128/JVI.02518-07.

Kim, M. J., Kim, H. R., and Paek, K.-H. (2006). Arabidopsis tonoplast proteins TIP1 and TIP2 interact with the cucumber mosaic virus 1a replication protein. J. Gen. Virol. 87, 3425–3431. doi: 10.1099/vir.0.82252-0.

King, A. M. Q., Lefkowitz, E., Adams, M. J., and Carstens, E. B. (2011). Virus Taxonomy: Ninth Report of the International Committee on Taxonomy of Viruses. Elsevier Science Available at: https://books.google.es/books?id=aFYaE9KXEXUC.

King, L. B., Fusco, M. L., Flyak, A. I., Ilinykh, P. A., Huang, K., Gunn, B., et al. (2018).

The Marburgvirus-Neutralizing Human Monoclonal Antibody MR191 Targets a Conserved Site to Block Virus Receptor Binding. Cell Host Microbe 23, 101-109.e4. doi: 10.1016/j.chom.2017.12.003.

Kiselyova, O. I., Yaminsky, I. V, Karger, E. M., Frolova, O. Y., Dorokhov, Y. L., and Atabekov, J. G. (2001). Visualization by atomic force microscopy of tobacco mosaic virus movement protein-RNA complexes formed in vitro. J. Gen. Virol. 82, 1503–1508. doi: 10.1099/0022-1317-82-6-1503.

Kleijnen, M. F., Kirkpatrick, D. S., and Gygi, S. P. (2007). The ubiquitin-proteasome system regulates membrane fusion of yeast vacuoles. EMBO J. 26, 275–287. doi: 10.1038/sj.emboj.7601486.

Klinghammer, M., and Tenhaken, R. (2007). Genome-wide analysis of the UDP-glucose dehydrogenase gene family in Arabidopsis, a key enzyme for matrix polysaccharides in cell walls. J. Exp. Bot. 58, 3609–3621. doi: 10.1093/jxb/erm209.

Knowlton, J. J., Fernández de Castro, I., Ashbrook, A. W., Gestaut, D. R., Zamora, P. F., Bauer, J. A., et al. (2018). The TRiC chaperonin controls reovirus replication through outer-capsid folding. Nat. Microbiol. 3, 481–493. doi: 10.1038/s41564-018-0122-x.

Kobori, T., Ohki, S. T., and Osaki, T. (2000). Movement of Cucumber mosaic virus is restricted at the interface between mesophyll and phloem pathway in Cucumis figarei. J. Gen. Plant Pathol. 66, 159–166.

Kogovšek, P., Pompe-Novak, M., Petek, M., Fragner, L., Weckwerth, W., and Gruden, K. (2016). Primary Metabolism, Phenylpropanoids and Antioxidant Pathways Are Regulated in Potato as a Response to Potato virus Y Infection. PLoS One 11, e0146135. Available at: https://doi.org/10.1371/journal.pone.0146135.

Kolberg, L., Raudvere, U., Kuzmin, I., Vilo, J., and Peterson, H. (2020). gprofiler2 -- an R package for gene list functional enrichment analysis and namespace conversion toolset g:Profiler. F1000Research 9. doi: 10.12688/f1000research.24956.2.

Kong, D., Zhu, Y., Wu, H., Cheng, X., Liang, H., and Ling, H.-Q. (2008). AtTHIC, a gene involved in thiamine biosynthesis in Arabidopsis thaliana. Cell Res. 18, 566–576. doi: 10.1038/cr.2008.35.

Kong, J., Wei, M., Li, G., Lei, R., Qiu, Y., Wang, C., et al. (2018). The cucumber mosaic

virus movement protein suppresses PAMP-triggered immune responses in Arabidopsis and tobacco. Biochem. Biophys. Res. Commun. 498, 395–401. doi: https://doi.org/10.1016/j.bbrc.2018.01.072.

Kragler, F. (2012). Plasmodesmata: intercellular tunnels facilitating transport of macromolecules in plants. Cell Tissue Res. 352, 49–58.

Kragler, F., Curin, M., Trutnyeva, K., Gansch, A., and Waigmann, E. (2003). MPB2C, a microtubule-associated plant protein binds to and interferes with cell-to-cell transport of tobacco mosaic virus movement protein. Plant Physiol. 132, 1870–1883. doi: 10.1104/pp.103.022269.

Krogh, A., Larsson, B., Von Heijne, G., and Sonnhammer, E. L. L. (2001). Predicting transmembrane protein topology with a hidden Markov model: Application to complete genomes. J. Mol. Biol. 305, 567–580. doi: 10.1006/jmbi.2000.4315.

Kumar, S., and Trivedi, P. K. (2018). Glutathione S-transferases: Role in combating abiotic stresses including arsenic detoxification in plants. Front. Plant Sci. 9, 751. doi: 10.3389/fpls.2018.00751.

Kumari, R., Kumar, S., Singh, L., and Hallan, V. (2016). Movement Protein of Cucumber Mosaic Virus Associates with Apoplastic Ascorbate Oxidase. PLoS One 11, e0163320. doi: 10.1371/journal.pone.0163320.

Künzl, F., Früholz, S., Fäßler, F., Li, B., and Pimpl, P. (2016). Receptor-mediated sorting of soluble vacuolar proteins ends at the trans-Golgi network/early endosome. Nat. plants 2, 1–10.

Kutchukian, C., Vivas, O., Casas, M., Jones, J. G., Tiscione, S. A., Simó, S., et al. (2021). NPC1 regulates the distribution of phosphatidylinositol 4-kinases at Golgi and lysosomal membranes. EMBO J. 40, e105990. doi: 10.15252/embj.2020105990.

Kuźniak, E., and Kopczewski, T. (2020). The Chloroplast Reactive Oxygen Species-Redox System in Plant Immunity and Disease. Front. Plant Sci. 11, 572686. doi: 10.3389/fpls.2020.572686.

Kwon, Y., Shen, J., Lee, M. H., Geem, K. R., Jiang, L., and Hwang, I. (2018). AtCAP2 is crucial for lytic vacuole biogenesis during germination by positively regulating vacuolar protein trafficking. Proc. Natl. Acad. Sci. U. S. A. 115, E1675–E1683. doi:

10.1073/pnas.1717204115.

Lamb, D. C., Follmer, A. H., Goldstone, J. V., Nelson, D. R., Warrilow, A. G., Price, C. L., et al. (2019). On the occurrence of cytochrome P450 in viruses. Proc. Natl. Acad. Sci. U. S. A. 116, 12343–12352. doi: 10.1073/pnas.1901080116.

Lambertucci, S., Orman, K. M., Das Gupta, S., Fisher, J. P., Gazal, S., Williamson, R. J., et al. (2019). Analysis of Barley Leaf Epidermis and Extrahaustorial Proteomes During Powdery Mildew Infection Reveals That the PR5 Thaumatin-Like Protein TLP5 Is Required for Susceptibility Towards Blumeria graminis f. sp. hordei. Front. Plant Sci. 10, 1138. doi: 10.3389/fpls.2019.01138.

Lazar, C., Gatto, L., Ferro, M., Bruley, C., and Burger, T. (2016). Accounting for the Multiple Natures of Missing Values in Label-Free Quantitative Proteomics Data Sets to Compare Imputation Strategies. J. Proteome Res. 15, 1116–1125. doi: 10.1021/acs.jproteome.5b00981.

Lecoq, H., Labonne, G., and Pitrat, M. (1980). Specificity of resistance to virus transmission by aphids in Cucumis melo. in Annales de Phytopathologie (Institut National de la Recherche Agronomique), 139–144.

Lecoq, H., and Pitrat, M. (1982). Effect on cucumber mosaic virus incidence of the cultivation of partially resistant muskmelon cultivars. in IV Conference on recent Advances in Vegetable Virus Research 127, 137–146.

Lecoq, H., and Pitrat, M. (1983). Field experiments on the integrated control of aphid-borne viruses in muskmelon. F. Exp. Integr. Control aphid-borne viruses muskmelon., 169–176.

Lee, J.-Y., and Frank, M. (2018). Plasmodesmata in phloem: different gateways for different cargoes. Curr. Opin. Plant Biol. 43, 119–124. doi: 10.1016/j.pbi.2018.04.014.

Lefeuvre, P., Martin, D. P., Elena, S. F., Shepherd, D. N., Roumagnac, P., and Varsani, A. (2019). Evolution and ecology of plant viruses. Nat. Rev. Microbiol. 17, 632–644. doi: 10.1038/s41579-019-0232-3.

Lellis, A. D., Kasschau, K. D., Whitham, S. A., and Carrington, J. C. (2002). Loss-of-susceptibility mutants of Arabidopsis thaliana reveal an essential role for eIF (iso) 4E during potyvirus infection. Curr. Biol. 12, 1046–1051.

Lewsey, M., Surette, M., Robertson, F. C., Ziebell, H., Choi, S. H., Ryu, K. H., et al. (2009). The role of the Cucumber mosaic virus 2b protein in viral movement and symptom induction. Mol. Plant. Microbe. Interact. 22, 642–654. doi: 10.1094/MPMI-22-6-0642.

Li, B., Dong, X., Li, X., Chen, H., Zhang, H., Zheng, X., et al. (2018a). A subunit of the HOPS endocytic tethering complex, FgVps41, is important for fungal development and plant infection in Fusarium graminearum. Environ. Microbiol. 20, 1436–1451.

Li, D., Wei, T., Abbott, C. M., and Harrich, D. (2013a). The Unexpected Roles of Eukaryotic Translation Elongation Factors in RNA Virus Replication and Pathogenesis. Microbiol. Mol. Biol. Rev. 77, 253–266. doi: 10.1128/MMBR.00059-12.

Li, D., Wei, T., Abbott, C. M., Harrich, D., Sasikumar, A. N., Perez, W. B., et al. (2013b). The Unexpected Roles of Eukaryotic Translation Elongation Factors in RNA Virus Replication and Pathogenesis. Microbiol. Mol. Biol. Rev. 77, 253–266. doi: 10.1128/MMBR.00059-12.

Li, N., Yin, Y., Wang, F., and Yao, M. (2018b). Construction of a high-density genetic map and identification of QTLs for cucumber mosaic virus resistance in pepper (Capsicum annuum L.) using specific length amplified fragment sequencing (SLAF-seq). Breed. Sci. 68, 233–241. doi: 10.1270/jsbbs.17063.

Li, Q., Ryu, K. H., and Palukaitis, P. (2001). Cucumber mosaic virus-plant interactions: identification of 3a protein sequences affecting infectivity, cell-to-cell movement, and long-distance movement. Mol. plant-microbe Interact. 14, 378–385.

Li, S. (2019). Regulation of ribosomal proteins on viral infection. Cells 8, 508.

Li, X., Wang, J., Coutavas, E., Shi, H., Hao, Q., and Blobel, G. (2016). Structure of human Niemann-Pick C1 protein. Proc. Natl. Acad. Sci. U. S. A. 113, 8212–8217. doi: 10.1073/pnas.1607795113.

Li, Y., Wu, M. Y., Song, H. H., Hu, X., and Qiu, B. S. (2005). Identification of a tobacco protein interacting with tomato mosaic virus coat protein and facilitating long-distance movement of virus. Arch. Virol. 150, 1993–2008. doi: 10.1007/s00705-005-0554-5.

Li, Z. P., Paterlini, A., Glavier, M., and Bayer, E. M. (2021). Intercellular trafficking via plasmodesmata: molecular layers of complexity. Cell. Mol. Life Sci. 78, 799–816. doi: 10.1007/s00018-020-03622-8.

Lim, S. H., Witty, M., Wallace-Cook, A. D. M., Ilag, L. I., and Smith, A. G. (1994). Porphobilinogen deaminase is encoded by a single gene in Arabidopsis thaliana and is targeted to the chloroplasts. Plant Mol. Biol. 26, 863–872. doi: 10.1007/BF00028854.

Lionetti, V., Raiola, A., Cervone, F., and Bellincampi, D. (2014). How do pectin methylesterases and their inhibitors affect the spreading of tobamovirus? Plant Signal. Behav. 9, e972863-1-e972863-4. doi: 10.4161/15592316.2014.972863.

Liu, C., and Nelson, R. S. (2013). The cell biology of Tobacco mosaic virus replication and movement. Front. Plant Sci. 4, 12. doi: 10.3389/fpls.2013.00012.

Liu, D. Y. T., Smith, P. M. C., Barton, D. A., Day, D. A., and Overall, R. L. (2017). Characterisation of Arabidopsis calnexin 1 and calnexin 2 in the endoplasmic reticulum and at plasmodesmata. Protoplasma 254, 125–136. doi: 10.1007/s00709-015-0921-3.

Liu, D., Zhao, Q., Cheng, Y., Li, D., Jiang, C., Cheng, L., et al. (2019a). Transcriptome analysis of two cultivars of tobacco in response to Cucumber mosaic virus infection. Sci. Rep. 9, 3124. doi: 10.1038/s41598-019-39734-w.

Liu, M., and Lu, S. (2016). Plastoquinone and Ubiquinone in Plants: Biosynthesis, Physiological Function and Metabolic Engineering . Front. Plant Sci. 7, 1898. Available at: https://www.frontiersin.org/article/10.3389/fpls.2016.01898.

Liu, N. J., Zhang, T., Liu, Z. H., Chen, X., Guo, H. S., Ju, B. H., et al. (2019b). Phytosphinganine Affects Plasmodesmata Permeability via Facilitating PDLP5-Stimulated Callose Accumulation in Arabidopsis. Mol. Plant. doi: 10.1016/j.molp.2019.10.013.

López-Gresa, M. P., Lisón, P., Kim, H. K., Choi, Y. H., Verpoorte, R., Rodrigo, I., et al. (2012). Metabolic fingerprinting of Tomato Mosaic Virus infected Solanum lycopersicum. J. Plant Physiol. 169, 1586–1596. doi: https://doi.org/10.1016/j.jplph.2012.05.021.

Love, A. J., Geri, C., Laird, J., Carr, C., Yun, B.-W., Loake, G. J., et al. (2012). Cauliflower mosaic virus protein P6 inhibits signaling responses to salicylic acid and regulates innate immunity. PLoS One 7, e47535. doi: 10.1371/journal.pone.0047535.

Lu, D.-P., and Christopher, D. A. (2008). Endoplasmic reticulum stress activates the expression of a sub-group of protein disulfide isomerase genes and AtbZIP60

modulates the response in Arabidopsis thaliana. Mol. Genet. Genomics 280, 199–210. doi: 10.1007/s00438-008-0356-z.

Luan, H., Shine, M. B., Cui, X., Chen, X., Ma, N., Kachroo, P., et al. (2016). The Potyviral P3 Protein Targets Eukaryotic Elongation Factor 1A to Promote the Unfolded Protein Response and Viral Pathogenesis. Plant Physiol. 172, 221–234. doi: 10.1104/pp.16.00505.

Luo, K.-R., Huang, N.-C., and Yu, T.-S. (2018). Selective targeting of mobile mRNAs to plasmodesmata for cell-to-cell movement. Plant Physiol. 177, 604–614.

Madeira, F., Park, Y. M., Lee, J., Buso, N., Gur, T., Madhusoodanan, N., et al. (2019). The EMBL-EBI search and sequence analysis tools APIs in 2019. Nucleic Acids Res. 47, W636–W641. doi: 10.1093/nar/gkz268.

Mahdavi, F., Sariah, M., and Maziah, M. (2012). Expression of rice thaumatin-like protein gene in transgenic banana plants enhances resistance to fusarium wilt. Appl. Biochem. Biotechnol. 166, 1008–1019. doi: 10.1007/s12010-011-9489-3.

Makuch, L., Storch, J., Xu, Z., Jorrin-Novo, J. V., Jiménez-Guerrero, I., Cubo, M., et al. (2014). Plant proteomics methods and protocols. 1st ed. Elsevier Inc. doi: 10.1201/b15251-10.

Malik, A. A., Vashisht, V. K., Singh, K., Sharma, A., Singh, D. K., Singh, H., et al. (2014). Diversity among melon (Cucumis melo L.) landraces from the Indo-Gangetic plains of India and their genetic relationship with USA melon cultivars. Genet. Resour. Crop Evol. 61, 1189–1208.

Malter, D., and Wolf, S. (2011). Melon phloem-sap proteome: developmental control and response to viral infection. Protoplasma 248, 217–224. doi: 10.1007/s00709-010-0215-8.

Mandadi, K. K., and Scholthof, K.-B. G. (2013). Plant Immune Responses Against Viruses: How Does a Virus Cause Disease? Plant Cell 25, 1489–1505. doi: 10.1105/tpc.113.111658.

Marín, M., Thallmair, V., and Ott, T. (2012). The intrinsically disordered N-terminal region of AtREM1.3 remorin protein mediates protein-protein interactions. J. Biol. Chem. 287, 39982–39991. doi: 10.1074/jbc.M112.414292.

Marri, L., Sparla, F., Pupillo, P., and Trost, P. (2005). Co-ordinated gene expression of photosynthetic glyceraldehyde-3-phosphate dehydrogenase, phosphoribulokinase, and CP12 in Arabidopsis thaliana. J. Exp. Bot. 56, 73–80. doi: 10.1093/jxb/eri020.

Martelli, G. P., Gallitelli, D., and Russo, M. (1999). "An appraisal of pathogen-derived resistance for the control of virus diseases," in Genetics and breeding for crop quality and resistance (Springer), 223–232.

Marti, L., Fornaciari, S., Renna, L., Stefano, G., and Brandizzi, F. (2010). COPII-mediated traffic in plants. Trends Plant Sci. 15, 522–528. doi: 10.1016/j.tplants.2010.05.010.

Martín-Hernández, A. M., and Picó, B. (2021). Natural resistances to viruses in cucurbits. Agronomy 11, 23.

Maruyama, D., Endo, T., and Nishikawa, S. (2010). BiP-mediated polar nuclei fusion is essential for the regulation of endosperm nuclei proliferation in Arabidopsis thaliana Proc. Natl. Acad. Sci. 107, 1684 LP – 1689. doi: 10.1073/pnas.0905795107.

Maruyama, D., Sugiyama, T., Endo, T., and Nishikawa, S.-I. (2014). Multiple BiP genes of Arabidopsis thaliana are required for male gametogenesis and pollen competitiveness. Plant Cell Physiol. 55, 801–810. doi: 10.1093/pcp/pcu018.

Mascia, T., Vučurović, A., Minutillo, S. A., Nigro, F., Labarile, R., Savoia, M. A., et al. (2019). Infection of Colletotrichum acutatum and Phytophthora infestans by taxonomically different plant viruses. Eur. J. Plant Pathol. 153, 1001–1017.

Masiri, J., Velasquez, N. V, and Murphy, J. F. (2011). Cucumber mosaic virus 2b-deficient mutant causes limited, asymptomatic infection of bell pepper. Plant Dis. 95, 331–336.

Mateyak, M. K., and Kinzy, T. G. (2010). eEF1A: Thinking outside the ribosome. J. Biol. Chem. 285, 21209–21213. doi: 10.1074/jbc.R110.113795.

Matsusaki, M., Kanemura, S., Kinoshita, M., Lee, Y. H., Inaba, K., and Okumura, M. (2020). The Protein Disulfide Isomerase Family: from proteostasis to pathogenesis. Biochim. Biophys. Acta - Gen. Subj. 1864, 129338. doi: 10.1016/J.BBAGEN.2019.04.003.

Maule, A. J., and Havelda, Z. (2008). In situ detection of plant viruses and virus-specific products. Methods Mol. Biol. 451, 201–216. doi: 10.1007/978-1-59745-102-4_14.

Maule, A. J., and Palukaitis, P. (1991). Virus movement in infected plants. CRC. Crit. Rev.

Plant Sci. 9, 457–473.

McBride, Z., Chen, D., Reick, C., Xie, J., and Szymanski, D. B. (2017). Global Analysis of Membrane-associated Protein Oligomerization Using Protein Correlation Profiling. Mol. Cell. Proteomics 16, 1972–1989. doi: 10.1074/mcp.RA117.000276.

Mekuria, T., Bamunusinghe, D., Payton, M., and Verchot-Lubicz, J. (2008). Phloem unloading of potato virus X movement proteins is regulated by virus and host factors. Mol. Plant. Microbe. Interact. 21, 1106–1117. doi: 10.1094/MPMI-21-8-1106.

Melcher, U. (2000). The "30K" superfamily of viral movement proteins. J. Gen. Virol. 81, 257–266. doi: 10.1099/0022-1317-81-1-257.

Mi, H., Ebert, D., Muruganujan, A., Mills, C., Albou, L.-P., Mushayamaha, T., et al. (2021). PANTHER version 16: a revised family classification, tree-based classification tool, enhancer regions and extensive API. Nucleic Acids Res. 49, D394–D403. doi: 10.1093/nar/gkaa1106.

Michel, V., Julio, E., Candresse, T., Cotucheau, J., Decorps, C., Volpatti, R., et al. (2018). NtTPN1: a RPP8-like R gene required for Potato virus Y-induced veinal necrosis in tobacco. Plant J. doi: 10.1111/tpj.13980.

Mifflin, H., and Littell, M. (2008). McDougal Littell Biology. Houghton Mifflin School Available at: https://books.google.es/books?id=s2zNbwAACAAJ.

Mine, A., Hyodo, K., Tajima, Y., Kusumanegara, K., Taniguchi, T., Kaido, M., et al. (2012). Differential roles of Hsp70 and Hsp90 in the assembly of the replicase complex of a positive-strand RNA plant virus. J. Virol. 86, 12091–12104. doi: 10.1128/JVI.01659-12.

Mine, A., and Okuno, T. (2012). Composition of plant virus RNA replicase complexes. Curr. Opin. Virol. 2, 669–675. doi: 10.1016/j.coviro.2012.09.014.

Misra, R. C., Sandeep, Kamthan, M., Kumar, S., and Ghosh, S. (2016). A thaumatin-like protein of Ocimum basilicum confers tolerance to fungal pathogen and abiotic stress in transgenic Arabidopsis. Sci. Rep. 6, 25340. doi: 10.1038/srep25340.

Mitra, S. K., Walters, B. T., Clouse, S. D., and Goshe, M. B. (2009). An efficient organic solvent based extraction method for the proteomic analysis of Arabidopsis plasma membranes. J. Proteome Res. 8, 2752–2767. doi: 10.1021/pr801044y.

Miura, E., Kato, Y., Matsushima, R., Albrecht, V., Laalami, S., and Sakamoto, W. (2007). The Balance between Protein Synthesis and Degradation in Chloroplasts Determines Leaf Variegation in Arabidopsis yellow variegated Mutants. Plant Cell 19, 1313–1328. doi: 10.1105/tpc.106.049270.

Mizutani, M. (2012). Impacts of Diversification of Cytochrome P450 on Plant Metabolism. Biol. Pharm. Bull. 35, 824–832. doi: 10.1248/BPB.35.824.

Mochizuki, T., and Ohki, S. T. (2005). Amino acid 129 in the coat protein of Cucumber mosaic virus primarily determines invasion of the shoot apical meristem of tobacco plants. J. Gen. Plant Pathol. 71, 326–332.

Moffett, P. (2017). Transfer and modification of NLR proteins for virus resistance in plants. Curr. Opin. Virol. 26, 43–48. doi: https://doi.org/10.1016/j.coviro.2017.07.008.

Molho, M., Prasanth, K. R., Pogany, J., and Nagy, P. D. (2021). Targeting conserved co-opted host factors to block virus replication: Using allosteric inhibitors of the cytosolic Hsp70s to interfere with tomato bushy stunt virus replication. Virology 563, 1–19. doi: https://doi.org/10.1016/j.virol.2021.08.002.

Monforte, A. J., Diaz, A., Caño-Delgado, A., and van der Knaap, E. (2014). The genetic basis of fruit morphology in horticultural crops: lessons from tomato and melon. J. Exp. Bot. 65, 4625–4637. doi: 10.1093/jxb/eru017.

Monforte, A. J., Oliver, M., Gonzalo, M. J., Alvarez, J. M., Dolcet-Sanjuan, R., and Arus, P. (2004). Identification of quantitative trait loci involved in fruit quality traits in melon (Cucumis melo L.). Theor. Appl. Genet. 108, 750–758.

Moreno, I. M., Thompson, J. R., and García-Arenal, F. (2004). Analysis of the systemic colonization of cucumber plants by Cucumber green mottle mosaic virus. J. Gen. Virol. 85, 749–759. doi: 10.1099/vir.0.19540-0.

Mugford, S. G., Matthewman, C. A., Hill, L., and Kopriva, S. (2010). Adenosine-5′-phosphosulfate kinase is essential for Arabidopsis viability. FEBS Lett. 584, 119–123. doi: https://doi.org/10.1016/j.febslet.2009.11.014.

Munro, A. W., Girvan, H. M., and McLean, K. J. (2007). Cytochrome P450-redox partner fusion enzymes. Biochim. Biophys. Acta - Gen. Subj. 1770, 345–359. doi: 10.1016/j.bbagen.2006.08.018.

Murtagh, F., and Legendre, P. (2014). Ward's Hierarchical Agglomerative Clustering Method: Which Algorithms Implement Ward's Criterion? J. Classif. 31, 274–295. doi: 10.1007/s00357-014-9161-z.

Nagano, H., Mise, K., Furusawa, I., and Okuno, T. (2001). Conversion in the requirement of coat protein in cell-to-cell movement mediated by the cucumber mosaic virus movement protein. J. Virol. 75, 8045–8053. doi: 10.1128/jvi.75.17.8045-8053.2001.

Nagy, P. D., and Pogany, J. (2012). The dependence of viral RNA replication on co-opted host factors. Nat. Rev. Microbiol. 10, 137–149. doi: 10.1038/nrmicro2692.

Nakatsu, F., Hase, K., and Ohno, H. (2014). The Role of the Clathrin Adaptor AP-1: Polarized Sorting and Beyond. Membranes (Basel). 4, 747–763. doi: 10.3390/membranes4040747.

Nakatsukasa, K., Huyer, G., Michaelis, S., and Brodsky, J. L. (2008). Dissecting the ER-Associated Degradation of a Misfolded Polytopic Membrane Protein. Cell 132, 101–112. doi: 10.1016/J.CELL.2007.11.023.

Nakhasi, H. L., Ramanujam, M., Atreya, C. D., Hobman, T. C., Lee, N., Esmaili, A., et al. (2001). Rubella virus glycoprotein interaction with the endoplasmic reticulum calreticulin and calnexin. Arch. Virol. 146, 1–14. doi: 10.1007/s007050170186.

Naoumkina, M. A., Zhao, Q., Gallego-Giraldo, L., Dai, X., Zhao, P. X., and Dixon, R. A. (2010). Genome-wide analysis of phenylpropanoid defence pathways. Mol. Plant Pathol. 11, 829–846. doi: 10.1111/j.1364-3703.2010.00648.x.

Naslavsky, N., and Caplan, S. (2018). The enigmatic endosome - sorting the ins and outs of endocytic trafficking. J. Cell Sci. 131. doi: 10.1242/jcs.216499.

Nasu, Y., Karasawa, A., Hase, S., and Ehara, Y. (1996). Cry, the resistance locus of cowpea to cucumber mosaic virus strain Y. Phytopathology 86, 946–951.

Navarro, J. A., and Pallás, V. (2017). An Update on the Intracellular and Intercellular Trafficking of Carmoviruses. Front. Plant Sci. 8, 1801. doi: 10.3389/fpls.2017.01801.

Navarro, J., Sanchez-Navarro, J., and Pallas, V. (2019). "Chapter One - Key checkpoints in the movement of plant viruses through the host," in Virus Entry, eds. M. Kielian, T. C. Mettenleiter, and M. J. B. T.-A. in V. R. Roossinck (Academic Press), 1–64. doi: https://doi.org/10.1016/bs.aivir.2019.05.001.

Nebenfuhr, A., Gallagher, L. A., Dunahay, T. G., Frohlick, J. A., Mazurkiewicz, A. M., Meehl, J. B., et al. (1999). Stop-and-go movements of plant Golgi stacks are mediated by the acto-myosin system. Plant Physiol. 121, 1127–1141.

Nguyen, D. H., and Hildreth, J. E. (2000). Evidence for budding of human immunodeficiency virus type 1 selectively from glycolipid-enriched membrane lipid rafts. J. Virol. 74, 3264–3272. doi: 10.1128/jvi.74.7.3264-3272.2000.

Nicaise, V. (2014). Crop immunity against viruses: Outcomes and future challenges. Front. Plant Sci. 5, 660. doi: 10.3389/fpls.2014.00660.

Nicaise, V., German-Retana, S., Sanjuán, R., Dubrana, M.-P., Mazier, M., Maisonneuve, B., et al. (2003). The Eukaryotic Translation Initiation Factor 4E Controls Lettuce Susceptibility to the Potyvirus Lettuce mosaic virus . Plant Physiol. 132, 1272–1282. doi: 10.1104/pp.102.017855.

Niehl, A., Amari, K., Gereige, D., Brandner, K., Mély, Y., and Heinlein, M. (2012). Control of Tobacco mosaic virus Movement Protein Fate by CELL-DIVISION-CYCLE Protein48. Plant Physiol. 160, 2093–2108. doi: 10.1104/pp.112.207399.

Niehl, A., and Heinlein, M. (2011). Cellular pathways for viral transport through plasmodesmata. Protoplasma 248, 75–99. doi: 10.1007/s00709-010-0246-1.

Niehl, A., Peña, E. J., Amari, K., and Heinlein, M. (2013). Microtubules in viral replication and transport. Plant J. 75, 290–308. doi: 10.1111/tpj.12134.

Niehl, A., Wyrsch, I., Boller, T., and Heinlein, M. (2016). Double-stranded RNAs induce a pattern-triggered immune signaling pathway in plants. New Phytol. 211, 1008–1019. doi: 10.1111/nph.13944.

Nieto, C., Morales, M., Orjeda, G., Clepet, C., Monfort, A., Sturbois, B., et al. (2006). An eIF4E allele confers resistance to an uncapped and non-polyadenylated RNA virus in melon. Plant J. 48, 452–462.

Noël, L. D., Cagna, G., Stuttmann, J., Wirthmüller, L., Betsuyaku, S., Witte, C.-P., et al. (2007). Interaction between SGT1 and Cytosolic/Nuclear HSC70 Chaperones Regulates Arabidopsis Immune Responses. Plant Cell 19, 4061. doi: 10.1105/TPC.107.051896.

Nováková, P., Hirsch, S., Feraru, E., Tejos, R., van Wijk, R., Viaene, T., et al. (2014). SAC

phosphoinositide phosphatases at the tonoplast mediate vacuolar function in Arabidopsis. Proc. Natl. Acad. Sci. U. S. A. 111, 2818–2823. doi: 10.1073/pnas.1324264111.

Nováková, S., Šubr, Z., Kováč, A., Fialová, I., Beke, G., and Danchenko, M. (2020). Cucumber mosaic virus resistance: Comparative proteomics of contrasting Cucumis sativus cultivars after long-term infection. J. Proteomics 214, 103626. doi: 10.1016/j.jprot.2019.103626.

Novick, P., Field, C., and Schekman, R. (1980). Identification of 23 complementation groups required for post-translational events in the yeast secretory pathway. Cell 21, 205–215. doi: 10.1016/0092-8674(80)90128-2.

Oliveros, J. C. (2008). Venny. An interactive tool for comparing lists with Venn's diagrams. Available at: https://bioinfogp.cnb.csic.es/tools/venny/index.html.

Ouko, M. O., Sambade, A., Brandner, K., Niehl, A., Peña, E., Ahad, A., et al. (2010). Tobacco mutants with reduced microtubule dynamics are less susceptible to TMV. Plant J. 62, 829–839. doi: 10.1111/j.1365-313X.2010.04195.x.

Paape, M., Solovyev, A. G., Erokhina, T. N., Minina, E. A., Schepetilnikov, M. V, Lesemann, D.-E., et al. (2006). At-4/1, an interactor of the Tomato spotted wilt virus movement protein, belongs to a new family of plant proteins capable of directed intra- and intercellular trafficking. Mol. Plant. Microbe. Interact. 19, 874–883. doi: 10.1094/MPMI-19-0874.

Pallas, V., and García, J. A. (2011). How do plant viruses induce disease? Interactions and interference with host components. J. Gen. Virol. 92, 2691–2705. doi: 10.1099/vir.0.034603-0.

Pallas, V., and Gómez, G. (2013). Phloem RNA-binding proteins as potential components of the long-distance RNA transport system. Front. Plant Sci. 4, 130. doi: 10.3389/fpls.2013.00130.

Palukaitis, P., and García-Arenal, F. (2003). Cucumoviruses. Adv. Virus Res. 62, 241–323.

Palukaitis, P., Roossinck, M. J., Dietzgen, R. G., and Francki, R. I. (1992). Cucumber mosaic virus. Adv. Virus Res. 41, 281–348. doi: 10.1016/s0065-3527(08)60039-1.

Palukaitis, P., and Yoon, J.-Y. (2020). R gene mediated defense against viruses. Curr. Opin.

Virol. 45, 1–7. doi: 10.1016/j.coviro.2020.04.001.

Pascual, L., Yan, J., Pujol, M., Monforte, A. J., Picó, B., and Martín-Hernández, A. M. (2019). CmVPS41 Is a General Gatekeeper for Resistance to Cucumber Mosaic Virus Phloem Entry in Melon. Front. Plant Sci. 10, 1219. doi: 10.3389/fpls.2019.01219.

Pathak, K. B., Pogany, J., and Nagy, P. D. (2011). Non-template functions of the viral RNA in plant RNA virus replication. Curr. Opin. Virol. 1, 332–338. doi: 10.1016/j.coviro.2011.09.011.

Pathak, K. B., Sasvari, Z., and Nagy, P. D. (2008). The host Pex19p plays a role in peroxisomal localization of tombusvirus replication proteins. Virology 379, 294–305. doi: 10.1016/j.virol.2008.06.044.

Peña, E. J., and Heinlein, M. (2012). RNA transport during TMV cell-to-cell movement . Front. Plant Sci. 3. Available at: https://www.frontiersin.org/article/10.3389/fpls.2012.00193.

Pereira, C., Pereira, S., Satiat-Jeunemaitre, B., and Pissarra, J. (2013). Cardosin A contains two vacuolar sorting signals using different vacuolar routes in tobacco epidermal cells. Plant J. 76, 87–100.

Pereira, L., Pujol, M., Garcia-Mas, J., and Phillips, M. A. (2017). Non-invasive quantification of ethylene in attached fruit headspace at 1 p.p.b. by gas chromatography-mass spectrometry. Plant J. 91, 172–183. doi: 10.1111/tpj.13545.

Perraki, A., Gronnier, J., Gouguet, P., Boudsocq, M., Deroubaix, A.-F., Simon, V., et al. (2018). REM1.3's phospho-status defines its plasma membrane nanodomain organization and activity in restricting PVX cell-to-cell movement. PLoS Pathog. 14, e1007378. doi: 10.1371/journal.ppat.1007378.

Peters, W. S., Jensen, K. H., Stone, H. A., and Knoblauch, M. (2021). Plasmodesmata and the problems with size: Interpreting the confusion. J. Plant Physiol. 257, 153341. doi: https://doi.org/10.1016/j.jplph.2020.153341.

Pfeffer, S. R. (2019). NPC intracellular cholesterol transporter 1 (NPC1)-mediated cholesterol export from lysosomes. J. Biol. Chem. 294, 1706–1709. doi: 10.1074/jbc.TM118.004165.

Pinot, F., and Beisson, F. (2011). Cytochrome P450 metabolizing fatty acids in plants:

characterization and physiological roles. FEBS J. 278, 195–205. doi: 10.1111/j.1742-4658.2010.07948.x.

Piper, R. C., Bryant, N. J., and Stevens, T. H. (1997). The membrane protein alkaline phosphatase is delivered to the vacuole by a route that is distinct from the VPS-dependent pathway. J. Cell Biol. 138, 531–545.

Pisetsky, D. S. (2012). The origin and properties of extracellular DNA: from PAMP to DAMP. Clin. Immunol. 144, 32–40. doi: 10.1016/j.clim.2012.04.006.

Pitrat, M. (2008). "Melon," in Vegetables I (Springer), 283–315.

Pitrat, M. (2016). "Melon genetic resources: phenotypic diversity and horticultural taxonomy," in Genetics and genomics of Cucurbitaceae (Springer), 25–60.

Poirier, S., Mayer, G., Murphy, S. R., Garver, W. S., Chang, T. Y., Schu, P., et al. (2013). The Cytosolic Adaptor AP-1A Is Essential for the Trafficking and Function of Niemann-Pick Type C Proteins. Traffic 14, 458–469. doi: 10.1111/tra.12046.

Pols, M. S., ten Brink, C., Gosavi, P., Oorschot, V., and Klumperman, J. (2013). The HOPS proteins hVps41 and hVps39 are required for homotypic and heterotypic late endosome fusion. Traffic 14, 219–232. doi: 10.1111/tra.12027.

Popescu, S. C., and Tumer, N. E. (2004). Silencing of ribosomal protein L3 genes in N. tabacum reveals coordinate expression and significant alterations in plant growth, development and ribosome biogenesis. Plant J. 39, 29–44. doi: 10.1111/j.1365-313X.2004.02109.x.

Pouwels, J., van der Velden, T., Willemse, J., Borst, J. W., van Lent, J., Bisseling, T., et al. (2004). Studies on the origin and structure of tubules made by the movement protein of Cowpea mosaic virus. J. Gen. Virol. 85, 3787–3796. doi: 10.1099/vir.0.80497-0.

Price, A., Seals, D., Wickner, W., and Ungermann, C. (2000). The docking stage of yeast vacuole fusion requires the transfer of proteins from a cis-SNARE complex to a Rab/Ypt protein. J. Cell Biol. 148, 1231–1238.

Printen, J. A., and Sprague, G. F. (1994). Protein-protein interactions in the yeast pheromone response pathway: Ste5p interacts with all members of the MAP kinase cascade. Genetics 138, 609–619. doi: 10.1093/genetics/138.3.609.

Pulido, P., Zagari, N., Manavski, N., Gawronski, P., Matthes, A., Scharff, L. B., et al. (2018).

CHLOROPLAST RIBOSOME ASSOCIATED Supports Translation under Stress and Interacts with the Ribosomal 30S Subunit. Plant Physiol. 177, 1539–1554. doi: 10.1104/pp.18.00602.

Qian, L., Zhao, J., Du, Y., Zhao, X., Han, M., and Liu, Y. (2018a). Hsp90 Interacts With Tm-22 and Is Essential for Tm-22-Mediated Resistance to Tobacco mosaic virus. Front. Plant Sci. 9, 411. doi: 10.3389/fpls.2018.00411.

Qian, X., Xiang, Q., Yang, T., Ma, H., Ding, X. S., and Tao, X. (2018b). Molecular Co-Chaperone SGT1 Is Critical for Cell-to-Cell Movement and Systemic Infection of Tomato Spotted Wilt Virus in Nicotiana benthamiana. Viruses 10. doi: 10.3390/v10110647.

Radford, J. E., Vesk, M., and Overall, R. L. (1998). Callose deposition at plasmodesmata. Protoplasma 201, 30–37. doi: 10.1007/BF01280708.

Rafalski, J. A., Vogel, J. M., Morgante, M., Powell, W., Andre, C., and Tingey, S. V (1996). "4 - Generating and Using DNA Markers in Plants," in, eds. B. BIRREN and E. B. T.-N. G. A. LAI (San Diego: Academic Press), 75–134. doi: https://doi.org/10.1016/B978-012101285-4/50005-9.

Rapala-Kozik, M., Wolak, N., Kujda, M., and Banas, A. K. (2012). The upregulation of thiamine (vitamin B1) biosynthesis in Arabidopsis thaliana seedlings under salt and osmotic stress conditions is mediated by abscisic acid at the early stages of this stress response. BMC Plant Biol. 12, 2. doi: 10.1186/1471-2229-12-2.

Rappsilber, J., Ishihama, Y., and Mann, M. (2003). Stop And Go Extraction tips for matrix-assisted laser desorption/ionization, nanoelectrospray, and LC/MS sample pretreatment in proteomics. Anal. Chem. 75, 663–670. doi: 10.1021/ac026117i.

Raschke, M., Bürkle, L., Müller, N., Nunes-Nesi, A., Fernie, A. R., Arigoni, D., et al. (2007). Vitamin B1 biosynthesis in plants requires the essential iron–sulfur cluster protein, THIC. Proc. Natl. Acad. Sci. 104, 19637 LP – 19642. doi: 10.1073/pnas.0709597104.

Rehling, P., Darsow, T., Katzmann, D. J., and Emr, S. D. (1999). Formation of AP-3 transport intermediates requires Vps41 function. Nat. Cell Biol. 1, 346–353. doi: 10.1038/14037.

Reichel, C., and Beachy, R. N. (2000). Degradation of tobacco mosaic virus movement

protein by the 26S proteasome. J. Virol. 74, 3330–3337.

Requena, A., Simón-Buela, L., Salcedo, G., and García-Arenal, F. (2006). Potential involvement of a cucumber homolog of phloem protein 1 in the long-distance movement of Cucumber mosaic virus particles. Mol. Plant. Microbe. Interact. 19, 734–746. doi: 10.1094/MPMI-19-0734.

Reynolds, C. R., Islam, S. A., and Sternberg, M. J. E. (2018). EzMol: A Web Server Wizard for the Rapid Visualization and Image Production of Protein and Nucleic Acid Structures. J. Mol. Biol. 430, 2244–2248. doi: 10.1016/j.jmb.2018.01.013.

Risser, G. (1977). ETUDE DE LA RESISTANCE DU MELON (CUCUMIS MELO L.) AU VIRUS DE LA MOSAIQUE DU CONCOMBRE. Available at: https://pascal-francis.inist.fr/vibad/index.php?action=getRecordDetail&idt=PASCAL7810235041 [Accessed June 10, 2021].

Rissler, H. M., Collakova, E., DellaPenna, D., Whelan, J., and Pogson, B. J. (2002). Chlorophyll biosynthesis. Expression of a second chl I gene of magnesium chelatase in Arabidopsis supports only limited chlorophyll synthesis. Plant Physiol. 128, 770–779. doi: 10.1104/pp.010625.

Ritschel, P. S., Lins, T. C. de L., Tristan, R. L., Buso, G. S. C., Buso, J. A., and Ferreira, M. E. (2004). Development of microsatellite markers from an enriched genomic library for genetic analysis of melon (Cucumis melo L.). BMC Plant Biol. 4, 9. doi: 10.1186/1471-2229-4-9.

Ritzenthaler, C., and Hofmann, C. (2007). “Tubule-Guided Movement of Plant Viruses,” in Viral Transport in Plants, ed. H. M. Waigmann E. (Berlin, Heidelberg: Springer Berlin Heidelberg), 63–83. doi: 10.1007/7089_2006_105.

Rives, A. W., and Galitski, T. (2003). Modular organization of cellular networks. Proc. Natl. Acad. Sci. U. S. A. 100, 1128–1133. doi: 10.1073/pnas.0237338100.

Robinson, R. W., and Decker-Walters, D. S. (1999). Cucurbits. CAB International, Wallingford. Oxon (GB). pp 226.

Rojas, C. M., Senthil-Kumar, M., Tzin, V., and Mysore, K. S. (2014). Regulation of primary plant metabolism during plant-pathogen interactions and its contribution to plant defense. Front. Plant Sci. 5, 17. doi: 10.3389/fpls.2014.00017.

Rolland, N., Bouchnak, I., Moyet, L., Salvi, D., and Kuntz, M. (2018). The Main Functions of Plastids. Methods Mol. Biol. 1829, 73–85. doi: 10.1007/978-1-4939-8654-5_5.

Roossinck, M. J. (2001). Cucumber mosaic virus, a model for RNA virus evolution. Mol. Plant Pathol. 2, 59–63. doi: 10.1046/j.1364-3703.2001.00058.x.

Roossinck, M. J., Zhang, L., and Hellwald, K.-H. (1999). Rearrangements in the 5′ nontranslated region and phylogenetic analyses of cucumber mosaic virus RNA 3 indicate radial evolution of three subgroups. J. Virol. 73, 6752–6758.

Ross-Elliott, T. J., Jensen, K. H., Haaning, K. S., Wager, B. M., Knoblauch, J., Howell, A. H., et al. (2017). Phloem unloading in Arabidopsis roots is convective and regulated by the phloem-pole pericycle. Elife 6. doi: 10.7554/eLife.24125.

Roy, D., Sin, S.-H., Damania, B., and Dittmer, D. P. (2011). Tumor suppressor genes FHIT and WWOX are deleted in primary effusion lymphoma (PEL) cell lines. Blood, J. Am. Soc. Hematol. 118, e32–e39.

Ruan, Q., Harrington, A. J., Caldwell, K. A., Caldwell, G. A., and Standaert, D. G. (2010). VPS41, a protein involved in lysosomal trafficking, is protective in Caenorhabditis elegans and mammalian cellular models of Parkinson's disease. Neurobiol. Dis. 37, 330–338.

Ruffel, S., Dussault, M.-H., Palloix, A., Moury, B., Bendahmane, A., Robaglia, C., et al. (2002). A natural recessive resistance gene against potato virus Y in pepper corresponds to the eukaryotic initiation factor 4E (eIF4E). Plant J. 32, 1067–1075. doi: 10.1046/j.1365-313x.2002.01499.x.

Ruffel, S., Gallois, J.-L., Lesage, M. L., and Caranta, C. (2005). The recessive potyvirus resistance gene pot-1 is the tomato orthologue of the pepper pvr2-eIF4E gene. Mol. Genet. Genomics 274, 346–353.

Ruggieri, V., Alexiou, K. G., Morata, J., Argyris, J., Pujol, M., Yano, R., et al. (2018). An improved assembly and annotation of the melon (Cucumis melo L.) reference genome. Sci. Rep. 8, 8088. doi: 10.1038/s41598-018-26416-2.

Ruiz-Medrano, R., Moya, J. H., Xoconostle-Cázares, B., and Lucas, W. J. (2007). Influence of cucumber mosaic virus infection on the mRNA population present in the phloem translocation stream of pumpkin plants. Funct. Plant Biol. 34, 292–301. doi:

10.1071/FP06300.

Sager, R. E., and Lee, J.-Y. (2018). Plasmodesmata at a glance. J. Cell Sci. 131. doi: 10.1242/jcs.209346.

Salie, M. J., Zhang, N., Lancikova, V., Xu, D., and Thelen, J. J. (2016). A Family of Negative Regulators Targets the Committed Step of de Novo Fatty Acid Biosynthesis. Plant Cell 28, 2312–2325. doi: 10.1105/tpc.16.00317.

Sánchez-Navarro, J. A., Carmen Herranz, M., and Pallás, V. (2006). Cell-to-cell movement of Alfalfa mosaic virus can be mediated by the movement proteins of Ilar-, bromo-, cucumo-, tobamo- and comoviruses and does not require virion formation. Virology 346, 66–73. doi: 10.1016/j.virol.2005.10.024.

Sanderson, L. E., Lanko, K., Alsagob, M., Almass, R., Al-Ahmadi, N., Najafi, M., et al. (2021). Bi-allelic variants in HOPS complex subunit VPS41 cause cerebellar ataxia and abnormal membrane trafficking. Brain 144, 769–780. doi: 10.1093/brain/awaa459.

Sané, A. T., Sinnett, D., Delvin, E., Bendayan, M., Marcil, V., Ménard, D., et al. (2006). Localization and role of NPC1L1 in cholesterol absorption in human intestine. J. Lipid Res. 47, 2112–2120. doi: 10.1194/jlr.M600174-JLR200.

Sanfaçon, H. (2015). Plant Translation Factors and Virus Resistance. Viruses 7, 3392–3419. doi: 10.3390/v7072778.

Sanseverino, W., Hénaff, E., Vives, C., Pinosio, S., Burgos-Paz, W., Morgante, M., et al. (2015). Transposon insertions, structural variations, and SNPs contribute to the evolution of the melon genome. Mol. Biol. Evol. 32, 2760–2774.

Sáray, R., Fábián, A., Palkovics, L., and Salánki, K. (2021). The 28 Ser Amino Acid of Cucumber Mosaic Virus Movement Protein Has a Role in Symptom Formation and Plasmodesmata Localization. Viruses 13. doi: 10.3390/v13020222.

Sasaki, N., Park, J.-W., Maule, A. J., and Nelson, R. S. (2006). The cysteine-histidine-rich region of the movement protein of Cucumber mosaic virus contributes to plasmodesmal targeting, zinc binding and pathogenesis. Virology 349, 396–408. doi: 10.1016/j.virol.2006.02.035.

Sasikumar, A. N., Perez, W. B., and Kinzy, T. G. (2012). The many roles of the eukaryotic elongation factor 1 complex. Wiley Interdiscip. Rev. RNA 3, 543–555. doi:

10.1002/wrna.1118.

Schoppe, J., Mari, M., Yavavli, E., Auffarth, K., Cabrera, M., Walter, S., et al. (2020). AP-3 vesicle uncoating occurs after HOPS-dependent vacuole tethering. EMBO J. 39, e105117. doi: 10.15252/embj.2020105117.

Sebastian, P., Schaefer, H., Telford, I. R. H., and Renner, S. S. (2010). Cucumber (Cucumis sativus) and melon (C. melo) have numerous wild relatives in Asia and Australia, and the sister species of melon is from Australia. Proc. Natl. Acad. Sci. 107, 14269–14273.

Seemanpillai, M., Elamawi, R., Ritzenthaler, C., and Heinlein, M. (2006). Challenging the role of microtubules in Tobacco mosaic virus movement by drug treatments is disputable. J. Virol. 80, 6712–6715. doi: 10.1128/JVI.00453-06.

Sekine, K.-T., Nandi, A., Ishihara, T., Hase, S., Ikegami, M., Shah, J., et al. (2004). Enhanced resistance to Cucumber mosaic virus in the Arabidopsis thaliana ssi2 mutant is mediated via an SA-independent mechanism. Mol. Plant. Microbe. Interact. 17, 623–632. doi: 10.1094/MPMI.2004.17.6.623.

Seo, J.-K., and Kim, K.-H. (2016). "Long-Distance Movement of Viruses in Plants BT - Current Research Topics in Plant Virology," in, eds. A. Wang and X. Zhou (Cham: Springer International Publishing), 153–172. doi: 10.1007/978-3-319-32919-2_6.

Seo, J.-K., Kwon, S.-J., Choi, H.-S., and Kim, K.-H. (2009). Evidence for alternate states of Cucumber mosaic virus replicase assembly in positive- and negative-strand RNA synthesis. Virology 383, 248–260. doi: https://doi.org/10.1016/j.virol.2008.10.033.

Serra-Soriano, M., Navarro, J. A., Genoves, A., and Pallás, V. (2015). Comparative proteomic analysis of melon phloem exudates in response to viral infection. J. Proteomics 124, 11–24. doi: https://doi.org/10.1016/j.jprot.2015.04.008.

Serra-Soriano, M., Pallás, V., and Navarro, J. A. (2014). A model for transport of a viral membrane protein through the early secretory pathway: minimal sequence and endoplasmic reticulum lateral mobility requirements. Plant J. 77, 863–879. doi: 10.1111/tpj.12435.

Serrano, I., Buscaill, P., Audran, C., Pouzet, C., Jauneau, A., and Rivas, S. (2016). A non canonical subtilase attenuates the transcriptional activation of defence responses in Arabidopsis thaliana. Elife 5. doi: 10.7554/eLife.19755.

Serva, S., and Nagy, P. D. (2006). Proteomics analysis of the tombusvirus replicase: Hsp70 molecular chaperone is associated with the replicase and enhances viral RNA replication. J. Virol. 80, 2162–2169. doi: 10.1128/JVI.80.5.2162-2169.2006.

Shadle, G. L., Wesley, S. V., Korth, K. L., Chen, F., Lamb, C., and Dixon, R. A. (2003). Phenylpropanoid compounds and disease resistance in transgenic tobacco with altered expression of l-phenylalanine ammonia-lyase. Phytochemistry 64, 153–161. doi: https://doi.org/10.1016/S0031-9422(03)00151-1.

Shannon, P., Markiel, A., Ozier, O., Baliga, N. S., Wang, J. T., Ramage, D., et al. (2003). Cytoscape: a software environment for integrated models of biomolecular interaction networks. Genome Res. 13, 2498–2504. doi: 10.1101/gr.1239303.

Shi, L., Yang, Y., Xie, Q., Miao, H., Bo, K., Song, Z., et al. (2018). Inheritance and QTL mapping of cucumber mosaic virus resistance in cucumber (Cucumis Sativus L.). PLoS One 13, e0200571.

Shimada, T., Takagi, J., Ichino, T., Shirakawa, M., and Hara-Nishimura, I. (2018). Plant Vacuoles. Annu. Rev. Plant Biol. 69, 123–145. doi: 10.1146/annurev-arplant-042817-040508.

Shimaoka, T., Nakayama, T., Fukumoto, N., Kume, N., Takahashi, S., Yamaguchi, J., et al. (2004). Cell surface-anchored SR-PSOX/CXC chemokine ligand 16 mediates firm adhesion of CXC chemokine receptor 6-expressing cells. J. Leukoc. Biol. 75, 267–274. doi: 10.1189/jlb.1003465.

Shimura, H., Pantaleo, V., Ishihara, T., Myojo, N., Inaba, J., Sueda, K., et al. (2011). A viral satellite RNA induces yellow symptoms on tobacco by targeting a gene involved in chlorophyll biosynthesis using the RNA silencing machinery. PLoS Pathog. 7, e1002021.

Soards, A. J., Murphy, A. M., Palukaitis, P., and Carr, J. P. (2002). Virulence and differential local and systemic spread of Cucumber mosaic virus in tobacco are affected by the CMV 2b protein. Mol. Plant-Microbe Interact. 15, 647–653.

Soler-Garzón, A., McClean, P. E., and Miklas, P. N. (2021). Genome-Wide Association Mapping of bc-1 and bc-u Reveals Candidate Genes and New Adjustments to the Host-Pathogen Interaction for Resistance to Bean Common Mosaic Necrosis Virus in Common Bean. Front. Plant Sci. 12, 699569. doi: 10.3389/fpls.2021.699569.

Solinger, J. A., and Spang, A. (2013). Tethering complexes in the endocytic pathway: CORVET and HOPS. FEBS J. 280, 2743–2757. doi: https://doi.org/10.1111/febs.12151.

Solovyev, A., Kalinina, N., and Morozov, S. (2012). Recent advances in research of plant virus movement mediated by triple gene block. Front. Plant Sci. 3, 276.

Sotelo-Silveira, M., Cucinotta, M., Chauvin, A. L., Chávez Montes, R. A., Colombo, L., Marsch-Martínez, N., et al. (2013). Cytochrome P450 CYP78A9 is involved in arabidopsis reproductive development. Plant Physiol. 162, 779–799. doi: 10.1104/pp.113.218214.

Spirin, V., and Mirny, L. A. (2003). Protein complexes and functional modules in molecular networks. Proc. Natl. Acad. Sci. U. S. A. 100, 12123–12128. doi: 10.1073/pnas.2032324100.

Stahl, E., Hartmann, M., Scholten, N., and Zeier, J. (2019). A Role for Tocopherol Biosynthesis in Arabidopsis Basal Immunity to Bacterial Infection. Plant Physiol. 181, 1008–1028. doi: 10.1104/pp.19.00618.

Stalder, D., and Gershlick, D. C. (2020). Direct trafficking pathways from the Golgi apparatus to the plasma membrane. Semin. Cell Dev. Biol. 107, 112–125. doi: https://doi.org/10.1016/j.semcdb.2020.04.001.

Steel, D., Zech, M., Zhao, C., Barwick, K. E. S., Burke, D., Demailly, D., et al. (2020). Loss-of-function variants in HOPS complex genes VPS16 and VPS41 cause early onset dystonia associated with lysosomal abnormalities. Ann. Neurol. 88, 867–877.

Stein, N., Perovic, D., Kumlehn, J., Pellio, B., Stracke, S., Streng, S., et al. (2005). The eukaryotic translation initiation factor 4E confers multiallelic recessive Bymovirus resistance in Hordeum vulgare (L.). Plant J. 42, 912–922.

Stoeck, I. K., Lee, J.-Y., Tabata, K., Romero-Brey, I., Paul, D., Schult, P., et al. (2018). Hepatitis C Virus Replication Depends on Endosomal Cholesterol Homeostasis. J. Virol. 92. doi: 10.1128/JVI.01196-17.

Strange, R. C., MA, S., S, R., and AA, F. (2001). Glutathione-S-transferase family of enzymes. Mutat. Res. 482, 21–26. doi: 10.1016/S0027-5107(01)00206-8.

Streb, S., and Zeeman, S. C. (2012). Starch Metabolism in Arabidopsis. Arab. B. 2012. doi:

10.1199/tab.0160.

Stroupe, C., Collins, K. M., Fratti, R. A., and Wickner, W. (2006). Purification of active HOPS complex reveals its affinities for phosphoinositides and the SNARE Vam7p. EMBO J. 25, 1579–1589.

Struk, S., Jacobs, A., Sánchez Martín-Fontecha, E., Gevaert, K., Cubas, P., and Goormachtig, S. (2019). Exploring the protein-protein interaction landscape in plants. Plant. Cell Environ. 42, 387–409. doi: 10.1111/pce.13433.

Su, S., Liu, Z., Chen, C., Zhang, Y., Wang, X., Zhu, L., et al. (2010). Cucumber Mosaic Virus Movement Protein Severs Actin Filaments to Increase the Plasmodesmal Size Exclusion Limit in Tobacco . Plant Cell 22, 1373–1387. doi: 10.1105/tpc.108.064212.

Suga, T. (1991). The Man'yo-shu: A Complete English Translation in 5-7 Rythm. Kanda Inst. Foreign Lang., Tokyo.

Sun, Y., Huang, D., and Chen, X. (2019). Dynamic regulation of plasmodesmatal permeability and its application to horticultural research. Hortic. Res. 6, 47. doi: 10.1038/s41438-019-0129-3.

Sun, Z., and Brodsky, J. L. (2019). Protein quality control in the secretory pathway. J. Cell Biol. 218, 3171–3187. doi: 10.1083/jcb.201906047.

Suzuki, K., Kuroda, T., Miura, Y., and Murai, J. (2003a). Screening and field trials of virus resistant sources in Capsicum spp. Plant Dis. 87, 779–783.

Suzuki, M., Hibi, T., and Masuta, C. (2003b). RNA recombination between cucumoviruses: possible role of predicted stem-loop structures and an internal subgenomic promoter-like motif. Virology 306, 77–86. doi: https://doi.org/10.1016/S0042-6822(02)00050-8.

Szponarski, W., Sommerer, N., Boyer, J.-C., Rossignol, M., and Gibrat, R. (2004). Large-scale characterization of integral proteins from Arabidopsis vacuolar membrane by two-dimensional liquid chromatography. Proteomics 4, 397–406. doi: 10.1002/pmic.200300607.

Takahashi, H., Miller, J., Nozaki, Y., Sukamto, Takeda, M., Shah, J., et al. (2002). RCY1, an Arabidopsis thaliana RPP8/HRT family resistance gene, conferring resistance to cucumber mosaic virus requires salicylic acid, ethylene and a novel signal transduction mechanism. Plant J. 32, 655–667.

Takahashi, H., Suzuki, M., Natsuaki, K., Shigyo, T., Hino, K., Teraoka, T., et al. (2001). Mapping the virus and host genes involved in the resistance response in cucumber mosaic virus-infected Arabidopsis thaliana. Plant cell Physiol. 42, 340–347.

Takemoto, K., Ebine, K., Askani, J. C., Krüger, F., Gonzalez, Z. A., Ito, E., et al. (2018). Distinct sets of tethering complexes, SNARE complexes, and Rab GTPases mediate membrane fusion at the vacuole in Arabidopsis. Proc. Natl. Acad. Sci. U. S. A. 115, E2457–E2466. doi: 10.1073/pnas.1717839115.

Taliansky, M., Torrance, L., and Kalinina, N. O. (2008). Role of plant virus movement proteins. Methods Mol. Biol. 451, 33–54. doi: 10.1007/978-1-59745-102-4_3.

Tang, W., Ma, Y., Jia, L., Ioannou, Y. A., Davies, J. P., and Yu, L. (2009a). Genetic inactivation of NPC1L1 protects against sitosterolemia in mice lacking ABCG5/ABCG8. J. Lipid Res. 50, 293–300. doi: https://doi.org/10.1194/jlr.M800439-JLR200.

Tang, Y., Leao, I. C., Coleman, E. M., Broughton, R. S., and Hildreth, J. E. K. (2009b). Deficiency of niemann-pick type C-1 protein impairs release of human immunodeficiency virus type 1 and results in Gag accumulation in late endosomal/lysosomal compartments. J. Virol. 83, 7982–7995. doi: 10.1128/JVI.00259-09.

TerBush, D. R., Maurice, T., Roth, D., and Novick, P. (1996). The Exocyst is a multiprotein complex required for exocytosis in Saccharomyces cerevisiae. EMBO J. 15, 6483–6494.

Thackray, D. J., Diggle, A. J., Berlandier, F. A., and Jones, R. A. C. (2004). Forecasting aphid outbreaks and epidemics of Cucumber mosaic virus in lupin crops in a Mediterranean-type environment. Virus Res. 100, 67–82. doi: 10.1016/j.virusres.2003.12.015.

Thomas, C. L., Bayer, E. M., Ritzenthaler, C., Fernandez-Calvino, L., and Maule, A. J. (2008). Specific targeting of a plasmodesmal protein affecting cell-to-cell communication. PLoS Biol. 6, e7. doi: 10.1371/journal.pbio.0060007.

Tian, T., Liu, Y., Yan, H., You, Q., Yi, X., Du, Z., et al. (2017). agriGO v2.0: a GO analysis toolkit for the agricultural community, 2017 update. Nucleic Acids Res. 45, W122–W129. doi: 10.1093/nar/gkx382.

Till, B. J., Reynolds, S. H., Greene, E. A., Codomo, C. A., Enns, L. C., Johnson, J. E., et al. (2003). Large-scale discovery of induced point mutations with high-throughput TILLING. Genome Res. 13, 524–530.

Tilsner, J., Linnik, O., Christensen, N. M., Bell, K., Roberts, I. M., Lacomme, C., et al. (2009). Live-cell imaging of viral RNA genomes using a Pumilio-based reporter. Plant J. 57, 758–770. doi: 10.1111/j.1365-313X.2008.03720.x.

Tilsner, J., Linnik, O., Louveaux, M., Roberts, I. M., Chapman, S. N., and Oparka, K. J. (2013). Replication and trafficking of a plant virus are coupled at the entrances of plasmodesmata. J. Cell Biol. 201, 981–995.

Travis, S. M., DAmico, K., Yu, I.-M., McMahon, C., Hamid, S., Ramirez-Arellano, G., et al. (2020). Structural basis for the binding of SNAREs to the multisubunit tethering complex Dsl1. J. Biol. Chem. 295, 10125–10135. doi: 10.1074/jbc.RA120.013654.

Turner, K. A., Sit, T. L., Callaway, A. S., Allen, N. S., and Lommel, S. A. (2004). Red clover necrotic mosaic virus replication proteins accumulate at the endoplasmic reticulum. Virology 320, 276–290. doi: https://doi.org/10.1016/j.virol.2003.12.006.

Tyanova, S., Temu, T., and Cox, J. (2016). The MaxQuant computational platform for mass spectrometry-based shotgun proteomics. Nat. Protoc. 11, 2301–2319. doi: 10.1038/nprot.2016.136.

Ueki, S., and Citovsky, V. (2002). The systemic movement of a tobamovirus is inhibited by a cadmium-ion-induced glycine-rich protein. Nat. Cell Biol. 4, 478–486. doi: 10.1038/ncb806.

Ueki, S., and Citovsky, V. (2005). Identification of an interactor of cadmium ion-induced glycine-rich protein involved in regulation of callose levels in plant vasculature. Proc. Natl. Acad. Sci. U. S. A. 102, 12089–12094. doi: 10.1073/pnas.0505927102.

Uemura, T., Yoshimura, S. H., Takeyasu, K., and Sato, M. H. (2002). Vacuolar membrane dynamics revealed by GFP-AtVam3 fusion protein. Genes Cells 7, 743–753. doi: 10.1046/j.1365-2443.2002.00550.x.

UniProt Consortium (2021). UniProt: the universal protein knowledgebase in 2021. Nucleic Acids Res. 49, D480–D489. doi: 10.1093/nar/gkaa1100.

Van der Maelen, E., Rezaei, M. N., Struyf, N., Proost, P., Verstrepen, K. J., and Courtin, C.

M. (2019). Identification of a Wheat Thaumatin-like Protein That Inhibits Saccharomyces cerevisiae. J. Agric. Food Chem. 67, 10423–10431. doi: 10.1021/acs.jafc.9b03432.

van Zeist, W., and de Roller, G. J. (1993). Plant remains from Maadi, a Predynastic site in Lower Egypt. Veg. Hist. Archaeobot. 2, 1–14.

Vandereyken, K., Van Leene, J., De Coninck, B., and Cammue, B. P. A. (2018). Hub Protein Controversy: Taking a Closer Look at Plant Stress Response Hubs. Front. Plant Sci. 9, 694. doi: 10.3389/fpls.2018.00694.

Verchot-Lubicz, J., Torrance, L., Solovyev, A. G., Morozov, S. Y., Jackson, A. O., and Gilmer, D. (2010). Varied movement strategies employed by triple gene block–encoding viruses. Mol. plant-microbe Interact. 23, 1231–1247.

Verchot, J. (2012). Cellular chaperones and folding enzymes are vital contributors to membrane bound replication and movement complexes during plant RNA virus infection. Front. Plant Sci. 3, 275. doi: 10.3389/fpls.2012.00275.

Verchot, J. (2016). Plant Virus Infection and the Ubiquitin Proteasome Machinery: Arms Race along the Endoplasmic Reticulum. Viruses 8. doi: 10.3390/v8110314.

Verchot, J., Driskel, B. A., Zhu, Y., Hunger, R. M., and Littlefield, L. J. (2001). Evidence that soilborne wheat mosaic virus moves long distance through the xylem in wheat. Protoplasma 218, 57–66. doi: 10.1007/BF01288361.

Vinatzer, B. A., Teitzel, G. M., Lee, M., Jelenska, J., Hotton, S., Fairfax, K., et al. (2006). The type III effector repertoire of Pseudomonas syringae pv. syringae B728a and its role in survival and disease on host and non-host plants. Mol. Microbiol. 62, 26–44.

Vogel, F., Hofius, D., and Sonnewald, U. (2007). Intracellular trafficking of potato leafroll virusmovement protein in transgenic arabidopsis. Traffic 8, 1205–1214.

von Bargen, S., Salchert, K., Paape, M., Piechulla, B., and Kellmann, J.-W. (2001). Interactions between the tomato spotted wilt virus movement protein and plant proteins showing homologies to myosin, kinesin and DnaJ-like chaperones. Plant Physiol. Biochem. 39, 1083–1093. doi: https://doi.org/10.1016/S0981-9428(01)01331-6.

Vukašinovic, N., and Žárský, V. (2016). Tethering complexes in the Arabidopsis endomembrane system. Front. Cell Dev. Biol. 4, 46. doi: 10.3389/fcell.2016.00046.

Wachter, A., Tunc-Ozdemir, M., Grove, B. C., Green, P. J., Shintani, D. K., and Breaker, R. R. (2007). Riboswitch Control of Gene Expression in Plants by Splicing and Alternative 3′ End Processing of mRNAs. Plant Cell 19, 3437–3450. doi: 10.1105/tpc.107.053645.

Waigmann, E., Chen, M. H., Bachmaier, R., Ghoshroy, S., and Citovsky, V. (2000). Regulation of plasmodesmal transport by phosphorylation of tobacco mosaic virus cell-to-cell movement protein. EMBO J. 19, 4875–4884. doi: 10.1093/emboj/19.18.4875.

Walsh, D., and Naghavi, M. H. (2019). Exploitation of Cytoskeletal Networks during Early Viral Infection. Trends Microbiol. 27, 39–50. doi: 10.1016/j.tim.2018.06.008.

Wan, J., Cabanillas, D. G., Zheng, H., and Laliberté, J.-F. (2015). Turnip mosaic virus moves systemically through both phloem and xylem as membrane-associated complexes. Plant Physiol. 167, 1374–1388. doi: 10.1104/pp.15.00097.

Wang, D. Y., Kamuda, K., Montoya, G., and Mesa, P. (2020a). The TRiC/CCT Chaperonin and Its Role in Uncontrolled Proliferation. Adv. Exp. Med. Biol. 1243, 21–40. doi: 10.1007/978-3-030-40204-4_2.

Wang, H., Shi, Y., Song, J., Qi, J., Lu, G., Yan, J., et al. (2016). Ebola Viral Glycoprotein Bound to Its Endosomal Receptor Niemann-Pick C1. Cell 164, 258–268. doi: 10.1016/j.cell.2015.12.044.

Wang, H., Shi, Y., Song, J., Qi, J., Lu, G., Yan, J., et al. (2020b). Cryo-EM structures of NPC1L1 reveal mechanisms of cholesterol transport and ezetimibe inhibition. Sci. Adv. 6, 258–268. doi: 10.1016/j.cell.2015.12.044.

Wang, T., Ming, Z., Xiaochun, W., and Hong, W. (2011). Rab7: role of its protein interaction cascades in endo-lysosomal traffic. Cell. Signal. 23, 516–521.

Wang, X., Sager, R., Cui, W., Zhang, C., Lu, H., and Lee, J.-Y. (2013). Salicylic Acid Regulates Plasmodesmata Closure during Innate Immune Responses in Arabidopsis . Plant Cell 25, 2315–2329. doi: 10.1105/tpc.113.110676.

Wang, Y., Tzfira, T., Gaba, V., Citovsky, V., Palukaitis, P., and Gal-On, A. (2004). Functional analysis of the Cucumber mosaic virus 2b protein: pathogenicity and nuclear localization. J. Gen. Virol. 85, 3135–3147. doi: 10.1099/vir.0.80250-0.

Watson, J., and Crick, F. (1953). Genetical Implications of the Structure of Deoxyribonucleic Acid. Nature 171, 964–967.

Watt, L. G., Crawshaw, S., Rhee, S.-J., Murphy, A. M., Canto, T., and Carr, J. P. (2020). The cucumber mosaic virus 1a protein regulates interactions between the 2b protein and ARGONAUTE 1 while maintaining the silencing suppressor activity of the 2b protein. PLOS Pathog. 16, e1009125. Available at: https://doi.org/10.1371/journal.ppat.1009125.

Wei, J., Fu, Z. Y., Li, P. S., Miao, H. H., Li, B. L., Ma, Y. T., et al. (2014). The clathrin adaptor proteins ARH, Dab2, and numb play distinct roles in Niemann-Pick C1-Like 1 versus low density lipoprotein receptor-mediated cholesterol uptake. J. Biol. Chem. 289, 33689–33700. doi: 10.1074/jbc.M114.593764.

Wheeler D, B. M. (2007). "BLAST QuickStart: Example-Driven Web-Based BLAST Tutorial.," in Comparative Genomics: Volumes 1 and 2, ed. editor. Bergman NH (Totowa (NJ): Humana Press).

Whitham, S., Dinesh-Kumar, S. P., Choi, D., Hehl, R., Corr, C., and Baker, B. (1994). The product of the tobacco mosaic virus resistance gene N: similarity to toll and the interleukin-1 receptor. Cell 78, 1101–1115.

Wichmann, C., Meier, F., Virreira Winter, S., Brunner, A.-D., Cox, J., and Mann, M. (2019). MaxQuant.Live Enables Global Targeting of More Than 25,000 Peptides. Mol. Cell. Proteomics 18, 982–994. doi: https://doi.org/10.1074/mcp.TIR118.001131.

Williams, R. C., and Smith, K. M. (1958). The polyhedral form of the Tipula iridescent virus. Biochim. Biophys. Acta 28, 464–469. doi: 10.1016/0006-3002(58)90507-9.

Willows, R. D. (2003). Biosynthesis of chlorophylls from protoporphyrin IX. Nat. Prod. Rep. 20, 327–341. doi: 10.1039/b110549n.

Wolf, S., Deom, C. M., Beachy, R. N., and Lucas, W. J. (1989). Movement protein of tobacco mosaic virus modifies plasmodesmatal size exclusion limit. Science 246, 377–379. doi: 10.1126/science.246.4928.377.

Woloshen, V., Huang, S., and Li, X. (2011). RNA-Binding Proteins in Plant Immunity. J. Pathog. 2011, 278697. doi: 10.4061/2011/278697.

Woo, J. Y., Jeong, K. J., Kim, Y. J., and Paek, K.-H. (2016). CaLecRK-S.5, a pepper L-type lectin receptor kinase gene, confers broad-spectrum resistance by activating priming. J. Exp. Bot. 67, 5725–5741. doi: 10.1093/jxb/erw336.

Xiang, L., Etxeberria, E., and Van den Ende, W. (2013). Vacuolar protein sorting mechanisms in plants. FEBS J. 280, 979–993. doi: 10.1111/febs.12092.

Xu, X. M., Wang, J., Xuan, Z., Goldshmidt, A., Borrill, P. G. M., Hariharan, N., et al. (2011). Chaperonins facilitate KNOTTED1 cell-to-cell trafficking and stem cell function. Science 333, 1141–1144. doi: 10.1126/science.1205727.

Yamaguchi, N., Seshimo, Y., Yoshimoto, E., Ahn, H. Il, Ryu, K. H., Choi, J. K., et al. (2005). Genetic mapping of the compatibility between a lily isolate of Cucumber mosaic virus and a satellite RNA. J. Gen. Virol. 86, 2359–2369.

Yamaji, Y., Kobayashi, T., Hamada, K., Sakurai, K., Yoshii, A., Suzuki, M., et al. (2006). In vivo interaction between Tobacco mosaic virus RNA-dependent RNA polymerase and host translation elongation factor 1A. Virology 347, 100–108. doi: 10.1016/j.virol.2005.11.031.

Yamaji, Y., Sakurai, K., Hamada, K., Komatsu, K., Ozeki, J., Yoshida, A., et al. (2010). Significance of eukaryotic translation elongation factor 1A in tobacco mosaic virus infection. Arch. Virol. 155, 263–268. doi: 10.1007/s00705-009-0571-x.

Yan, J. (2018). Study of the resistance to Cucumber mosaic virus aggressive strains in the melon (Cucumis melon L.) accession PI 161375.

Yang, P., Lüpken, T., Habekuss, A., Hensel, G., Steuernagel, B., Kilian, B., et al. (2014). PROTEIN DISULFIDE ISOMERASE LIKE 5-1 is a susceptibility factor to plant viruses. Proc. Natl. Acad. Sci. 111, 2104–2109. doi: 10.1073/PNAS.1320362111.

Yano, R., Ariizumi, T., Nonaka, S., Kawazu, Y., Zhong, S., Mueller, L., et al. (2020). Comparative genomics of muskmelon reveals a potential role for retrotransposons in the modification of gene expression. Commun. Biol. 3, 432. doi: 10.1038/s42003-020-01172-0.

Yano, R., Nonaka, S., and Ezura, H. (2018). Melonet-DB, a Grand RNA-Seq Gene Expression Atlas in Melon (Cucumis melo L.). Plant Cell Physiol. 59, e4–e4. doi: 10.1093/pcp/pcx193.

Ye, J., Qu, J., Zhang, J.-F., Geng, Y.-F., and Fang, R.-X. (2009). A critical domain of the Cucumber mosaic virus 2b protein for RNA silencing suppressor activity. FEBS Lett. 583, 101–106. doi: 10.1016/j.febslet.2008.11.031.

Yoshii, M., Nishikiori, M., Tomita, K., Yoshioka, N., Kozuka, R., Naito, S., et al. (2004). The Arabidopsis cucumovirus multiplication 1 and 2 loci encode translation initiation factors 4E and 4G. J. Virol. 78, 6102–6111.

Yoshii, M., Yoshioka, N., Ishikawa, M., and Naito, S. (1998a). Isolation of an Arabidopsis thaliana mutant in which accumulation of cucumber mosaic virus coat protein is delayed. Plant J. 13, 211–219.

Yoshii, M., Yoshioka, N., Ishikawa, M., and Naito, S. (1998b). Isolation of an Arabidopsis thaliana mutant in which the multiplication of both cucumber mosaic virus and turnip crinkle virus is affected. J. Virol. 72, 8731–8737.

Yoshinari, A., Fujimoto, M., Ueda, T., Inada, N., Naito, S., and Takano, J. (2016). DRP1-Dependent Endocytosis is Essential for Polar Localization and Boron-Induced Degradation of the Borate Transporter BOR1 in Arabidopsis thaliana. Plant Cell Physiol. 57, 1985–2000. doi: 10.1093/pcp/pcw121.

Yuan, C., Lazarowitz, S. G., and Citovsky, V. (2018). The Plasmodesmal Localization Signal of TMV MP Is Recognized by Plant Synaptotagmin SYTA. MBio 9. doi: 10.1128/mBio.01314-18.

Zavaliev, R., Levy, A., Gera, A., and Epel, B. L. (2013). Subcellular dynamics and role of Arabidopsis β-1,3-glucanases in cell-to-cell movement of tobamoviruses. Mol. Plant. Microbe. Interact. 26, 1016–1030. doi: 10.1094/MPMI-03-13-0062-R.

Zeenko, V. V, Ryabova, L. A., Spirin, A. S., Rothnie, H. M., Hess, D., Browning, K. S., et al. (2002). Eukaryotic elongation factor 1A interacts with the upstream pseudoknot domain in the 3' untranslated region of tobacco mosaic virus RNA. J. Virol. 76, 5678–5691. doi: 10.1128/jvi.76.11.5678-5691.2002.

Zhang, H., Cui, F., Wu, Y., Lou, L., Liu, L., Tian, M., et al. (2015). The RING Finger Ubiquitin E3 Ligase SDIR1 Targets SDIR1-INTERACTING PROTEIN1 for Degradation to Modulate the Salt Stress Response and ABA Signaling in Arabidopsis. Plant Cell 27, 214–227. doi: 10.1105/tpc.114.134163.

Zhang, R. guang, Andersson, C. E., Savchenko, A., Skarina, T., Evdokimova, E., Beasley, S., et al. (2003). Structure of Escherichia coli ribose-5-phosphate isomerase: a ubiquitous enzyme of the pentose phosphate pathway and the Calvin cycle. Structure 11, 31–42. doi: 10.1016/s0969-2126(02)00933-4.

Zhang, S., Ren, J., Li, H., Zhang, Q., Armstrong, J. S., Munn, A. L., et al. (2004). Ncr1p, the yeast ortholog of mammalian Niemann Pick C1 protein, is dispensable for endocytic transport. Traffic 5, 1017–1030. doi: 10.1111/j.1600-0854.2004.00241.x.

Zhang, Y., Chen, W., Sang, X., Wang, T., Gong, H., Zhao, Y., et al. (2021). Genome-Wide Identification of the Thaumatin-like Protein Family Genes in Gossypium barbadense and Analysis of Their Responses to Verticillium dahliae Infection. Plants (Basel, Switzerland) 10. doi: 10.3390/plants10122647.

Zhang, Y., and Hughson, F. M. (2021). Chaperoning SNARE folding and assembly. Annu. Rev. Biochem. 90, 581–603.

Zhang, Z. J., and Peck, S. C. (2011). Simplified enrichment of plasma membrane proteins for proteomic analyses in Arabidopsis thaliana. Proteomics 11, 1780–1788. doi: 10.1002/pmic.201000648.

Zhao, J., Zhang, X., Hong, Y., and Liu, Y. (2016). Chloroplast in plant-virus interaction. Front. Microbiol. 7, 1565.

Zheng, H., and Staehelin, L. A. (2011). Protein storage vacuoles are transformed into lytic vacuoles in root meristematic cells of germinating seedlings by multiple, cell type-specific mechanisms. Plant Physiol. 155, 2023–2035. doi: 10.1104/pp.110.170159.

Zhong, S., Zhao, M., Shi, T., Shi, H., An, F., Zhao, Q., et al. (2009). EIN3/EIL1 cooperate with PIF1 to prevent photo-oxidation and to promote greening of Arabidopsis seedlings. Proc. Natl. Acad. Sci. 106, 21431 LP – 21436. doi: 10.1073/pnas.0907670106.

Zhong, Y., Gu, L. J., Sun, X. G., Yang, S. H., and Zhang, X. H. (2014). Comprehensive analysis of patched domain-containing genes reveals a unique evolutionary pattern. Genet. Mol. Res. 13, 7318–7331. doi: 10.4238/2014.February.13.11.

Zhuang, X., Chung, K. P., Luo, M., and Jiang, L. (2018). Autophagosome Biogenesis and the Endoplasmic Reticulum: A Plant Perspective. Trends Plant Sci. 23, 677–692. doi: 10.1016/j.tplants.2018.05.002.

Zouhar, J., Muñoz, A., and Rojo, E. (2010). Functional specialization within the vacuolar sorting receptor family: VSR1, VSR3 and VSR4 sort vacuolar storage cargo in seeds and vegetative tissues. Plant J. 64, 577–588. doi: 10.1111/j.1365-313X.2010.04349.x.

Supplementary material

The supplementary material can be accessed using the following link or QR code. This is restricted data that is not published yet. Please, do not share this content.

Link:
https://drive.google.com/drive/folders/1Ty8TdUGnIGgX5JSr5_0VjFj1G7EjXRsm?usp=sharing

QR code: